EXPRESSION DYNAMICS OF THE HEPATIC MITOCHONDRIAL PROTEOME OF THE *SOD2*$^{+/-}$ MOUSE IN RESPONSE TO TROGLITAZONE ADMINISTRATION

LEE YIE HOU
HT051163E

A THESIS SUBMITTED FOR THE DEGREE OF DOCTOR OF PHILOSOPHY

DEPARTMENT OF BIOCHEMISTRY,
YONG LOO LIN SCHOOL OF MEDICINE,
NATIONAL UNIVERSITY OF SINGAPORE

2009

ACKNOWLEDGEMENTS

For many, obtaining a postgraduate degree involves conducting experiments decided by our supervisors and doing well in courses. If done right, this is enough to earn one a Ph.D. Needless to say, it isn't always the case. Scientific research is immersion into the unknown, and when factors such as fund (in)sufficiency, ensuring publishing within journals' already limited room for articles and foreseeing unlimited possibilities of problems, doing good research is no longer that easy. Confronting this vast number of daunting tasks alone, while remaining productive in a multi-disciplinary project was not a simple task. That realization was discouraging, but also liberating because of who my academic advisor is.

I am indebted to my academic supervisor, Professor Maxey Chung Ching Ming. Professor Chung was my mentor, teacher, role model and friend. I was always motivated and inspired by his attitude, outlook and vision. He reached so many people as a result of his unwavering belief in individuals and their strengths, as he did to my Ph.D and life. Professor Chung has always been positive, and he gave me many opportunities, supported and encouraged me in bad times. And that was how I was touched by his sincerity and patience, creating a climate of friendliness and emotional support as I muddled through my way to doing productive good science. On the research front, I was granted ample freedom to steer my project, but of course with his constant guidance. With much appreciation and respect, his guidance has changed my Ph.D course

tremendously, and I would not be where I am today if not for Professor Chung's patience and mentorship that saw me through. Professor Chung has left a mark in my life.

My sincere gratitude towards Professor Urs Alex Boelsterli for hatching this brilliant research proposal and imparting the many skills required in this field. Professor Urs made me rediscover research – that science is more than just benchwork, requiring an intimate interplay of soft skills that are essential in this field, as in any other.

Colleagues from Protein and Proteomics Centre, Professor Lin Qingsong, Dr Tan Hwee Tong, Lim Teck Kwang, Cynthia Liang, Tan Gek San, Zubaida, and others whom I fail to mention, thank you for your warmth, friendliness and generosity. Among them, Professor Lin maintained my desire for questioning the unlimited boundaries of knowledge, and facing them with strong analytical skills and sound, systematic thinking. I would like to thank the National University of Singapore for the award of my research scholarship and the various institutions for the grants they have provided, without which this project could not have been completed.

Lastly, I especially want to thank my family and many close friends who had stood by me and supported me all the while. I appreciate your every presence in my life. The years spent doing my Ph.D has been fulfilling, challenging and at times daunting. Were the support from my family, friends and colleagues placed elsewhere, I wonder if the outcome will be entirely different.

TABLE OF CONTENTS

SUMMARY

Idiosyncratic drug-induced liver injuries (DILI) are rare adverse events that inflict susceptible patients exposed to certain normally-mild drugs. A major obstacle in understanding idiosyncratic DILI etiology includes the lack of ideal animal models for its reproduction in the laboratory. Recently, ROS has been implicated in idiosyncratic DILI and the heterozygous superoxide dismutase 2 or *Sod2*$^{+/-}$ mouse (HET) is an ideal mutant model for studying DILI arising from diminished mitochondrial antioxidant defence. Using highly purified mitochondrial proteins from the HET liver, we performed comparative proteomics. The up-regulation of antioxidants such GPX1, GSTK1 and MGST1 suggested the increased effort to restore redox equilibrium. Our proteomic analysis indicated that HET mice exhibit a mild mitochondrial oxidative stress which is partly compensated by the antioxidant defense system linked to the tricarboxylic acid (TCA) cycle, urea cycle, β-oxidation, and oxidative phosphorylation (OXPHOS). This discreet and phenotypically silent mitochondrial proteome alteration represents a "1st hit" which is compatible with studying pathological DILI conditions ("2nd hit").

Applying integrative proteomics on the HET hepatic mitochondria treated with troglitazone, a withdrawn drug due to unacceptable hepatic liability, we generated a comprehensive view of proteomic changes that correlated well with toxicological and histological endpoints. 2D-DIGE and iTRAQ™ coupled to MALDI-TOF/TOF MS/MS analysis revealed a two-stage mitochondrial response upon short-term and long-term troglitazone administration, similar to the delayed hepatotoxicity observed in humans.

The small number of proteins common to both time-points (3 out of 70 proteins) reflected distinct changes that occurred at the molecular level. Early changes involved the induction of a mitochondrial stress response such as seen by increased levels of heat shock protein family members (mortalin, HSP7C), Lon protease, and catalase. In contrast, after 4 weeks, a number of critical proteins including ATP synthase β-subunit, aconitase-2 (ACO2), and mitochondrial dicarboxylate carrier (DIC) exhibited decreased abundance. In addition, mitochondrial protein carbonyls and nitrotyrosine adducts were significantly increased, suggesting uncompensated oxidative damage. Even in the presence of increased SOD2 levels, the threshold for toxicity has been reached and liver injury ensued. Building on clinical and biological evidence of mitochondrial ROS perturbation on troglitazone DILI, we observed that impairment of mitochondrial glutathione transport may play a role in precipitating the toxic effects of troglitazone under compromised mitochondrial ROS defence. This further confirms the contribution of glutathione and inheritable mitochondrial dysfunction in idiosyncratic DILI susceptibility. ACO2 was decreased at both time points, making this protein a potential sensitive and early biomarker for mitochondrial oxidative stress. ACO2 was decreased at both time points, making this protein a potential sensitive and early biomarker for mitochondrial oxidant stress. This integrative approach could signify a new paradigm in advancing and predicting mechanistic toxicity of idiosyncratic DILI.

LIST OF TABLES

LIST OF FIGURES

LIST OF ABBREVIATIONS

$\Delta\Psi_m$	Transmembrane potential
[Fe-S]	Iron-sulfur
1D	1-dimensional
2DE	2-dimensional gel electrophoresis
2D-DIGE	2-dimensional difference gel electrophoresis
2D-LC	2-dimensional liquid chromatography
3-NT	3-nitrotyrosine
3-MGC	3-methylglutaconic aciduria
8-OHdG	8-hydroxydeoxyguanosine
8-oxodG	8-oxo-hydrodeoxyguanosine
ALT	Alanine aminotransferase
AST	Asparate aminotransferase
AUC	Area under curve
$CO_3^{\bullet-}$	Carbonate radical anion
ChIP	Chromatin Immunoprecipitation
DAVID	Database for Annotation, Visualization and Integrated Discovery
DILI	Drug-induced liver injury
ELISA	Enzyme-linked immunosorbent assay
EMSA	Electrophoretic Mobility Shift Assay
ESI	Electrospray ionization
ETC	Electron transport chain
FDA	U.S. Food and drug administration
FDR	False discovery rate
GO	Gene Ontology
GSH	Glutathione
H_2O_2	Hydrogen peroxide
HET	*Sod2*$^{+/-}$
HPLC	High performance liquid chromatography
IEF	Isoelectric focusing
IPG	Immobiline pH gradient
IPI	International Protein Index
iTRAQ™	Isobaric tag for relative and absolute quantitation
KEGG	Kyoto Encyclopaedia of Genes and Genomes
LC	Liquid chromatography
LPS	Liposaacharide
MALDI	Matrix-assisted laser desorption/ionization
MnTBAP	Manganese 5, 10, 15, 20-tetrakis (4-benzoic acid) porphyrin
mPT	Mitochondrial permeability transition
MRM	Multiple reaction monitoring
MS	Mass spectrometry
MS/MS	Tandem mass spectrometry
MudPIT	Mulitdimensional Protein Identification Technology
mtDNA	Mitochondrial DNA
nDNA	Nuclear DNA

$^{\bullet}NO$	Nitric oxide
NO_x^-	Nitrate/ nitrite
$^{\bullet}NO_2$	Nitrogen dioxide
s/n	Signal-to-noise ratio
SOD	Superoxide dismutase
$O_2^{\bullet-}$	Superoxide anion
$OH^{\bullet}$	Hydroxyl radical
$ONOO^-$	Peroxynitrite
OXPHOS	Oxidative phosphorylation
PPARγ	Peroxisome proliferator-activated receptor gamma
PPRE	PPAR response element
PTM	Post-translational modification
ROS	Reactive oxygen species
RNS	Reactive nitrogen species
RXR	Retinoid X receptor
SILAC	Stable isotope labelling by amino acids in cell culture
TOF	Time of flight
TCA	Tricarboxylic acid
ULN	Upper limit of normal
WT	Wild-type

INTRODUCTION

1.1. Idiosyncratic drug-induced liver injury

Drug-induced liver injury (DILI) is a major cause for the withdrawal of drugs from the market, regulatory actions and restriction of prescribing indications (US Food and Drug Administration. Draft guidance for industry. Drug-Induced Liver Injury: Premarketing Clinical Evaluation http://www.fda.gov/cder/guidance/7507dft.htm; accessed 13 March 2009). Figure 1 shows that from 1976 to 2005, hepatotoxicity formed the single most common toxicity as to why drugs were removed from the market. As such, there has been immense attention to address the challenges of detecting drugs early that can potentially cause DILI and mitigate their adverse consequential effects.

Idiosyncratic DILI, by definition, is difficult to understand. It is unpredictable, rare occurring at the frequency of about $1{:}10^4$ or more, delayed onset, dose-independent and may have an immune component (although the last two points are arguable). It is highly likely that genetic risk factors are also involved. The term "idiosyncratic reaction" can be defined as "toxic responses determined by individual susceptibility to (host) factors that increase the penetrance and expressivity of the intrinsic toxicity of a drug or a drug metabolite" (Boelsterli, 2003b). This would imply that these factors encompass the penetrance (the proportion of individuals affected) and the expressivity (consistency or severity of the DILI phenotype) of such a drug. A distinct feature of idiosyncratic DILI is that these drugs do not cause liver injury in the vast majority of patients. It only manifests the injuries in a very small fraction of patients featuring susceptibility factors coupled

with by drug exposure over time. It is likely that a combination of susceptibility factors within an individual, rather than a single factor, that will trigger idiosyncratic DILI (Ulrich, 2007). Clinically, idiosyncratic DILI can be manifested by parenchymal necrosis, hepatocellular or cholestatic injury in the absence of necrosis, or a combination of both (Kaplowitz, 2005). In certain cases, delayed hypersensitivity or inflammatory responses may accompany the insult and drug rechallenge. Several clinical signatures can be recognized from serum chemistries – (i) marked increases in serum aminotransferases and bilirubin, and mild increases in alkaline phosphatases which resembles hepatitis, (ii) prominent elevations in alkaline phosphatase levels, more than serum aminotransferases which resembles cholestasis or (iii) a mix of hepatocellular and cholestatic features (Navarro & Senior, 2006). Typically, increases in serum alanine aminotransferase (ALT) levels and overt liver injury set in after a variable latency period (weeks to months and even after more than 1 year of treatment). Once started, the progression of the liver disease can often precipitate abruptly. When symptoms are present, drug-induced hepatotoxicity can be diagnosed and drug treatment halted. In most instances, the patient situation would improve. However liver injury can worsen in some cases even with progressive falls in ALT levels, the latter usually taken as a sign of liver recovery (Navarro & Senior, 2006). On rare occasions, the hepatic injury can result in acute liver failure and death. The reasons for these typical hallmarks of idiosyncratic DILI have remained poorly understood so far.

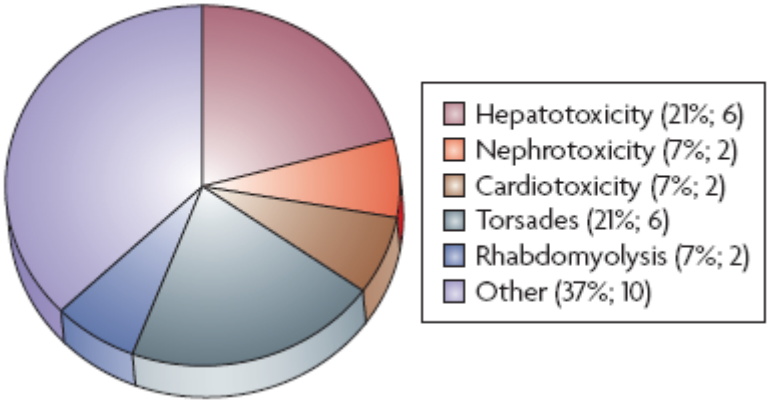

Figure 1. Drug toxicities leading to market withdrawals in the period 1976 to 2005. Hepatotoxicity or DILI (21%) formed the majority cause for drug withdrawals. Cardiotoxicity refers to heart-related toxicities other than torsades de pointes. Torsades is a life-threatening arrhythmia and may present as sudden cardiac death in patients with structurally normal hearts. Rhabdomyolysis is the breakdown of muscle fibres resulting in the release of muscle fibre contents (myoglobin) into the bloodstream. 'Other' refers to haemolytic anaemia (1), skin disease (1), immune toxicity (2), gastrointestinal toxicity (1), respiratory toxicity (1), fatal (1), neurotoxicity (1), blood-related toxicity (1) and birth defects (1). Percentage of total and number of cases shown in brackets. Figure taken from *Nature Reviews: Drug Discovery* (2007), 6: 904-916.

1.1.1. Susceptibility factors and mechanisms of idiosyncratic DILI

Many attempts have been made to describe the mechanisms or hypotheses that underlie idiosyncratic DILI. The occasional susceptibility of patients to adverse effects of otherwise mild drugs means there is no intuitive consensus as to how idiosyncrasy occurs.

Drug-allergic reactions have been suspected to play a role in various idiosyncratic drug-induced hepatotoxicities (Uetrecht, 2007). Fever, rash, eosinophilia, auto-antibodies accompanying hepatotoxicity and the rapid recurrence of liver injury upon drug re-challenge (Gunawan & Kaplowitz, 2004) are features supporting the hypothesis of

immune-mediated idiosyncratic DILI. However, not all idiosyncratic DILI-causing drugs have an allergic-mediated component (Kaplowitz, 2005). The frequent encounter of drugs that elicit hypersensitivity and non-allergic reactions prompted Kaplowitz to classify idiosyncratic reactions into allergic and non-allergic drug-induced reactions (Kaplowitz, 2005). Yet it is difficult to exclude allergic reactions based solely on the presentation of clinical evidence noted above. Furthermore, the development of hapten, a reactive drug metabolite that covalently binds to proteins, elicits an immune response one to five weeks after drug exposure. In contrast, the clinical latency of idiosyncratic DILI usually occurs several months to more than a year after the first drug exposure. In this regard, Zimmerman classified this as metabolic idiosyncrasy (Zimmerman, 1976), although no metabolic pathway or mechanism has yet been associated with the cause for idiosyncratic DILI. Another hypothesis that has been put forward is the inflammagen hypothesis (Uetrecht, 2008). This is based on a combination of drugs in doses normally tolerated and inflammagens such as liposaacharide (LPS) that lead to acute hepatic injury in mice. In contrast to an acute inflammatory phase, the onset of idiosyncratic drug reactions is characteristically delayed and chronic. LPS itself is a confounding factor, thus making it difficult to differentiate if the hepatic injuries were potentiated or caused by LPS, or the drug was amplifying the liver toxic effects of LPS. Therefore it can be argued that immune-mediated toxic response and inflammagens cannot satisfactorily explain the uniqueness and pathogenesis of idiosyncratic DILI.

Genetic risk factors may increase the toxic potency of drugs by shifting the dose-response curve (effectively LC_{50}) to the left. However, presently, clinical evidence

supporting the presence of polymorphisms in causing idiosyncratic DILI has been sporadic. Therefore, current hypotheses do not adequately describe possible mechanisms that predispose susceptible patients to the adverse effects of drug and new paradigms are urgently needed to explain the unpredictable nature of idiosyncratic DILI.

1.2. Troglitazone as a model drug for the study of idiosyncratic DILI

Troglitazone (Rezulin™, Pfzier; Figure 2), a first-generation thiazolidinedione drug used in the treatment of type-2 diabetes mellitus was withdrawn from the market due to an unacceptable risk of idiosyncratic hepatotoxicity (Graham et al., 2002). In early drug safety assessments, even in long-term studies, troglitazone did not cause hepatotoxicity in normal healthy rodents and monkeys, (Matsunuma et al., 1993, Mayfield et al., 1993, Rothwell et al., 1997). Moreover, while subsequent post-market withdrawal experiments showed that troglitazone caused mitochondrial injury *in vitro* at high concentrations, troglitazone was allowed to progress to the clinical testing phase stage.

A hallmark of troglitazone-induced hepatic injury is the seemingly random and delayed onset of liver injury, which could abruptly progress to life-threatening and irreversible liver failure ranging from one month to more than a year's interval (Graham, et al., 2002, Iwase et al., 1999). This idiosyncratic hepatotoxicity of troglitazone was not repeated in 13 double-blind clinical trial studies with the other thiazolidinedione members of safer profiles, namely rosglitazone and pioglitazone. In this clinical trial study, 1.91% of 2510 patients (versus 0.6% in the placebo group), 0.26% of 1526

patients, and 0.17% of 3503 patients who received troglitazone, pioglitazone, and rosiglitazone respectively had three times the upper limit of normal (ULN) of ALT (Lebovitz et al., 2002). ALT is released from dead or injured hepatocytes and is generally used as indicators to measure liver health[1]. However, it must be stated that ALT above three times ULN alone does not always predict severe liver toxicity and therefore may require use of additional clinical parameters (Kaplowitz, 2005). Out of these patients, two individuals were hospitalised with drug-induced hepatitis while another two individuals had jaundice although no cases of acute liver failure was reported (Graham et al., 2001, Watkins & Whitcomb, 1998). Despite the mild elevations in ALT, such irregularity was not necessarily indicative of subsequent cases of equal or worse severity and hence troglitazone was brought into the market in 1997. Soon thereafter, several cases of acute liver failure associated with troglitazone prescription was reported and by 2000, troglitazone was removed from the market culminating in 94 reported cases of troglitazone-associated liver failure (U.S. Department of Health and Human Services, March 21, 2000). Ever since, numerous attempts to study the underlying mechanisms troglitazone-induced liver toxicity have been made, but the *in vitro* results and ensuing hypotheses provided little mechanistic relevance to address clinical troglitazone-induced DILI (Chojkier, 2005, Smith, 2003). Studying the mechanisms behind the idiosyncratic toxicity of troglitazone not only explain why only a subset of patients develop liver injury, but also bring us closer to explain how a spectrum of drugs can induce idiosyncratic DILI. With better understanding of the idiosyncractic DILI mechanisms,

[1] Healthy ALT range is placed at around 5 IU/L to 50 IU/L but this range changes slightly with the ethnicity of the population and gender with males slightly higher. IU, international units

potential idiosyncratic liabilities of drugs in preclinical development can be identified early.

Being lipophilic, troglitazone readily enters the cell and nucleus and bind to PPARγ with K_d[2] around 40 nM (Lehmann et al., 1995). When liganded, this causes a conformational change of PPARγ and its heterodimer partner, retinoid X receptor (RXR) and binds to specific PPAR-response element (PPRE) in or near the transcriptional start site of target genes (Germain et al., 2002, Kliewer et al., 1992). The conformational change of PPAR also causes the recruitment of co-activator and co-repressor proteins that influences the set of transcribed genes (Heinaniemi & Carlberg, 2008). PPRE consists of two hexameric half-sites of the consensus motif AGGTCA in a direct repeat interspaced by a nucleotide. PPARγ binds to the first PPRE site while RXR binds the second, resulting in the initiation of DNA transcription and expression of PPARγ-responsive genes (Chandra et al., 2008). However, the PPRE sequences are not PPAR isoform-specific (Lemay & Hwang, 2006). In a similar fashion, troglitazone binds to and activate PPARγ to elicit its therapeutic effects in tissues. It is therefore interesting to understand how a normally-mild and beneficial drug used for ameliorating diabetic symptoms can cause severe hepatotoxicity in certain groups of patients.

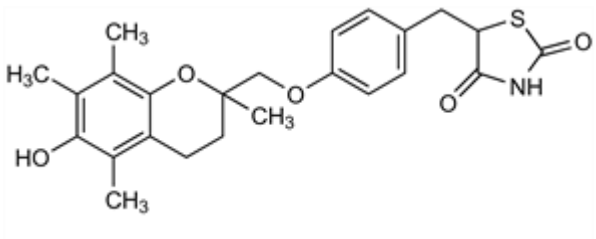

[2] K_d is the concentration of a drug that results in binding to 50% of the receptors

Figure 2. Chemical structure of troglitazone

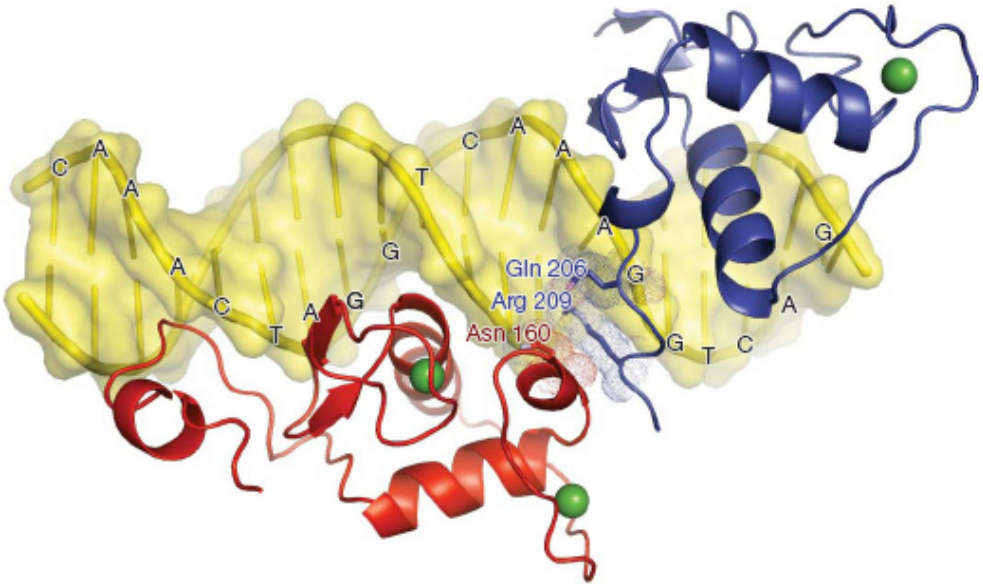

Figure 3. Crystal structure of PPARγ and RXR
Crystal structure at 3.1 to 3.2Å resolution of PPARγ (red) and RXRα (blue) binding to PPRE to initiate DNA transcription. The optimal PPRE consensus motif AGGTCA-A-AGGTCAG.The spacer nucleotide which also forms the minor groove of PPRE consensus sequence interacts with the DNA-binding domains of PPARγ and RXRα and shields the highly polar side chains of the interacting residues (Asn 160 from PPARγ, and Arg 209 and Gln 206 of RXRα) from an aqueous environment. Figure taken from *Nature* (2008), 456: 350-356

1.2.1. Mitochondrial dysfunction and threshold effect as a possible mechanism for idiosyncratic DILI

There is growing evidence showing the linkage of mutations in mitochondrial proteins to reactive oxygen species / reactive nitrogen species (ROS /RNS) in the pathogenesis of both rare and common human diseases (Droge, 2002). Mitochondrial diseases due to mutations in nDNA and mtDNA encoding for mitochondrial proteins are complex, and are confounded by a heterogeneous mix of clinical symptoms and inheritance patterns (Wallace, 1999). Elevated levels in free radicals under non-regulated conditions have been implicated with pathophysiological conditions that include neurodegenerative diseases, aging, ischemia / reperfusion cycles, cancer and mitochondrial diseases arising from mtDNA mutations and drug-induced toxicities (Wallace, 1999).

mtDNA has high mutation rates, presumably due to their proximity to sites of mitochondrial ROS production and the lack of protective histones (Ott et al., 2007). As some mtDNA gets mutated, each cell could possess a mix of mtDNA variants, some mutant and some WT, a condition known as heteroplasmy. During cell division of heteroplasmic cells, cytokinesis will lead to the distribution of mutant mtDNA to other daughter cells, and as a consequence may lead to an expansion of homoplasmic cells of mutant mtDNA. Likewise, mtDNAs copy numbers can increase within cells during clonally expansion, fission and fusion of mitochondria. A mutant mtDNA variant could be tolerated at low copies, but once a dominance of detrimental mtDNA has been

reached, the mitochondrial dysfunction set in and clinical symptoms become apparent. This is known as the threshold effect (DiMauro & Schon, 2003).

Defects in any of the many mitochondrial functions can in principle manifest as diseases. However, due to the mode of genetic inheritance, it is likely that there are many clinically silent mitochondrial abnormalities that would only be unmasked after exposure to hazardous chemicals and toxic substances. Moreover, mitochondrial diseases are not as rare as commonly thought – the prevalence of pathologies associated with ETC dysfunction was estimated at 10 to 15 per 100, 000 persons (Chinnery & Turnbull, 2001). A epidemiological study of mtDNA disease in Finland (3243A>G mutation[3]) which has an estimated prevalence of 16.3 per 100, 000 persons, found that 14% of patients had hypertrophic cardiomyopathy, 13% of patients with ophthalmoplegia, 7.4% of maternally inherited deafness, and 6.9% of those with occipital stroke (Majamaa et al., 1998). This highlighted the wide-ranging implications of mitochondrial diseases in many organs. Many lines of evidence have also implicated inherited mitochondrial defects (mtDNA and nDNA encoded) in the etiology of type 2 diabetes (Guo et al., 2005, Petersen et al., 2004), neurodegenerative diseases (Lin & Beal, 2006), cardiac disorders (Corral-Debrinski et al., 1992b, Murray et al., 2007) and obesity and alcohol-induced liver diseases (Mantena et al., 2008).

Inherited mitochondrial mutations are known to affect tissues with high energy requirements, and mitochondrial disorders in the liver are uncommon (Schon, 2000). However, this can dramatically change under chemical insults. The selective hepatic

[3] The most frequent mtDNA mutation found in humans is the A to G transition at nucleotide 3243

targeting of liver by drugs and xenobiotics appear to be the consequence of two dominant features of the liver, vascular and metabolic. About 75% of hepatic blood comes directly from the gastrointestinal tract and spleen via the portal vein, bringing blood with concentrated amounts drugs and xenobiotics absorbed by the gut directly to the liver. Drug-metabolizing enzymes detoxify many xenobiotics but bioactivate the toxicity of others to reactive intermediates. This leads to the hypothesis that underlying silent mitochondrial abnormalities could sensitise the liver to such normally mild drugs, and overwhelm any inherent biological defence, eventually triggering overt liver injury. The notion of abnormal mitochondria playing the role of a susceptibility factor in DILI is relatively new, and recent evidence implicates the role of mitochondrial ROS in drug-induced toxicity in various organs (Pessayre et al., 1999, Wallace, 2008, Wallace & Starkov, 2000). Experimentally, it has been shown that many of the drugs implicated in idiosyncratic DILI impair mitochondrial function or induce mitochondrial permeabilization (Table 1). In humans, a recent review of clinical evidence suggests the contribution of mitochondrial dysfunction in the development of idiosyncratic DILI (Table 2), providing a plausible link between the two (Boelsterli & Lim, 2007).

Although most pieces of clinical evidence are sporadic and indirect, they fuel the working hypothesis that heteroplasmic mitochondria undergo gradual damage until the critical threshold is crossed. For example, the late onset and abrupt progression of idiosyncratic DILI can be explained by an accumulation of a drug effect rather than an accumulation of the drug itself. If a drug causes cumulative injury to mitochondria, these changes may not become detectable until the threshold effect comes into play (i.e., a large number of mitochondria have been severely damaged and many hepatocytes being

compromised that is sufficient to trigger detectable hepatic injury). Because many mitochondria are lethally damaged, the injury may sometimes progress even after discontinuation of the drug (Boelsterli, 2003b).

By far, as for many drugs, age is the major risk factors in idiosyncratic DILI (Navarro & Senior, 2006). It is well established that mtDNA accumulates mutations with aging, especially large-scale deletions and point mutations (Corral-Debrinski et al., 1992a). The accumulation of these deletions and point mutations with aging results in the decline in ETC activity and ATP production. In addition to being primary targets of elevated ROS themselves, net production of ROS is another important mechanism by which mitochondria are thought to contribute to aging. Thus, it is conceivable that aging mitochondria become sensitized and susceptible to ROS-damaging effects, and the effect is even more pronounced if it stems from superimposed drug stress.

Table 1. Selected drugs causing idiosyncratic DILI experimentally incriminated with mitochondrial dysfunction

Drug	Therapeutic class	Reference
Amiodarone	Anti-arhythmic	Fromenty et al. (1990); Berson et al. (1998); Spaniol et al. (2001); Kaufmann et al. (2005)
Dantrolene	Antiepileptic	Darios et al. (2003); Munns et al. (2005)
Diclofenac	NSAID[a]	Petrescu and Tarba (1997); Bort et al. (1998); Masubuchi et al. (1998); Masubuchi et al. (1999); Masubuchi et al. (2000); Masubuchi et al. (2003); Gomez-Lechon et al. (2003a); Gomez-Lechon et al. (2003b); Lim et al. (2006)
Fialuridine	Anti-viral (Hepatitis B)	McKenzie et al. (1995); Horn et al. (1997); Lewis et al. (1997)
Flutamide	Anti-cancer (Prostate)	Coe et al. (2007)
Isoniazid	Antibiotics	Schwab and Tuschl (2003); Chowdhury et al. (2006)
Lamivudine	Anti-viral (HIV)	Note et al. (2003); Desai et al. (2008)
Leflunomide	DMARD[b]	Spodnik et al. (2002)
Mefenamic acid	NSAID	McDougall et al. (1983); Masubuchi et al. (2000)
Nimesulide	NSAID	Mingatto et al. (2000); Caparroz-Assef et al. (2001); Mingatto et al. (2002); Tay et al. (2005); Ong et al. (2006); Lim et al. 2008
Perhexiline	Anti-aginal	Deschamps et al. (1994); Berson et al. (1998)
Simvastatin	Statin[c]	Velho et al. (2006)
Sulindac	NSAID	Leite et al. (2006)
Stavudine	NSAID	Gaou et al. (2001); Gerschenson et al. (2001); Pace et al. (2003); Velsor et al. (2004)
Tolcapone	Parkinson's	Haasio et al. (2002a,b,c)
Troglitazone	Diabetes	Bedoucha et al. (2001); Haskins et al. (2001); Tirmenstein et al. (2002); Narayanan et al. (2003); Shishido et al. (2003); Bova et al. (2005); Masubuchi et al. (2006); Ong et al. (2007)
Trovafloxacin	Antibiotics	Liguori et al. (2005)
Valproic acid	Antiepileptic	Bjorge and Baillie (1991); Keller et al. (1992); Ponchaut et al. (1992); Tang et al. (1995); Trost and Lemasters (1996); Sobaniec-Lotowska (1997); Tong et al. (2005)

Mitochondrial dysfunction is defined as having experimental *in vitro* or *in vivo* evidence of one or a combination of the following traits: depolarization of the inner transmembrane potential due to either uncoupling or inhibiting ETC complexes, induction of the mPT, cytochrome c release, inhibition of β-oxidation, ATP depletion by reasons not specified. [a], non-steroidal anti-inflammatory drugs by inhibiting both cyclooxygenase-1and 2; [b], disease-modifying antirheumatic drug, and in leflunomide, inhibits dihydroorotate dehydrogenase, a mitochondrial enzyme involved in *de novo* pyrimidine synthesis; [c], Statins control cardiovascular complications by lowering cholesterol through inhibiting HMG-CoA reductase, a mitochondrial, rate-limiting enzyme of the metabolic pathway responsible for the production of cholesterol.

Table 2. Summary of clinical evidence linking DILI with mitochondrial dysfunction

Clinical evidence
• Ultrastructural alterations in hepatocellular mitochondria (megamitochondria, swollen mitochondria, changes in cristae structure)
• Delayed time to onset of overt DILI after drug administration (weeks to months), compatible with the threshold effect (accumulating but clinically silent mitochondrial injury)
• Abrupt progression of DILI, in line with crossing a threshold at the point-of-no-return
• Continued course of disease, in some severe cases despite discontinuation of drug administration, consistent with the concept of accumulation of an irreversible effect (e.g., mtDNA damage), rather than of the drug
• Lactic acidosis (in severe cases, e.g. NRTI), as a result of liver mitochondria's failure to oxidize substrate
• Symptoms accompanied by diarrhoea or rhabdomyolysis (rare), compatible with intestinal or striated muscle mitochondrial injury
• Similar incidence (same order of magnitude) of mitochondrial abnormalities and DILI. For both conditions, the real number is probably higher
• Age as a major risk factor for idiosyncratic DILI—both mtDNA abnormalities and oxidative injury increases with age
• Estrogen protection against oxidative mitochondrial changes in skeletal muscle of young versus postmenopausal women, possibly in line with the increased preponderance of DILI in elderly women
• Decreased activity of certain ETC complexes in susceptible DILI patients (e.g., valproic acid) has been documented as direct evidence
• Genetic/acquired mitochondrial abnormalities in certain type 2 diabetes, Alzheimer, and Parkinson patient subsets have been consistently found. DILI has occurred in patients treated against these indications
• In rare cases, mitochondrial mutations have been found in DILI patients

Table taken from *Toxicology and Applied Pharmacology* (2007) 220: 92–107

Perhaps the most interesting clinical observation of idiosyncratic DILI is the higher occurrence in older women (Navarro & Senior, 2006), which is common across the heterogeneous variety of pharmacologically-unrelated drugs. While such information does suggest the convergence of estrogen as a cytoprotective hormone, it is difficult to elucidate any mechanisms in such diverse patient populations and drug types, and thus the scientific basis of this observation remains unanswered. However, experimental data suggest that estrogen and estradiol regulate mitochondrial function (Nilsen & Diaz Brinton, 2003, Stirone et al., 2005), increased expression of mitochondrial proteins (Nilsen et al., 2007) and enhanced mitochondrial antioxidant defence in the hippocampus (Nilsen, et al., 2007, Strehlow et al., 2003), neurons and vascular systems (Brinton, 2008, Duckles et al., 2006). Furthermore, a recent report has indicated that elderly postmenopausal women exhibited more significant markers of oxidative stress in muscle tissue than elderly men, suggesting a gender-differential mechanism in the redox regulation of aging muscles (Barreiro et al., 2006). However, the association of gender-specific susceptibility, aging and estrogen-mediated mitochondrial liability to idiosyncratic DILI requires further investigation.

1.2.2. Mitochondria and idiosyncratic troglitazone DILI

Continual usage of troglitazone was linked to cumulative risk of developing liver failure and this was not associated with diabetes (Figure 4) (Graham, et al., 2002). Type 2 diabetes, which troglitazone was used to treat can arise from genetic mitochondrial dysfunctions in the OXPHOS or mitochondrial biogenesis (Mantena, et al., 2008, Mootha et al., 2003, Patti et al., 2003, Petersen, et al., 2004). These observations connotes that clinically latent, genetically acquired mitochondrial defects may be partially due to mtDNA heteroplasmy and could aid progression of troglitazone-induced hepatotoxicity. Experimental *in vitro* evidence demonstrated that troglitazone adversely affected a multitude of mitochondrial functions, such as (i) lowering of mitochondrial membrane potential ($\Delta\Psi_m$) and cellular ATP, (ii) inducing the mitochondrial outer membrane permeabilization (MOMP), (iii) enlargement of mitochondria with intramitochondrial myelin-like structures, (iv) elevation of H_2O_2, and $O_2^{\bullet-}$, (v) uncoupling of State 2 and inhibition of State 3 respiration, (vi) inhibition of OXPHOS Complexes II + III, IV and V activities and sometimes (vii) inducing apoptosis (Lim et al., 2008, Masubuchi et al., 2006, Nadanaciva et al., 2007, Shishido et al., 2003, Tirmenstein et al., 2002). Interestingly, troglitazone improved OXPHOS in patients with insulin resistance (Arioglu et al., 2000). However it is important to note that the doses of troglitazone used in these experiments are considerably several orders of magnitude higher (ranging from 50 to 150 μM) than the therapeutic dose in humans. Furthermore, the cells were incubated with drugs in the absence of albumin, where albumin sequesters 95 to 99% of plasma troglitazone, thereby reducing the bioavailability (pharmacologically and toxicologically)

of the drug (Chojkier, 2005, Loi et al., 1999). Finally, some of the cell lines are transformed cell lines which make extrapolation to *in vivo* conditions unrealistic. Hence such information should be considered cautiously when interpreting and translating *in vitro* data to the more complex *in vivo* system.

As noted earlier, mitochondria are sensitive to troglitazone exposure but mitochondrial dysfunction triggered by troglitazone alone is insufficient in explaining the idiosyncrasy of troglitazone-mediated liver injury. Rather, a "1st and 2nd hit" paradigm may explain why a small fraction of the patients seemingly suffer such sudden hepatic injuries while the rest does not develop overt liver injuries. In other words patients with underlying clinically silent mitochondrial abnormalities may be more predisposed to the mitochondrial toxic effects of troglitazone. This is more compatible with the idiosyncratic DILI nature of troglitazone toxicity. Such a model also explains the independence of correlation of drug dosage and toxicity in troglitazone and other idiosyncratic DILI incriminated with inflicting idiosyncratic DILI (Dykens & Will, 2007). To summarize, a low degree of mitochondrial abnormality is insufficient to elicit any obvious phenotypic effects but provide a source for cumulative damage to act on, and by lowering the threshold required to maintain normal cellular functions. When this threshold is exceeded, presumably through overwhelming the system's ability to mitigate exogenous stresses, there is a sudden, rapid onset of cellular and tissue injuries as shown in Figure 5.

Unfortunately, preclinical testing for mitochondrial toxicity has not gained wide acceptance in drug companies and is also hampered by a lack of an established suite of mitochondrial toxicity assays (Dykens & Will, 2007). Another complication is the difficulty in unmasking natural occurrences of uncommon genetic, silent mutations and toxicities during clinical trials. For instance, if a particular drug inflicts 0.1% of the patients, it will require more than 10000 patients in a Phase III clinical trial to even realistically uncover it. Therefore, outdated tools needs to be urgently replaced and it is incumbent for the innovative development and adoption of better tools for the rigorous identification of mitochondrial toxic drugs. In addition, the use of preclinical mutant models can help in unmasking drugs with mitochondrial liabilities.

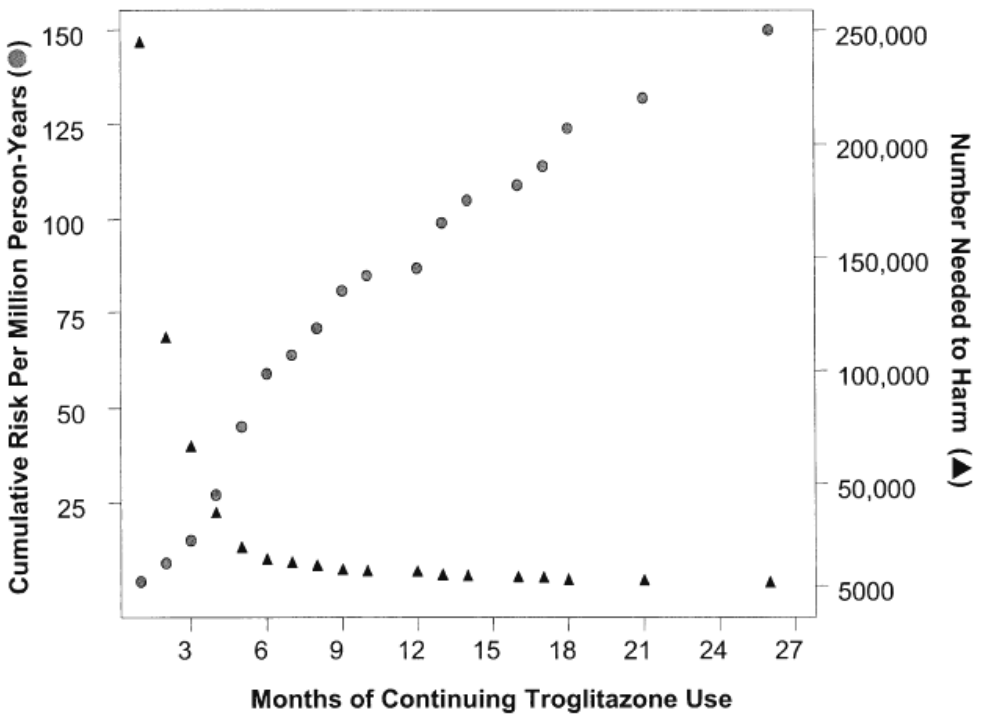

Figure 4. Chart showing relationships between troglitazone exposure and risk of troglitazone-induced liver injury.
Cumulative risk of liver failure in patients treated with troglitazone increases, together with decreases in the number of patients needed to harm, with longer durations of troglitazone use. Figure taken from *The American Journal of Medicine* (2003), 114: 299 - 306

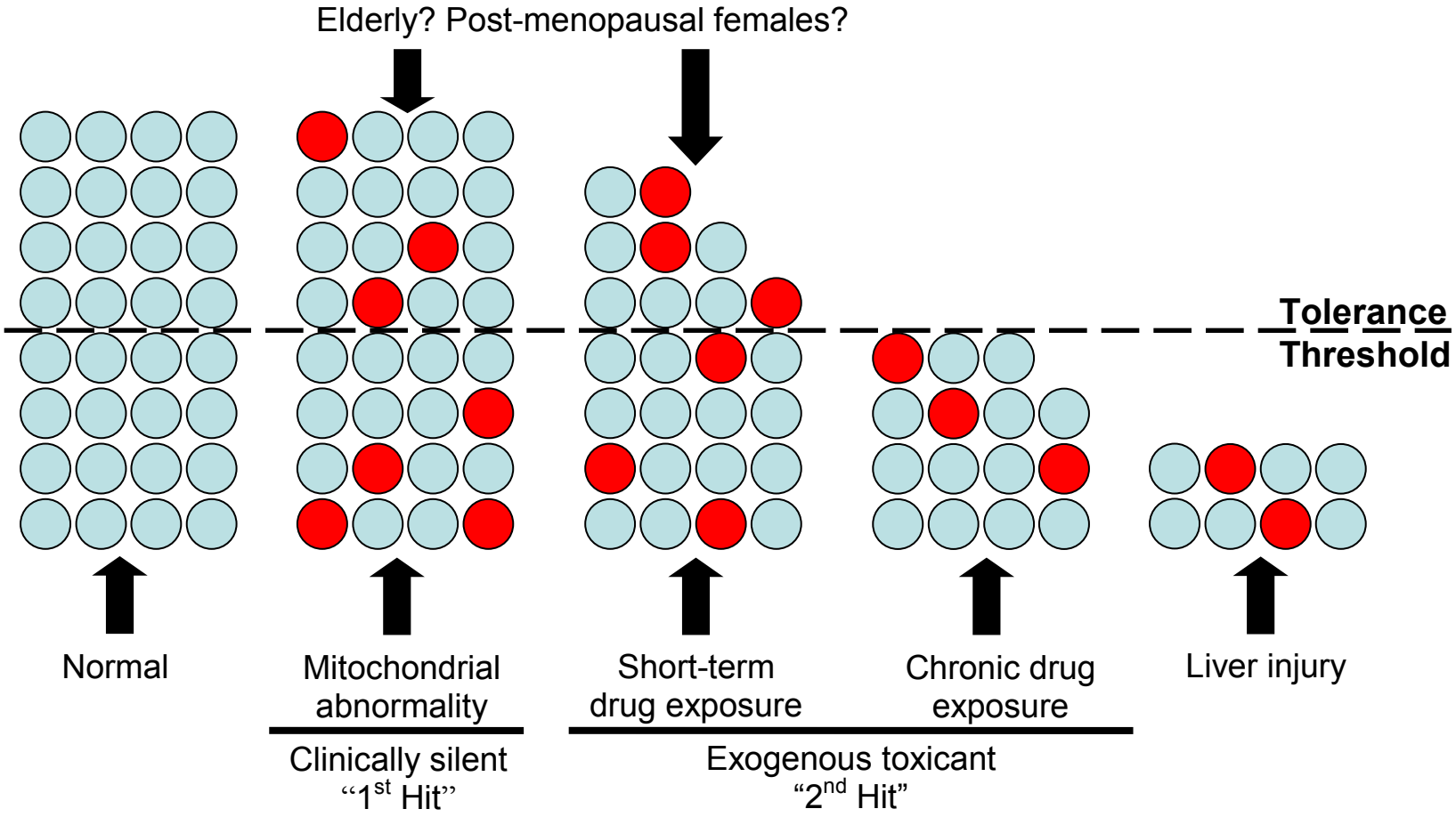

Figure 5. Clinically silent mitochondrial abnormality and threshold effect.
Red circles represent hepatocytes with mitochondrial abnormality (due to heteroplasmy) that is silent but represents a susceptibility factor. This is observed in a small subset of individuals (second column from left), unlike the general populace (blue circles; left most column). Aged or post-menopausal women may also be more predisposed. Short-term exposure to the drug may result in a loss of hepatocytes but this is tolerated, given the regenerative abilities of the liver. However, with chronic drug exposure there is accumulating mitochondrial damage and hepatocytic death which upon crossing the tolerance threshold, triggers the abrupt progression of DILI. The number of cells needed to tolerate insults is indicated by the dash line.

1.3. Heterozygous *Sod2*$^{+/-}$ mouse

During oxidative phosphorylation, it is inevitable that a small portion of the oxygen consumed within the ETC escapes to form superoxide anion ($O_2^{\bullet-}$) as toxic by-products of respiration. Approximately 0.4 to 4% of the oxygen is reduced to $O_2^{\bullet-}$ (Chance et al., 1979, Hansford et al., 1997) and it is generally accepted that the main sites of ROS production are Complex I and Complex III (Orrenius et al., 2007). In addition, Complex II which serves Complex I and III has been implicated in ROS genesis (Zhang et al., 1998). Therefore it has been suggested, and is widely accepted that the mitochondrion is the primary locus for free radical and other reactive oxidant species (ROS) generation. $O_2^{\bullet-}$ is a relatively short-lived species and is restricted to biomembranes, including the mitochondrial outer and inner membranes whereas H_2O_2 is freely diffusible. Although H_2O_2 reacts slowly with most biological molecules, its damaging effects stem from the production of hydroxyl radicals ($^{\bullet}OH$) via Fenton chemistry (Gutteridge & Halliwell, 2000). $NO^{\bullet}$ is another poor oxidant but because it reacts with $O_2^{\bullet-}$ to form the highly reactive peroxynitrite ($ONOO^-$) it is biologically important. $ONOO^-$ is a short-lived free radical formed from $^{\bullet}NO$ and $O_2^{\bullet-}$ and is highly diffusible across biomembranes (Marla et al., 1997). In biological systems, $ONOO^-$ can react with carbon dioxide to form carbonate ($CO_3^{\bullet-}$) and nitrogen dioxide ($^{\bullet}NO_2$) radicals. There are clearly other secondary reactive products of ROS and RNS, but the physiologically more important ones (Winterbourn, 2008) and that are relevant to this study are $O_2^{\bullet-}$, H_2O_2, $^{\bullet}OH$, $CO_3^{\bullet-}$, $^{\bullet}NO$, $^{\bullet}NO_2$ and $ONOO^-$ (Figure 6). Thus any further discussion on ROS/RNS should be perceived with these free radical species as the focus.

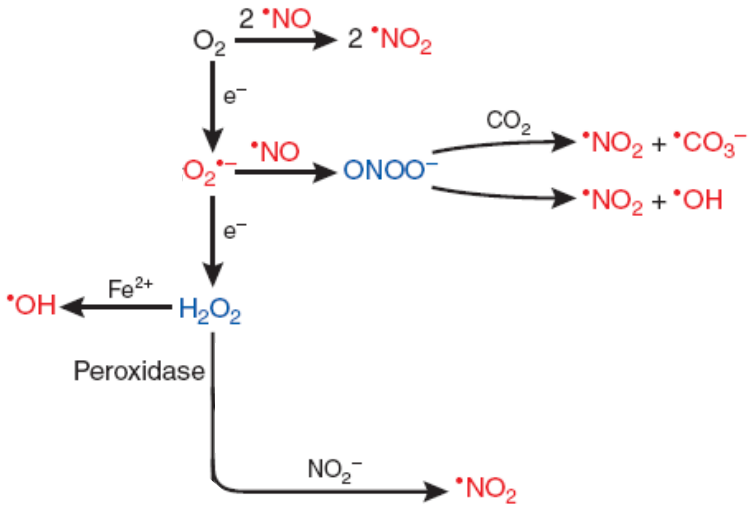

Figure 6. Physiologically relevant ROS/RNS
Most reactive free radical species that are physiologically important are featured in this figure. Although relatively poorer oxidants, hydrogen peroxide and nitric oxide (H_2O_2 and $^{\bullet}NO$) reacts readily with other oxidants, yielding other more biologically damaging ROS/RNS. Peroxynitrite chemistry is more complex, generating carbonate ($CO_3^{\bullet-}$), nitrogen dioxide ($^{\bullet}NO_2$) and hydroxyl ($^{\bullet}OH$) radicals. $^{\bullet}OH$ has the highest oxidizing strength and can also be generated from H_2O_2 via Fenton chemistry with iron (Fe^{2+}). Red, one-electron oxidants (radicals); blue, two-electron oxidants (non-radicals). Not included are hypochlorous acid (HOCI), phenoxyl radicals ($PhO^{\bullet}$) are produced from tyrosine and other phenolic metabolites and xenobiotics and gluthionyl radical ($GS^{\bullet}$) are generated from other thiols such as cysteine residues. Figure modified from *Nature Chemical Biology* (2008) 4: 278 - 286

To cope with the generation of ROS/RNS, cells have a pool of antioxidants to detoxify free radicals and maintain redox homeostasis, of which are three forms of superoxide dismutases (SOD) that are found in mammalian cells, viz., copper-zinc SOD (SOD1 or CuZnSOD), manganese SOD (SOD2 or MnSOD) and extracellular SOD (SOD3 or EcSOD). SOD2 is the predominant form of $O_2^{\bullet-}$ catalyzing enzyme within the mitochondrial matrix by dismutating $O_2^{\bullet-}$ (Equation 1). It should not be assumed that SOD-mediated dismutation of $O_2^{\bullet-}$ always lead to increased H_2O_2. This is because under different biological conditions, $O_2^{\bullet-}$ can be diverted to reactions generating $ONOO^-$ and/or oxidation of Fe-S clusters (which also produces H_2O_2 but is not a result of SOD detoxification of $O_2^{\bullet-}$) (Winterbourn, 2008). Equations 2 and 3 show this.

$$2O_2^{\bullet-} + H^+ \xrightarrow{SOD} H_2O_2 + O_2 \qquad \text{(Eq. 1)}$$

$$O_2^{\bullet-} + {}^{\bullet}NO \longrightarrow ONOO^- \qquad \text{(Eq. 2)}$$

$$O_2^{\bullet-} + [4Fe\text{-}S]^{2+} + 2H^+ \longrightarrow [4Fe\text{-}S]^{3+} + H_2O_2 \qquad \text{(Eq. 3)}$$

While $O_2^{\bullet-}$ is a substrate of SOD2, this enzyme itself can be subjected to post-translational modification via protein tyrosine nitration. Mass spectrometric analysis revealed that $ONOO^-$ reacts with the Mn center of SOD2, leading to its inactivation due to the nitration of Tyr^{34} which is critical for enzyme activity (Quijano et al., 2001, Yamakura et al., 1998). The inactivation of SOD2 would lead to an increase in $O_2^{\bullet-}$ and hence favour the formation of more $ONOO^-$. Excessive $ONOO^-$ can then inhibit numerous mitochondrial proteins, including SOD2. This synergistic effect would in turn cause mitochondrial injury, initiating a vicious cycle leading to cellular demise (Brown &

Borutaite, 2002). The critical importance of this enzyme in maintaining mitochondrial redox status is highlighted by the early and high incidence of neo-natal and pre-natal fatalities in *Sod2*-null mice (Huang et al., 2001, Lebovitz et al., 1996, Li et al., 1995). This deleterious consequence of complete ablation of *Sod2* gene indicated that the toxicity of the mitochondrial ROS is particularly deleterious to health. If the high and early incidence of death among *Sod2*$^{-/-}$ pups remained as technical limitations, then the exogenous, synthetic mimetics of SOD2 enzyme can be used to overcome such problems. The deleterious phenotypes of the *Sod2* null mouse can be rescued and their life spans extended by pharmacological rescue of the SOD mimetic, Mn-TBAP and low molecular weight SOD and catalase mimetics, EUK8 and EUK189 (Doctrow et al., 2005, Melov et al., 2001). In contrast, HET mice do not share the same neo-natal fatal consequences as the homozygous knockouts and do not exhibit any gross phenotypic abnormalities. Therefore, their heterozygous mutations and intermediate phenotypes make them potentially valuable as murine models for studying the role of SOD2 in antioxidant protection and mitochondria-associated pathophysiological conditions.

Mice lacking SOD2 enzyme have been generated in numerous genetic backgrounds (Table 3). Figure 7 shows the extensive research had been conducted using the *Sod2* deficient mouse model for defining various oxidative stress-induced disorders including senescence, neurology, cardiology, ophthalmology, drug safety and oncology. However, the discussion here will be limited to the use of the HET mouse in drug toxicity assessment.

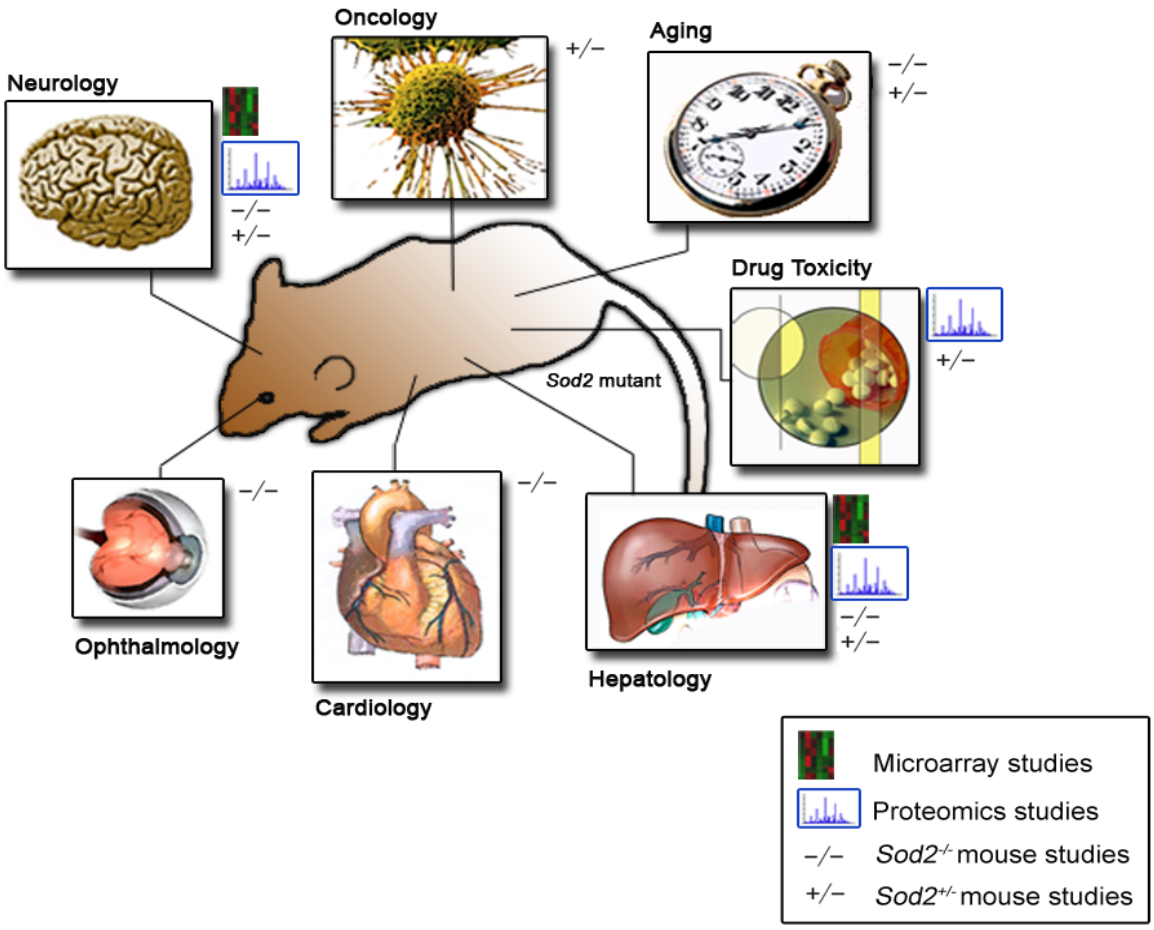

Figure 7. Areas of research that utilizes the *Sod2* mutant mouse.
Both the heterozygous and homozygous *Sod2* knock-out mouse model have been used in numerous scientific fields, namely aging, research, cardiology, drug safety assessment, hepatology, neurology, oncology and ophthalmology. Symbols represented: heat map, microarray studies; MS-spectrum, proteomics; -/-, studies using the *Sod2*$^{-/-}$ mouse; +/-, studies using the HET mouse

1.3.1. The utility of HET mouse in toxicological studies

Idiosyncratic adverse drug reactions are inadvertently impossible to reproduce *in vitro* and usually slips detection during clinical testing (Dixit & Boelsterli, 2007). This problem is compounded by the fact that there are currently no ideal 'normal' animal models for the reproduction of idiosyncratic drug toxicity in the laboratory (Boelsterli, 2003, Kaplowitz, 2005, Shenton et al., 2004). The impact of this is the huge economic, time and social loss associated with withdrawal of such normally-mild drugs (Figures 8 and 9). The use of drugs at supra-therapeutic doses in healthy, laboratory animal during toxicity testing remains a question on the biological relevance to humans. There are genetic mouse models, for example, $JNK^{-/-}$ and $ASK^{-/-}$ mice used in the study of drug-induced toxic effects of acetaminophen or doxorubicin-induced toxicity but they are limited to drugs with predictable or non-idiosyncratic toxic effects (Gunawan et al., 2006, Nakagawa et al., 2008, Oliveira & Wallace, 2006). Hence there is an urgent need for valid animal models to replicate the idiosyncratic DILI situation in humans for they are important and practical tools for drug safety assessments. A mutant murine model for drug toxicology research that has found application for the study of rare or idiosyncratic DILI is the HET mouse (Dykens & Will, 2007). The clinically silent phenotype of the HET mouse offers a novel alternative animal model to studying the mechanisms behind idiosyncratic drug toxicity (Boelsterli & Lee, 2008).

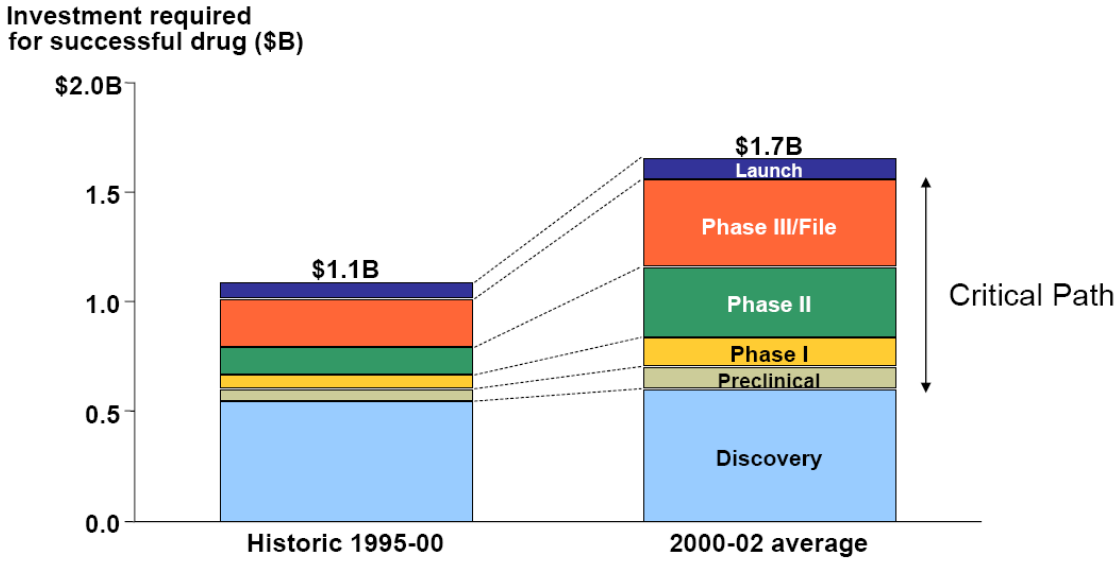

Figure 8. Change in investment of successful new drug launch over time.
The Critical Path refers to the development process beyond the discovery phase and is the 'critical bottleneck' to bring development of products into the clinic. Modified from Bain drug economics model, 2003

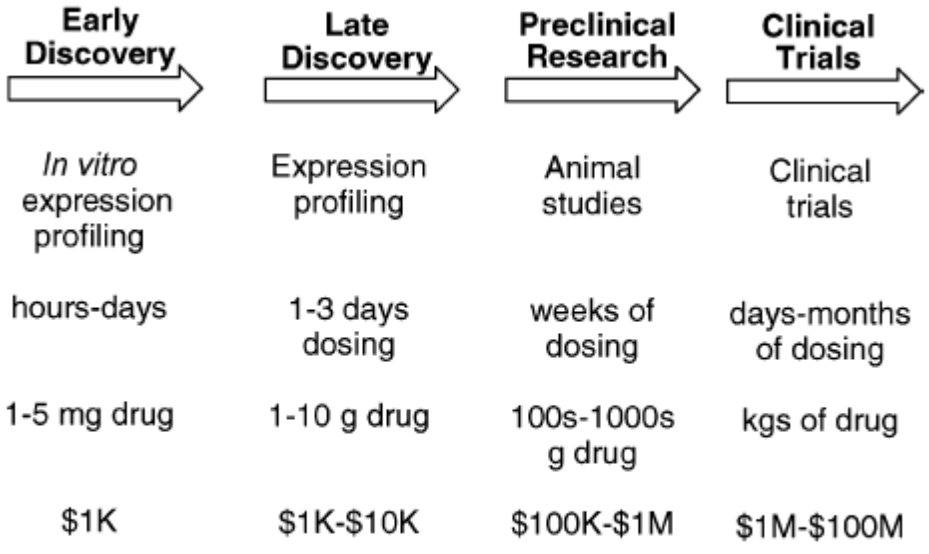

Figure 9. Increase in cost, time and drug amounts with drug development progession
Significant cost and time savings can be made if toxicity assessments are made earlier in drug discovery and development pipeline. Figure taken from *Chem. Res. Toxicol.* (2007) 20: 344-369

Genetic mitochondrial abnormalities in the partial *Sod2* knockout mouse generate a mitochondrial environment of cumulative endogenous ROS/RNS production which predisposes these mice to toxicants (Ong et al., 2007). They are morphologically normal but biochemically different from the WT mice, thus exhibiting a premature decline in mitochondrial functions and activities of some mitochondrial proteins including oxidative damage to mitochondrial biomolecules. For example, enzymatic assays revealed reductions in liver and heart mitochondrial aconitase and Complex I activities and increases in 8-OHdG levels in liver and skeletal muscle mtDNA (Mansouri et al., 2006, Van Remmen et al., 2001, Williams et al., 1998) (Table 3). The implication is that the chronic detrimental effect of cumulative oxidative stress over time can be simulated by sensitizing the HET mouse with mitochondria-targeting toxicants. The B6-*Sod2*tm1Leb$^{+/-}$ mouse has been shown to exhibit higher sensitivity towards the mitochondrial damaging effects of xenobiotics such as NSAID nimesulide, the nucleoside reverse transcriptase inhibitor stavudine or troglitazone and this aids in unmasking certain mechanistic pathways in rare drug-induced adverse reactions (Leitner et al., 2005, Ong et al., 2007, Ong et al., 2006). Thus the potentiality of this mouse model in toxicological studies has been demonstrated.

Various lines of evidence propose that genetic variability is an important genetic factor in the pathogenesis and increased risk of idiosyncratic DILI (Larrey & Pageaux, 1997, Wilke et al., 2007). This is compatible with our hypothesis of acquired genetic mitochondrial abnormality as a risk factor for idiosyncratic DILI (Figure 5; also see above, Section 1.1.1 for discussion) and the low incidence of idiosyncratic reactions. It is

important to note that the *Sod2* deficiency represents a generic model of mitochondrial abnormality for the testing of drugs with potential mitochondrial liabilities. For reasons stated in above (Section 1.2.2), it is attractive that at the preclinical stage, high-throughput technologies, namely genomics, transcriptomics, proteomics and metabolomics can test and generate hypotheses at the global-scale of the impact of DILI-causing drugs on biological systems such as the *Sod2* mutant mouse. Information generated from such technologies may lead to the discovery of genetic risk factors that predispose certain groups of exposed patients to toxicants. Also, comparative studies can be performed using the different risk factors in large cohort of patients or animal models. At a time when drug-induced toxicities are a growing concern, the US. Food and Administration has initiated the Critical Path Activities to modernize the drug development process and drug safety evaluation, among which mechanisms underlying DILI and its prediction came under the priority topic of "Better Evaluation Tools" (FDA, 2008, Hennessy & Strom, 2007). The use of proteomics on a mutant mouse model of acquired mitochondrial abnormality may therefore help to advance our understanding on the association of risk factors in the pathogenesis of idiosyncratic DILI.

Table 3. Summary of functional characterization studies in *Sod2*$^{-/-}$ and *Sod2*$^{+/-}$ deficient mice

Genotype	Strain	Changes found	Organ	Reference
Sod2$^{-/-}$	CD1-tm1Cje[†]	Decreased Complex I activity	Brain, heart	Melov et al., 1999, Hinerfeld et al., 2004
	CD1-tm1Cje	Decreased Complex II activity	Brain. heart, skeletal muscles	Melov et al., 1999, Hinerfeld et al., 2004, Morten et al., 2006
	CD1-tm1Cje, B6D2F1-tm1Cje[*]	Decreased ACO2 activity	Brain, heart	Melov et al., 1999, Lynn et al., 2005
	CD1-tm1Cje	Decreased KGDH, HMG-CoA lyase activities	Brain, liver	Melov et al., 1999, Hinerfeld et al., 2004
	CD1-tm1Cje	Increased mPT propensity	Liver	Kokoszka et al., 2001
	B6D2F1-tm1Cje (5 days old)	Increased SOD1activity	Brain, heart, lung, liver	Huang et al., 2001
	B6D2F1-tm1Cje (15 days old)	Increased activity (CATA, liver) Decreased activity (GPX, kidney & liver)	Kidney, liver	Huang et al., 2001
	D2- tm1Cje (5 days old)	Increased SOD1 activity	Heart	Huang et al., 2001
	D2-tm1Cje (5 days old)	Increased activity (CATA) Decreased activity (GPX)	Kidney, liver	Huang et al., 2001
Sod2$^{+/-}$	B6-tm1Cje[‡]	Decreased ACO2, Complex I, Complex V activities	Liver, heart, skeletal muscle	Williams et al., 1998, Mansouri et al., 2006, Van Remmen et al., 2001, Liang & Patel, 2004
	B6-tm1Cje	No change in GS, ACO1, fumarase, SOD1, CATA, GPX activities	Brain, heart, kidney, liver, lung muscle, spleen, stomach	Williams et al., 1998, Van Remmen et al., 1999, Van Remmen et al., 2003
	B6-tm1Cje, B6-tm1Leb[#]	Increased mitochondrial protein carbonyls	Liver, skin	Williams et al., 1998, Zhao et al., 2002, Ong et al., 2006
	B6-tm1Cje, CD1-tm1Cje	Increased rate of mPT induction	Liver, heart	Williams et al., 1998, Kokoszka et al., 2001, Van Remmen et al., 2001
	CD1-tm1Cje	Lowered $\Delta\psi_m$	Liver	Kokoszka et al., 2001
	CD1-tm1Cje (20-25 mths old)	Increased Complex I, II, II+III, IV activities	Liver	Kokoszka et al., 2001
	B6-tm1Cje	Increased DNA binding activity	Skin	Zhao et al., 2002
	B6-tm1Leb	No change in Cyt c release, CASP3 activity	Skin, liver	Zhao et al., 2002, Ong et al., 2006

Abbreviations: $\Delta\psi_m$, transmembrane potential; ACO1, cytosolic aconitase; ACO2, mitochondrial aconitase; AP-1, activator protein 1; CASP3, caspase-3; CATA, catalase; Cyt c; cytochrome c; GS, Glutamine synthase; GPX, glutathione peroxidise; HMG-CoA lyase, 3-hydroxy-3-methylglutaryl CoA lyase; KDGH, ketoglutarate dehydrogenase; mPT, mitochondrial permeability transition; SOD1, CuZn Superoxide dismutase. [†] CD1-tm1Cje *Sod2* mutant mouse produced on CD1 background. [*] B6D2F1-tm1Cje *Sod2* mutant mouse generated from intercrossing C57BL/6J and DBA/2J. [‡] B6-tm1Cje *Sod2* mutant mouse originally produced in CD1 strain but backcrossed to C57BL/6 background for 13-14 generations. [#] B6-*Sod2*tm1Leb *Sod2* mutant mouse produced on C57BL/6 background.

1.4. Proteomics

Elucidation of gene-product function and regulation is a fundamental objective in biology. However the one gene-one product paradigm is out-dated, slow and luck-dependent; hence systems-wide analyses have gained much interest recently. Profiling the genome and transcriptome can be readily done through the use of microarrays and sequencers. Yet, DNA and mRNA are proxy to proteins, the molecules truly reflecting a cell state. Aside from this, it is widely acknowledged that mRNA and protein abundance correlate modestly, or average at best (Kislinger et al., 2006). Therefore, proteomics bridges the gap between what is known at the genome level and what is translated and modified from the genome.

Because proteins are biological molecules that directly related to physiological conditions, high-resolution proteomic technologies are in the best position to systemically probe complex biological systems and determine the roles of the protein complement in different biological states (Figure 10). Proteomics offers more complexity and potentially more specificity than examining genes and transcripts alone, fostering advances in understanding physiological and pathological conditions, development of biomarkers for diagnosis and prognosis of diseases, all for moving bench-top science to bed-side applications (Azad et al., 2006, Diamond et al., 2006, Hanash, 2003).

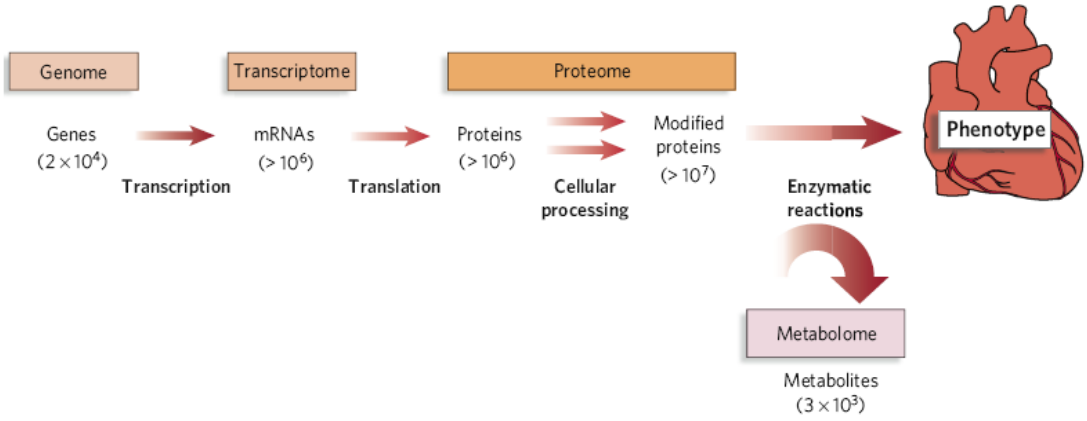

Figure 10. A schematic diagram of the level of complexity from genome to the proteome.
The increase in complexity of biological molecules moving from genome to transcriptome to proteome level. The number of estimated analytes is in parentheses. Figure taken from *Nature* 451: 949 – 952.

Proteomics can be broadly divided into three main platforms – (i) top-down approach which includes the classical two dimensional electrophoresis or 2DE, (ii) bottom-up approach, also known as shot-gun proteomics which encompasses chemical labelling and label-free mass-spectrometry-based proteomics and (iii) and protein-chip-based arrays. There are advantages and disadvantages to both platforms and they are listed in Table 4. Due to the numerous facets of protein characteristics that make up a proteome, complementary proteomic technologies are believed to capture as much information as possible. The two main proteomics platforms used in this study will be discussed briefly.

2DE is one of the central tools for proteomic analysis (Gorg et al., 2004). Separation of proteins is based first on isoelectric focusing (IEF) according to differences in net charge in the first dimension followed by molecular weight in the second

dimension using standard SDS-PAGE. Hundreds to thousands of proteins can be resolved on a single 2D gel that can then be identified by mass spectrometry (MS) and their relative abundances are determined. Hence, each well-resolved spot on a gel should, in principle, represent one protein species. A more recent technological innovation, two-dimensional difference gel electrophoresis (2D-DIGE), incorporates the labelling of two pools of protein samples and an internal standard with fluorescent cyanine dyes (Cy2, Cy3 and Cy5) permitted the multiplexing of samples in a single 2D gel (Unlu et al., 1997). The dyes are each composed of a peptide reactive group (*N*-hydroxysuccinimide ester; NHS) to derivitize the ε-amino groups of lysine residues. The molecular mass of each CyDye is approximately 450 Da and should not significantly alter the labelled proteins' M_r, and even if they do, the labelled proteins should move in tandem. Therefore, the same protein found in both sample pools but labelled with different Cydyes will migrate to the same spot, minimising the gel-to-gel reproducibility problem of conventional 2DE gels. Figure 11 shows a typical 2D-DIGE experimental setup. The gel can then be post-stained with silver (see Methods & Materials, sections 2.10 and 2.11 for further details) and the spot excised for protein identification (Figure 11). This multiplexing of samples in a single gel circumvents many technical limitations of conventional 2DE, including (i) improved intra and inter-gel reproducibility, (ii) a standard reference for eliminating experimental errors, (iii) less laborious, resource and time-saving by reducing the number of gels runs and (vi) increasing the confidence of spot quantification.

While conventional 2DE and 2D-DIGE have little problems identifying changes in the abundance of the hydrophilic proteins (for example, such as the mitochondrial matrix proteins, with respect to this study), membrane proteins are poorly resolved by the fact that many of these proteins precipitate at the basic end of the IEF strips (Eravci et al., 2008, Hanson et al., 2001). Therefore, alternate protein separation techniques are required to define changes for membrane proteins. Shotgun or MS-based proteomics based on liquid chromatography (LC) separation is a gel-free method. It separates complex biological samples after proteolytic digestion and when combined with chemical labelling (such as isobaric Tag for Relative and Absolute Quantitation or iTRAQ™) allows the quantification of these peptides. In the multidimensional LC assay, which is more ideal for complex samples, a typical experiment involves the digestion of proteins into peptides prior to separation first by strong cation exchange, followed by C18 reversed-phase column chromatography. Multidimensional separation is useful in its orthogonal nature, defined as the lack of correlation between analyte retention in two modes (Slonecker et al., 1996), thereby increasing the coverage of peptides of different physiochemical characteristics. In other words, the separation mechanisms between the first and second LC dimensions should be as dissimilar (or correlated) as possible, analogous to the independence of right-angles in geometry. A strong-cation exchanger separates peptides based on their positive charges , that is, a stationary phase that contains ionic groups which interact with the cationic samples) while reversed-phase column separates on the basis of hydrophobic differences, that is, the stationary phase is less polar than the mobile phase and the retention of samples is based on how polar (water-soluble) they are. This approach is termed Mulitdimensional Protein Identification Technology (MudPIT)

(Washburn et al., 2001), which is ideally suited for shotgun proteomics. The advantage of such an approach is that the resolved peptides from the C18 column can be directly introduced into a mass spectrometer. This is also known as online setup. In contrast, an offline 2D-LC setup allows less restriction on the compatibility of the mobile phase composition between the first and second LC dimension (Gilar et al., 2005, Peng et al., 2003) while remaining fully automated. The flexibility offered by the offline 2D-LC setup is especially useful for this study, since the collected fractions cannot be injected directly in MALDI, but rather the collected fractions from the second dimensional separation can be evaporated or diluted and mixed with the matrix. iTRAQ™ allows the multiplexing of four samples and recently, multiplexing up to eight samples is now possible (Wiese et al., 2007). Proteolytic peptides are chemically labelled with iTRAQ™ reagents of masses 113.1 – 119.1 Da and 121.1 Da. 120.1 Da was omitted to avoid contamination from phenylalanine immonium ion at *m*/*z* 120.08 (Pierce et al., 2008). Each label also exploits the NHS ester and an isobaric tag of 145 Da that consists of a balance group (carbonyl group) and a reporter group (based on *N*-methylpiperazine) via the formation of an amide bond. Due to the isobaric mass of the labels, digested peptides labelled with different iTRAQ™ channels do not differ in mass and appear as single peaks in MS scans. In MS/MS fragment ion spectra of iTRAQ™ labelled peptides, additional peaks appear in the m/z range of 113 to 121, originating from the singly charged reporter group fragment of each iTRAQ™ label. Between the balance and the reporter group is a fragmentation site thereby liberating reporter ion as a neutral ion. The peptide reactive group attaches specifically to free primary amino groups – *N*-termini and ε-amino groups of lysine residues. Peptide quantification can be performed by

interpretation of these peaks. Using this approach, in combination with 2D-DIGE, changes in the expression levels of mitochondrial proteome that comprise the ETC complexes and others can be assessed. In summary, 2D-DIGE and iTRAQ™-coupled to LC enables the labelling and protein/peptide fractionation which can then be successfully detected and analyzed by Matrix-assisted laser desorption/ionization (MALDI).

Table 4. Advantages and disadvantages of major proteomic platforms.

Technique	Advantages	Disadvantages
2D-DIGE[1,3]	Quantitative, retains information on p*I* and *M*r and subsequently gives direct information on PTM. Because each resolved spot is in principle one protein, the information generated from this pool of peptides is often more reliable.	Time-consuming technique, lack of automation for spot picking from gels, low throughput (~only 25–30 samples can be analysed per day). Biases against high- and low- molecular proteins and hydrophobic proteins
MS-based proteomics[2]	Excellent for differentially expressed proteins, measures the relative abundance of labelled peptides. Increased ability to detect hydrophobic proteins.	Expensive equipment and processing costs. Proteins digested into peptides are generally not uniform and generates various redundant peptides which makes it a challenge for accurately protein identification.
SELDI / protein array	Extremely sensitive (femtomolar range), high throughput (more than 100 samples can be analysed per day). Less complicated to use, offers convenience to the clinics	Not quantitative to semi-quantitative, antibodies used arrays are incomplete for entire protein complement, epitopes lie in different segments of a peptide and may not be represented on the array

[1, 2] The two platforms used in this study. [3] 2D-DIGE is an improvement over the classical 2DE for its ability to multiplex and increase in reproducibility which is one of the major technical concerns for 2DE. 2DE, two-dimensional gel electrophoresis; DIGE, differential gel electrophoresis; MS, mass spectrometry; p*I*, isoelectric point; *M*r, molecular weight; SELDI, surface-enhanced laser desorption/ionization.

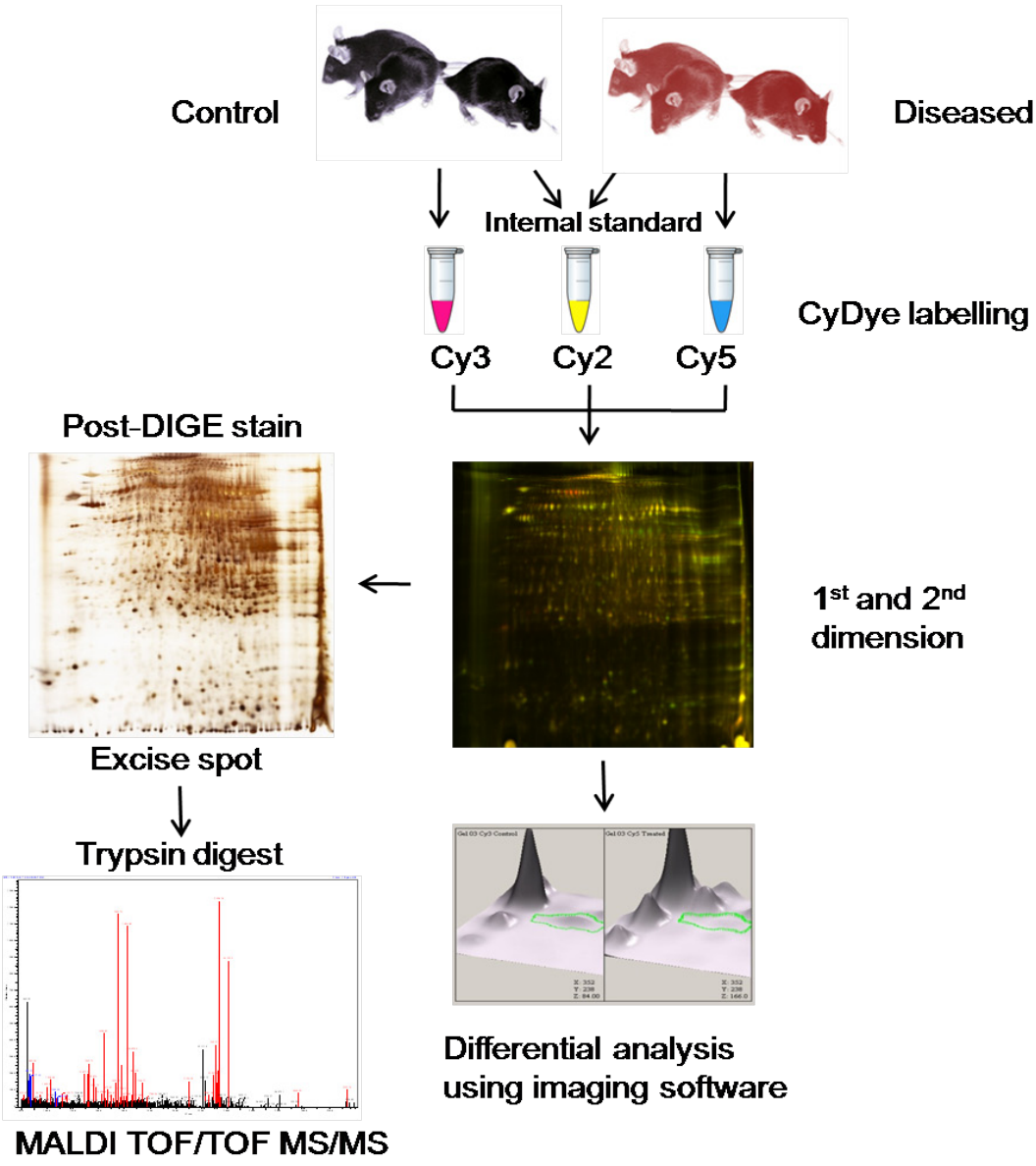

Figure 11. Experimental setup of a typical 2D-DIGE experiment
Protein extracted from biological samples (cells, medium, tissues) are labelled with Cydyes prior to 2D separation. The internal standard, labelled with Cy2 contains equal aliquots of the two sample pools. Spots that are detected to be differential on DIGE gels are matched with the post-stained gels, excised and identified by mass spectrometry.

1.4.1. Toxicoproteomics using the HET mouse in the mechanistic study of troglitazone toxicity

Toxicology focus on the study of adverse effects of chemicals on living organisms, and has traditionally been evaluated by the dosing of animals to measure their effects of chemicals and drugs on the cytology, physiology, metabolism, and morphology. Biochemical endpoints, histology and clinical chemistry have conventionally been used to assess the toxicity of exogenous stressors and in understanding the mechanisms by which these agents elicit their effects. Toxicology has progressively developed from studies predominantly based on individual chemicals to a knowledge-based science involving 'omics' and bioinformatics (Iannaccone, 2001). The effects of structurally and functionally similar agents can be characterized to a greater depth by assessing information of high-throughput data from databases. This will facilitate the rapid assessment of toxicant-related effects on diseases as well as gaining an understanding of the underlying mechanisms.

In drug discovery and development, preclinical drug safety assessments typically involve low-to-intermediate throughput and sometimes high-throughput *in vitro* and *in vivo* toxicity testing (Kramer et al., 2007). As toxicity continues to be a primary cause for compound attrition and long development cycle times, drug companies in the past 5–10 years have increasingly initiated and integrated new technologies for toxicity prediction (Walgren & Thompson, 2004). The rapid development of new drug candidates and subsequent screening for leads can be tightened and aligned by the use of high-throughput technologies for the early selection of leads with acceptable safety profiles,

which in turn gives important information to continue or discontinue the development of drug candidates before entry into the more expensive clinical development. Increasingly, new technologies, such as 'omics', stem cells and mutant animals have emerged to interpret and reinforce information gleaned from the more traditional mechanistic toxicology studies, and possibly save time and resources to achieve higher drug safety (Heijne et al., 2005, Ulrich & Friend, 2002). In Singapore, pharmaceutical companies like Eli Lilly and Schering-Plough has set up research programs aimed at supporting drug discovery/development that harness novel technologies to guide drug safety assessment.

One of the main goals of toxicoproteomics, besides the advancement of understanding of exogenous stressor associated with disease susceptibility and elucidating the mechanisms underlying toxicity is the identification of biomarkers of toxicity (Waters & Fostel, 2004). Biomarkers can be generally grouped into three major classes: diagnostic, prognostic, and predictive. The use of proteomics for predictive toxicity markers and toxicity profiling is especially informative given the simultaneous measure of a large number of proteins. Predictive markers can not only foretell the course of a drug-induced adverse effect but also help in understanding its route of toxicological mechanism. The larger implication will be the prediction and/or discerning of the type of toxicity judging from certain patterns of proteome changes. Toxicoproteomics can pave the way for reducing drug candidates with potential toxic effects by the early prediction of the modes of toxicity and managing the risks appropriately (Guengerich & MacDonald, 2007, Waters & Fostel, 2004, Wetmore & Merrick, 2004). Changes in the proteome profile induced by a candidate can be compared to profiles of known toxicants

and classified or discarded early in the development phase (Guengerich & MacDonald, 2007). In addition, toxicoproteomics may provide the framework for the extrapolation of toxicological data between species (Aardema & MacGregor, 2002, Stierum et al., 2005). Another advantage of toxicoproteomics is the extrapolation of *in vitro* cytotoxicity results to *in vivo* toxic results at the molecular level (Aardema & MacGregor, 2002). The use of extant clinical data may also help to correlate laboratory model toxicity profiles with that of human toxicity profiles in a similar fashion. The contribution of numerous indirect and direct pathways that has been hypothesized from *in vivo*, *in vitro* and clinical data that could aggravate or lead to troglitazone-induced DILI can be better explored and even reconciled through the application of highly accurate and objective assays such as proteomics.

Hitherto, one toxicoproteomic analysis of troglitazone-induced cytotoxicity has been described (Maniratanachote et al., 2005). Using 2D-DIGE analysis on HepG2 cells incubated with troglitazone versus similar doses of the less-toxic rosiglitazone, the authors showed that 78 kDa glucose-regulated protein (GRP78) and protein disulfide isomerase-related protein (ERp72) increased in a dose-dependent manner and suggested the involvement of chaperones in troglitazone-induced cytotoxicity (Maniratanachote, et al., 2005). However, such results have to be taken cautiously with the following considerations. The lethality of *in vitro* troglitazone toxicity depends very much on the dose and duration of the drug exposure to the cells. The dose used in the study was four to twenty fold greater than maximum plasma concentration (C_{max} of 3.6 to 6.3 μM) achieved in humans after 7 days of troglitazone exposure (Loi et al., 1999). Further to this

is the non-reproducibility of troglitazone-induced idiosyncratic and delayed toxicity in the petri dish. Hence it is our objective to extract information from the proteome at doses that is therapeutically used and in a complex *in vivo* biological system, by achieving as much relevance as possible to the clinical manifestation of troglitazone-induced idiosyncratic DILI.

Given the importance and complications of troglitazone mediation of mitochondrial dysfunction and its role and interplay with ROS / RNS production, our understanding of free radical-induced mitochondrial-associated pathologies can be advanced by studying protein expression dynamics under a genetically compromised condition. The mitochondrial abnormalities in the HET mutant mouse are associated with discreet mitochondria redox imbalance. This presents an interesting phenotype that is clinically silent, but represents a model for oxidative stress at the same time. Subtle yet chronic elevated production of endogenous free radical influences gene expression and post-translational modifications of proteins extensively (Bailey et al., 2005, Pryor et al., 2006). Assessing such alterations on a global-scale has been facilitated by advances in proteomic technologies using gel and MS-based platforms (Hamdan & Righetti, 2002). So far limited proteomic studies have been performed on the *Sod2* deficient mouse. Incidentally, and not surprisingly, published works have been directed at the analysis of the mitochondrial proteome where perturbations should occur most prominently at the site of free radical production and also where there is lowered antioxidant defence (Chang et al., 2004, Hinerfeld et al., 2004). From the standpoint of large-scale, global studies, using quantitative proteomics on HET mutant mouse will provide unbiased

information about the involvement of mitochondrial ROS on a proteome. Furthermore, the administration of drugs onto this susceptible mouse model can uncover the often obscure off-target (or toxic) ROS-inducing effects of drugs. In this sense, functional proteomics may help to illuminate the interaction of a proteome with a mitochondria-targeting toxicant under a state of compromised mitochondrial antioxidant defence.

1.5. Objectives

The main aims of this study are three-fold –

(1) To investigate to what degree is the HET hepatic mitoproteome different from the WT mouse. This will address its suitability as a preclinical surrogate model for assessing idiosyncratic DILI associated with discreet mitochondrial abnormalities.

(2) Secondly, building on the hypothesis of acquired abnormal or dysfunctional mitochondria as a susceptibility factor of troglitazone-induced toxicity, toxicoproteomics will be employed to analyze the dynamics of mitochondrial proteome and more clearly define the mechanisms and time course of troglitazone hepatotoxicity in the HET mouse.

(3) Finally, to understand the relationship between hepatic mitochondria oxidative stress on the mitoproteome and how it may lead to hepatic injury in the HET mouse.

Specifically, the unique properties of the HET mutant mouse will be exploited. Integrating unbiased, sensitive and comprehensive quantitative proteomics with conventional toxicological endpoints will provide complementary views on the ensemble

of mitochondrial proteins in which the adverse effects manifested with chronic troglitazone exposure. This approach may aid in deriving new understanding of troglitazone-related DILI in humans.

2. METHODS AND MATERIALS

2.1. Chemicals

The cyanine dyes, Cy2, Cy3, and Cy5, and Immobiline pH gradient (IPG) strips and two-dimensional electrophoresis reagents were purchased from GE Healthcare (Uppsala, Sweden). iTRAQ™ reagents were purchased from Applied Biosystems (Foster City, CA, USA). All other chemicals were of the highest purity grade and were purchased from Sigma unless otherwise stated.

2.2. Nomenclature

Gene symbols are italicized and begin with an uppercase letter, followed by all lowercase letters. Protein symbols are at upper case and not italicized. Genes coded by the mitochondrial genome have a prefix "mt-", lowercase mt followed by a hyphen.

The WT allele of a gene is indicated by "+" as superscript to the gene symbol and the deficiency (due to knock-out or mutation) is denoted by "-" as superscript to the gene symbol. For example, a wildtype mouse carrying two copies of *Sod2* alleles will be designated as WT, a heterozygous knock-out as HET ($Sod2^{+/-}$) and a homozygous mutant as $Sod2^{-/-}$.

With regards to proteomics, in the context of 2DE, the terms "protein abundance" and "differentially modulated" are used to reflect the variations in protein levels, including transcription (up-regulation and down-regulation), post-translational

modifications, translocation, degradation, accumulation and trafficking (Cohen et al., 2008, Godovac-Zimmermann et al., 2005, Nesvizhskii & Aebersold, 2005) that occur when proteomes are perturbed in various conditions especially. In contrast, the term "differentially expressed" is more tractable and suitable for describing detected protein from MS-based proteomics.

2.3. Animals, drug treatment and experimental design

All protocols involving animals were in compliance with the Institutional Animal Care and Use Committee, Singapore and in accordance with the guidelines of the National Advisory Committee for Laboratory Animal Care and Research, Singapore. Heterozygous *Sod2*^{tm1Leb}*/J* mice (breeding pairs), congenic in the C57BL/6 background, were obtained from Jackson Laboratory (Bar Harbor, ME, USA). A breeding colony was established by crossing male HET with female WT mice. The F_1 littermates were genotyped and subsequently used for the experiments. Genotyping of all mice was performed prior to weaning. The assays were performed by polymerase chain reaction (PCR) analysis according to the protocol provided by The Jackson Laboratory. Briefly, the DNA was extracted from a <4 mm tail piece using a DNA tissue kit (Promega, Madison, WI). PCR was performed with a Taq polymerase kit (Promega). The primers for the HPRT minigene (240 bp) were 5'-TgT TCT CCT CTT CCT CAT CTC C-3', oIMR0781, and 5'-ACC CTT TCC AAA TCC TCA gC-3', oIMR0782, synthesized by Research Biolabs (Singapore). As internal standard, the *Sod1* gene was used; primers for

the 123 bp product were 5'-TgA ACC AgT TgT gTT gTC Agg-3', and 5'-TCC ATC ACT ggT CAC Tag CC-3'.

Three WT C57BL/6 mice and three HET mice, 8 weeks old at the start of the experiment were used in the mitoproteome characterisation. The studies were conducted with a small number of laboratory mice because the tight, constant environmental conditions and due to inbreeding implies that their genetic variation should remain low. Following the characterisation study, a total of 15 HET mice were doused with either solutol or troglitazone for the toxicoproteomic analysis. Troglitazone ((±)-5-[4-(6-hydroxy-2,5,7,8-tetramethylchroman-2-ylmethoxy)benzyl]-thioazolidine-2,4-dione (Cayman Chemical, Ann Arbor, MI, USA) was dissolved in 9% (w/v) solutol HS-15 in phosphate buffered saline, a nontoxic solvent used for parenteral administration of water-insoluble compounds. Solutol HS-15 (BASF, Ludwigshafen, Germany) is composed of polyglycol mono- and di-esters of 12-hydroxystearic acid and 30% free polyethylene glycol served as the vehicle control. All animals used in this study were females and between 8 weeks to 14 weeks old at the start of the experiments. All mice kept under specified pathogen-free (SPF) conditions under controlled environmental conditions (22±2ºC, 75±5% relative humidity, 12-12 hr dark-light cycle) and had free access to standard rodent chow (Specialty Feeds Pte Ltd, Glen Forrest, Australia) and water *ad libitum*.

In the toxicological study, HET mice were randomly divided in four groups according to different treatments and duration of study. Groups 1 and 2 were injected

daily intraperitoneally with vehicle (10 μL/g body weight) or troglitazone (30 mg/kg body weight) for 14 days (assigned as VEH for vehicle administered mice and TRG for troglitazone administered mice, n = 3 per group). Groups 3 (n = 3) and 4 (n = 6) were injected intraperitoneally daily for 28 days (Table 5). In group 4, the allocation of six mice is to account for any unforeseen deaths from prolonged troglitazone administration (Ong et al., 2007). The troglitazone dose used here in mice is similar to the previously used therapeutic human dose (200 mg) (Loi, et al., 1999) if corrected for interspecies dose scaling factors (Kirman et al., 2005). Pharmacokinetic studies using UPLC-MS/MS showed that systemic exposure was also comparable to humans, as the plasma levels (C_{max}) and systemic exposure (AUC) in mice after a single dose of 30 mg/kg troglitazone were approximately 20 μM and 18.1 mgh/L respectively (New et al., 2007). The intraperitoneal route was selected in an attempt to target the drug to the liver and to guarantee maximal absorption. After 14 or 28 days of treatment, the mice were anesthetized with pentobarbital (60 mg/kg). Immediately after necropsy, the liver was excised and weighed; one portion of liver sample for histopathological evaluation was fixed in 4% neutral buffered formalin, another portion lysed in lysis buffer consisting of 7 M urea (USB, Cleveland, OH), 2 M thiourea (Fluka, Buchs, Switzerland), 4% (w/v) CHAPS (USB), 1 × Halt protease inhibitor cocktail (Pierce, Rockford, IL), 1 × PhosStop phosphatase inhibitor, 50 μg/mL DNase 1 and RNase A (Roche Applied Science, Mannheim, Germany) and the remaining used to prepare mitochondrial fractions. Blood was collected by cardiac puncture and serum prepared by allowing the blood allowed to stand at 25ºC for 30 min. After the blood has clotted, the tube was centrifuged at 1500 × g for 10 min at 20ºC and stored at 4ºC until further analysis.

Table 5. Experimental design of vehicle and drug-treatments of HET mice.
Fifteen HET mice were randomly assigned to four groups administered with either 9% solutol or 30 mg/kg troglitazone. Two weeks study comprises groups 1 and 2; four weeks study comprises groups 3 and 4.

	Vehicle-administered	**Troglitazone-administered**
2 weeks	*Group 1:*	*Group 2:*
	VEH1, 2, 3	TRG1, 2, 3
4 weeks	*Group 3:*	*Group 4* [‡]:
	VEH4, 5, 6	TRG4[¶], 5[¶], 6[¶], 7, 8, 9

[¶] Randomly-assigned troglitazone-treated mice used for proteomics analysis.
[‡] Larger sample size were used for the 4 weeks troglitazone-treated mice due to possible unforeseen deaths (Ong, et al., 2007).

2.4. Assessment of liver injury

Serum activity of ALT and AST was determined spectrophotometrically using Cobas Diagnoistics machine (Roche). For histopathological analysis, small pieces of liver were fixed in 4% phosphate-buffered formalin. The fixed tissues were subsequently processed with an automatic tissue processor (Leica TP 1020, Germany) and embedded in paraffin blocks. Tissue sections (2 - 5 μm) were stained with hematoxylin and eosin (H & E) and analyzed by light microscopy.

2.5. Isolation of liver mitochondria

All overnight food-deprieved mice were euthanized with CO_2. At all stages of preparation 1% protease inhibitor (Roche Complete) was added and all procedures conducted at 4°C unless stated. Liver tissue were quickly removed and rinsed with two washes of ice-cold isolation buffer (20 mM Hepes, 10 mM KCl, 1.5 mM $MgCl_2$, 1 mM

EDTA, 1 mM EGTA, 1 mM dithiothreitol (DTT) (Bio-Rad, Hercules, CA), 250 mM sucrose, pH 7.4). The washed livers were finely minced and homogenized with a Dounce homogenizer in 10 mL isolation buffer. Unbroken cells and cell debris were removed by centrifugation at 800 × *g* for 10 min. The resultant supernatant was centrifuged at 8,000 × *g* for 10 min. The crude mitochondria pellet (CM) were resuspended and washed twice in wash buffer (210 mM mannitol, 70 mM sucrose, 5 mM Hepes, 1 mM EGTA, pH 7.4), and centrifuged at 8,000 × *g* for 10 min. The supernatants from the first and second 8, 000 × g spins were collected for western blotting and were designated S1 and S2 respectively. To remove the contamination by endoplasmic reticulum, lysosomes or peroxisomes, the enriched mitochondrial pellet was resuspended in 5 mL of wash buffer and gently layered onto a modified discontinuous Percoll (GE Healthcare) gradient (Meisinger et al., 2000). A Percoll gradient was generated in place of sucrose in 38.5 mL polycarbonate tubes. By carefully layering stepwise, the discontinuous Percoll gradient consists of 1.5 mL of 60%, 4 mL of 32%, 1.5 mL of 23% and 1.5 mL of 15% (v/v) Percoll in wash buffer. Gradients were prepared on ice and used within 15 min of preparation. After centrifugation at 134,000 × g, 1 h in a Beckman SW41 Ti70 fixed-bucket rotor the purified mitochondria were recovered from the 32/60% interface. The mitochondria were then diluted with 4 volumes of wash buffer and sedimented at 12,000 × g. Thereafter the purified mitochondria (PM) were resuspended in lysis buffer, vortexed and sonicated. The suspension was centrifuged at 20,800 × g for 1.5 h at 15°C. Samples were stored at -80°C until use. Protein amount was determined using a modified Coomassie Plus protein assay kit (Pierce, IL, USA) with bovine serum albumin (BSA) as standard.

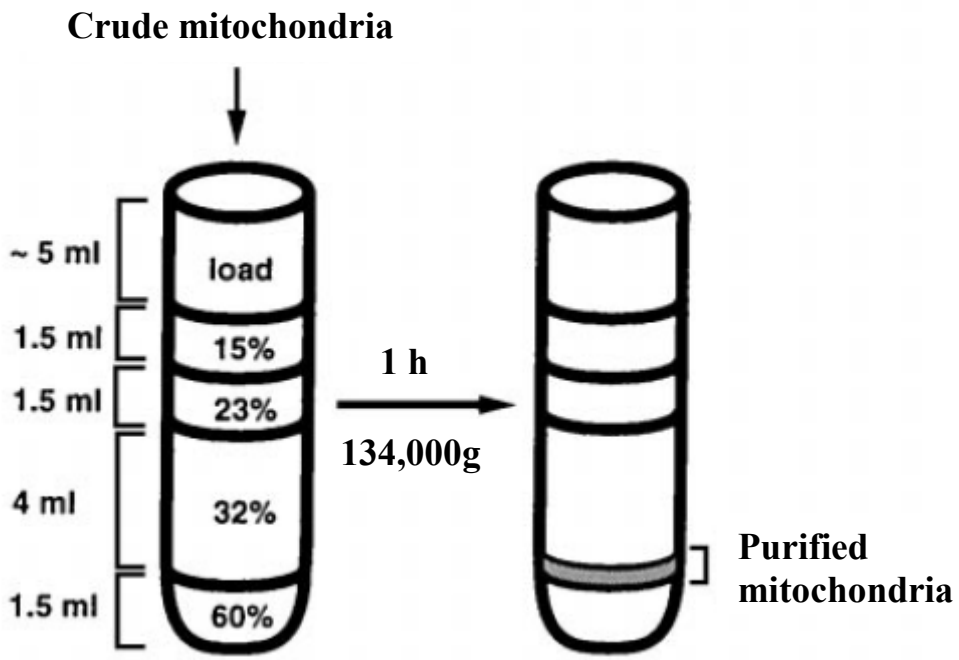

Figure 12. Schematic of discontinuous Percoll gradient.
The crude mitochondrial fraction (CM) is carefully layered onto a preformed discontinuous Percoll gradient (4ºC). This multi-step purification process resulted in highly pure mitochondrial fractions (PM; see Figure 16A for verificiation results).

2.6. Determination of mitochondrial GSH

Mitochondrial glutathione (mGSH) was determined in isolated mitochondria using monochlorobimane (MCB) as fluorochrome. MCB features a high selectivity for GSH and is conjugated to GSH by a glutathione-S-transferase (GST)–catalyzed reaction. Mitochondrial samples were incubated with MCB for 1 hr at 37ºC. The fluorescence was determined at 380/460 nm, and GSH levels were calculated from a standard curve formed from glutathione positive controls.

2.7. Determination of nitrite/nitrate levels

NO production was indirectly determined by measuring liver homogenate total nitrate/ nitrite (NO_x^-) levels with a fluorometric assay kit (Cayman Chemical, Ann Harbor, MI). Samples were ultra-filtered through a 10 kDa molecular weight cut-off centrifugal filter (Millipore, MA, USA) prior to the assay. Briefly, 20 μL of samples were incubated for 2 hr with nitrate reductase to convert nitrate to nitrite, followed by the addition of 2, 3-diaminonaphthalene and sodium hydroxide to enhance fluorescence. Fluorescence was measured using a fluorometer at excitation wavelengths of 365 nm and emission wavelengths of 430 nm.

2.8. Detection of total mitochondrial protein carbonyls and 3-nitrotyrosine adducts

To detect and quantify irreversible oxidative modification of total mitochondrial proteins, a protein carbonyl ELISA (Cell Biolab, San Diego, CA, USA) was used for its higher sensitivity and discrimination than the colorimetric assay (Buss et al., 1997) and according to the manufacturer's instructions. Briefly, the samples were compared with a standard curve generated from predetermined reduced and oxidized BSA standards. This assay was adapted from a protocol described by Buss and co-workers (Buss, et al., 1997) and subsequently modified for smaller sample volumes (Alamdari et al., 2005).

All samples were adjusted to 10 μg/mL protein concentration and incubated overnight in wells of a Nunc Maxisorp immunoplate (Nalge Nunc International) at 4°C. Similarly, reduced/oxidized BSA standards were incubated overnight. The samples and standards were washed three times with 1 × PBS and derivatized with 0.04 mg/mL DNPH diluted in 2 M HCl for 45 minutes at room temperature in the dark, and were subsequently washed 5 times with PBS: ethanol (1:1 v/v) and twice with PBS. The wells were blocked with 5 % BSA in 1 × PBS for 1.5 hour at room temperature and washed thrice with 1 × wash solution (100 mM Tris, pH 7.5, 1.5 M NaCl, 0.5% Tween-20 containing 0.02% thimerosal). Thereafter rabbit anti-DNP antibody (1: 1000) in 5% blocking solution was added to each well for 1 hour followed by HRP conjugated goat anti-rabbit secondary antibody (1: 1000) for another 1 hour and finally washed thrice with wash solution. The chromogen substrate, 3,3,5,5-tetramethylbenzidine (TMB) was added and incubated for 15 min at room temperature and the reaction stopped by adding 0.5 M H_2SO_4. Absorbance was quickly measured at 450 nm. Carbonyl content was expressed as nmol/mg protein using a fully reduced BSA standard as absorbance blank (Reznick & Packer, 1994). To quantify 3-nitrotyrosine (3-NT) levels, sandwich-based ELISA was used (Kamiya Biomedical, Seattle, WA). Diluted samples (20 × dilution) were pipetted into anti-nitrotyrosine coated wells, incubated with biotinylated second antibody for 1 hour. The wells were then flushed 4 times with wash solution, followed by streptavidin-peroxidase conjugate substrate for 1 hour before washing again with wash solution (4 times). Finally TMB was added to the wells for 30 min and the colour developed proportionally to the amount of 3-NT present in the sample.The enzyme

reaction was stopped by the addition of citric and absorbance was finally measured at 450 nm. 3-NT levels were expressed as nmol/mg protein using a calibration curve.

2.9. Two-dimensional Difference Gel Electrophoresis

2.9.1. Labelling with cyanine dyes

To prepare for CyDye labeling, 50 mM sodium hydroxide was first added to adjust the samples to pH 8.5. In the characterisation study, mitochondrial protein samples (40 μg) from WT and HET mice were labelled separately with 320 pmol Cy3 and Cy5, respectively (Table 6), and incubated for 30 min in the dark. An internal standard consisting of a mix of equal amounts of mitochondrial proteins from all WT and HET animals was prepared by labelling with Cy2. After 30 min, the labelling was stopped with 10 mM lysine. To check for labelling efficiency, 1.5 μg and 3 μg labelled proteins were subjected to 1D SDS-PAGE analysis, and the gels were scanned with a Typhoon 9400 scanner (GE Healthcare) at the wavelengths corresponding to Cy3 (532 nm). The same gel was stained after scanning to check for equal loading after pH adjustment.

In the toxicological study, 40 μg mitochondrial proteins from vehicle-administered and troglitazone-treated HET mice were labelled with 320 pmol Cy3 and Cy5, respectively (Table 7). An internal standard was generated using equal portions (3.33 μg) of all 12 samples and labelled with Cy2. Subsequent steps were followed essentially the same as above.

Table 6. Gel setup for 2D-DIGE experiments for HET hepatic mitochondrial proteome characterisation.
For each sample pair, there were duplicate gels and a dye swap for the third.

	Cy2 standard	Cy3	Cy5
Gel 1 – 2		WT1	HET 1
Gel 3 (Dye swap)		HET 1	WT1
Gel 4 - 5	Pooled WT1-3,	WT2	HET 2
Gel 6 (Dye swap)	HET 1-3	HET 2	WT2
Gel 7 - 8		WT3	HET 3
Gel 9 (Dye swap)		HET 3	WT3

Table 7. Gel setup for 2D-DIGE experiments for analysis of troglitazone-induced changes in HET hepatic mitochondrial proteome.
VEH1 - 3, HET mice dosed with solutol (9%/day. i.p. for 2 weeks) and TRG1 - 3, HET mice dosed with troglitazone (30 mg/kg/day, i.p. for 2 weeks). VEH4 - 6, HET mice dosed with solutol (9%/day. i.p. for 4 weeks) and TRG4 -6, HET mice dosed with troglitazone (30 mg/kg/day, i.p. for 4 weeks). For each sample pair, there were duplicate gels and a dye swap for the third.

	Cy2 standard	Cy3	Cy5
Gel 1 – 2		VEH1	TRG 1
Gel 3 (Dye swap)		TRG 1	VEH 1
Gel 4 - 5		VEH 2	TRG 2
Gel 6 (Dye swap)		TRG 2	VEH 2
Gel 7 - 8		VEH 3	TRG 3
Gel 9 (Dye swap)	Pooled VEH1-3, TRG1-3,	TRG 3	VEH 3
Gel 10 – 11	VEH4-6, TRG4-6	VEH 4	TRG 4
Gel 12 (Dye swap)		TRG 4	VEH 4
Gel 13 – 14		VEH 5	TRG 5
Gel 15 (Dye swap)		TRG 5	VEH 5
Gel 16 – 17		VEH 6	TRG 6
Gel 18 (Dye swap)		TRG 6	VEH 6

2.9.2. Isoelectric focusing and two-dimensional gel electrophoresis

Isoelectric focusing was conducted as described (Lee et al., 2008a). Briefly, a 40 μg portion of each Cy3-, Cy5- or Cy2- labelled samples were combined and subjected to isoelectric focusing using an IPGphor isoelectric focusing unit (GE Healthcare). IPG strips were rehydrated overnight using rehydration buffer, consisting of 7 M urea, 2 M thiourea, 4% (w/v) CHAPS, 2 M DTT, 0.2% (v/v) pH 3-10 non-linear (NL) IPG buffer or pH 3-11 NL IPG buffer, trace amounts of bromophenol blue (Merck). IPG strips used were 18 cm, pH 3-10 NL for drug-treatment study and pH 3-11 NL for mitochondrial proteome characterization. For analytical gels, approximately 50 μg of sample was loaded into the strip using the cup-loading method. The rehydrated strips were subjected to focusing at 200 V for 400 Vh, 500 V for 250 Vh, 1 kV for 500 Vh, gradient ramp from 1 kV to 8 kV for 2250 Vh, 8 kV for 36 kVh at 20°C at a maximum of 50 μA per strip.

Equilibration of strips was done prior to SDS-PAGE gel electrophoresis as described (Lee, et al., 2008a). Briefly, the strips were equilibrated for 15 min in equilibration buffer, consisting of 6 M urea, 50 mM Tris-Cl, 30% (v/v) glycerol, 2% (w/v) SDS, 1% (w/v) DTT, trace of bromophenol blue, pH 6.8, then re-equilibrated for 15 min in the same equilibration buffer containing 2.5% iodoacetamide (Fluka, Buchs, Switzerland), pH 8.8 in place of DTT pH 6.8. Subsequently, for characterization studies the equilibrated strips were loaded onto a 13% Laemmli SDS-PAGE polyacrylamide gel (20 × 20 cm) using a Protean II XL (Bio-Rad) cell and ran at 10°C, 15 mA per gel, for 20 min followed by 30 mA per gel. To observe differential protein modulation in high to

moderate molecular weights proteins, 11% SDS-PAGE polyacrylamide gels were used in the troglitazone-treated studies. Duplicate gels were run per study group. To avoid Cy3- or Cy5-specific effects, a dye swap was run for a third gel.

2.10. Image visualization and analysis

Fluorescent images of the 2D DIGE gels were obtained using a Typhoon Variable Mode Imager 9410 (GE Healthcare). Determination of protein spot abundance and analysis of the 2D DIGE gels were performed using DeCyder v5.02 software (GE Healthcare) as described in the Ettan DIGE User Manual. Normalization and quantitative profiling of proteins in the 2-DE gels were performed using the Differential In-gel Analysis (DIA) module and Biological Variance Analysis (BVA) module of the DeCyder software. The spots were also manually screened to ensure correct matching across gels. For the first DIGE experiment, significant alteration in ratio relative to WT mouse was defined as equal or more than a 1.5-fold (≥ 1.5 or 33.3%) difference in spots that were present in at least 6 of the 9 gels run for each experiment. For the second DIGE experiment, significant alteration in ratio relative to vehicle-dosed HET mouse was defined as ≥ 1.45-fold (31%) difference in spots that were present in all gels run for the troglitazone study. The fold change criterion was lowered to expand on the possibility of capturing proteins that may fit into a particular pathway. Student's *t*-test at 99% statistical confidence ($P < 0.01$) was set for both experiments. A 1% false discovery rate was applied in the BVA module to control false positives. Together they increase the stringency of matching gel spots and lower variability of gels, thereby generating high

statistical confidence of the proteomic data. For visualization, gels were silver-stained using the Vorum protocol (Mortz et al., 2001) and followed by in-gel tryptic digestion of the selected spots.

2.11. Protein identification by MALDI-TOF/TOF MS/MS

Gel pieces were excised from silver stained 2D-DIGE gels and washed twice with 150 µL of 2.5 mM NH_4HCO_3 in 50% v/v acetonitrile (ACN) and incubated at 37°C for 15 min. After drying, gel pieces underwent reduction with 10 mM DTT for 1 h at 56°C with constant shaking. This was followed by alkylation with 55 mM IAA for 45 min at room temperature in the dark. Trypsin (Promega) in 25 mM NH_4HCO_3. Five µg/µL was added to intense spots, while 2.5 µg/µL trypsin was added to faint spots, and incubated at 37°C for 16 h. Upon sonication, peptides were extracted in 20 µL 0.1% v/v trifluoroacetic acid (TFA) in 50% ACN and dried in a speedvac evaporator. Peptide digests from each gel spot were spotted onto a 100-well MALDI sample plate and mixed with an equal volume of CHCA matrix solution (5 mg/mL α–cyano-4-hydroxy-cinnamic acid in 0.1% TFA, 50% ACN). MS and MS/MS spectra were obtained using the ABI 4800 Proteomics Analyzer MALDI-TOF/TOF Mass Spectrometer (Applied Biosystems) operating in a result-dependent acquisition mode. For MS analysis, 2,000 shots were accumulated for each well of sample. Peptide digests from each gel spot were spotted onto a 384-well MALDI sample plate and mixed with an equal volume of CHCA matrix solution (5 mg/mL α–cyano-4-hydroxy-cinnamic acid in 0.1% TFA, 50% ACN). MS and MS/MS spectra were obtained using the ABI 4800 Proteomics Analyzer MALDI-TOF/TOF Mass

Spectrometer (Applied Biosystems) operating in a result-dependent acquisition mode. For MS analysis, 2,000 shots were accumulated for each well of sample. Six external standards (mass standard kit for the 4700 Proteomics Analyzer, Applied Biosystems) were used to calibrate each spectrum to a mass accuracy within 50 ppm. Peaks were detected without smoothing. Peaks were deisotoped and only the peaks with s/n≥ 10 were submitted for database search. Common keratin contamination peaks (804.4097, 973.5313, 1179.6, 1234.68, 1320.583, 1475.785, 1707.773, 1791.728, 1993.977, 2705.161) and trypsin autolytic peaks (842.51, 1045.56, 1940.95, 2211.10, 2225.12, 2239.13, 2283.18, 2299.17, 2807.30) were excluded with a mass tolerance of 200 ppm. Peak density filter was implemented with a limit of 50 peaks per 200 Da, and the maximum number of peaks was set to 65. The ten most intense ions from each sample excluding trypsin autolytic and keratin tryptic peptides were selected for MS/MS. The MS/MS analyses were performed at collision energy of 2 kV and a collision gas pressure ~ 1×10^{-6} Torr, using air as the collision gas. Stop conditions were implemented so that 2,000 to 3,000 shots were accumulated depending on the quality of the spectra. No smoothing was applied before peak detection. Only the peaks from 60 Da to 20 Da below each precursor mass, and with s/n≥ 10 were picked. Peak density was limited to 30 peaks per 200 Da, and the maximum number of peaks was set to 125. GPS explorer™ software Version 3.6 (Applied Biosystems) was used to create and search files with MASCOT search engine (Version 2.1; Matrix Science) for peptide and protein identification. Both MS and MS/MS spectra were combined for database search. International Protein Index (IPI) (Kersey et al., 2004) mouse database Version 3.23 (51536 entries) or Version 3.25 (52407 entries) was used for the search and was restricted

to tryptic peptides. *N*-terminal acetylation, cysteine carbamidomethylation, and methionine oxidation were selected as variable modifications. One missing cleavage was allowed. Peptide mass tolerance and fragment mass tolerance were set at 150 ppm and 0.4 Da, respectively. Maximum peptide rank was set to 2 and the minimum ion score C. I. % (peptide) was set to 50. Expectation values for protein and best peptide identification were≤ 0.0.5 except for ECHM, 3HIDH and HMCS2 (expectation values can be found in Appendix). If more than one database entries were matched to the same set of MS data, the entry first entered on the database was reported in the table with the exception of 3HIDH / HMCS2.

2.12. iTRAQ™ labelling

Labelling of samples was performed according to manufacturer's protocols (Applied Biosystems). This study comprised of two iTRAQ™ experiments done in duplicates, the 4-plex system for the heterozygous versus WT mouse comparison study and the 8-plex system for the toxicological study (Figure 13).

4-plex iTRAQ™ labelling was performed as followed: iTRAQ™ label reagents 114 and 116 (1st replicate) – a pool of three WT mice and iTRAQ™ label reagents 115 and 117 (2nd replicate) – a pool of three HET mice. Duplication provided two advantages, firstly to eliminate label reagent-specific bias and secondly, to ensure quantification reproducibility. After extraction and purification of the mitochondrial proteins, the samples were precipitated using the 2D-clean up kit (GE Healthcare) and reconstituted in

0.5 M triethylammonium bicarbonate, 1.0% SDS (w/v). A total of 90 μg hepatic mitochondrial proteins, comprising of a pool of 30 μg portions from the 3 mice of each genotype were reduced, alkylated and digested. Following this, the samples were incubated with their corresponding labels for 1 h. The four labelled samples were then combined and pass through a strong cation exchange cartridge (Applied Biosystems) and the eluate desalted via a SepPak cartridge (Millipore). The iTRAQ™-labelled mixture was then vacuum dried and stored at -80°C until further use.

8-plex iTRAQ™ labelling was also performed according to manufacturer's instructions. With the exception of 50 μL isopropanol and the additional labels, the rest of the protocol remains the same as the 4-plex system. Similarly, the experimental design consists of two technical replicates. For the 2-weeks study, the vehicle-dosed mice (Groups 1 and 2) were labelled with iTRAQ™ label reagents 113 and 115 (replicate) and troglitazone-treated mice with reagents 114 and 116 (replicate). For the 4-weeks study, the vehicle-dosed mice (Groups 3 and 4) were labelled with iTRAQ™ label reagents 117 and 119 (replicate) and troglitazone-treated mice with reagents 118 and 121 (replicate). A schematic diagram of the experimental design can be found in Figure 13B.

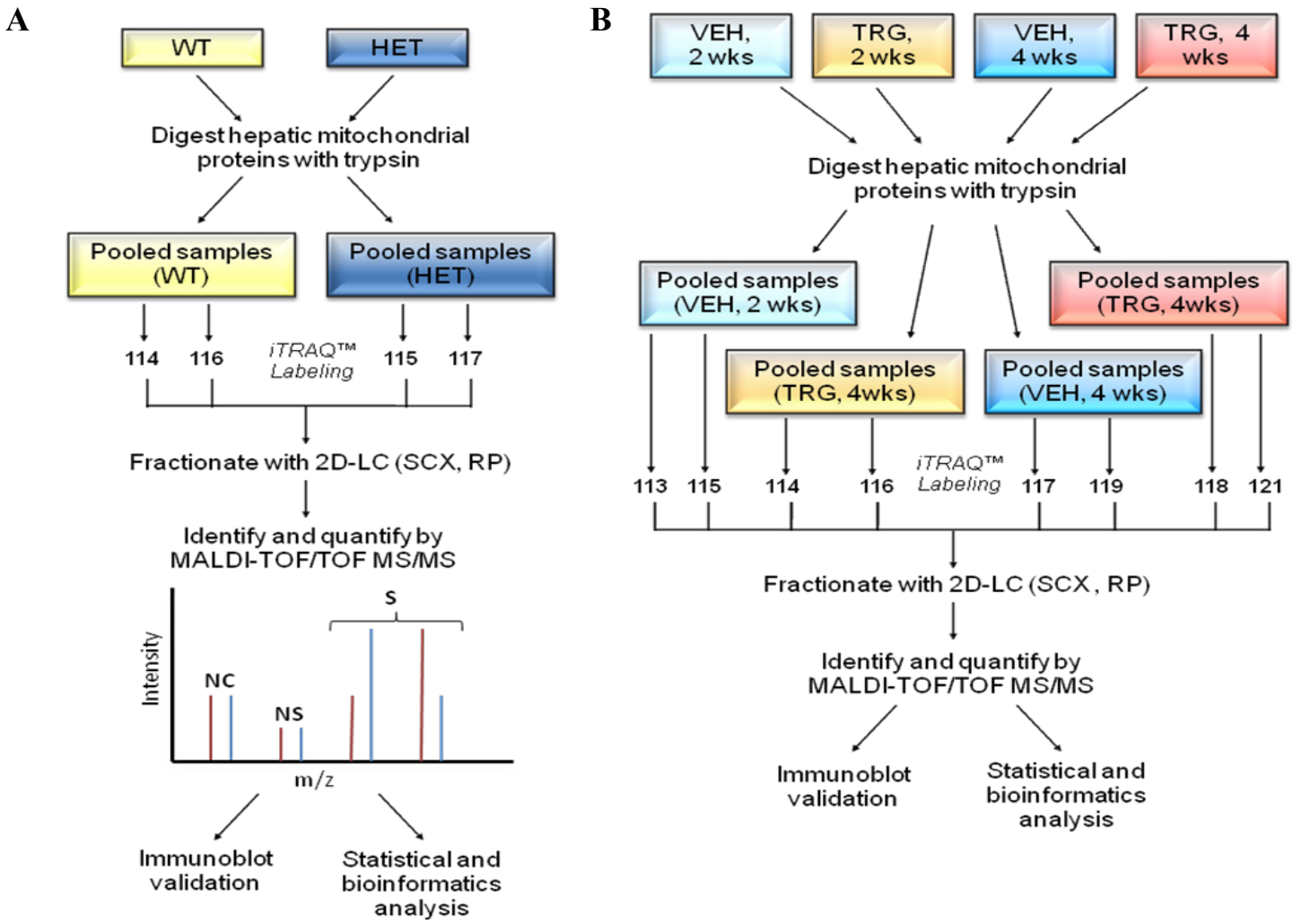

Figure 13. A flow-chart summary of the iTRAQ™ experiment design of 4-plex and 8-plex systems.
(A) The quantification of proteins differentially expressed in the WT and HET hepatic mitochondria using 4-plex iTRAQ™. (B) Quantitative shotgun proteomics using 8-plex iTRAQ™ to elucidate and identify mitoproteome dynamics over two periods of daily vehicle (VEH) or troglitazone (TRG) dosing. See text for details to experimental design. NC, no change; NS, not significant; S, significant; SCX, strong cation exchange; RP, reverse phase.

2.12.1. Two-dimensional Liquid Chromatography-MS/MS of iTRAQ™ samples

Each of the iTRAQ™-labeled peptide mixtures was separated using an Ultimate™ dual gradient LC system (Dionex-LC Packings) equipped with a Probot™ MALDI spotting device. A 2D-LC separation was performed as follows. The labeled peptide mixture was dissolved in 2% ACN with 0.05% TFA and injected into a 0.3 × 150-mm strong cation exchange column (SCX300 Å, NanoEase Trap Column 0.50 × 47 mm; Waters) for the first dimensional separation. The flow rate was 6 µL/min. Five fractions were obtained using step gradients of Mobile phase B (5 mM KH_2PO_4 buffer, 5% ACN, 125 mM KCl, pH3) for the HET comparative study: unbound, 0–17, 17–26, 26–36, 36–50, 50–100% and eight fractions for the toxicoproteomics study were obtained using step gradients of Mobile phase B: unbound, 0–10, 10–20, 20–40, 40–50, 50–75, 75–100 and 100% of Mobile C (5 mM KH_2PO_4 buffer, pH 3, 5% ACN, 500 mM KCl). Mobile A was 5 mM KH_2PO_4 buffer, 5% ACN, pH 3. The eluting fractions were captured alternatively onto two 0.18 × 23.5 mm trap columns (5 µm C18 Symmetry 300; Waters) and washed with 0.05% TFA followed by gradient elution in a 300 µm × 150 mm reverse phase column (Symmetry C18; Waters). The mobile phases used for this second dimensional separation were 2% ACN with 0.05% TFA (A) and 100% ACN with 0.04% TFA (B). The gradient elution step was 0–45% B in 40 min at a flow rate of 2.7 µL/min. The LC fractions were mixed directly with MALDI matrix solution (7 mg/ml α-cyano-4-hydroxycinnamic acid and 130 µg/mL ammonium citrate in 75% ACN) at a flow rate of 5.4 µL /min via a 25-nL mixing tee (Upchurch Scientific) before they were spotted

onto a 192-well stainless steel MALDI target plate (Applied Biosystems) using a Probot Micro Precision Fraction Collector (Dionex-LC Packings) at a speed of 5 s/well.

2.12.2. Mass Spectrometry for iTRAQ™

The samples on the MALDI target plates were analyzed using a 4700 Proteomics Analyzer mass spectrometer (Applied Biosystems). MS/MS analyses were performed using nitrogen at a collision energy of 1 kV and a collision gas pressure of 1×10^{-6} torr. One thousand shots were accumulated for each MS spectrum. For MS/MS, 6,000 shots were combined for each precursor ion with signal to noise (S/N) ratio greater or equal to 100. For precursors with S/N ratio between 50 and 100, 10,000 shots were acquired. The resolution used to select the parent ion was 200. No smoothing was applied before peak detection for both MS and MS/MS, and the peaks were deisotoped. For MS/MS, only the peaks from 60 to 20 Da below each precursor mass and with S/N$\geq$ 10 were selected. Peak density was limited to 30 peaks per 200 Da, and the maximum number of peaks was set to 125. Cysteine methanethiolation, N-terminal iTRAQ™ labeling, and iTRAQ™ labeled lysine were selected as fixed modifications; methionine oxidation was considered as a variable modification. One missed cleavage was allowed. Precursor error tolerance was set to 100 ppm; MS/MS fragment error tolerance was set to 0.4 Da. Maximum peptide rank was set to 2.

2.13. Immunblotting

In order to show mitochondrial enrichment during the isolation process, immunoblot analysis was performed using standard methods. Polyvinylidene difluoride membrane blots (PVDF, Bio-Rad) were developed with primary antibodies directed against either cytochrome oxidase subunit IV or COX IV (Molecular Probes, Invitrogen, CA, USA) or SOD2 (Abcam, Cambridge, UK). Blots were incubated against antibodies in 0.1% Tween 20 (Duchefa, Netherlands), 5% blocking non-fat milk (Bio-Rad) in PBST (20 mM Tris, 150 mM NaCl, pH7.5, 0.2% Tween 20) or 2.5% BSA in TBST. Primary antibodies were incubated overnight at 4°C, while secondary antibodies were incubated for 1 h at room temperature. Primary antibody binding was visualized utilizing horseradish peroxidase-conjugated secondary antibody and appropriate chemiluminescent substrate (ECL or ECL plus, GE Healthcare, Uppsala, Sweden). All quantifications were done by scanning the blots with a GS-800 densitometer (Bio-Rad). COX IV was used as a loading control.

To validate the mass spectrometry results in HET mitoproteome profiling, a range of mitochondrial antibodies were selected with respect to their molecular weights and sub-mitochondrial localizations via 1D or 2D immunoblotting. Antibodies against NDUFS3 (MitoSciences, Invitrogen), COX IV, succinate dehydrogenase [Fe-S] subunit (Molecular Probes, Invitrogen), medium-chain acyl-CoA dehydrogenase (ACADM), methionine sulfoxide reductase, SOD2, thiosulfate sulfurtransferase, hydroxyacyl-coenzyme A dehydrogenase, (Abcam) and cytochrome c (BD Pharmingen, San Jose, CA)

were used. In 2D-immunoblots, 20 μg of mitochondrial proteins were separated on first dimension using 7-cm IPG strips (pH3-10 non-linear), followed by second dimension separation on 13% polyacrylamide minigels and subsequently incubated with antibodies against SOD1 (Santa Cruz Biotechnology), SOD2 or GPX1 (Abcam). 2D-PAGE immunoblotting was also performed to ascertain that aconitase-2 (Abnova) and thioredoxin-2 (Abcam) were not altered in their abundance levels in the HET mouse.

For the toxicological studies, equal amounts of mitochondrial protein (5 μg) were loaded onto acrylamide gels, resolved, transferred to PVDF and incubated with primary antibodies directed against LAMP-1 (Santa Cruz Biotechnology), calnexin (Chemicon), PEX-19 (Santa Cruz Biotechnology), or cytochrome *c* oxidase subunit IV (Molecular Probes, Invitrogen) to demonstrate the level of purity of the mitochondrial fractions. As a confirmatory step to our mass spectrometry results, we performed 1D and 2D-immunoblotting (pH3-10 non-linear and pH6-11 linear; 11% and 14% gels respectively) as above. Antibodies against ACO2 (Abnova), ornithine transcarboxylase, medium-chain specific acyl-CoA dehydrogenase, methionine sulfoxide reductase, SOD2, thiosulfate sulfurtransferase, hydroxyacyl-coenzyme A dehydrogenase, (Abcam), VDAC1 (Calbiochem, CA, USA), NDUFS3 (MitoSciences, Invitrogen), cytochrome *c* oxidase subunit IV, succinate dehydrogenase [Fe-S] subunit (Invitrogen), cytochrome c (BD Pharmingen, San Jose, CA, USA) in 5% non-fat milk or 2.5% BSA in TBST. Total cytochrome c levels were determined from liver extracts.

To detect activation of MAPK and AKT signalling cascade, liver lysates were immunoblotted. Equal amounts of proteins were separated and subjected to immunblotting with antibodies as follows. Antibodies specific for ASK1, phospho-ASK1$^{\text{Serine 83}}$, phospho-ASK1$^{\text{Threonine 845}}$, JNK, phospho-JNK$^{\text{Threonine183/Tyrosine185}}$, p38 MAPK, phospho-p38 MAPK$^{\text{Threonine180/Tyrosine182}}$, AKT, phosphor-AKT$^{\text{Serine 473}}$ (Cell Signaling Technology, Beverly, MA) and visualized using peroxidase-conjugated secondary antibodies and advanced chemiluminescence (GE Healthcare). To assess the transcriptional regulatory circuits leading to expression of mitochondria gene products, liver lysates were immunoblotted using antibodies against NRF-1, ERRα, (Abcam), PGC-1β (Santa Cruz Biotechnology), PGC-1α (Aviva Systems Biology, San Diego, CA), PPARγ, pFOXO3a$^{\text{Serine 253}}$ and FOXO3a (Cell Signalling Technology) to check for levels and/or activation of such transcription factors or transcriptional co-activators.

All blots were checked for equal loading by post-colloidal silver staining. After development with chemiluminescent substrate, the membrane blots were washed with three times with fresh changes of ddH_2O and rocked with colloidal silver solution (40% $NaNO_3$, 20% $FeSO_4$, 20% $AgNO_3$; w/v) for 15 to 30 min until the colour develop. The colloidal silver solution was discarded and the membrane washed with ddH_2O for 15 min before being air-dried.

2.14. Aconitase-2 aggregation and degradation study

Polyclonal antibodies against residues 767 to 780 of the C-terminus of aconitase 2 (ACO2) were raised in rabbits (generously provided by Dr. Bi Xuezhi, National University of Singapore, Singapore) and cross-reacted with murine aconitase 2 (Bota et al., 2002). This antibody recognises murine ACO2 in the non-oxidized, intact form (corresponding to bands of ~85 kDa) and oxidized, degraded form (corresponding to bands detectable at ~43 kDa). Additional ACO2 antibodies were bought from Abnova (Taipei, Taiwan), and were used for the detection of aggregates which formed an extended smear of >100 kDa.

For isolation of ACO2 aggregates and proteins bigger than 100 kDa, mitochondria samples were diluted 20 × and filtered through Ultracel YM-50 centrifugal filters (Millipore) at 14,000 × g at 10°C. The 50, 000 Da nominal molecular weight cut-off was chosen according to the manufacturer's recommendation of using a cut-off two times smaller than the molecular weight of the protein to be concentrated, i.e. proteins above the molecular weight of 100 kDa will be retained as the retentive and proteins below 100 kDa, including non-aggregated ACO2 will pass through the membrane as filtrate. Lyses buffer was used as a negative control. To test for aggregation (>100 kDa), 25 µg of protein from the retentate fraction was loaded onto 8% SDS-PAGE gels (3% stacking gel), allowed to run beyond the dye front for an additional 30 min and immunoblotting was performed by transferring to PVDF membrane blots and incubated with ACO2

antibodies. Detection was by ECL Plus. Another replicate gel was stopped when the dye front reaches the edge of the gel and was immunoblotted for the analysis of intact ACO2.

To study the degradation of ACO2, the filtrate fraction was analyzed by immunblotting. 20 μg per lane from the filtrate samples were loaded onto 13% SDS-PAGE gels and the gel was stopped when the dye front reached the end of the gel. Similarly, the bands were detected by using ACO2 antibodies and ECL Plus substrates as described above.

2.15. Immunohistochemistry

Dewaxed paraffin-embedded liver sections (2 μm) were rehydrated and antigen retrieval was by heating in 0.01 M sodium citrate buffer for 20 min. Endogenous peroxidase activity was blocked using 0.3% hydrogen peroxide for 10 min. Sections were then blocked and immunostained using Envision + System-HRP Labelled Polymer Kit (Dako, Denmark). Anti-pFOXO3a$^{\text{Serine 253}}$ antibodies (Cell Signalling Technology) were incubated overnight, 4°C. After that the sections were rinsed thrice with PBS, incubated with secondary antibody for 1 hr at room temperature, washed thrice with PBS and immunoreactivity detected using 3, 3-diaminobenzidine. The sections were counterstained using Lillie's modified Mayers Hematoxylin, dehydrated, mounted and viewed under light microscope (Carl Zeiss).

2.16. *In silico* analysis

2.16.1. Mass spectra analysis – ProteinPilot™

The data analysis for 8-plex iTRAQ™ was performed using ProteinPilot™ (Applied Biosystems/MDS-Sciex) by searching the spectra against either species-specific subset (mouse in this case) concatenated with a reversed "decoy" version of itself. The decoy database is constructed by reversing all the protein sequences in the database (IPI mouse database) and appending these reversed sequences to the original database. The list of identifications obtained by searching of the concatenated target and a randomized decoy database is ordered from highest confidence to lowest confidence (or sorted from highest score to lowest score).

The data analysis for 4-plex and 8-plex iTRAQ™ was performed using ProteinPilot™ (Applied Biosystems/MDS-Sciex) by searching the spectra against mouse database (IPI mouse version 3.48) concatenated with a randomized "decoy" version of itself (Feng et al., 2007). “Instantaneous” false discovery rate (FDR) estimation of 5%, as calculated from the slope of the accumulated Decoy database hits by the PSPEP algorithm were applied (Tang et al., 2008). As a further refinement, proteins have to meet the criteria of (i) ProteinPilot™ Unused ProtScore of≥ 2.0 (99% C.I.) and (ii) two or more tryptic peptides of which at least one unique peptide of high confidence (> 99%) (Shilov et al., 2007) before proteins were accepted for further analysis. The software calculates a percentage confidence which reflects the probability that the hit is a false

positive, so that at the 99% confidence level, there is a false positive identification rate of 1%. Low confidence peptides do not identify a protein by themselves, but support the identification of the protein and hence is the true indicator of a protein (Shilov, et al., 2007). The Unused ProtScore is a measure of all the peptides evidence specific for a protein and prevents reuse of the same unique peptide to support the identification of another protein. Manual bias correction was applied to account for any experimental error that may arise from unequal sample mixing during combination of the differently labelled samples (seven potential biases due to the 8-plex system).

Confidently-identified proteins passing the global 5% FDR, and the micro-level criteria were selected for relative protein quantification using the Pro Group algorithm™ (Kapp et al., 2005, Sadygov et al., 2004). Because the iTRAQ™ experiments were performed in pairs (technical replicates; Figure 13), the denominator of the reagent corresponding to the first reagent pair was swapped to the other reagent pair, thereby generating four independent fold change ratios. For example, 114 of the 115/114 pair was swapped with 116 to form 117/114 fold change ratio. Fold changes, *FC* was defined as $1.2 \leq FC \leq 0.83$ (reciprocal of 1.2). For quantification purposes, MS and MS/MS spectra were manually examined and detected sequences rejected based on one or more of the following criteria – (i) C.I. ≥ 99, (ii) partially cleaved tryptic sequences or internal miscleavages, except proline is C-terminus of lysine or arginine (sequences cleaved by trypsin should end with arginine or lysine at its C-terminus), (iii) within a window of ±5 Da around the main precursor peak, "crowding" of one or more adjacent peaks whose intensity is half or more than the matched experimental precursor, (iv) unlabeled

iTRAQ™, (v) non-specific iTRAQ™ labelling, (vi) plausible PTMs, (vii) weak absolute quantification peaks for iTRAQ™ reporter labels (<3500 relative intensity for 4-plex and <2000 for 8-plex, based on 5th percentile cut-off; Figure 14) and main precursor peak (Keil, 1992, Nesvizhskii & Aebersold, 2005, Olsen, et al., 2004). Keratin was considered as contamination during processing and was disregarded.

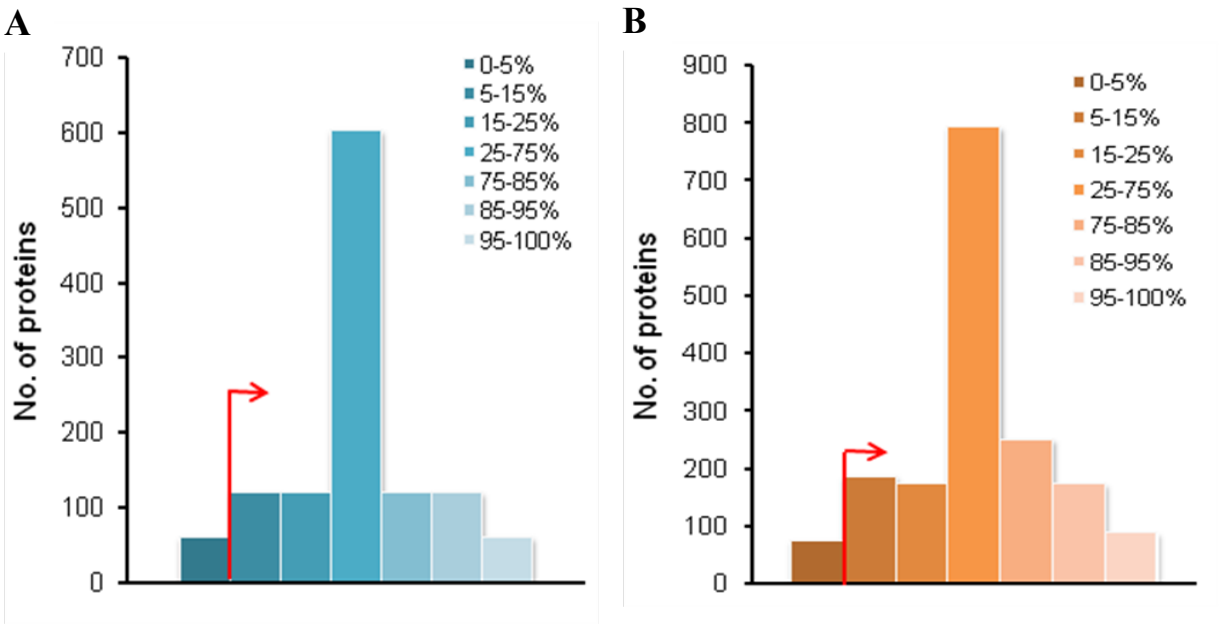

Figure 14. Histogram of mean signal area (intensity) of reporter channels.
(A) 4-plex. (B) 8-plex systems. The peptides were binned according to percentile ranks.

2.16.2. Gene Ontology over-representation and pathway analysis

Gene Ontology (GO) over-representation analysis was performed using Ontologizer 2.0 (http://compbio.charite.de/index.php/ontologizer2.html). GO is a widely used classification system of gene functions and other gene attributes that uses a controlled

vocabulary. Statistically enrichment of GO terms were tested using "Term-for-Term" analysis and enrichment of GO "biological process" terms was defined at adjusted $P < 0.05$ after using Bonferroni correction for multiple testing against 18080 gene products (filtered *Mus musculus* database, http://www.geneontology.org/GO.current.annotations.shtml) that forms the population sample accessed 26 Jan 2008 (Bauer et al., 2008). GO terms "Metabolic process, cellular metabolic process and primary metabolic process" were considered broad terms and were not included in the analysis. KEGG and GO enrichment of 2-weeks and 4-weeks intersecting and non-overlapping "biological process" was performed using Database for Annotation, Visualization and Integrated Discovery (DAVID; version 6) (Dennis et al., 2003). Ingenuity Pathway analysis (IPA; version 7.1) was used for the analysis of over-represented biological pathways. The information is obtained from Ingenuity's Knowledge Base, a manually curated database. Right-tailed Fisher's Exact test ($P < 0.05$) is used for multiple testing of over-represented pathways.

2.17. Statistical evaluation

The mean ± SD was calculated for each treatment group. For biochemical analyses, all assays were performed in triplicate, and the mean was taken as 1 data point. Linear regression (Pearson correlation) analysis and agglomerative hierarchical clustering were performed using Microsoft Excel and XLSTAT (Addinsoft, New York, USA). Significant differences between means were determined by ANOVA and Newman-Keuls multiple comparison or Tukey post-tests (InStat, GraphPad software, San Diego, CA,

USA). *P* values of < 0.05 were considered significant. Mean centroid value (MCV) is simply the ratio of averaged fold change of a group of functionally-related proteins, that is proteins of the same distribution (statistical population), treated fold-change as a function to vehicle fold-change. By letting *i* be the expression for proteins 1, 2, 3, …*n*, of functional cluster *k* = 1, 2, 3, …*n*, the MCV, *m* is determined using the following equation:

$$m_{ik} = \frac{\bar{x}_{ik}}{\bar{y}_{ik}} \qquad \text{(Eq. 4)}$$

where *m* is the shrunken centroid value, $\bar{x}_{ik}$ is the class average of functional cluster *ik* in week 2, $\bar{y}_{ik}$ is the class average of functional cluster *ik* in week 4

To do so, proteins were first determined if they are mitochondrially-localized through the use of Bioinformatic Harvester IV (http://harvester.fzk.de/harvester/). Bioinformatic Harvester is a meta-search engine that collects information from various scientifically curated proteins and genes databases. For each mitochondrial-localized protein entry, the description and associated literature was examined for its GO and/or Kyoto Encyclopaedia of Genes and Genomes (KEGG) annotated function as well as its interactions with other proteins; the latter being able to provide additional information about its functions. This is based on the presumption that the association of proteins would suggest their common involvement in a biological function or pathway, analogous to the 'guilt-by-association' concept. On top of this, published literature was manually curated to further assess a protein's function so as not to miss out additional lines of experimental evidence that was left out due to reasons such as recent publications (not

updated on databases) or just not included in the databases for other reasons. For example, it was shown very recently that thioesterase superfamily member 2 (also known as acyl-CoA thioesterase 13) is involved with mitochondrial fatty acid metabolism (Wei et al., 2009). Often there is a time-lag in the annotation of new information and given the above example, such recent information would not be captured on the databases and escape further analysis. Some proteins have promiscuous functions and hence may overlap in different functional clusters. The proteins are then included under a functional class with focus for biological functions and pathways associated with the mitochondrion. Finally, the MCV is a value of 4-weeks averaged fold change relative to 2-weeks. Of note, the functional cluster 'Apoptosis' was listed but expression values of associated proteins do not dictate an up- or down-regulation of this pathway; additionally, the incomplete detection of proteins such as Bax, Bcl-2 and caspases implies that the MCV should only serve as a reference point.

3. RESULTS

3.1. High level of mitochondrial purity

Prior to proteomics investigation, the genotypes of the mice were validated (Figure 15A). Having confirmed the genotypes, liver mitochondria from the HET and WT mice were isolated and enriched. Purity assessment of the mitochondria-enriched fractions is important to establish the level of contamination of other cellular compartments. As shown in Figure 15B (CM fraction), an enrichment of mitochondrial proteins can be observed using simple density differential centrifugation.

To further purify this fraction, density differential centrifugation followed by ultracentrifugation with discontinuous Percoll™ gradient was employed, which separates molecules purely by its density and not by particle size. This Percoll™-purified mitochondrial fraction demonstrated a high abundance of cytochrome c oxidase subunit IV (COX IV), and an apparent lack of lysosomal, endoplasmic reticulum, or peroxisomal markers, indicating a high degree of purification of mitochondria (PM fraction, Figure 15B).

3.1.1. Comparative proteomics of HET liver mitoproteome by 2D-DIGE

To detect a large range of proteins including low molecular weight proteins, 2-D DIGE analysis was conducted on 13% polyacrylamide gels using a p*I* range of 3 to 11. A total of approximately 1500 protein spots were found on the 2D-DIGE gels (Figure 16B). In 2D-DIGE, WT and HET mouse hepatic mitochondria lysate were labelled with three fluorescent dyes, *i.e.*, Cy2, Cy3, and Cy5, before the IEF step.

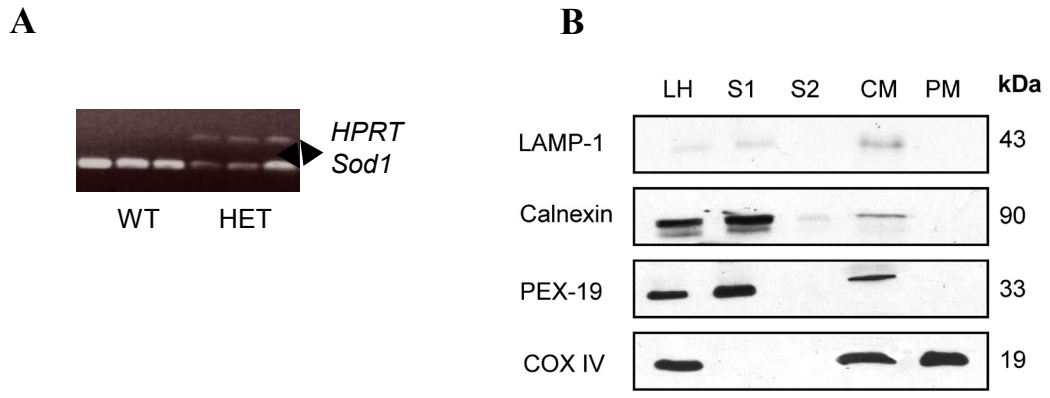

Figure 15. Assessment of genotype and mitochondria purification
(A) Genotyping of mice used for proteomic analysis. Hypoxanthine phosphoribosyltransferase minigene (HPRT) was used to replace part of exon 1 of *Sod2*. (B) Immunoblots demonstrating a high degree of purification of hepatic mitochondria used for proteomics analysis. At each step of the Percoll purification, fractions were collected and the proteins probed with antibodies against markers of lysosomes (LAMP-1), endoplasmic reticulum (calnexin), peroxisomes (PEX-19), and mitochondria (COX IV). LH, liver homogenate; S1 and S2, first and second-spin supernatants; CM, crude mitochondria; PM, purified mitochondria.

Protein spots that exhibited an average fold change of ≥ 1.5 as determined by DeCyder software were selected for further analysis. It must be stressed that in order to preserve biologically meaningful interpretations, a number of differentially expressed proteins that fell below the average fold change cut-off threshold were not accepted. On this basis, 57 proteins were found to be differentially modulated in the HET mouse as compared to the WT (Student's t-test $P < 0.01$). Among these, 57 proteins (46 unique spots and 11 redundant spots) were identified, while two failed to be identified by MS (Supplemental Table 1; Figure 16). However, about three-quarters of these proteins were affected mildly, with only one being highly modulated (Figure 20A). The proteins identified above are involved in a wide range of pathways and biological processes (Figure 20B). Also, of the 54 proteins, a large number (58%) increased in abundance. Collectively, this has led to the proposition that the extent of oxidative stress within the HET mitochondria has not reached a critical threshold that would adversely impact the mitoproteome. Most of the proteins identified have expectation values ≤ 0.05 and at least one MS/ MS expectation value ≤ 0.05. Although enoyl-CoA hydratase has a protein expectation value > 0.05, its best MS/MS score is 33 (expectation value = 0.088) with a relatively good *y*-ion series assignment (Figure 17; Appendix Figure 45). Thus it was included as a positive identification. Another spot was identified as 3-hydroxyisobutyrate dehydrogenase and hydroxymethylglutaryl-CoA synthase. 3HIDH has a protein expectation value of 0.0071 and best peptide score of 32 (expectation value = 0.13), with a relatively good *b*-ion-series assignment. Hydroxymethylglutaryl-CoA synthase has a protein expectation value of 0.11 and best peptide score of 33 (expectation value = 0.069) with a relatively good *b*-ion-series assignment. Together, both 3-hydroxyisobutyrate

dehydrogenase and hydroxymethylglutaryl-CoA synthase were therefore included as positive identifications (Appendix Figure 44 and Figure 46). However, which of these two proteins contributed to the calculated fold change could not be determined.

First, there was confirmation of lower SOD2 expression in the HET mice (*FC* = 2.17 *versus* WT) as a result to the partial ablation of the *Sod2* allele (Figure 18). This is consistent with a 50–55% decrease in SOD2 activity and a decrease immunoreactivity of immunoblots found in other studies (Li et al., 1995, Ong, et al., 2006, Van Remmen et al., 1999). Subsequently, SOD2 was used as an internal control, supporting the use of 2D-DIGE/MS as a valuable tool in quantifying changes in protein expression. Interestingly, mitochondrial SOD1 abundance level was also decreased by 1.77-fold (Figure 18). In contrast, other redox-sensitive proteins with antioxidant activity were up-regulated or increased in abundance; GPX1 and catalase levels increased by 2.01- and 1.73-fold respectively (Figure 18), thus indicating a mildly pro-oxidant environment in the liver mitochondria of the heterozygous mutants. To further validate the observed differences in protein expression from 2D-DIGE/MS, the levels of three crucial enzymes (SOD1, SOD2, and GPX1) by 2D immunoblotting was examined. The results clearly show that both SOD1 and SOD2 amounts were decreased in the HETmice, whereas GPX1 amounts increased, corroborating our MS analysis (Figure 18).

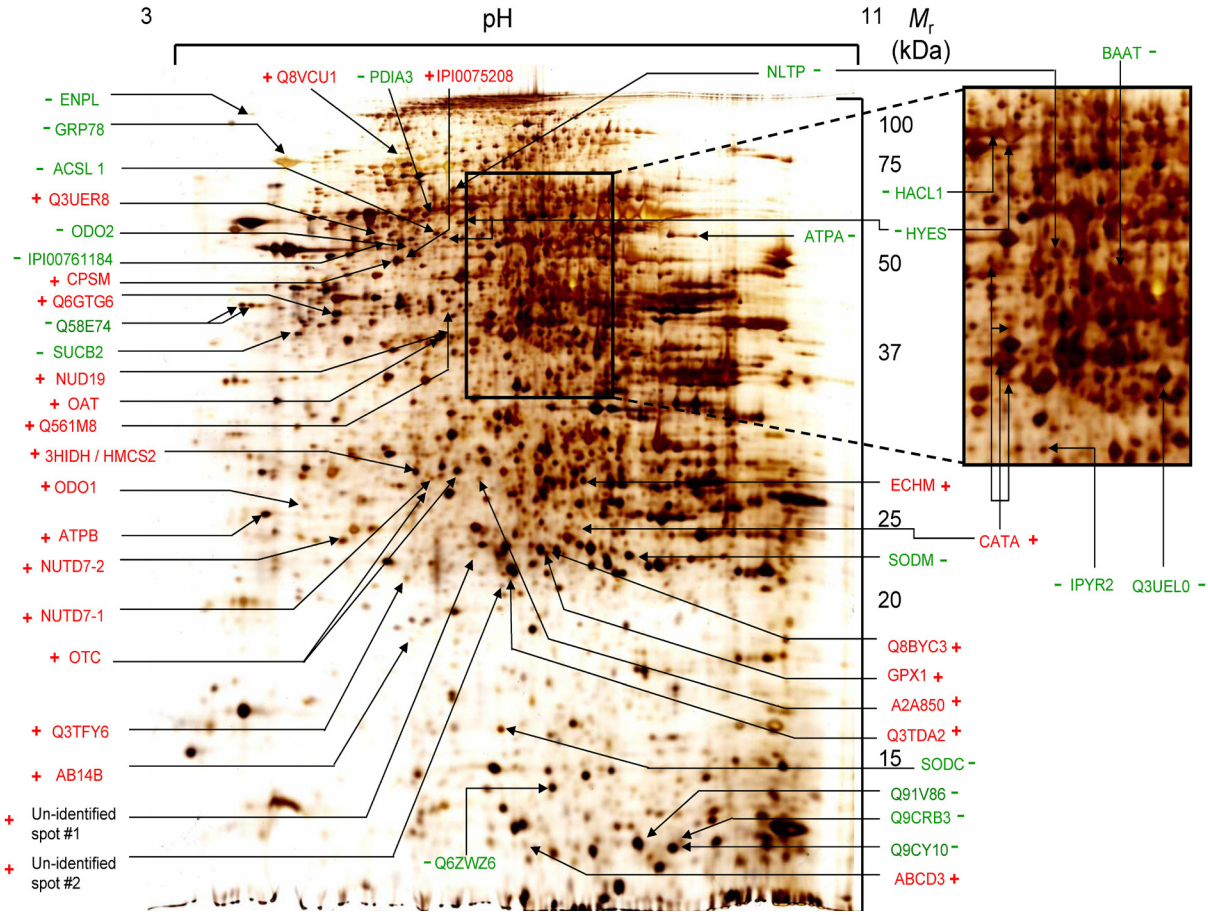

Figure 16. Representative proteome map of mouse liver mitochondria.
Mitochondrial proteins were separated on a 13% gel and identified using MALDI TOF/TOF-MS/MS. Annotations of differentially modulated proteins indicated on the silver-stained proteome map are shown in Supplemental Table 2. – correspond to proteins level that decreased in abundance in the HET mouse while + correspond to proteins that increased.

A

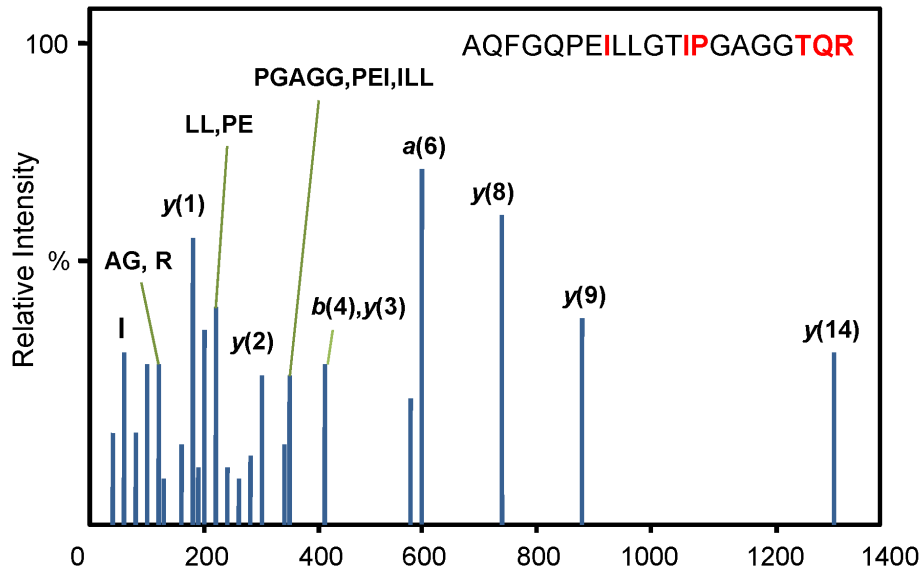

B

Seq.	y	#
A		21
Q	2040.1	20
F	1912	19
G	1765	18
Q	1707.9	17
P	1579.9	16
E	1482.8	15
I	1353.8	14
L	1240.7	13
L	1127.6	12
G	1014.5	11
T	957.51	10
I	856.46	9
P	743.38	8
G	646.33	7
A	589.31	6
G	518.27	5
G	461.25	4
T	404.23	3
Q	303.18	2
R	175.12	1

Figure 17.Tandem mass spectrum of enoyl-CoA hydratase generated from MALDI-TOF/TOF MS/MS.
The relatively good *y*-ions series (bold red) and a good match of a majority of intense peaks make it a reliable assignment despite a low protein and ion score in (A) the MS/MS spectrum and (B) the table showing the m/z of fragment ions.

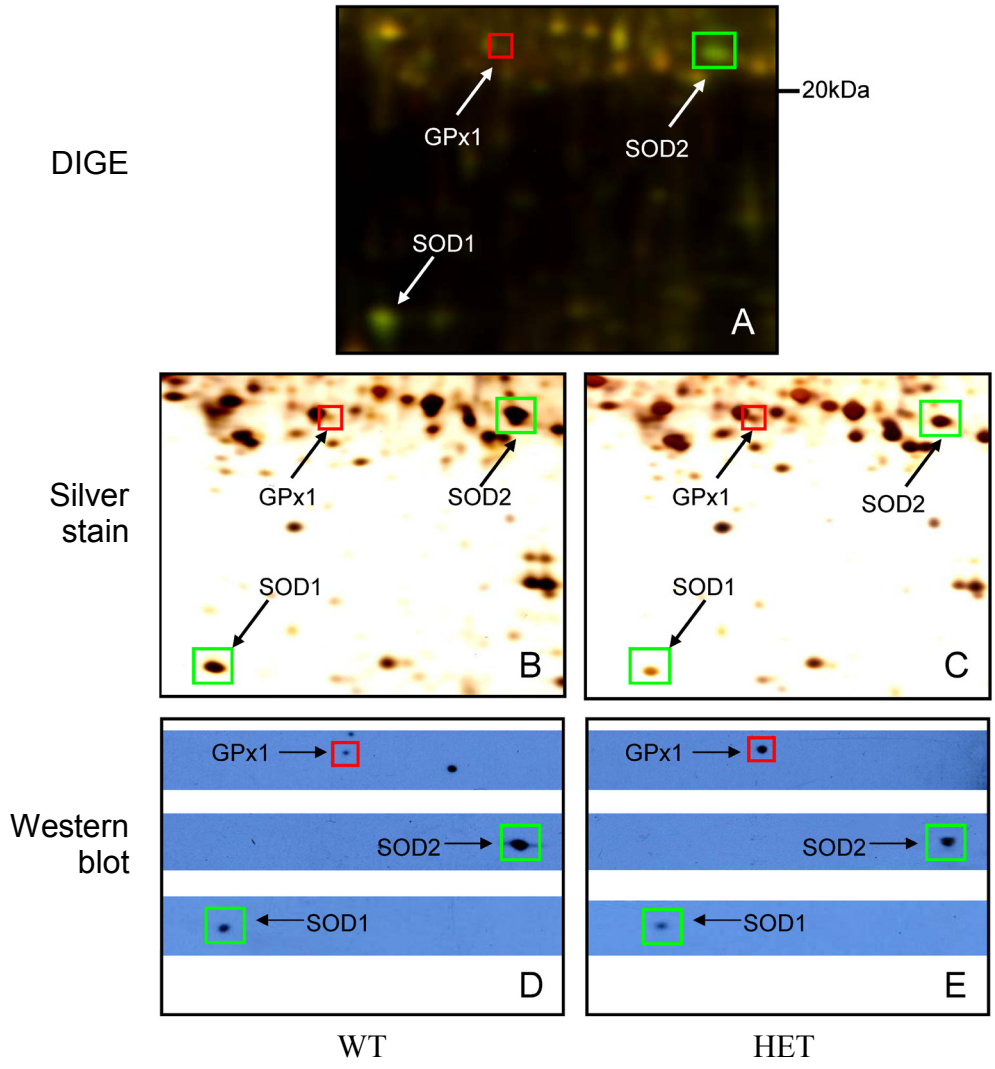

Figure 18. Comparison of SOD1, SOD2, and GPX1 abundance levels by DIGE, silver-staining of DIGE gel, and immunoblotting.
(A) Decreased abundance of SOD1 and SOD2 (green spots) and increased abundance of GPX1 (red spot) by DIGE imaging. (B & C) Silver staining; the arrows correspond to the gel spots on DIGE gel. (D & E) Verification by immunoblotting of selected spots was used to validate the MS results.

Interestingly, other proteins that are normally considered to be very sensitive to oxidative stress were unaltered in their expressions/abundances. For example, Complex I and ACO2 are sensitive to oxidative damage due to their [4Fe-4S] clusters (Gardner et al., 1995), yet ACO2 and thioredoxin-2 abundance levels were not altered within the defined 1.5-fold threshold. This was determined by 2D immunoblot analysis with antibodies directed against these proteins, which showed no significant difference between their amounts in mitochondria isolated from HET or WT liver (Figure 19). Certain mitochondrial enzymes involved in energy metabolism were also altered in the HET mice. For example, succinyl-CoA ligase (β-chain) and E1k and E2k components of a-ketoglutarate dehydrogenase (KGDH) were also affected. Furthermore, the decreased abundance of long-chain fatty acid-CoA ligase 1 and inorganic pyrophosphatase 2, the first and second enzymes of the β-oxidation cascade, points toward a down-regulation of fatty acyl β-oxidation in the liver mitochondria.

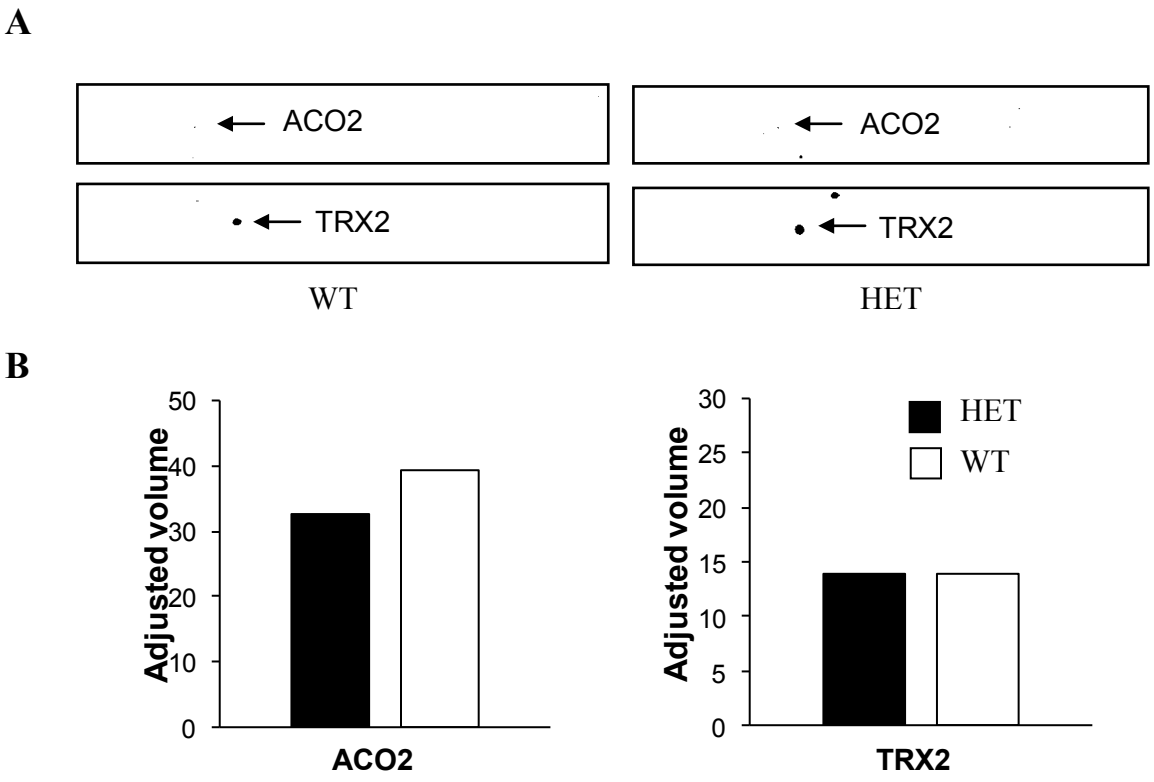

Figure 19. Immunoblotting of thioredoxin-2 and aconitase-2
(A) To ascertain effects of oxidative stress-sensitive ACO2 (*M*r = 85 kDa, p*I* = 8.08) and thioredoxin-2 (TRX2; *M*r = 18 kDa, p*I* = 7.73) in HET mouse, immunoblot analysis was used. (B) Densitometric analysis demonstrated that both mitochondrial proteins were insignificantly differentially expressed relative to WT mouse.

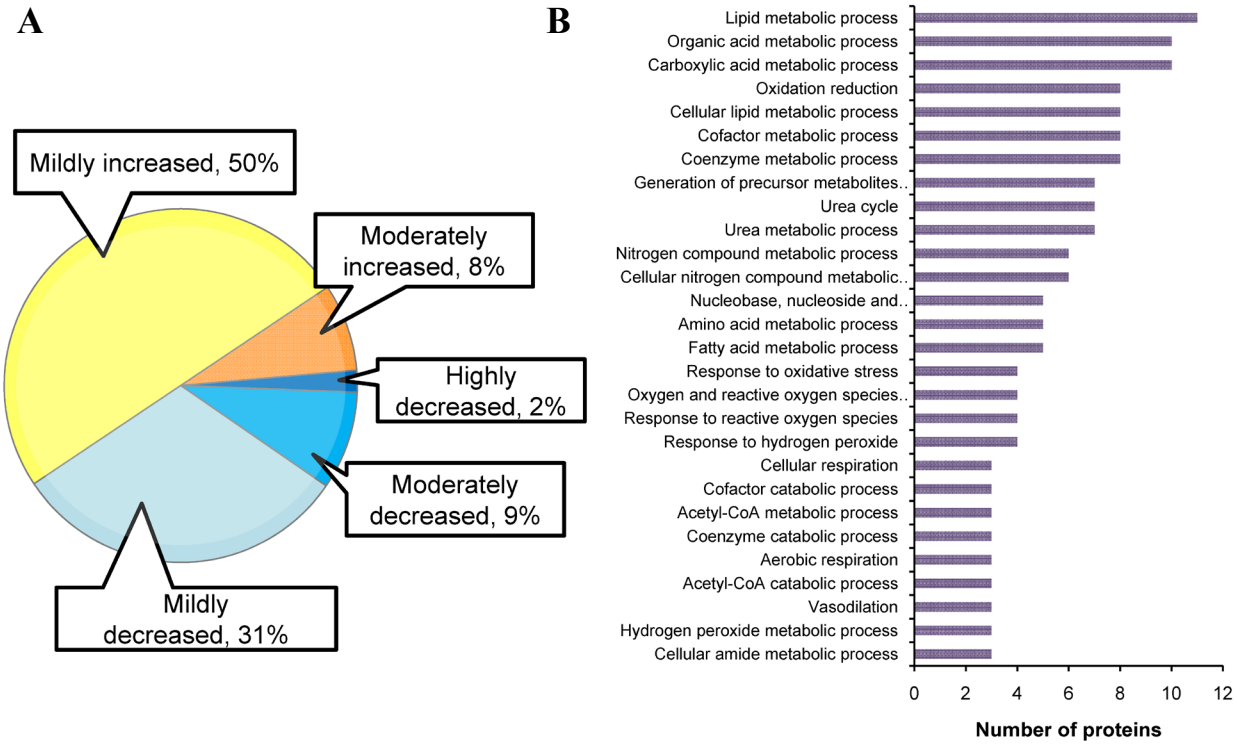

Figure 20. 2D-DIGE observations of HET hepatic mitochondrial proteome.
(A) Pie chart depicting the proportion of mildly, moderately or highly differentially modulated HET mitochondrial proteins relative to WT mouse. The low percentage of highly differentially modulated proteins versus a large majority of proteins that were mildly differentially modulated suggests a subtle pro-oxidant status within the mitochondria. (B) Classification of differentially modulated proteins identified by 2D-DIGE coupled to MALDI-TOF/TOF MS/MS according to GO "biological process" ($P < 0.001$).

3.1.2. Quantitative proteomics HET liver mitoproteome by 4-plex iTRAQ™

The 4-plex iTRAQ™ chemical labelling methodology coupled to 2DLC-MS/MS permitted the running of duplicate experiments to control for reagent bias as well as to increase statistical confidence. In the absence of IEF, membrane and hydrophobic proteins are expected to be better represented using chemically-labelled, MS-based proteomics. A large number of proteins from the inner and outer mitochondrial membranes were obtained using iTRAQ™ coupled LC-MS/MS approach (Figure 21A). A total of 321 proteins was identified positively with high confidence using a stringent set of criteria of Unused ProtScore ≥ 2 (C.I. = 99%) and identification was based on two tryptic peptides of which at least one unique peptide is of high confidence (>99%) and 5% "instantaneous" FDR at protein level. At a less stringent selection criterion of 5% "aggregate" FDR, 416 proteins were identified from the same set of data. Although "aggregate" FDR estimations generated a higher number of protein identifications, this set of proteins are more likely to contain more false positives than the more conservative "instantaneous" FDR (Tang, et al., 2008). Low reporter ion intensity resulted in less robust quantification whereas higher ion intensities contributed to more accurate and reliable quantification; hence one-tailed cut-off at the 5^{th} percentile to restrict peptides of low reporter ion signals was applied (Figure 14A). The reproducibility of the proteome-wide quantification analysis to detect *Sod2* haplodeficiency was tested (Pearson $r = 0.69$, $P = 1.33 \times 10^{-36}$; Figure 21B). Next the robustness and specificity of the MS-based analysis was verified by confirmation of the HET heterozygosity ($FC = 0.527$, Figure 22A). Following this, the extent to which the proteins were responsive to the partial loss

of the *Sod2* allele was quantified (Supplemental Table 4). To ascertain the accuracy of MS quantification, selected mitochondrial proteins were validated by immunoblotting. The fold changes of 9 out of 9 selected proteins were confirmed which was consistent with MS results (Figure 22B). This also demonstrated the critical need for manual filtering that underpinned the accuracy of MS analysis.

Next the question of whether the apparent homeostatic maintenance of the HET hepatic mitoproteome was maintained in part by the antioxidant enzymes housed within the mitochondria to curtail redox imbalance was assessed. Glutathione (GSH; L-γ-glutamyl-L-cysteinylglycine), one of the major protective molecules against elevated free radicals is regulated by a network of enzymes and oxidoreductases (Fernandez-Checa & Kaplowitz, 2005). From the mass spectrometric survey, the amounts of glutathione S-transferase kappa 1 (GSTK1) and microsomal glutathione S-transferase increased (MGST is also found in the mitochondria; *FC* = 0.71 and 0.70 respectively), thus suggesting increased recycling of mGSH to restore redox equilibrium. Consistent with 2D-DIGE results, GPX 1 was up-regulated (Figure 18). Mitochondrial GSH (mGSH) depletion is a hallmark of oxidative stress. Subsequently, endogenous mGSH levels of WT and HET mice were determined and there was no significant difference between both genotypes (Figure 22C).

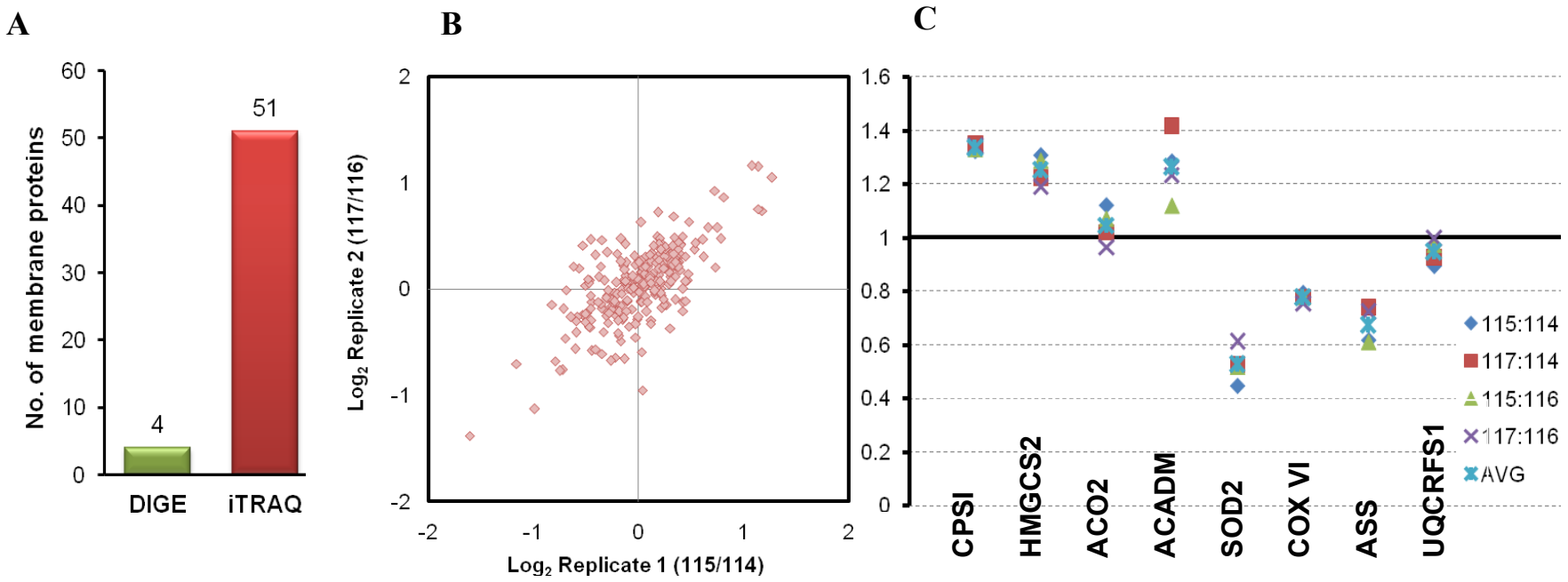

Figure 21. Global analysis HET mouse hepatic mitochondrial proteome by 4-plex iTRAQ™.
(A) Improvement in number of detected membrane proteins using iTRAQ™/LC-MS/MS. (B) Reproducibility of 4-plex iTRAQ™ (Pearson $r = 0.69$, $P = 1.33 \times 10^{-36}$). (C) Duplicate analysis of the same samples labelled with different iTRAQ™ reagents demonstrate high degree of reproducibility in detecting fold change and low level of regent-specific biasness. Random mitochondrial proteins were selected for the comparison. ACADM, medium-chain specific acyl-CoA dehydrogenase; ACO2, aconitate hydratase; ASS, argininosuccinate synthase; CPSI, carbamoyl-phosphate synthase; COX VI, cytochrome *c* oxidase subunit VIb; HMGCS2, hydroxymethylglutaryl-CoA synthase; UQCRFS1, ubiquinol-cytochrome c reductase core protein 1.

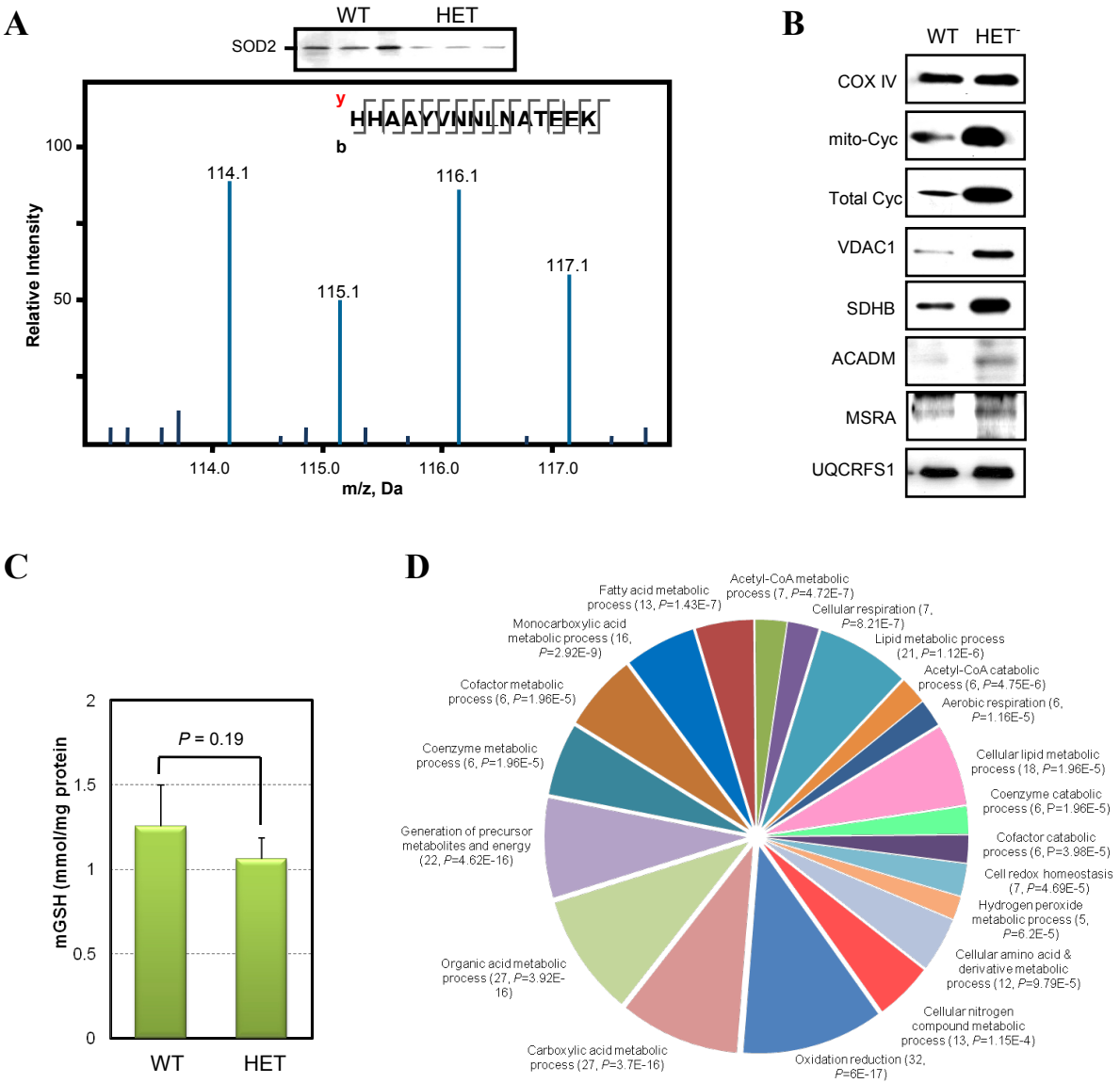

Figure 22. Enrichment of function of proteins responsive to *Sod2* haplodeficiency.

(A) Immunblot agrees with iTRAQ™ quantification of SOD2. Note that channels 114/115 and 116/117 form a pair of replicates. (B) Validation of selected detected mitochondrial proteins by immunoblotting demonstrates accuracy of mass-spectrometry results. (C) Mitochondrial GSH levels isolated from WT and HET mice (n = 4, two-tailed Student's t-test). (D) The 134 hit proteins from the 2D-DIGE and iTRAQ™ analysis were classified into molecular function categories for mouse genes according to the Gene Ontology classification system. Proteins for which no annotations could be assigned were excluded from the analysis for both the hits and the global set. The number of proteins assigned to each category and enrichment adjusted P values ($P < 0.01$) are shown in brackets.

To fully describe the mitoproteome changes, DIGE and iTRAQ™ fold change values are to be transformed before they can be combined and analyzed together. Because measures of fold change were different in the two methods as shown below (Equations 5-7), the fold change values were standardised and expressed as percentage fold change.

2D-DIGE fold change:

$$\text{if } \frac{y}{x} > 1, \qquad E = (R - 1) \times 100 \tag{Eq.5}$$

$$\text{if } \frac{y}{x} < 1, \qquad E = (1 + \frac{1}{R}) \times 100 \tag{Eq.6}$$

iTRAQ™ fold change:

$$E = (1 - R) \times 100 \tag{Eq.7}$$

where:

- y is the normalized spot volume to the HET mouse,
- x is the normalized spot volume to the WT mouse,
- E is the percentage expression ratio and
- R is the average fold ratio reported by the particular platform.

3.1.3. Combined proteomic analysis using 2D-DIGE and iTRAQ™ labelling

Using two independent and technologically different proteomic platforms is a formidable way of comprehensively describing the mitochondrial proteome in a global view by minimising individual technological shortcomings, complementing each other so as to potentiate the total proteome profile. By combining the number of proteins detected by the two unbiased proteomic screens, the HET liver mitochondria profile of differentially modulated proteins (detected with high statistical confidence) was expanded.

Gene Ontology or GO over-representation analysis of detected proteins revealed 'oxidation reduction' as the top biological process in terms of gene products number *and* confidence level for total and positively modulated proteins (32 proteins, $P = 6 \times 10^{-17}$; Figure 23). Biologically, this is not unexpected as the singular loss of the *Sod2* allele will result in fluctuations of proteins that are involved in redox activities. It was surprising, however, to see lipid metabolism ranking high in the GO analysis (12 proteins) – ACADM, acyl-Coenzyme A oxidase 1, acyl-CoA synthetase family member 2, acyl-CoA synthetase long-chain family member 1, acyl-coenzyme A synthetase isoform 2, ATP synthase subunit beta, catalase, carnitine *O*-palmitoyltransferase 2, delta(3,5)-Delta(2,4)-dienoyl-CoA isomerase, enoyl-CoA hydratase, GPX1, hydroxymethylglutaryl-CoA synthase. Further evidence of altered glutathione cycling ($P = 1.19 \times 10^{-5}$) was also demonstrated in this over-representation analysis (Figure 23). Proteins under negative modulation were classified into classes that are predominantly involved in maintaining

homeostasis, including redox homeostasis. Apart from SOD1 and SOD2, thioredoxin domain-containing protein 4, thioredoxin domain-containing protein 5, protein disulfide isomerase associated 4 and PDIA 5 were listed under 'redox homeostasis'. While these proteins are generally not annotated to the mitochondrion (Pagliarini et al., 2008), the mitochondria form interacting networks with the endoplasmic reticulum to facilitate Ca^{2+} uptake and mitochondrial lipid synthesis (de Brito & Scorrano, 2008, Rizzuto & Pozzan, 2006), and these proteins might be mitochondrial-associated proteins, or could be just contaminants.

Taken together, these results imply that despite an increase in the level of ROS within the HET mouse mitochondria, it is insufficient to elicit major perturbations in the mitoproteome, possibly attenuated by adjustments made in the mitochondria. This is compatible with the alternative hypothesis of using a phenotypically normal mouse model but with clinically silent redox abnormalities for picking up mitochondrial toxic effects (Dixit & Boelsterli, 2007).

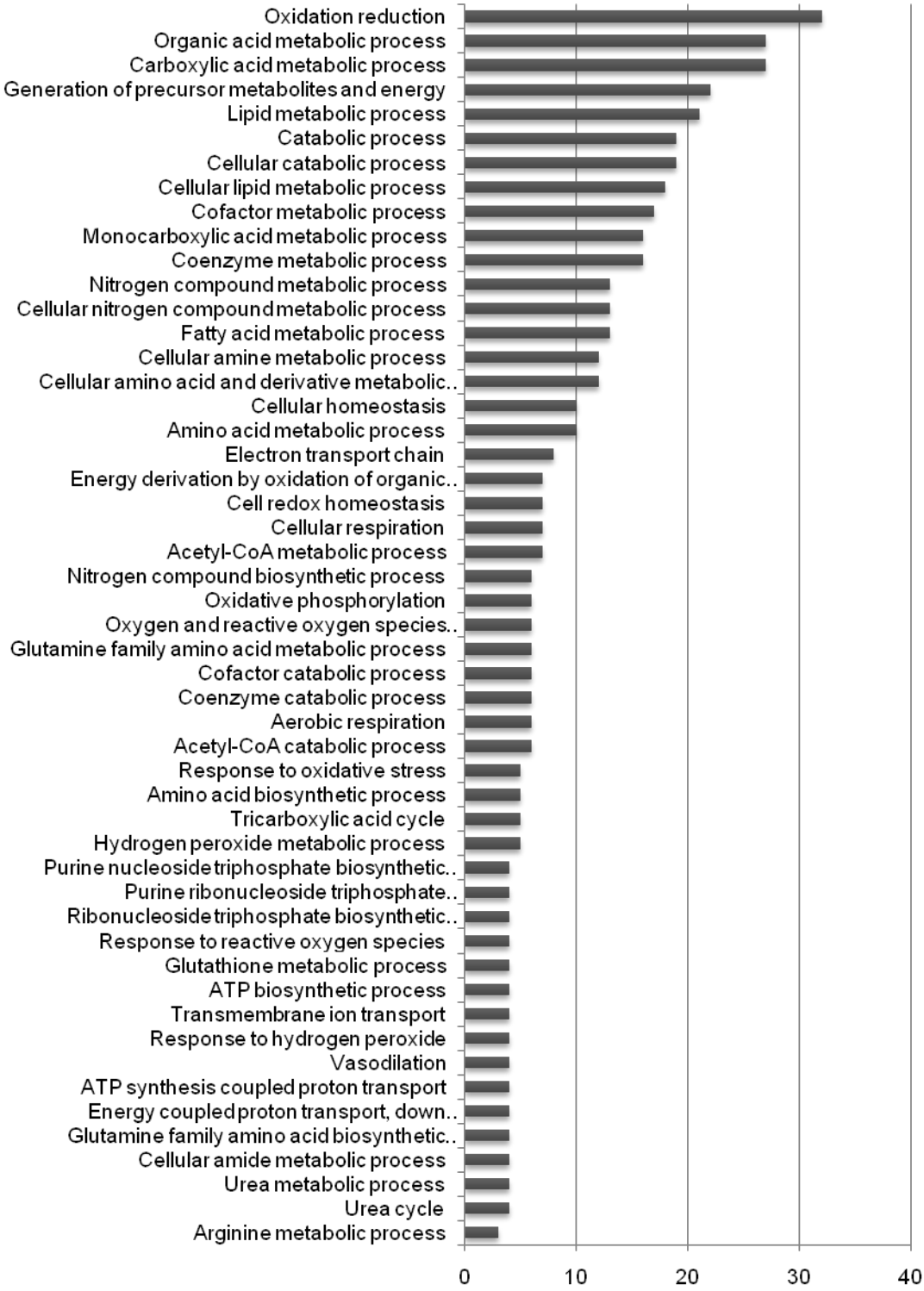

Figure 23. Classification of HET hepatic mitochondrial proteins based on GO annotation

Number of proteins are represented on the x-axis.

3.2. Prolonged troglitazone administration causes oxidative stress in mitochondria and moderate liver injury in HET mice

Genotyping verified *Sod2* haplodeficiency in all the mice used for the toxicity study (Figure 24A). Histopathological evaluation revealed the presence of small areas of hepatic necrosis (4/6 mice) in the 4-week troglitazone-treated group (Figure 24B), while no such alterations were seen in the 2-week drug-treated or in all vehicle controls (Table 8). This indicates that the small repeated doses of troglitazone cause a delayed-type moderate hepatocellular injury which is not yet manifested after 2 weeks. Although no significant increases in serum ALT activity was observed between 4 weeks troglitazone-treated mice and the vehicle controls ($P = 0.4$ and $P = 0.66$ respectively; Table 9), a general trend of increase in ALT activity was observed (47.73 U/L in 4-weeks TRG group versus approximately 33 U/L in the controls).

To quantify the depletion of mGSH with troglitazone administration, MCB was used as fluorochrome for sensitive detection of GSH. As shown in Figure 25A, in isolated HET hepatic mitochondria, mGSH levels were significantly depleted after 4 weeks of troglitazone administration ($P < 0.05$). By comparison, vehicle administration did not deplete mGSH levels, demonstrating the minimal adverse biological effects of 9% solutol and that mGSH depletion was a result of prolonged troglitazone treatment. Further, 2 weeks of troglitazone treatment did not significantly altered mGSH levels versus vehicle control (Figure 25A).

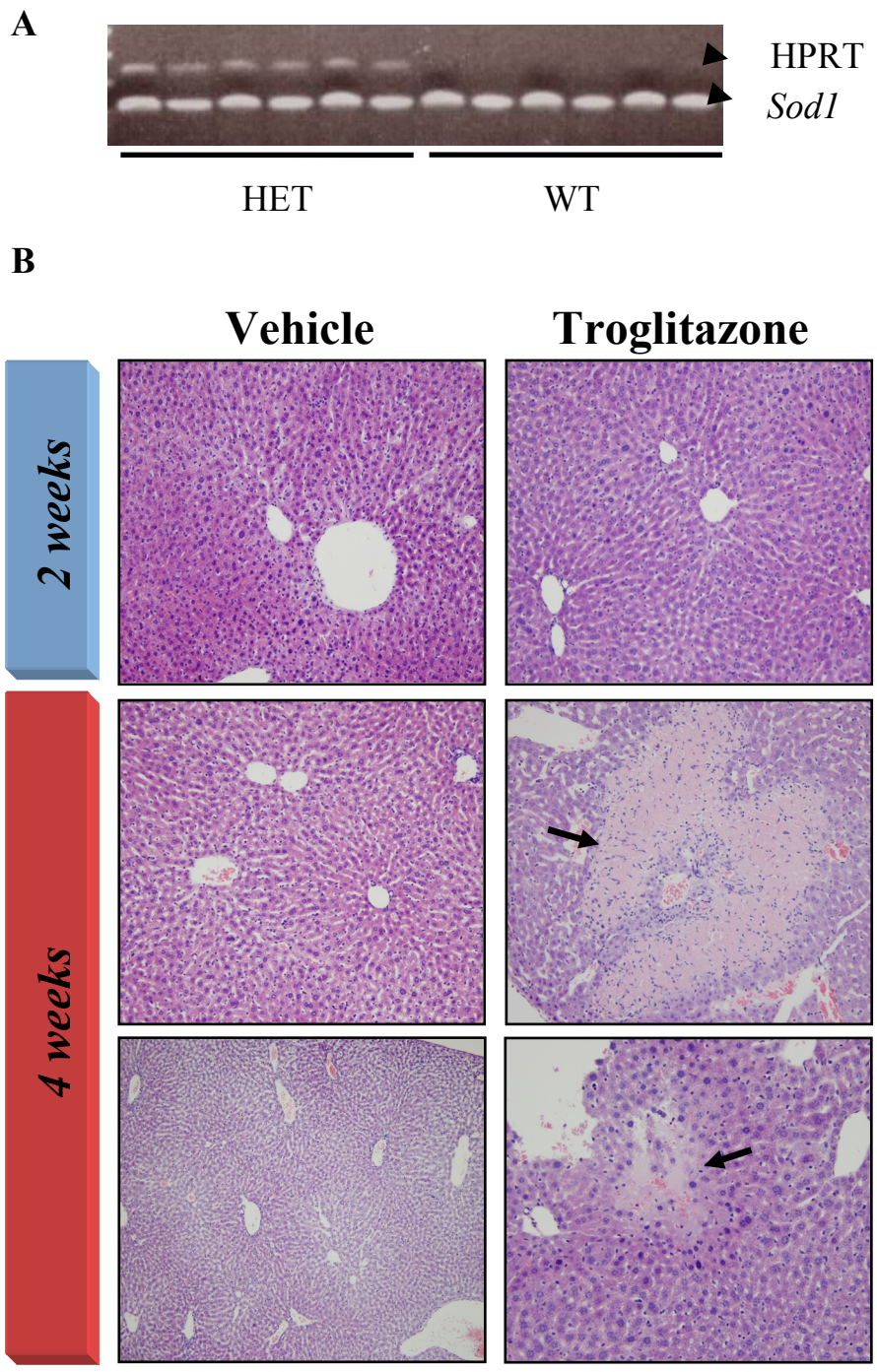

Figure 24. Liver histopathology in troglitazone-treated HET mice.
(A) Genotyping of WT and HET mice by PCR analysis before drug treatment showed the partial loss of *Sod2* allele. *Sod1* gene was used as a control. (B) Representative micrographs (H & E staining) showing areas of hepatocellular necrosis in 4 weeks troglitazone-exposed (original (black arrows), but not in 4 weeks vehicle-treated or 2 weeks-troglitazone treated mice (original magnification × 200)

Table 8. Hepatotoxicity score of HET mice treated with troglitazone for 2 or 4 weeks.

Histological sections were obtained from livers of mice treated daily with i.p. injections of troglitazone in 9% solutol. Mice were sacrificed after 14 or 28 days. Slides stained with H&E were reviewed under low and high power by two individuals.

	Histopathology types and scores																	
Treatment	Necrosis (Inflammation)						Apoptotic cells						Foci of infarction					
2 weeks																		
Vehicle control ($n = 3$)	0	1	0	-	-	-	0	0	0	-	-	-	0	0	0	-	-	-
Troglitazone, 30 mg/kg/day ($n = 3$)	1	0	0	-	-	-	0	0	2	-	-	-	0	0	0	-	-	-
4 weeks																		
Vehicle control ($n = 3$)	1	1	0	-	-	-	1	0	0	-	-	-	0	0	0	-	-	-
Troglitazone, 30 mg/kg/day ($n = 6^{\dagger}$)	1	5	3	1	2	3	1	5	2	1	2	2	1	0	0	1	0	0

Hepatocellular degeneration was graded based on frequency of occurrence regardless of extent of damage i.e. 0 (no occurence); 1 (stated degeneration occurring once) and so on. Values are total number of animals featuring the indicated score. † A larger number of mice were administered with 30 mg/kg troglitazone to account for any potential deaths resulting from the hepatotoxic effects of troglitazone.

Table 9. Biochemical and clinical chemistry properties of female HET mice

	2 weeks, VEH	2 weeks, TRG	4 weeks, VEH	4 weeks, TRG
n	3	3	3	6
Age (weeks)	12.3±2.52	11.3±3.06	10.7±2.08	11.7±3.27
Weight (g)				
Week 0	21.2±1.31	19.6±0.80	20.33±1.67	20.95±1.77
Week of Sacrifice*	18.3±1.11	17.3±1.04	19.5±2.15	18.165±1.06
ALT (U/L)	40.47±1.29	33±7.79	33.67±5.78	47.73±23.1
AST (U/L)	160.4±40	121.4±28.9	126.5±40.7	139.9±41.8
Creatinine (μmol/L)	14.5±0.52	14.33±0.9	13.83±1.85	11.98±1.55

* Mice from Groups 1 and 2 were sacrificed after 2 weeks and mice from Groups 3 and 4 were sacrificed after 4 weeks. All differences across groups were statistically insignificant (two-tailed Student's *t*-test, $P > 0.05$). Data presented shows the mean ± standard deviation.

A hallmark of ROS-induced protein modification is the addition of carbonyl groups to the amino acid side chains of proteins. The stability, early formation and irreversibility make protein carbonyls an excellent biomarker of protein oxidation (Alamdari et al., 2005, Nystrom, 2005). Total hepatic mitochondrial protein carbonyls increased significantly in HET mice treated with troglitazone for 4 weeks as compared to 2 weeks (41%, Student's *t*-test, $P < 0.05$; Figure 25B). Prolonged troglitazone treatment in HET mice resulted in increased production of NO levels, determined by liver homogenate levels of its metabolites nitrate and nitrite (Figure 25C; Student's *t*-test, $P < 0.01$). 3-NT is a relevant biomarker of $NO^{\bullet}$-dependent oxidative stress, arising from unregulated increased $^{\bullet}NO$ production and its secondary intermediates such as $ONOO^{-}$ and $^{\bullet}NO_2$ (Abello et al., 2009, Radi, 2004, Souza et al., 2008). To investigate for protein tyrosine nitration, total hepatic mitochondrial proteins were assayed for 3-NT and were found to significantly increased in HET mice administrated for 4-weeks with troglitazone (Student's *t*-test, $P < 0.01$; Figure 25D). No significant increase in 3-NT was observed in the solutol-administered mice and mice administered with troglitazone for 2-weeks.

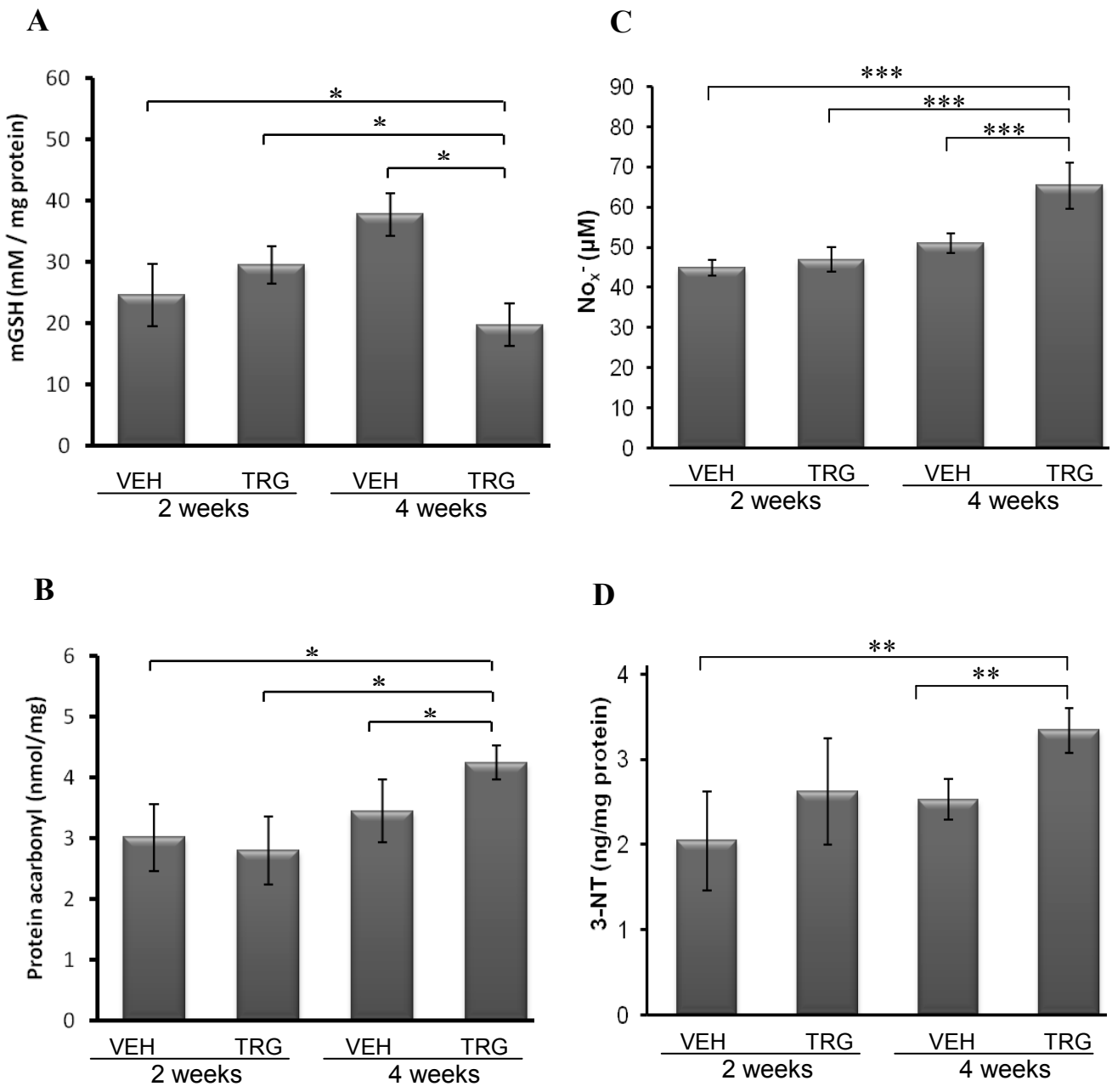

Figure 25. Prolonged troglitazone exposure leads to elevated •NO and mitochondrial oxidative stress.

(A) Mitochondrial GSH (mGSH) was depleted by two-fold after 4 weeks of administrating troglitazone to HET mice (Student's *t*-test, $n = 4$). The resultant loss of mGSH left the mitochondria less protected from the oxidation damaging effects of free radicals. (B) Protein carbonyls and (D) nitrotyrosine adducts (3-NT), established markers of oxidative damage to proteins were significantly increased after 4 weeks of troglitazone treatment. (C) The increase in 3-NT is due to •NO-dependent oxidative stress stemming from increased hepatic nitrate/nitrite levels and ROS (Student's *t*-test, $n = 3$) *$P < 0.05$, **$P < 0.01$, *** $P < 0.001$

3.3. HET Mitochondrial Proteome Dynamics induced by prolonged troglitazone treatment

3.3.1. 2D-DIGE Analysis of Troglitazone-induced HET Mitoproteome

To better understand the underlying mechanisms of this delayed toxicity and to identify potential early biomarkers of liver injury, the proteomics profiles after 2 and 4 weeks of treatment were analyzed. Using 2D-DIGE coupled with MALDI-TOF/TOF MS/MS analysis, the 2-weeks group showed that 24 proteins were differentially modulated relative to the corresponding vehicle controls, and that the vast majority (~80%) showed an increase in abundance ($FC \geq 1.45$, $P < 0.01$) (Figure 26, Supplemental Table 1). Specifically, a number of heat shock proteins, catalase, and Lon protease exhibited increased abundance levels which are commensurate with an adaptive response against mild oxidative stress (Douette et al., 2006, Maniratanachote, et al., 2005, Rabilloud et al., 2001). Among the proteins with decreased abundance, ACO2 was conspicuous, suggesting that a mild oxidant stress had actually lowered the levels of this exquisitely redox sensitive protein.

In contrast, the 4-week treatment with troglitazone affected a much larger number of mitochondrial proteins, and with a distinct proteome profile (Figure 26B). Specifically, among the 46 differentially expressed proteins, ~65% exhibited reduced levels as compared to vehicle controls ($FC \leq -1.45$, $P < 0.01$). For example, besides ACO2, catalase and the ATP synthase β-subunit (Complex V) also exhibited decreased abundance. It is likely that these changes have inflictions for mitochondrial function and

energy homeostasis. Some of these proteins, exhibiting decreased expression levels, may reflect decreases in the amounts due to more severe and sustained oxidant stress. It is also possible that a number of these proteins underwent modifications that were then selectively directed towards proteolytic degradation (Grune et al., 2003). On the other hand, a number of proteins exhibited increased expression levels. For example, VDAC, a component of Complex III, and SOD2. This likely points toward a compensatory up-regulation of critical (yet sensitive) components of the mitochondrial ATP biosynthesis machinery and antioxidant defence to cope with increased oxidative stress. Another important oxidoreductive stress-regulated mitochondrial protein is the redox sensor and antioxidant TRX2. TRX2 was not detected in 2D-DIGE, probably due to its small molecular mass (18 kDa). However, in a separate immunoblotting experiment using a high-percentage polyacrylamide gel, TRX2 abundance was positively modulated after 4 weeks, but not after 2 weeks.

The number of DIGE-detected overlapping proteins between 2-weeks and 4-weeks of troglitazone treated mice showed only 6 proteins (Supplemental Tables 2 and 3). This low number of overlapping proteins between the two time-points strongly suggested that the early effects on the liver, and also the toxic response, may be different from the latter effects. For some proteins, several distinct spots were identified on the gels, representing the same protein but featuring different isoelectric points or molecular weights (corresponding to the multiple entries in Supplemental Tables 2 and 3). These multiple spots suggested the occurrence of either different protein isoforms or post-translationally modified proteins. To validate the results from the MALDI-TOF/TOF

MS/MS analysis, 2D immunoblotting for selected proteins spanning a wide range of molecular weights were performed. Specifically, the abundance levels of five proteins: ACO2, CATA, OTC, SOD2, and VDAC1 (Figure 27) were examined. For the 2-week treated samples, the immunoblot for ACO2 exhibited a decrease in abundance, concordant with the MALDI-TOF results. Furthermore, the identity of HADH was confirmed, but not HIBCH due to a lack of commercially available antibody. As for 4-week treated samples, the identity of all five proteins and their relative change in expression levels were confirmed by immunoblotting.

3.3.2. Analysis of different ACO2 fates under different oxidative stress conditions

2D-DIGE was able to partially demonstrate the changes occurring in ACO2 protein modification and abundance (Figure 26, Supplemental Tables 1 and 2). In the 2-weeks study, the HET mouse was mildly sensitized to oxidative stress stemming from the toxicant, troglitazone. We observed a decrease in ACO2 abundance levels (~80 kDa), which becomes a substrate for Lon protease degradation under mild prooxidant conditions (Bota & Davies, 2002). Immunoblotting against ACO2 confirmed the 40 kDa band as cleaved ACO2 (Figure 28). This correlated well with the observation of increased Lon abundance. With prolonged troglitazone treatment and an increase in ROS, ACO2 should form aggregates. However, aggregated ACO2 (beyond the upper separation range of 2D gels of ~ 220 kDa) and Lon were not detected on the 2D-DIGE gels. By using a different approach, we were able to observe the aggregation of ACO2 after extended troglitazone administration (Figure 28). This is consistent with the three different fates of ACO2 under varying stages of oxidative stress (Bota & Davies, 2002, Delaval et al., 2004).

From these integrative proteomics results, the two-stage mitochondrial and cellular response complemented the potential of ACO2 as a potential biomarker for distinguishing varying degrees of mitochondrial redox status effects. While further in-depth studies are still required, ACO2 can be a promising oxidative stress marker for early detection as well as for diagnosing a biological system's redox status in response to oxidative insults.

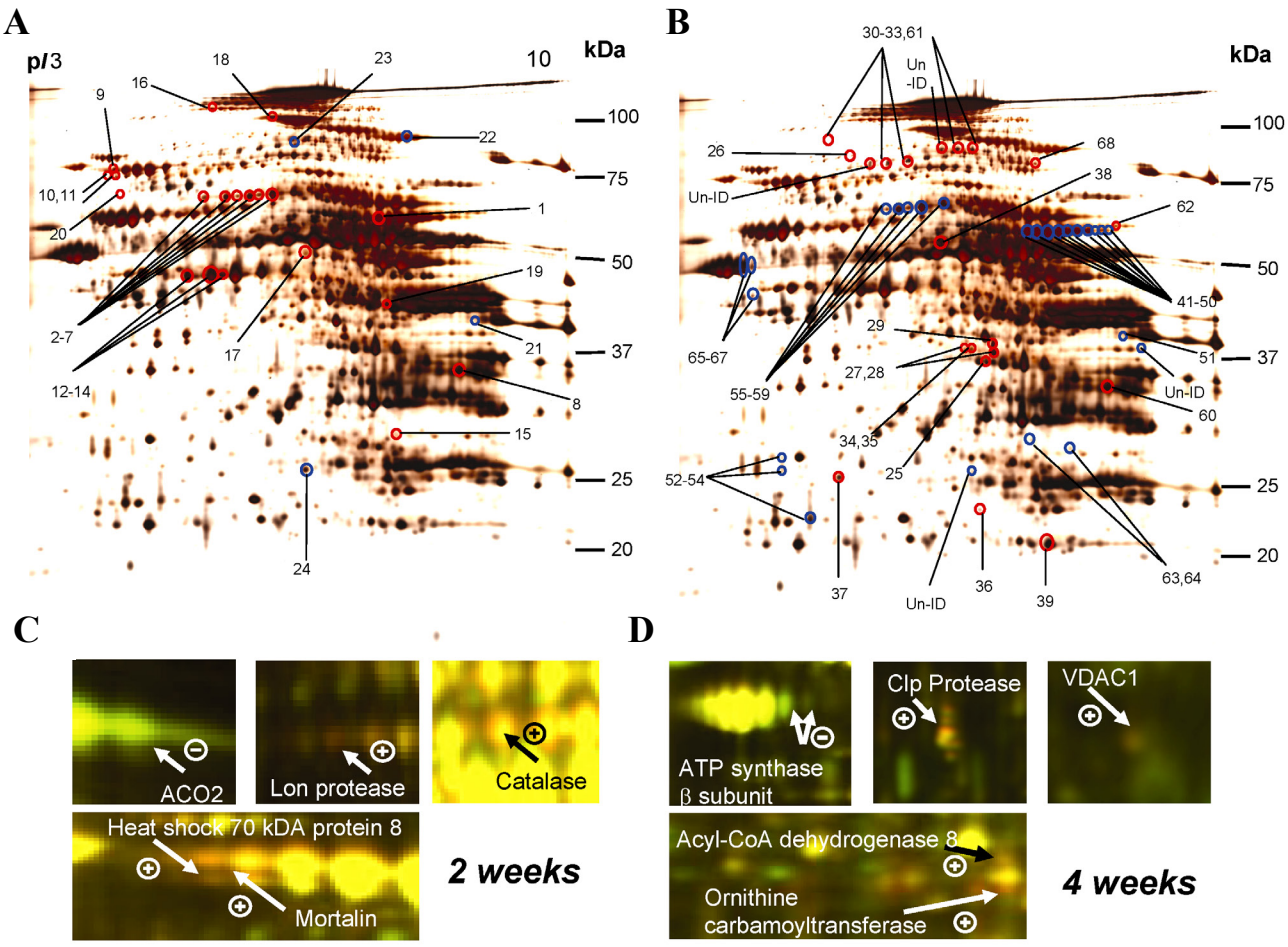

Figure 26. 2DE profile of HET mouse hepatic mitochondrial protein expression with solutol or troglitazone treatment.

Representation silver-stained (A, B) and DIGE profiles (C, D) of HET mouse hepatic mitochondrial protein expression after 2 weeks (A, C) or 4 weeks (B, D) treatment with troglitazone (30 mg/kg/day). +, increased amounts of protein relative to vehicle control; −, decreased amounts of protein relative to vehicle control. ACO2, aconitase-2; VDAC1, voltage-dependent anion channel-1. For numbering of proteins see Supplemental Tables 1 and 2.

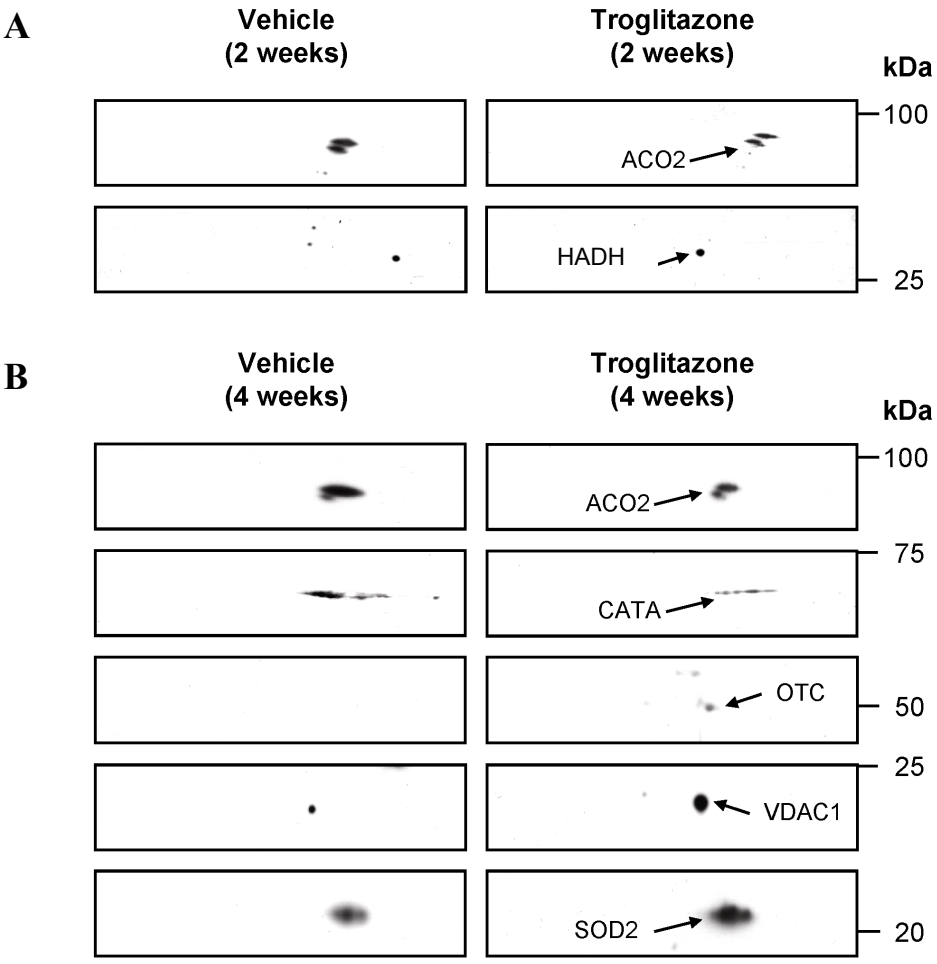

Figure 27. Validation using 2D immunoblotting.
Confirmation of MS results using 2D immunoblots on the differential expression of selected mitochondrial proteins after 2 weeks (A) or 4 weeks (B) troglitazone treatment. Note that while ACO2 and SOD2 isoforms and/or post-translational modifications were found to be differentially expressed on the immunoblots, 2D-DIGE only detected spots that were within the ≥1.45 fold change cut-off. ACO2, aconitase-2; CATA, catalase; HADH, hydroxyacyl-coenzyme A dehydrogenase; OTC, ornithine carbamoyltransferase; VDAC1, voltage-dependent anion channel-1; SOD2, superoxide dismutase-2.

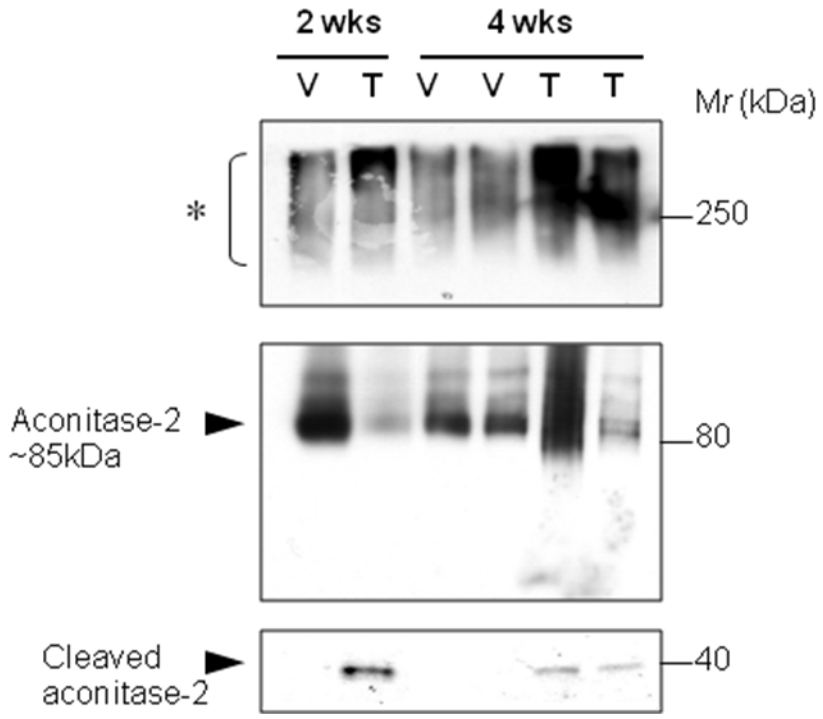

Figure 28. Varying fates of ACO2
ACO2 undertakes different forms with prolonged troglitazone administration and accompanying ROS levels in the HET mouse. Early administration with troglitazone already starts to induce ACO2 aggregation (> 100 kDa) and partial cleavage (~40 kDa; 2nd lane). With extended troglitazone treatment (4 weeks), large aggregation of ACO2 can be observed, in tandem with small amounts of non-aggregated and cleaved ACO2. (5th and 6th lanes). Arrowhead denotes the reduced amounts of ACO2 monomers and cleaved ACO2; ∗ denotes ACO2 aggregation. V, vehicle; T, troglitazone.

3.3.3. 8-plex iTRAQ™ Analysis of Troglitazone-induced HET Mitoproteome

The biasness of 2D-DIGE against certain classes of proteins is well-recognized (Hamdan & Righetti, 2002)) and the use of complementary proteomic approaches is an attractive way to adequately cover the proteome of any cell or organelle in depth (Andersen & Mann, 2006, Cox & Mann, 2007). Specifically, two main objectives were sought: (1) to gather a comprehensive proteome profile of the HET hepatic mitochondria upon challenge with therapeutic doses of troglitazone and (2) to determine which mitochondrial functional clusters were more sensitive to troglitazone-induced toxicity. 8-plex iTRAQ™ technology became available at a later part of this study and we adapted its multiplex chemical labelling for labelling the larger number of samples in this drug-treatment study.

Through quantitative MS analysis and post-MS acquisition filtering, approximately 277 proteins with high confidence (39 unquantified, total 314 detected proteins; Supplemental Tables 5 and 6) were quantified and a very good correlation between each set of technical replicates was found (channels 114/113 versus channels 116/115, Pearson $r = 0.79$, $P = 1.19 \times 10^{-57}$; channels 118/117 versus channels 121/119, Pearson $r = 0.91$, $P = 9.36 \times 10^{-111}$; Figures 33A and B). Identification of proteins was based on a stringent criteria which included that identification be based on the requirement of two tryptic peptides with at least one peptide unique to the protein sequence and not shared with any other database entry, 5% instantaneous FDR at protein level and finally Unused ProtScore ≥ 2 (99% C.I.).

An evaluation of the protein attributes of the detected proteins against the most complete list of mitochondrial proteins (Pagliarini, et al., 2008) revealed an undersampling of very basic proteins, low molecular weights and hydrophobic proteins (Figure 30). Nevertheless, the detected proteins followed the distribution of annotated mitochondrial proteins. In terms of functionality, the selection of detected proteins had the tendency to describe their functional clusters substantially, covering 44 out of 48 GO Slim terms annotated to the mitochondrial "Biological Process" (Figure 31).This permitted the investigation of which functional clusters were more susceptible to troglitazone mitotoxic effects and if these proteome changes correlated with alterations observed at the tissue level.

MS-based quantitative proteomics revealed 55 proteins (20.52%) that increased in abundance ($FC \geq 1.2$) as compared to 17 proteins (6.34%) that decreased in abundance ($FC \leq 0.833$) after 2-weeks of troglitazone administration (Supplemental Table 5; Figure 29C). In contrast, after 4-weeks of daily troglitazone administration, the proportion of mitochondrial proteins that increased versus those that decreased was markedly different, 22 proteins (8.21%) increased whereas 53 proteins (19.78%) decreased in abundance (Supplemental Table 6; Figure 29C). These results were therefore similar to the DIGE experiment. This therefore connoted a two-stage toxic phase: an early phase denoted by adaptory response to maintain mitoproteome homeostasis and a latter, sustained phase of mitoproteome changes that contributed to liver injury, as exemplified by confluent areas of hepatocytic death (Figure 24 and Figure 29D).

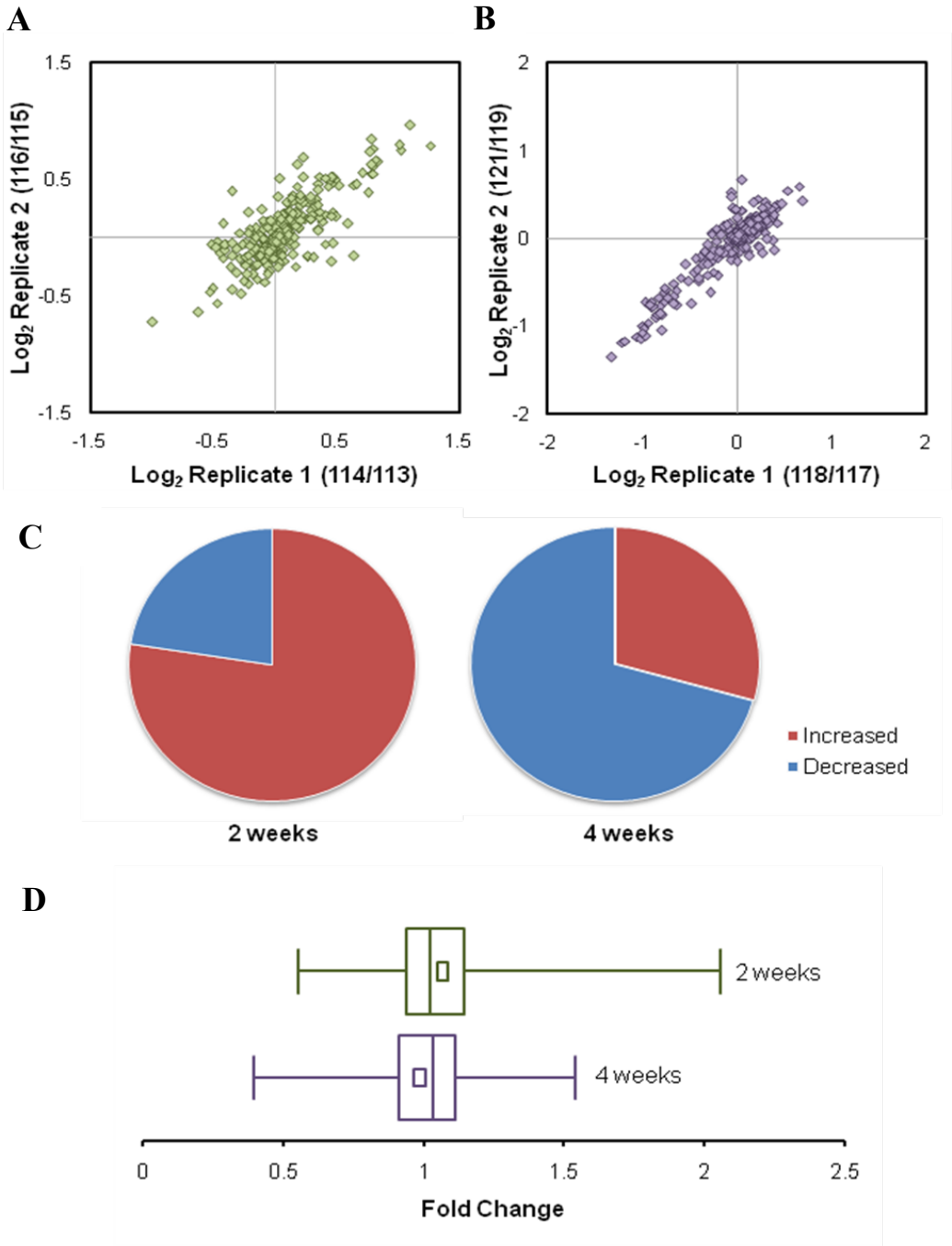

Figure 29. *Sod2* haplodeficiency delays troglitazone hepatotoxicity as revealed by quantitative proteomics.

(A and B) Linear regression of technical replicates show high levels of correlation and hence reproducibility of 8-plex iTRAQ™. (C) Pie charts showing the proportion of proteins that increased or decreased in abundance following 2 or 4 weeks of troglitazone treatment based on a threshold of 1.2 and 0.83. (D) Box plot of quantified proteins by iTRAQ™ for 2 weeks and 4 weeks study groups. Median - vertical line in box, interquartile range – box from end to end show 25% and 75% quartiles, minimum and maximum fold changes – whiskers and mean – insert box.

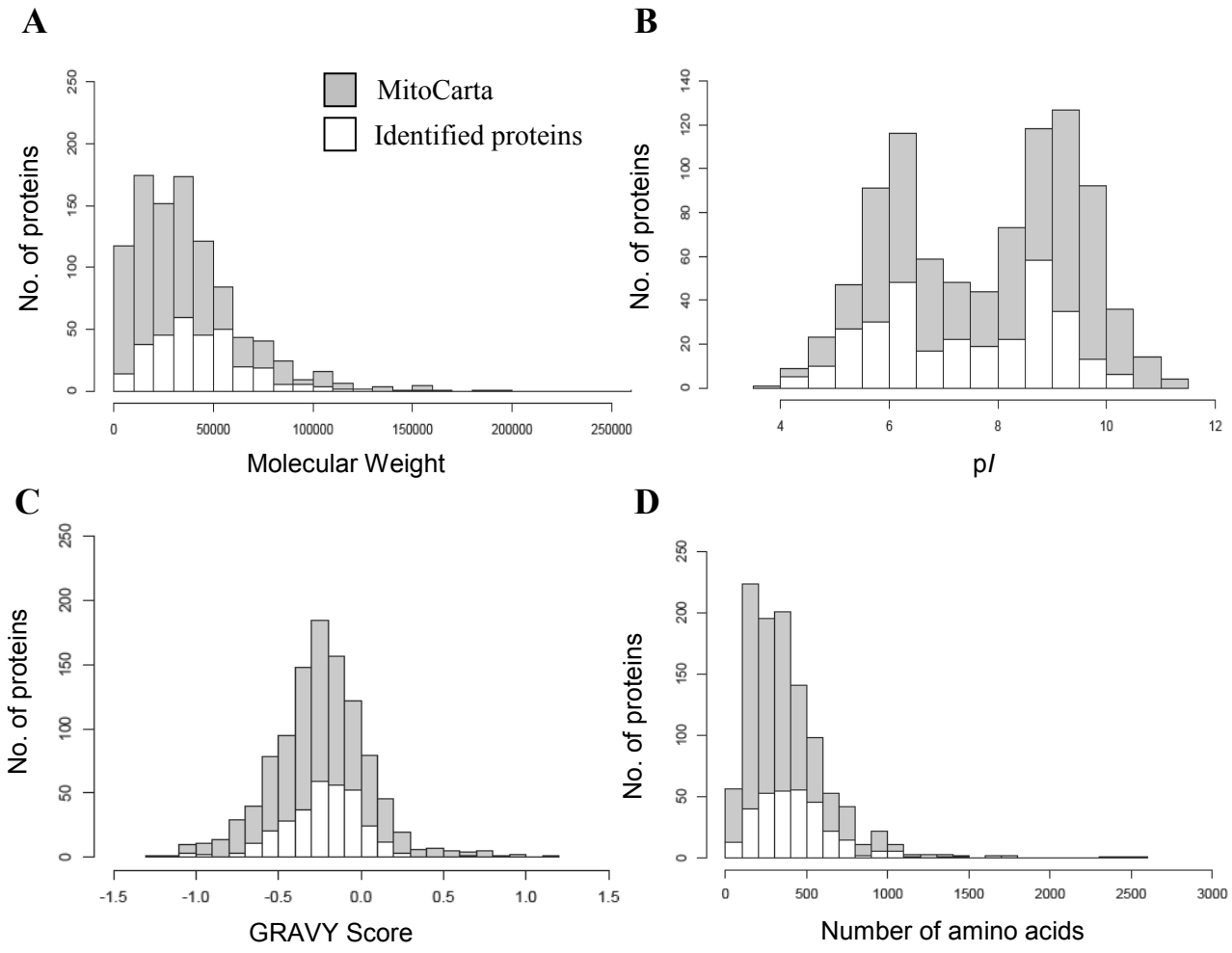

Figure 30. Bias analysis of protein attributes.
The detected proteins were classified according to their (A) molecular weight, (B) isoelectric point; p*I*, (C) hydrophobicity; the GRand AVerage hydropathicity or GRAVY score (a prediction of the hydrophobicity of a hypothetical translated gene product) and (D) length and compared against the 1098 annotated mouse mitochondrial genes fromMitoCarta (Pagliarini et al., 2008). Note that the detected proteins followed the distribution of annotated mitochondrial proteins, suggesting that the sampling was random and not biased towards proteins of any particular attribute.

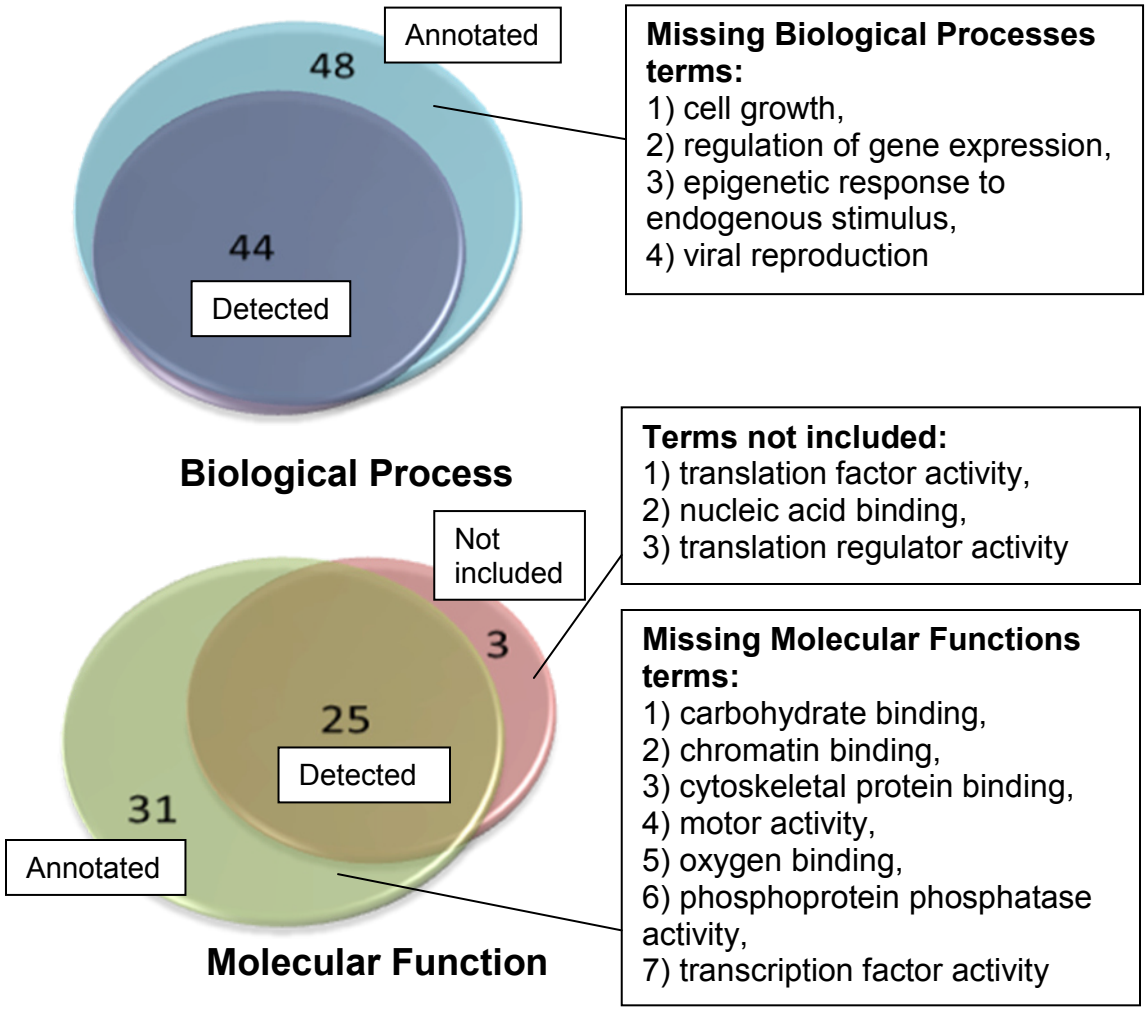

Figure 31. Pie charts of GO slim analysis.
GO slim analysis of detected mitochondrial proteins demonstrates substantial representation of functions annotated to the mitochondrion. Annotated GO terms not represented or included in our study (annotated excluding detected) were listed in boxes.

Using DAVID (Dennis, et al., 2003), we analyzed non-intersecting enriched biological functions as well as intersecting ones from the proteome dataset. Among the top-ranking and overlapping enriched KEGG functions, there was fatty acid metabolism ($P = 1.1\times10^{7}$) and expectedly, PPAR signalling ($P = 5.2\times10^{5}$) in both 2 and 4 weeks of troglitazone administration. Functions exhibiting over-representation in 2 weeks included OXPHOS and ATP generation (Figure 32). In general, GO analysis suggested the absence of a stress response and a normal functioning liver that is refractory to short-term troglitazone-induced toxicity. This is in agreement with histopathological analysis at 2 weeks (Figure 24). By comparison, which is unique to 4 weeks treatment, there was a marked enrichment of a number of stress responses, including apoptosis, oxidative stress (H_2O_2, $O_2^{\bullet-}$) response, GSH metabolism and cell death (Figure 32). There was also a chemical stimulus response, consistent with the toxicity arising from extended troglitazone administration. When viewed together with toxicological/biochemical endpoints and liver histopathology, it is apparent that after 4-weeks of troglitazone treatment, the liver of the HET mouse was subjected to considerable chemical insults in a pro-oxidant environment. Cellular (mitochondrial) compensatory responses were insufficient, which resulted in mitochondrial protein oxidation and liver injury.

IPA analysis revealed 'toxic' pathways manifested with long-term troglitazone administration, which included mitochondrial dysfunction, fatty acid metabolism and oxidative stress (Figure 33 and Figure 34). These altered pathways, which were affected with troglitazone-induced toxicity, were concordant with our 2D-DIGE results and biochemical endpoints reported here and elsewhere. This confirmed the importance of

mitochondria and oxidative stress in troglitazone hepatotoxicity (Smith, 2003). By agglomerative hierarchical clustering and simple scatterplot analysis, a large number of mitochondrial proteins displayed bimodal modulation and that they tended to group together by their functions (Figure 35). However, automated hierarchical clustering by statistical measures did not reveal GO biological process over-representation specific to any cluster. This is likely due to several reasons, such that hierarchical clustering was devoid of functional information and as a result the clustering was not thorough, or was it sufficiently biologically meaningful. This prompted us to cluster the mitochondrial proteins by their functions and to investigate which functional clusters were more sensitive and fragile to troglitazone-induced hepatotoxicity (Table 10).

Figure 32. Non-intersecting GO terms of proteins in 2 and 4 weeks treatment
Significantly enriched GO biological process terms within the 321 protein dataset. Enriched GO terms are listed together with *p* values and the number of proteins sorted in by statistical rank (A) 2 weeks and (B) 4 weeks. ATP, adenosine triphosphate; RNT, Ribonucleoside triphosphate; NTP, nucleoside triphosphate

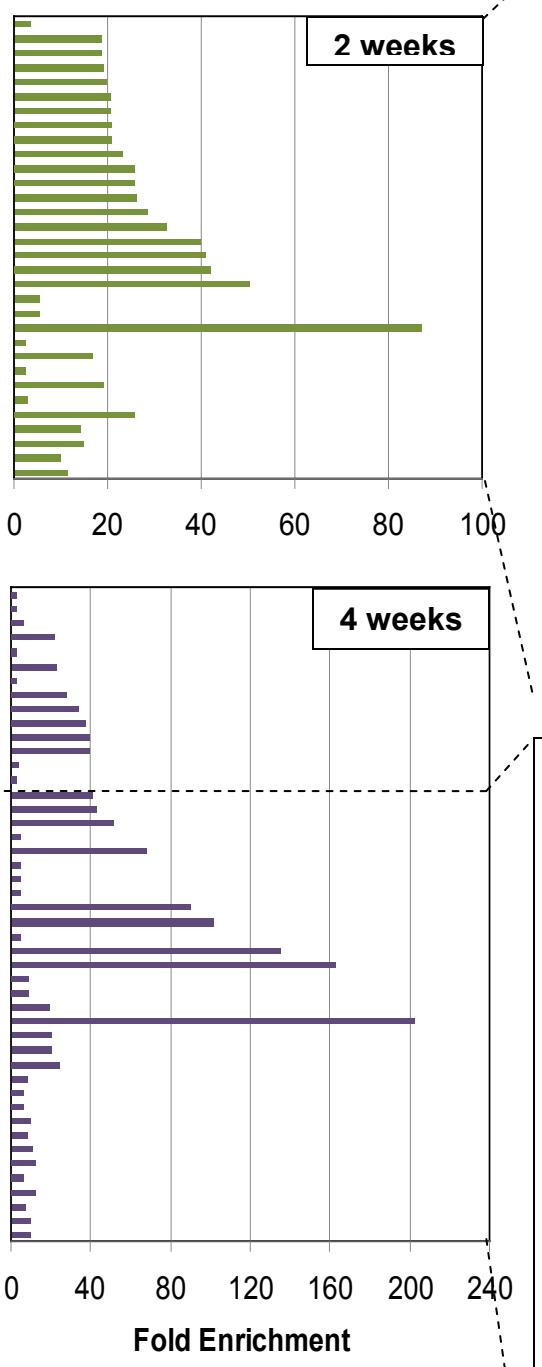

oxidative phosphorylation	5.5E-03
transport	8.3E-03
coenzyme biosynthetic process	9.9E-03
establishment of localization	9.9E-03
cofactor biosynthetic process	1.3E-02
localization	2.1E-02
apoptotic nuclear changes	2.2E-02
carboxylic acid metabolic process	3.7E-02
organic acid metabolic process	3.7E-02
negative regulation of cell growth	3.8E-02
nuclear organization and biogenesis	4.5E-02
negative regulation of cell size	4.6E-02
mitochondrial transport	4.7E-02
negative regulation of growth	5.7E-02
ATP synthesis coupled proton	6.5E-02
ATP biosynthetic process	7.2E-02
nucleoside phosphate metabolism	7.2E-02
ATP metabolic process	8.1E-02
purine RNT biosynthesis process	8.9E-02
purine NTP biosynthesis process	8.9E-02
RNT biosynthesis	9.0E-02
apoptotic program	9.0E-02
nucleoside triphosphate biosynthesis	9.4E-02
purine RNT metabolism process	9.7E-02
purine NTP metabolism	9.9E-02
RNT metabolism	9.9E-02
phosphorylation	1.0E-01

response to superoxide	0.009581
response to oxidative stress	0.010007
negative regulation of apoptosis	0.010402
negative regulation of programmed cell death	0.010854
response to oxygen radical	0.011962
glycine catabolic process	0.014338
catabolic process	0.015101
serine family amino acid catabolic process	0.019073
glycine metabolic process	0.021432
regulation of apoptosis	0.023981
electron transport	0.024318
regulation of programmed cell death	0.025003
response to hydrogen peroxide	0.028476
response to chemical stimulus	0.0327
acyl-CoA metabolic process	0.037792
response to reactive oxygen species	0.044722
serine family amino acid metabolic process	0.047021
response to stress	0.048717
generation of precursor metabolites & energy	0.04903
cellular response to stress	0.049315
glutathione metabolic process	0.049315
superoxide metabolic process	0.051603
double-strand break repair	0.056164
cellular response to stimulus	0.067472
apoptosis	0.081196
isoprenoid metabolic process	0.083083
programmed cell death	0.085302
oxygen & ROS metabolic process	0.087496
protein folding	0.091121
cell death	0.094547
death	0.095278

Figure 32. Figure legend can be found on page 122.

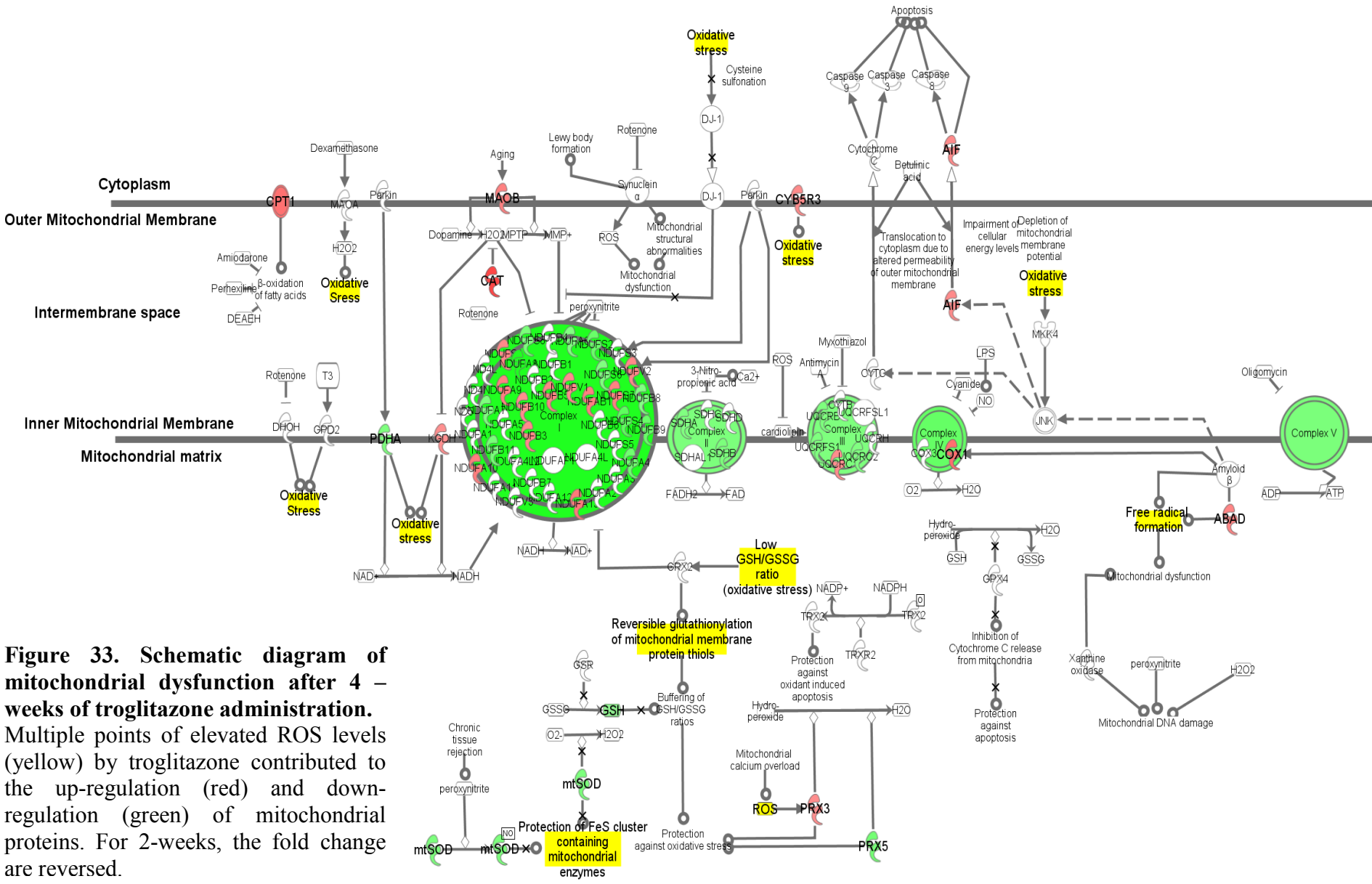

Figure 33. Schematic diagram of mitochondrial dysfunction after 4 – weeks of troglitazone administration. Multiple points of elevated ROS levels (yellow) by troglitazone contributed to the up-regulation (red) and down-regulation (green) of mitochondrial proteins. For 2-weeks, the fold change are reversed.

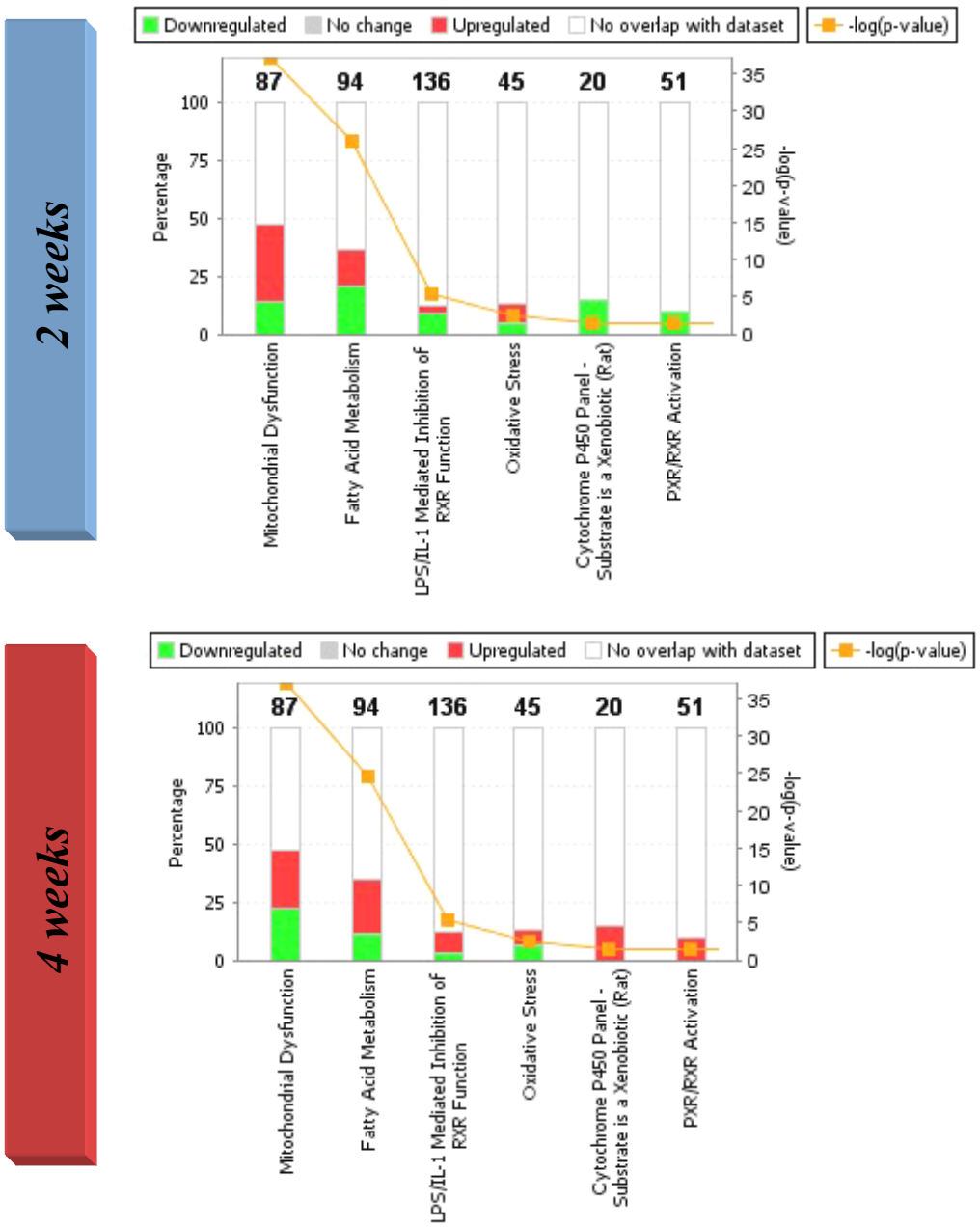

Figure 34. Histogram of "Toxic Pathways" affected by troglitazone treatment
The top 6 canonical pathways are shown due to space limitation. Mitochondrial dysfunction was also ranked highest under "Canonical Pathways" (Figure 33). This is likely due to the large proportion of detected ETC components which form part of annotated pathway. Of note, RXR activation and function were ranked highly in the analysis. Troglitazone activates PPAR, which in turns heterodimerize with RXR for transcriptional regulation. These chars provide an overview of affect pathways but may not be ideal for viewing the complex biological pathways as a whole. Significantly differentially expression was set at a threshold of 1.2 and 0.833 for IPA analysis.

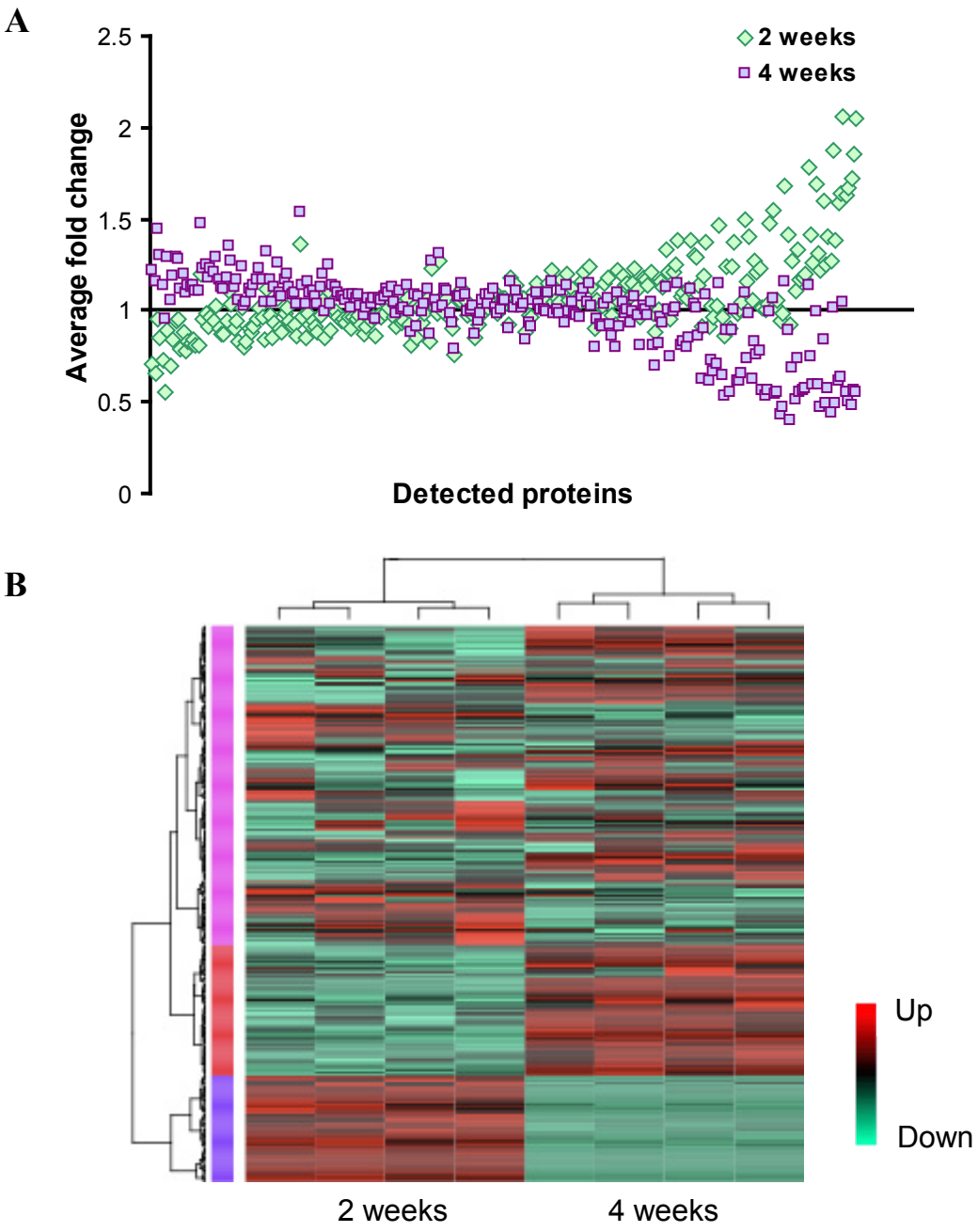

Figure 35. Cluster analysis of detected of proteins show bimodal expression
(A) Scatterplot shows biomodal expression can be seen for a large number of proteins at the extremes of the scatterplot. Proteins were sorted according the magnitude of expression difference (x-axis). (B) Agglomerative hierarchical clustering of quantified mitochondrial proteins with heatmap. The different colors on the side bars represent the three major clusters (red, blue and violet). Fold change is the variable attribute. Two proteins of similar attributes (shorter distance; y-axis) are grouped together and vice versa.

3.3.3.1. ETC components show bimodal response to acute and chronic troglitazone treatment

The ETC forms the defining and critical components for the ATP-generating capability of the mitochondria. MS analysis demonstrated that troglitazone has non-equitable effects on components of the OXPHOS both over short-term and long-term administration (Figure 36). Short-term treatment with troglitazone led to general down-regulation of the five ETC complexes. In particular, mitochondrially-encoded subunits of cytochrome c oxidase (mt-COX1 and mt-COX2) were up-regulated. Despite the exclusion of mt-COX1 based on FDR thresholds (Unused ProtScore= 2), manual inspection of the MS/MS spectrum revealed a highly confident fragmentation (99% confidence and complete *y* series for best scoring peptide sequence), mt-COX1 was deemed a positive identification (Figure 37A). To substantiate the claim, immunoblotting was performed. Indeed, mt-COX1 was up-regulated with 2-weeks treatment and was down-regulated with 4-weeks troglitazone treatment (Figure 36). It is interesting to note that mt-COX1, mt-COX2 and mt-COX3 form the catalytic and structural core of the functional complex while mt-COX1 and mt-COX2 constituted the catalytic core which contained the redox cofactors (Taanman, 1997). There could also be early ETC instability as suggested by a decreased in LETM1 levels (FC_{2weeks} = 0.91) (Tamai et al., 2008). Conversely, low ProtScores do not necessarily translate into accurate protein quantification. For example, NDFUS3 MS-quantified fold change did not agree with immunoblot density measurements (Figure 36 and Figure 37).

The observation that prolonged troglitazone treatment adversely affected the HET liver (Figure 24) suggested that a mitotoxicant-mediated increase in oxidative stress should potentiate the damage done on the ETC. Intriguingly, the hepatic injury at the tissue level was not associated with adverse changes on the ETC proteins which unexpectedly increased in abundance. With the exception of three ETC subunits including mt-COX1 ($FC_{4\ weeks}$ = 0.27), NDUFS4 ($FC_{4\ weeks}$ = 0.87) and ATP5F1 ($FC_{4\ weeks}$ = 0.91), most ETC members were up-regulated or at basal levels (Figure 36A and B). Because the majority of detected ETC members were at homeostatic levels or up-regulated (MCV = 1.07), this suggested that sustaining ATP generation remained an important cellular process during chronic toxicity events, and was unlikely a cause for hepatocyte death. In addition, there were instances of ETC subunits (~54%) showing bimodal differential expression (Student's *t*-test, $P < 0.05$) in the two study groups (Figure 36A and B). It is apparent that the bimodal dynamics of 54% of these ETC members were modulated in a concerted manner. Using immunoblotting, the MS-quantified abundance differences of selected components of the ETC and other mitochondrial proteins was confirmed (Figure 36C).

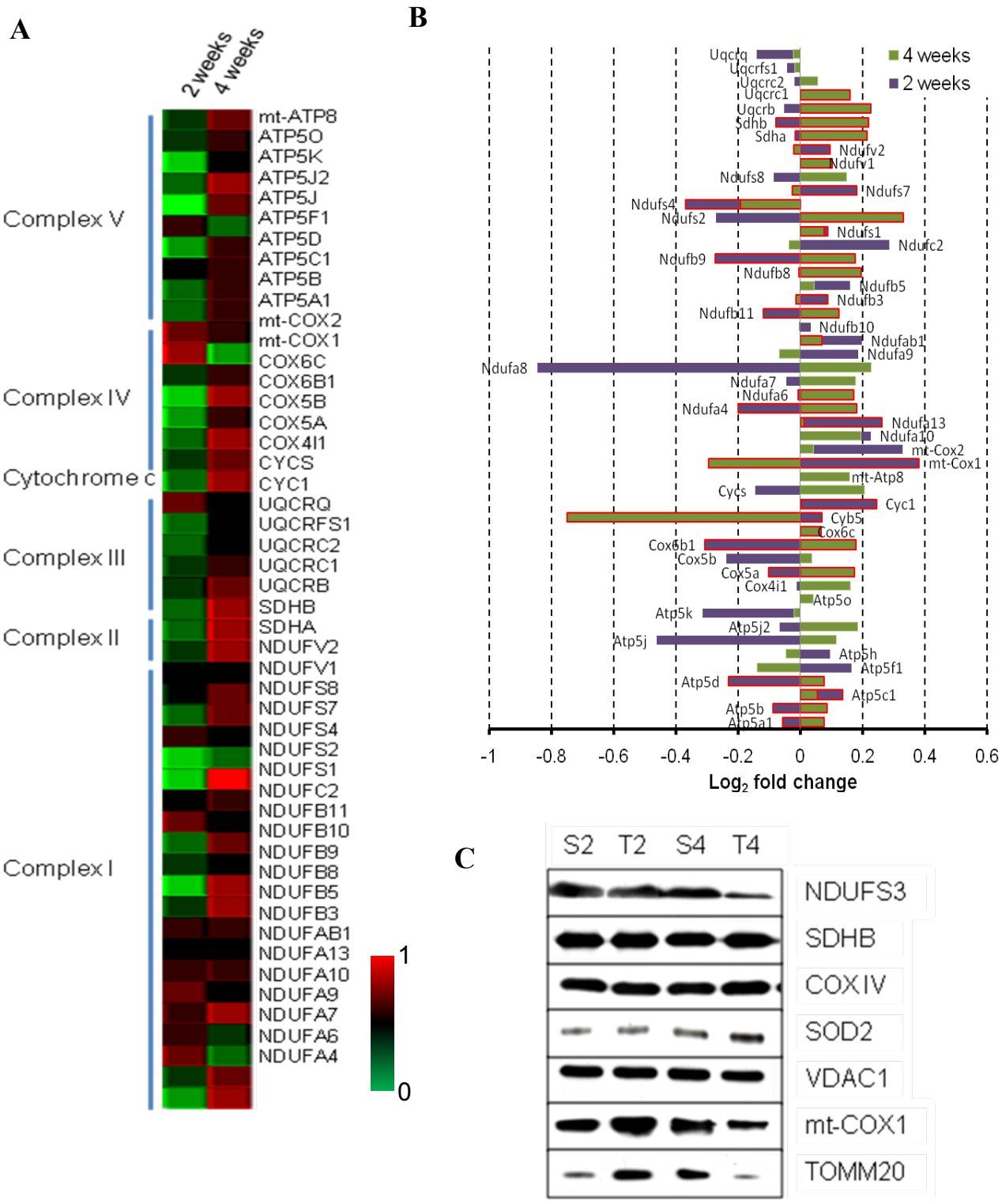

Figure 36. Impact of troglitazone on HET electron transport chain complexes
(A) Heatmap of quantified subunits of the ETC complexes. Fold change were centred to mean 0 and standard deviation 1 for better graphical presentation. (B) Histogram showing bimodal expression of most ETC components. Statistically significant differences of the same protein/subunit from 2 weeks to 4 weeks of troglitazone administration are marked with red borders (Student's *t*-test, $P < 0.05$). (C) Immunoblotted ratios are in agreement with MS-determined fold ratios except for NDUFS3.

A

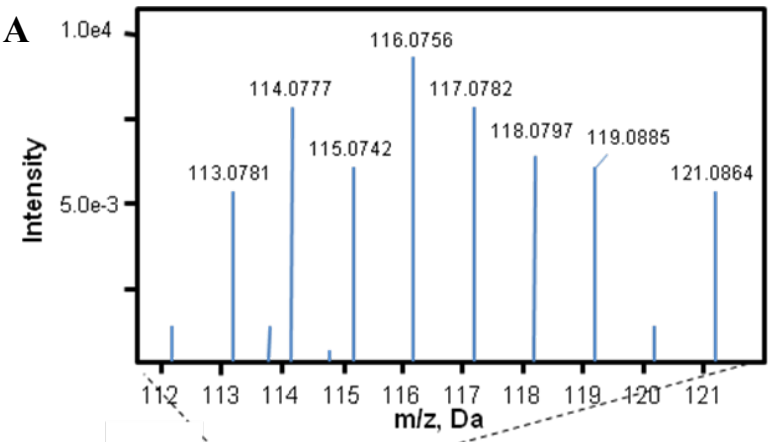

Residue	b	y
W	491.2919	1640.9369
L	604.3760	1150.6522
F	751.4444	1037.5681
S	838.4756	890.4997
T	939.5241	803.4677
N	1053.5671	702.4200
H	1190.6260	588.3771
K[IT8]	1622.9263	451.3182

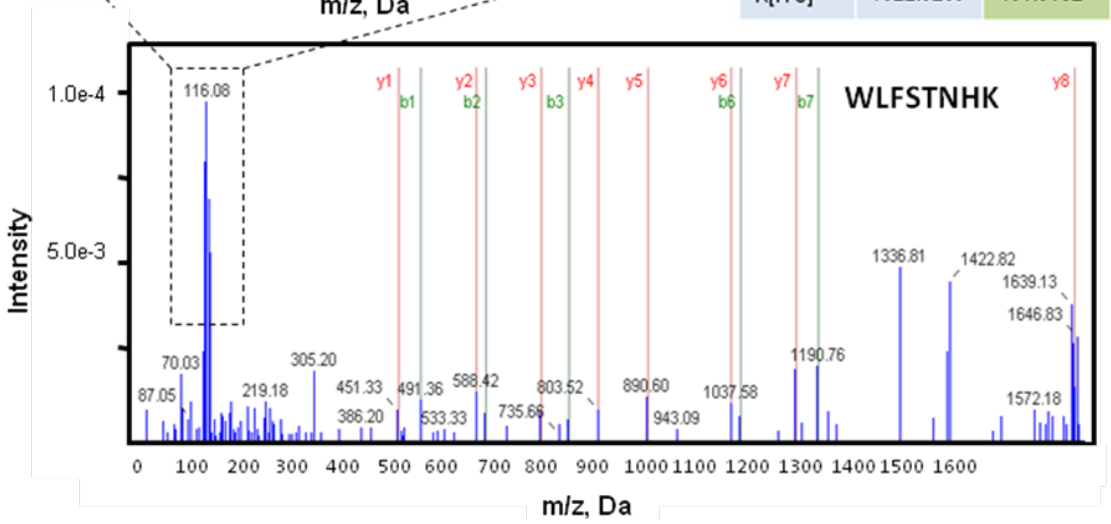

mt-COX1

B

Used	Conf.	Sequence	Modification	Theor m/z
☑	87	VVAEPVELAQEFR	iTRAQ8plex@N-term	1790.99
☐	4	DFPLTGYVELR	iTRAQ8plex@N-term	1613.88
☐	3	FDLNSPWEAFPAYR	iTRAQ8plex@N-term	2017.0
☐	<1	FEIVYNLLSLR	iTRAQ8plex@N-term	1670.97
☐	<1	LEAGDKKPETK	iTRAQ8plex@N-term iTRAQ8plex(K)@6 iTRAQ8plex(K)@7 iTRAQ8plex(K)@11	2432.47

NDUFS1

Figure 37. Mass spectrometric quantification of mt-COX1 and NDUFS3.
(A). MS/MS of best scoring peptide of mt-COX1 (99% C.I., ProtScore Unused =2) demonstrates a complete *y*-ion series (green boxes). Insert shows a zoomed-in area of low m/z which gives information on the iTRAQ™ reporter ions intensity and hence mt-COX1 quantification. (B). Peptide summary of NDUFS3 obtained from ProteinPilot software. Red arrow denotes the highest scoring unique peptide assigned to NDUFS3 which did not attain 99% C.I. (ProtScore Unused = 0.92).

3.3.3.2. Modulation of PPAR-agonist targets

Thiazolidinediones are known to transcriptionally induce expression of genes belonging to the β-oxidation pathway (Bogacka et al., 2005) and this motivated us to test if β-oxidation was affected. Short-term administration with troglitazone in HET mice brought about increases in ACAA1, CPT I and CAC (*Slc25a20*) levels. These changes are specific to the PPAR-agonist's mechanism of action to normalize glucose and lipids levels and are also consistent with no observable hepatic damage at this point. Prolonged troglitazone administration however, brought about the down-regulation of several β-oxidation enzymes such as CISD1, ECH1, ACAT1 and ACAA1 and suppressed the overall β-oxidation cluster (Figure 11).

Pioglitazone, a weaker PPARγ-agonist was discovered to bind to MitoNEET or CISD1 (Colca et al., 2004) and later it was found that pioglitazone stabilized its 2[Fe-S] cluster (Paddock et al., 2007). At different dosing regimens, CISD1 abundance varied (FC_{2weeks} = 1.23 and FC_{4weeks} = 0.83). CISD1 has been implicated as a redox sensor and/or in the formation of [Fe-S] clusters. Not much is known if and how binding to CISD1 has mediated PPAR-ligand specific actions. While it is tempting to speculate that troglitazone may also bind to CISD1, interactions with troglitazone, if any remained unknown.

Significantly, drugs intended for therapeutic indications often have inadvertent 'off-target' effects that cause drug-induced toxicities. Interestingly, there was IPA-qualified association of IL-1-mediated inhibition of RXR with troglitazone administration

(Figure 34). Mitochondrial dysfunction, apoptosis and oxidative stress can trigger inflammatory responses (Jaeschke, 2002, Smith, 2003, Uetrecht, 2008, Uetrecht, 2009) and while troglitazone has been shown to down-regulate IL-1 and IL-6 (Maggi et al., 2000a, Sigrist et al., 2000), the biological and toxicological consequences of such repression remain circumstantial (Desmet et al., 2005). To test for the potentiality of troglitazone-mediated PPAR-toxicity, we analyzed the fold change of differentially-regulated proteins with experimentally-verified PPAR-inducible genes (Nakachi et al., 2008, Tachibana, et al., 2005) in relation to the duration of the PPAR-agonist administration. The list included 186 genes, including those with established functional PPRE sites (true positives) such as catalase (Girnun et al., 2002), acyl-CoA oxidase (Varanasi et al., 1996), ACADM (Gulick et al., 1994), diazepam binding inhibitor isoform 1 (Helledie et al., 2002), HMG-CoA synthase (Rodriguez et al., 1994). Such an analysis revealed that after 2-weeks of troglitazone administration, PPAR-responsive proteins remained at basal levels (Wilcoxon rank sum test, $P = 0.2572$; Figure 38A). By contrast, after 4-weeks, down-regulation of PPAR-responsive proteins was observed (Wilcoxon rank sum test, $P = 0.002321$; Figure 38B).

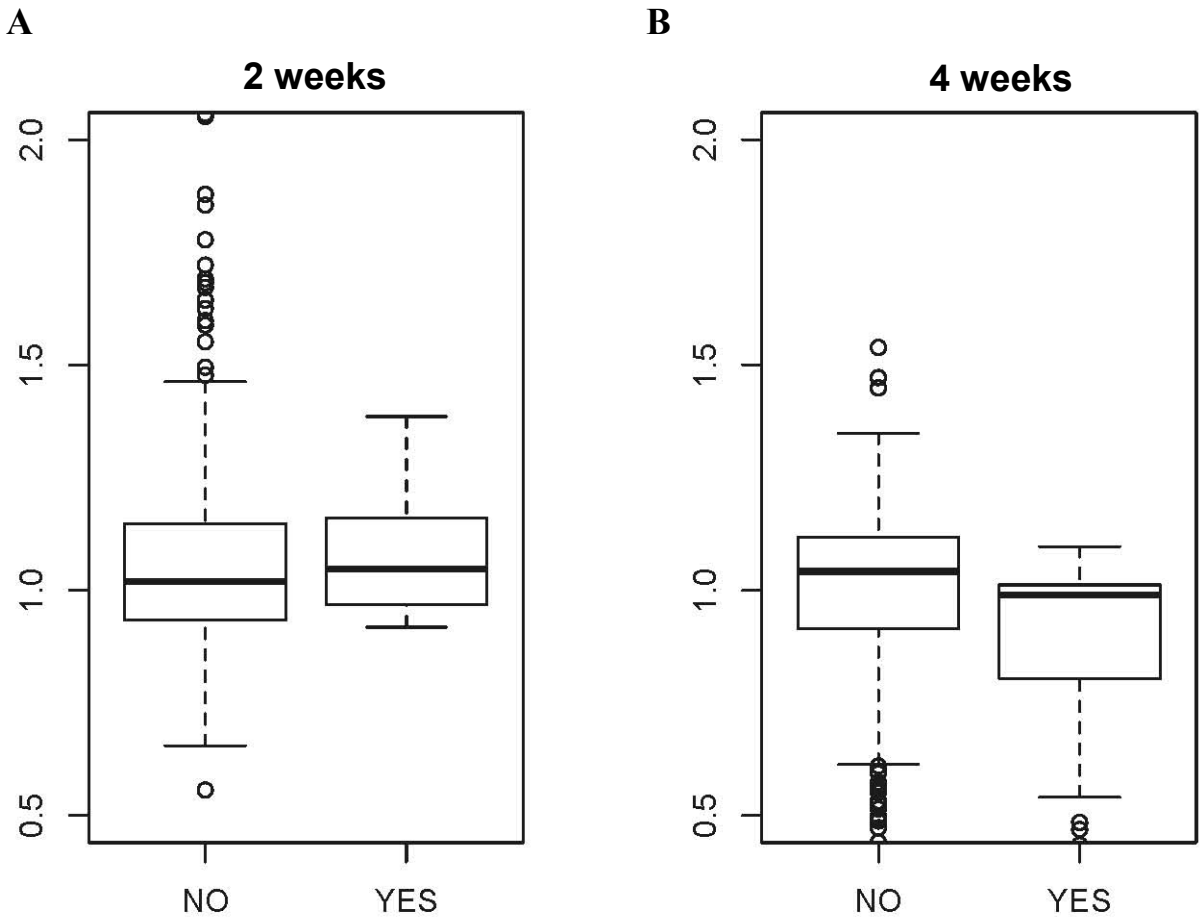

Figure 38. Boxplots of PPAR-responsive proteins with differential expression upon troglitazone administration

Boxplots showings the fold changes of proteins that are PPAR-responsive that changed with (A) 2 weeks and (B) 4 weeks of troglitazone adminstration. (A) At 2 weeks, there was no significant difference between the groups (Wilcoxon $P > 0.05$) (B) Signifcant differences (Wilcoxon $P < 0.01$) at 4 weeks implied that the presence of PPREs, and by extension, prolonged troglitazone treatment may play a role in troglitazone-induced toxicity under increased mitochondrial oxidative stress. Outliers were represented as dots (defined as 1.5 × interquantile range)

3.3.3.3. Parallel proteome shift suggests ROS-induced mitochondrial stress

Another important functional cluster to explore would be redox homeostasis. Despite the intrinsic partial loss of *Sod2* allele, the prolonged sensitization of the HET liver with troglitazone induced the up-regulation of SOD2 ($FC_{4\ weeks}$ = 1.23), and this occurred with troglitazone treatment (Figure 24A). Notably, two proteins involved in reducing protein disulfides and maintaining redox homeostasis, peroxiredoxin3 and glutaredoxin-related protein 5 exhibited an increase in their fold changes. Consistent with this, mitochondrial 3-NT protein adducts and protein carbonyls were significantly increased after 4 weeks of troglitazone administration (Figure 25B and C). Together, these data strongly illustrated an increasing redox imbalance in the HET mouse that required additional SOD2 and other ROS-detoxifying enzymes to overcome the elevated $O_2^{\bullet-}$ that stemmed from chronic administration of a PPARγ-agonist (Ong, et al., 2007).

In contrast to the redox homeostasis cluster, the mGSH transport cluster proved to be the most perturbed among the mitochondrial functional clusters, showing a highly reconfigured profile with prolonged troglitazone administration (MCV = 0.92). Anion transporters, dicarboxylate carrier (DIC; *Slc25a10*) and oxoglutarate carrier (OGC; *Slc25a11*), which mediated electroneutral exchange of dicarboxylates for inorganic phosphate and 2-oxoglutarate for other dicarboxylates, respectively have been suggested as GSH transporters (Fernandez-Checa & Kaplowitz, 2005, Lash, 2006). Mitochondrial uptake of GSH is essential for the maintenance of mGSH levels against elevated ROS levels. The impairment of GSH transport into the mitochondria will result in inadequate

mGSH to attenuate elevated ROS, as shown in Figure 25A. One adverse consequences of hepatic mGSH depletion is the potentiating of acetaminophen and usnic acid toxicity (Han et al., 2004, Zhao et al., 2002), thus highlighting the critical role of mGSH depletion in enhancing the toxicity of drugs. Noticeably, constituents of mGSH transport cluster, GPX1 and OGC were markedly up-regulated which suggested a compensatory response to an already compromised mGSH transport and protection. In summary, the results showed that troglitazone hit several mitochondrial functional clusters and in particular, exploited a compromised antioxidant environment due to *Sod2* haplodeficiency, and acted through disrupted mGSH cycling to propagate damage to the mitochondria and liver.

Table 10. Functional clustering of detected mitochondrial proteins.

No.	Functional Cluster	MCV
1	GSH homeostasis	0.9226491
2	Transporters	0.9255224
3	β-oxidation	0.9264068
4	Fatty acid metabolism	0.9375569
5	Detoxification	0.9545206
6	Redox homeostasis	0.9647358
7	Morphology and structure	0.9816671
8	Ca^{2+}	0.9834463
9	Bile salt biosynthesis	1.0398769
10	Nucleobase, nucleoside, nucleotide and nucleic acid metabolic process	1.0424324
11	Electron Transport Chain	1.0719918
12	Urea cycle	1.0769769
13	Mito translation/transcription	1.0789724
14	Tricarboxylic acid	1.1031997
15	Stress response	1.1094348
16	Amino acid metabolism	1.1094898
17	Protein import machinery	1.1470873

Only established mitochondrially-localized proteins were used for the Mean Centroid Value (MCV) calculations of 17 functional clusters. Probable proteins that are localized (or potentially organelle-promiscuous but not established) to the mitochondrion were excluded. Other mitochondrial functional clusters such as heme synthesis, ubiquinone biosynthesis and amino sugars metabolism were excluded due to insufficient data to calculate a feasible MCV. Functional clustering were manually curated from GO database, KEGG database, published literature and protein-protein interactions.

3.3.4. Prolonged troglitazone treatment activates FOXO3a through oxidative stress-mediated signals

In vertebrates and *C. elegans*, Forkhead box-containing, O3a subfamily (FOXO3a) has been implicated as a transcriptional activator in the up-regulation of SOD2 as a form of oxidative-stress defence (Honda & Honda, 1999, Kops et al., 2002). As shown in Figure 39A, endogenous FOXO3a was activated in the HET mouse liver (indicated by moderate dephosphorylation at Ser253), while FOXO3a remained phosphorylated in the WT mouse. Treatment with troglitazone for 4 weeks in HET mice caused the dephosphorylation of p-FOXO3a^{Ser253} (Figure 39B). By immunohistochemistry, control studies confirmed the sustained deactivation of FOXO3a (monitored by p-FOXO3a^{Ser253}; Figure 39B and C). Significantly, in areas of confluent hepatocytic degeneration of troglitazone-exposed HET livers, activation of FOXO3a occurred in a dephosphorylation-dependent manner and was translocated into the nucleus. In contrast, in the neighbouring surviving areas, FOXO3a remained phosphorylated at Ser253 and was retained in the cytoplasm (Figure 39D). Direct phosphorylation of Ser253, which is located at the nuclear localization signal domain of FOXO3a, is regulated by AKT/protein kinase B (AKT/PKB)-survival signalling which negatively regulates FOXO3a by promoting its interaction with 14-3-3 proteins and retention in the cytosol (Biggs et al., 1999). Subsequently, AKT/PKB activation was tested. In the control mice, FOXO3a inactivity and nuclear export was mediated by activated AKT/PKB (Figure 39E). Interestingly, AKT/PKB remained activated after 4 weeks of troglitazone treatment. The presence of activated AKT/PKB induces the phosphorylation, nuclear export and transcriptional inactivation of FOXO3a but this was

not observed (Figure 39D). This suggested that there was an interference of AKT/PKB-survival signalling by a competing signalling mechanism under increased oxidative stress and mGSH depletion that led to cell death.

ROS are potent stressors to activating stress kinases including JNK and p38, which form part of the mitogen-activated protein kinase (MAPK) pathway. Indeed, JNK has been implicated in its antagonistic action against AKT/PKB-mediated FOXO3a- (Sunayama et al., 2005) and FOXO4-inactivation (Essers et al., 2004). More notably, JNK and p38-dependent in troglitazone-induced cytotoxicity has been observed previously (Bae & Song, 2003, Lim et al., 2008). Apoptosis signal-regulating kinase 1 (ASK1) is the upstream kinase of JNK and p38 (Takeda et al., 2008). We observed that after 4 weeks of daily administration, troglitazone activated ASK1 (phosphorylation of Thr845 and dephosphoryation of inhibitory residue Ser83; Figure 39E). This resulted in the activation of JNK but not p38 (Figure 39E). By contrast, minimal levels of phosphorylated JNK were observed for control groups and a slight increase in 2-weeks treated group (Figure 39E). The phosphorylated form of p38 was minimal in all study groups. Therefore, increased troglitazone-mediated mitochondrial oxidative stress and this led to ASK1-JNK activation *in vivo* and to the delay in observed hepatotoxicity. This indicated, in agreement with other reports (Bae & Song, 2003, Lim, et al., 2008), that troglitazone-induced hepatotoxicity proceeded through mitochondrial ROS-activated JNK. In the HET mouse, however, this occurred irrespective of p38. Further, this is consistent with reports of antagonism between JNK and AKT/PKB in the regulation of

FOXO3a nuclear import and transcriptional activation when the balance was tipped towards stress-signalling (Sunayama, et al., 2005).

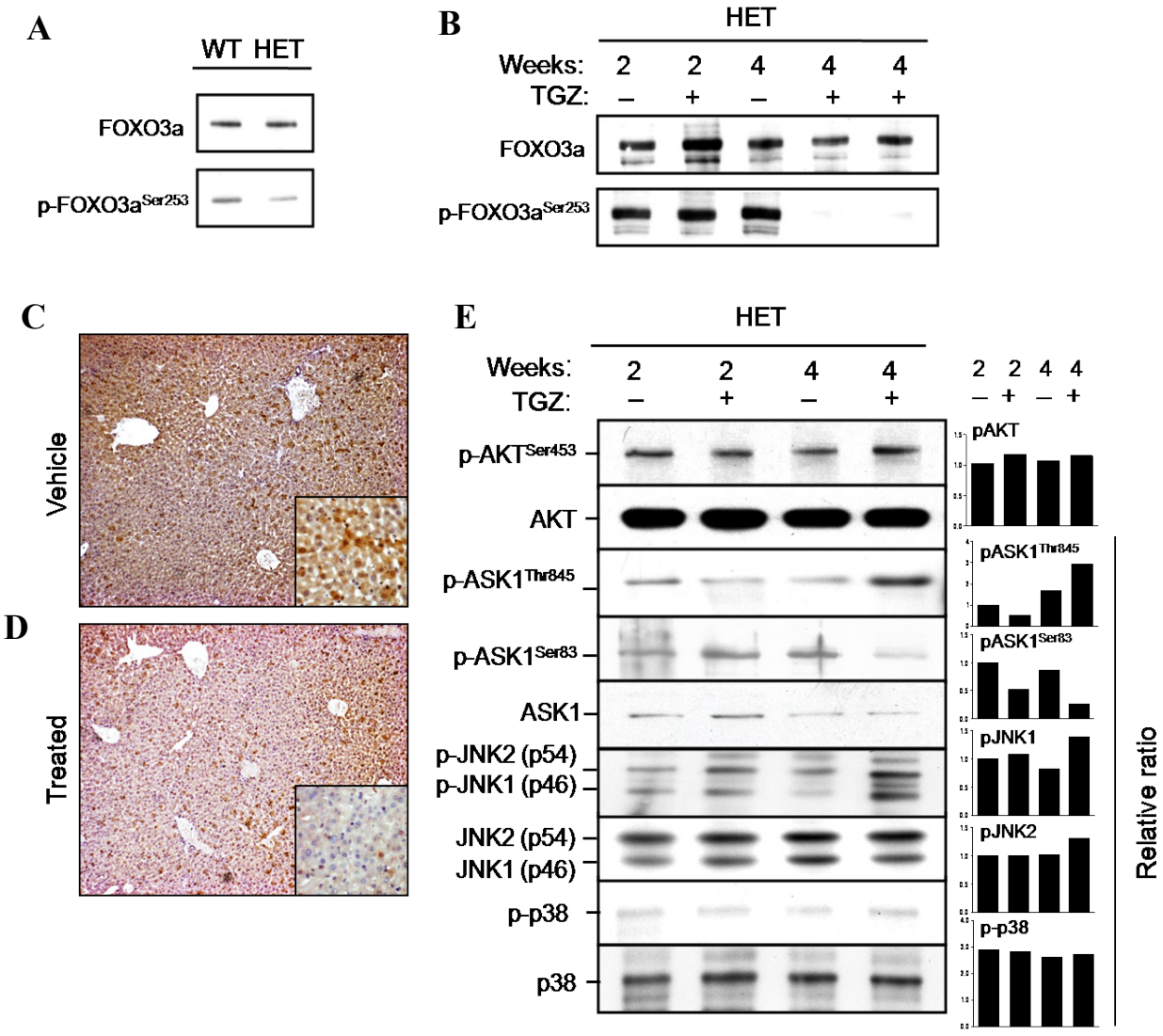

Figure 39. Prolonged troglitazone exposure causes ASK1-dependent JNK and p38 MAPK activation.

(A & B) Immunoblot analysis of FOXO3a in WT and HET mice and in HET mice treated with vehicle or troglitazone over a period of 2 or 4 weeks. (C & D) Immunohistochemistry of vehicle-administered HET mouse and troglitazone-administered HET mouse. Extended troglitazone administration caused FOXO3a dephosphorylation and nuclear translocation. Liver sections were incubated with anti-p-FOXO3a^{Ser253} antibody and counterstained. In areas with hepatocytic degeneration, FOXO3a was dephosphorylated and nuclearly imported (original magnification × 100). Insert illustrates the cytosolic localization of pFOXO3a (original magnification × 400). (E) The expression of pAKT at Ser453, AKT, pASK1 at Thr845 (activation pASK1^{Thr845}) or Ser83 (inhibitory pASK1^{Ser83}), pJNK at Thr183/Tyr185, JNK, p-p38 at Thr180/Tyr182, p38, were determined using immunoblot analysis. The relative ratios of phosphorylated to total, non-phosphorylated forms are shown as graphs (left).

3.3.5. Transcriptional regulation of SOD2 and the HET hepatic mitoproteome

SOD2 expression and other mitochondrial proteins are also regulated by transcription factors or activators other than FOXO3a. Given that PGC-1α, a co-activator of PPARγ, drove the gene expression of *Sod2* under pro-oxidant status (St-Pierre et al., 2006, Valle et al., 2005) and that troglitazone restored PGC-1α levels in the skeletal muscle of Zucker diabetic fatty rats (Jove et al., 2004), we investigated if prolonged troglitazone-induction of SOD2 was PGC-1α/PGC-1β-dependent. Unexpectedly, PGC-1α and PGC-1β levels remained at similar levels throughout the study and were independent of the form of treatment (Figure 40A). This is consistent with the lack of increase of LRPPRC levels which up-regulated PGC-1α and PGC-1β expression (Cooper et al., 2006). NO has been implicated in modulating PGC-1α expression and in parallel, affected mitochondrial ROS defense (Borniquel et al., 2006). Interestingly, increased NO did not translate into higher PGC-1α levels (Figure 25A).

However, in HET liver as compared to WT liver, PGC-1α but not PGC-1β may play a major role in orchestrating the mitoproteome profile under compromised mitochondrial antioxidant defense (Figure 40B). Other workers have reported that PGC-1α and PGC-1β share the induction of several mitochondrial genes such as ATP synthase β subunit, ACADM, cytochrome c and COX IV. This was in agreement with our proteomics profiling results as these proteins were found to be differentially expressed in the HET liver relative to WT mice (Figure 40C, Supplemental Table 4). PPARγ expression has been reported to increase with troglitazone treatment in hepatocytes

(Davies et al., 1999), and we ask if the HET mitoproteome might be influenced by PPARγ given its role as a transcriptional regulator. Immunoblot analysis of liver extracts of vehicle and troglitazone-treated HET mice revealed no significant differences in PPARγ amounts across the time-course study (Figure 40A). This is consistent with another proteomic study in which treatment with a PPARγ agonist did not increase PPARγ mRNA levels (Lanne et al., 2006). Taken together, this indicated that troglitazone-induced SOD2 up-regulation and mitoproteome dynamics was independent of PGC-1α, PGC-1β, NO and PPARγ but regulated by FOXO3a. In addition, no significant difference was observed with duration or drug-treatment for two other well-established transcriptional regulators of nuclear-encoded mitochondrial proteins, NRF-1 and ERR-α (Figure 40A). Of note, PGC-1α, PGC-1β, NRF-1 and ERR-α are part of the nuclear regulatory program for mitochondrial biogenesis, indicating that troglitazone-induced modification of the HET mitoproteome was not accompanied with mitochondrial biogenesis.

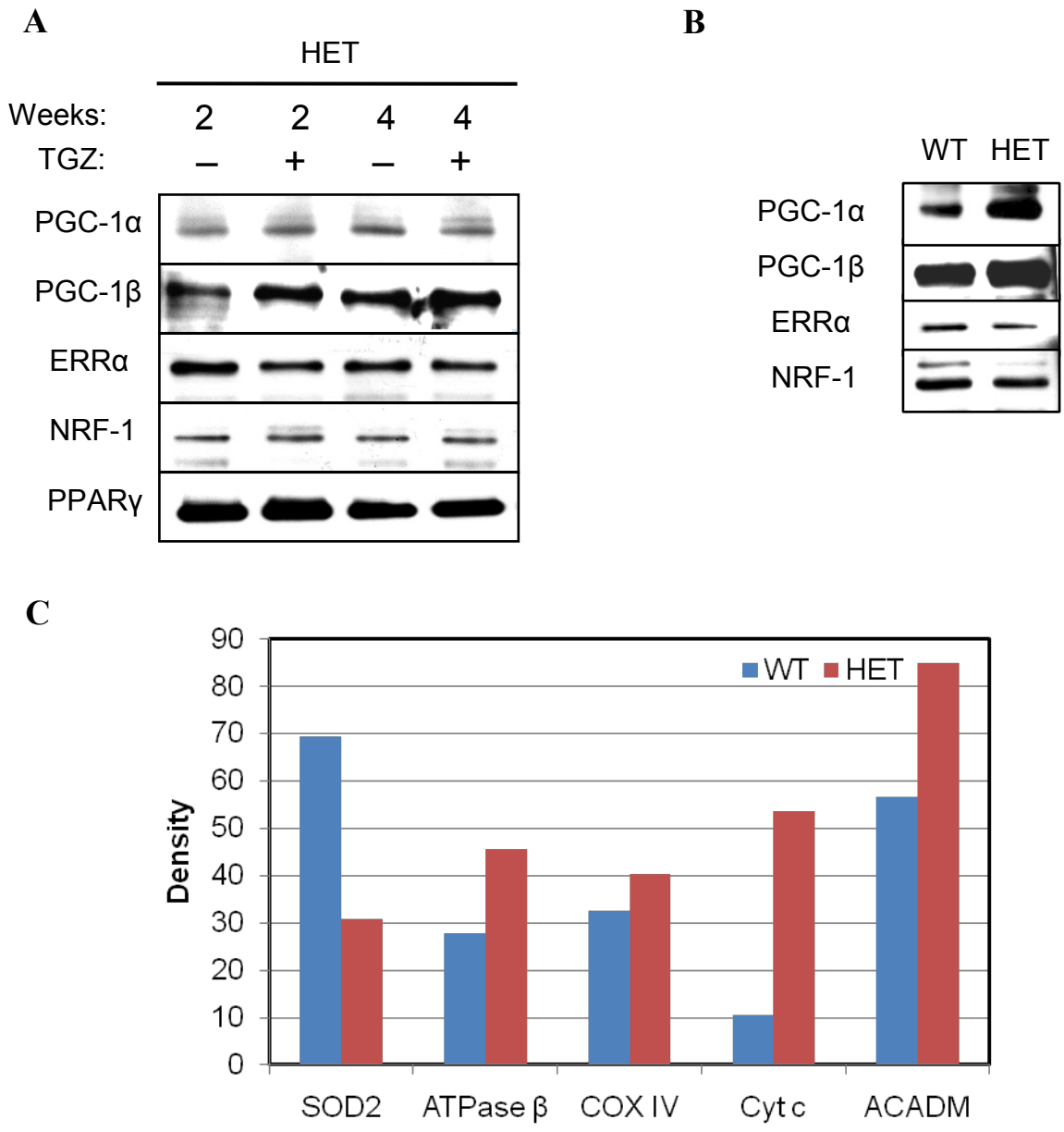

Figure 40. Transcriptional regulation over mitoproteome under elevated oxidative stress and troglitazone administration

(A) Immunoblot analysis of transcriptional regulators and co-activators involved in regulating nuclear-encoded mitochondrial proteins upon short and long-term troglitazone administration in the HET mouse. (B) Immunoblot analysis of transcriptional regulators and co-activators involved in regulating nuclear-encoded mitochondrial proteins in the HET mouse. (C) Bar graph showing the densitometric readings of several proteins regulated by PGC-1α detected in the proteomics screen.

4. DISCUSSION

4.1. Characterization of the HET liver mitoproteome

4.1.1. Introduction

One of the aims of this study is to characterize the hepatic mitochondrial proteome of the heterozygous HET mouse, an increasingly used murine model in neurobiology, cardiovascular biology, aging research, and toxicology, to address is suitability as a preclinical mouse model of drug toxicity. Although the HET mouse has been characterized with respect to mitochondrial function and transcript expression of certain individual genes, the effects of the singular loss of the *Sod2* allele on the global expression of hepatic mitochondrial proteins remains unknown. Specifically, we focused on the hepatic mitochondria because the partial reduction in SOD2 activity is likely to produce alterations in many of the important hepatic mitochondrial functions. This will address the suitability of the HET mouse as a surrogate animal model for studying DILI that arise as a result of clinically silent mitochondrial abnormalities.

4.1.2. Purity of mitochondria preparation

In this study we described an approach that uses discontinuous Percoll™ gradient to obtain a highly pure mitochondrial fraction. Preparation of highly pure mitochondrial fractions is critical to subcellular proteome research (Dunkley et al., 2006, Yates et al.,

2005). Based on immunoblotting against markers of ER, lysosomes and peroxisomes, we were able to confirm the lack of contaminating organelles. While we identified several nuclear, ER, lysosomal and peroxisomal proteins, they may represent minor contaminants, mitochondrial-associating proteins or multi-localized proteins. Sometimes their associations may even reflect a physiological condition. It is noteworthy that the mitochondria and the ER are spatially connected and organised, forming networks of interconnecting organelles (de Brito & Scorrano, 2008, Rizzuto & Pozzan, 2006). Such juxapositioning of the mitochondria and ER may facilitate the dual localization of proteins such as detoxifying cytochrome P450s (Omura, 2006) and phospholipid biosynthetic enzymes (Vance, 1990). We also identified cathepsins A, B, C, D, H and Z in the proteomics profiles. Cathepsins are proteases found mainly in the lysosome. Under stress, defective or mutant mitochondria may be degraded by engulfing autphagic machinery such as lysosomes (Yu et al., 2008). Our findings may suggest an ongoing dynamic degradation of the HET mitochondria for the maintainence of homeostasis. The biological significance of such non-mitochondrial-associations remained to be determined. Nevertheless, the level of mitochondrial purity gave us the confidence to conduct proteomic analyses of the hepatic HET mitoproteome.

4.1.3. The HET liver mitoproteome

The vast majority of mitochondrial proteins, estimated at approximately 1000–1500 (Pagliarini, et al., 2008, Taylor et al., 2003), are encoded by the nuclear genome, while 13 subunits of ETC complexes I, III, IV, and V (and the transfer RNA and

ribosomal RNA genes for protein synthesis) are encoded by the mtDNA. Proteomics analysis is a powerful method to assess the status of mitochondrial damage under pathological conditions of oxidative stress (Bailey, et al., 2005, Gibson, 2005). As a first step, 2D-DIGE coupled with MALDI-TOF/TOF MS/MS was used to resolve and identify these proteins. Because of the complexity of the mitochondrial proteome, additional proteomics methodologies would be required to reveal this protein complement. To increase proteome coverage, the mitochondrial samples were additionally profiled using a complementary MS-based proteomic approach. This approach has several merits, including no apparent biasness against proteins of any characteristics, higher dynamic range sensitivity as well as high level of reproducibility. Comparative proteomics by 4-plex iTRAQ™ and 2D-DIGE coupled to with MALDI-TOF/TOF MS/MS of HET mice versus WT mice revealed a mild redox perturbation in the mitochondrial proteome and demonstrated that mitochondrial proteins could cope with the mild pro-oxidant challenge. Overall, there was a good correlation between our findings and the functional or biochemical changes that have been described for this mouse model was observed (Huang et al., 1999, Kokoszka, et al., 2001, Lebovitz, et al., 1996, Liang & Patel, 2004, Ong, et al., 2006, Van Remmen et al., 2003, Van Remmen, et al., 1999, Van Remmen, et al., 2001, Williams, et al., 1998). Two features were particularly obvious. First, the changes in protein expression were mild and in the vast majority of proteins did not exceed two-fold changes. Although it is difficult to extrapolate from the observed change in abundance of a given protein to the possible consequences in a cell, these changes seemed relatively small when compared to other studies that have measured changes in protein expression after treatment with toxicants. Second, with the exception of SOD1

and 2, and thioredoxin domain-containing protein 4 and 5 (TXNDC4 and 5), most of the proteins involved in oxidant stress were up-regulated, rather than exhibiting decreased expression levels. Again, this is in contrast to other studies where rodents were treated with hepatotoxicants, including acetaminophen and bromobenzene, and where there was a bias towards lower protein levels (Fountoulakis et al., 2000, Fountoulakis et al., 2002). The reason for this is not entirely clear but it seems inviting to speculate that these changes are adaptive responses, likely compensatory mechanisms involved in counteracting the oxidative stress in mitochondria, rather than toxic responses leading to protein degradation.

While it is expected that certain ROS-sensitive proteins ought to be hit or damaged by the cumulative oxidative stress in the HET mice, and hence would exhibit a lower expression level, but the contrary is true. Importantly, the expression levels of enzymes with [Fe-S] clusters such as ACO2, Complexes I and II which have been shown to be exquisitely sensitive to oxidative stress do not seem to be affected by the pro-oxidant conditions and this was experimentally confirmed using iTRAQ™ quantitation analysis. This could be due to the constant signal feedback from mitochondria to the nucleus known as retrograde response (Poyton, 1996), resulting in compensatory homeostatic regulation of certain proteins. Another reason for this observation could be an up-regulation of the overall antioxidant defense systems, possibly via the nuclear transcriptional co-activator PGC-1α (St-Pierre, et al., 2006, Valle, et al., 2005) or it could be that the threshold for oxidative damage has not been attained (refer to Figure 5 for graphical explanation on the concept of thresholds). Thus, in the HET mouse, the partial

loss of SOD2 activity resulted in a pro-oxidant environment, whereby some form of compensatory mechanism is activated to achieve a new homeostatic condition. This implies that the singular loss of the *Sod2* allele results in a subtle redox imbalance.

4.1.3.1. Redox proteins

SOD2 (MnSOD) is one of the major mitochondrial antioxidant enzymes and is involved in the enzymatic dismutation of $O_2^{\bullet-}$ toH_2O_2. A lowered expression of SOD2 correlates with an increased redox imbalance in the mitochondria. It is therefore inviting to speculate that a number of the observed changes in the expression of the mitoproteome were a consequence of increased oxidant stress that is aimed at compensating the increases in superoxide levels. SOD1 (CuZnSOD) is primarily localized in the cytosol but can also be found in the intermembrane space in rat liver mitochondria (Okado-Matsumoto & Fridovich, 2001). In contrast to previous reports (Lebovitz, et al., 1996, Williams et al., 1998) we show for the first time there is a decrease in the expression of SOD1 in the HET mouse. This decrease in SOD1 expression suggests a coordinated effect of SOD2 levels on SOD1 expression under conditions of increased ROS. In heart tissue of a different transgenic HET model (Strassburger et al., 2005), it was shown that SOD1 activity was decreased by 50% in the absence of a decrease in *Sod1* mRNA and protein levels. The apparent discrepancy among several reports and the present data can be attributed in part that cytosolic SOD1 was measured while we focused entirely on mitochondria-associated SOD1. The reason for the decreased expression of mitochondrial intermembrane SOD1 is currently unknown.

Mitochondria are a key source of H_2O_2 generated either spontaneously or *via* enzymatic dismutation of $O_2^{\bullet-}$. In addition to the endogenous production of $O_2^{\bullet-}$ and H_2O_2, the partial deletion of *Sod2* adds further oxidative stress to the mitochondria and hepatocytes. The concomitant decrease in abundance of SOD2 and SOD1 would imply an accumulation of $O_2^{\bullet-}$ coupled with reduced amounts of H_2O_2. However, the general increased oxidative stress in mitochondria may induce compensatory feedback mechanisms resulting in upregulation of antioxidant enzymes including GPX1, GSTK1, MGST1 and catalase. This could explain the differentially increase expressed in levels of both H_2O_2-degrading enzymes. The up-regulation of GSTK1 and MGST1 suggested the increased recycling of mGSH to restore redox equilibrium with the partial ablation of *Sod2*. Depletion of mGSH is a hallmark to endogenous and chemically-induced oxidative stress. In the absence of intra-mitochondrial GSH synthesis, maintenance of the mGSH pool is crucial to ensure mitochondrial redox balance (Fernandez-Checa & Kaplowitz, 2005). Although GPX is the most important H_2O_2-degrading enzyme in liver, we found that catalase was also upregulated. Catalase is generally contained in the peroxisomal matrix; however, previous reports indicate that catalase can also be found in rat cardiac mitochondria (Radi et al., 1991). More recently, a combined proteomics and bioinformatics prediction strategy has indicated that catalase is localized in rat liver mitochondria (Jiang et al., 2005). Yet no direct evidence has been shown so far for mouse liver mitochondria.

4.1.3.2. OXPHOS

Several members of the ETC proteins were detected in our proteomic profiling. Subunits of the ATP synthase were the most commonly-detected ETC proteins. An interesting observation is that while the ATP synthase α-subunit was downregulated, the β-subunit was upregulated in an almost compensatory manner. Both form the F_1 catalytic portion necessary for phosphorylating ADP to ATP. The changes in α and β-subunits of ATP synthase probably reflect adaptive changes in the energy production as a result of mitochondrial oxidant stress. In contrast to these findings, other studies using protoxicant drugs that induce massive oxidant stress in mitochondria (*e.g.*, acetaminophen) found a decrease in the ATP synthase β-subunit, which is a consequence of oxidative damage to the ATP synthase (Ruepp et al., 2002). ATP synthase subunit δ was observed to be upregulated, possibly reflecting the sustained generation of ATP. We also identified the down-regulation of cytochrome b-c1 complex subunit 7 (UQCRB) and cytochrome c oxidase subunit VIb (COX6B1). The functional consequences of these changes are not known.

4.1.3.3. Urea cycle

Both carbamoyl phosphate synthase (CPS) and ornithine carbamoyltransferase (OTC) proteins are confined to the mitochondrial matrix. In particular CPS1 is one of the most abundant enzymes and rate limiting in catalyzing the first step of ureagenesis. The reason why both proteins are up-regulated in the HET mice is not entirely clear. However, besides playing a major role in the urea cycle, both CPS1 and OTC1 are involved in the synthesis and regulation of arginine, respectively. Arginine is a common substrate for arginase 1 and nitric oxide synthase. While arginase 1 is a known peroxisomal protein, close association of this enzyme with mitochondria is likely due to the functional link with the urea cycle enzymes OTC and CPS. More importantly, the decrease of arginase 1-like protein (Q3UEL0), a competitor of nitric oxide synthase for arginine, suggests that increased superoxide levels in the liver deplete NO (Aslan et al., 2001). Thus, a pool of arginine may be required to restore a physiological amount of beneficial nitric oxide to attenuate oxidative stress already present (Dasgupta et al., 2006). In contrast, $ONOO^-$ can be formed from excessive NO and a fine balanced NO production is mandatory. The decrease in arginine could signal both the upregulation of OTC and CPS to compensate for the generation of carbomyl phosphate and citrulline to ultimately regenerate arginine through the urea cycle. Thus, it is possible, that the increased levels reflect a response to altered NO synthesis from arginine as a consequence of accumulating $O_2^{\bullet-}$, and is indicative of an adaptive mechanism as part of the regenerative process by the hepatocyte (Minin et al., 2005).

4.1.3.4. β-Oxidation

The decreased expression of the first two enzymes involved in fatty acid β-oxidation (long-chain fatty acid-CoA ligase 1 and inorganic pyrophosphatase 2 may be a protective mechanism to reduce excessive NADH and $FADH_2$ formation from the β-oxidation process. Accumulation of reducing equivalents may pose a reductive stress and promote the formation of ROS (Adam-Vizi & Chinopoulos, 2006). Hence, down-regulation of both proteins suggests a reaction to balance the NAD^+/NADH ratio under the oxidative mitochondrial environment (Dawson et al., 1993). Consequently, the elevated expression of enoyl-CoA hydratase corresponds to the need to counteract further decreases in β-oxidation of fatty acids which yields acetyl-CoA that enters into the Krebs cycle.

4.1.3.5. α-ketoglutarate dehydrogenase (KGDH)

This mitochondrial matrix protein, also called 2-oxoglutarate dehydrogenase, is a TCA cycle enzyme catalyzing the oxidative decarboxylation of α-ketogluratate to succinyl-CoA, generating NADH. This protein complex comprises three protein subunits, KGDH (E1k), dihydrolipoamide succinyltransferase (E2k), and dihydrolipoyl dehydrogenase (E3). Mechanistic studies have revealed that KGDH is sensitive to oxidative stress and that it can be reversibly inactivated by ROS, suggesting that KGDH may serve an antioxidant function, limiting oxygen radical formation where H_2O_2 levels are high, and thus preventing further damage to mitochondria (Nulton-Persson & Szweda, 2001, Tretter & Adam-Vizi, 2005) In particular, the lipoic acid sulfhydryl group

of the E2k subunit make the protein exceptionally vulnerable to oxidative stress (Humphries & Szweda, 1998). Interestingly, the E1k subunit, which exhibited significantly increased protein expression in our study, was shown to be decreased approximately two-fold in the *Sod2*$^{-/-}$ mice (Hinerfeld et al., 2004) The reasons for the discrepancy are not known. However, it is possible that this protein which is highly sensitive to redox environment changes was up-regulated upon mild oxidant stress, while it becomes oxidatively damaged by extensive oxidative stress. The increase in E1k subunit could be reflective of a compensatory up-regulation, as it was found that the integrity of KGDH is extremely critical for NADH generation, especially in the early period of oxidative stress (Tretter, 2000).

Collectively, we found that apart from an obvious 50% reduction in SOD2, a number of oxidative stress-sensitive proteins were differentially regulated, but that the overall changes were minimal. However, the consequences of these subtle changes in mitochondrial redox status *in vivo* are not known; they could affect the function of OXPHOS, the TCA cycle, β-oxidation, the urea cycle, and other enzymes that form part of the mitochondrial antioxidant defense system.

Genetic mitochondrial abnormalities in the partial *Sod2* knockout mouse generate a mitochondrial environment of cumulative endogenous ROS production which is latent. Because the HET mouse is sensitized to the adverse effects of sustained mitochondrial oxidant stress, they hold the potential to unmask toxic effects of drugs otherwise not seen

in healthy mice. In fact, a genetic polymorphism (47T > C mutation) in *Sod2*[4] has been reported to predispose patients to a higher risk of DILI; that is, patients with C/C and C/T mutations have a higher propensity to DILI risk over the T/T genotype (Huang et al., 2007).

4.1.4. Summary

Our proteomics analysis of HET mouse liver mitochondria demonstrated that the overall changes in protein expression were quantitatively minor, and that most of the differentially expressed proteins were up-regulated. Part of this study (2D-DIGE) has already been published (Lee, et al., 2008a) and the iTRAQ™ work, which substantiated and extended the DIGE results will be published soon. The lack of a large number of down-regulated proteins suggested that the extent of oxidative stress had not attained a critical threshold that would adversely modify proteins. This implied that the singular loss of the *Sod2* allele resulted in a subtle redox imbalance, representing a "1st hit". The data confirmed biochemical and functional findings from earlier studies and are compatible with the hypothesis that the HET mouse is a suitable animal model for clinically silent mitochondrial abnormalities that can result in mild oxidative stress in mitochondria (Boelsterli & Lee, 2008). It has been generally recognized that heterozygous mutants could lead to interesting and novel genetic mouse models beyond knockout mice because such mice display partial-intermediate phenotypes. Heterozygous

[4] Thymine for cytosine substitution at nucleotide 47 results in an alanine for valine substitution which may augment import into the mitochondrial matrix (Shimoda-Matsubayashi et al., 1996, Sutton et al., 2003). It is arguable why more SOD2 leads to liver injury but may be explained by the higher production of H_2O_2 that overwhelms the system (Nahon et al., 2005, Sutton et al., 2006).

mice retain in part the function of the deleted gene, and compensatory mechanisms can ameliorate the mutation-evoked deficits (Kalueff et al., 2007). Importantly, this clinical scenario further supports the use of this murine model as a surrogate model for drug safety evaluation of biological relevance to humans.

4.2. Toxicoproteomics of Troglitazone-induced Mitoproteome Alterations

4.2.1. Introduction

Mitochondrial dysfunction is a common feature of troglitazone-induced toxic events (Bova et al., 2005, Haskins et al., 2001, Lim, et al., 2008, Masubuchi et al., 2006, Nadanaciva et al., 2007, Narayanan et al., 2003, Shishido et al., 2003, Tirmenstein et al., 2002) and that the underlying diminished redox defence of the HET mouse is a useful characteristic for the evaluation of mitochondrial toxic effects induced by hepatotropic drug challenges (Boelsterli & Hsiao, 2008, Boelsterli & Lee, 2008). However, the determinants of susceptibility to troglitazone-induced idiosyncratic liver injury have not yet been determined. Hence, the other major goal of this study is to obtain a global picture of the changes in the mitoproteome upon daily short- and long-term administration with troglitazone. We correlated molecular changes to histological and biochemical parameters. Figure 41 shows the toxicoproteomics workflow for this study. By doing so, it would allow a better understanding of the underlying molecular mechanisms and time-course of troglitazone hepatotoxicity, and that would facilitate the identification of potential early biomarkers of mitochondrial toxicity *in vivo*.

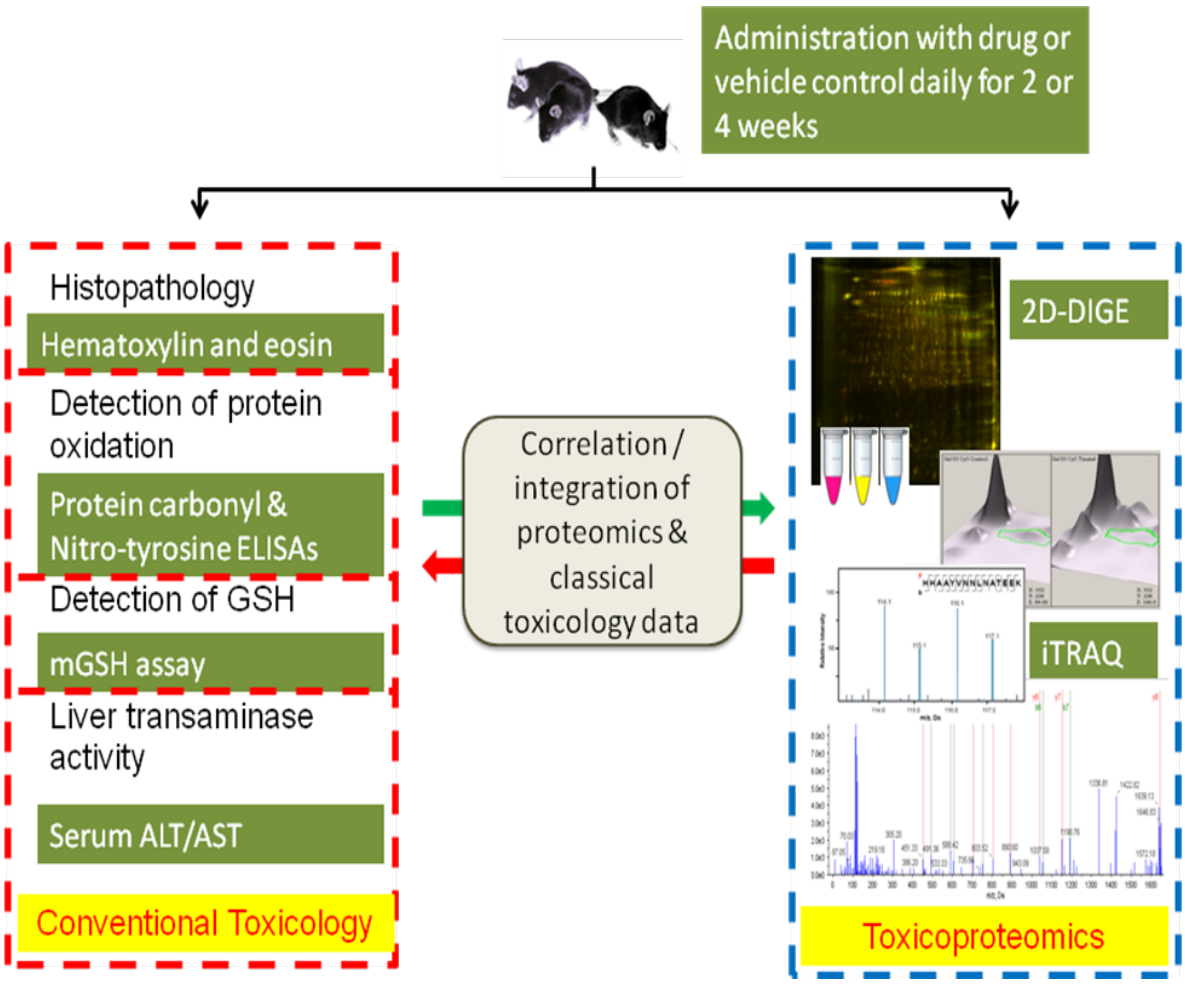

Figure 41. Workflow of toxicoproteomics
2D-DIGE and iTRAQ™ were the main tools used for increasing coverage of the mitochondrial proteome. Various toxicological and biochemical endpoints were integrated and correlated with proteomic data termed as 'phenotypic anchoring' to enhance and ascertain that the proteome changes were concordant to observable phenotypic changes.

4.2.2. Mitochondrial proteome expression dynamics induced by prolonged troglitazone treatment

Two separate proteomic platforms were performed to study the time-course of troglitazone-induced liver toxicity in the HET mouse. Using 2D-DIGE, we found 70 mitochondrial proteins that were differentially-modulated in the two time-points. To deepen our mechanistic understanding and increase the coverage of membraneous proteins, 8-plex iTRAQ™ in combination to MALDI TOF/TOF MS/MS was used. A total of 277 differentially-expressed proteins were revealed using this non-gel based method. For the 8-plex iTRAQ™ reporter structures have larger mass compared to the 4-plex iTRAQ™ reagents (Pierce, et al., 2008), the 8-plex iTRAQ™-labelled peptides cannot be fragmented as efficiently with the same set of MS parameters used in 4-plex. Using Glu-fibrinopeptide B, at different collision gas pressures (6.2×10^{-8}, 1.4×10^{-6} and 3.5×10^{-6} Torr), the intensity of the reporter ion is markedly reduced in the 8-plex system (Figure 42; compare Figures 42F and 42I). Low reporter ion intensity tends to suffer from poor ion statistics. To obtain efficient MS/MS fragmentation and subsequent reliable fold change values, initial optimization of the collision gas pressure to suit the 8-plex system was required. At high collision gas pressure (3.5×10^{-6} Torr), high quantification accuracy was achieved (Figure 42J) but at a cost in protein identification sensitivity, as indicated by a drop of ~55% in the fragment ion intensity (Figure 42K). Having established the optimal collision gas pressure for 8-plex iTRAQ™, the mitochondrial samples were detected and quantifed by MS.

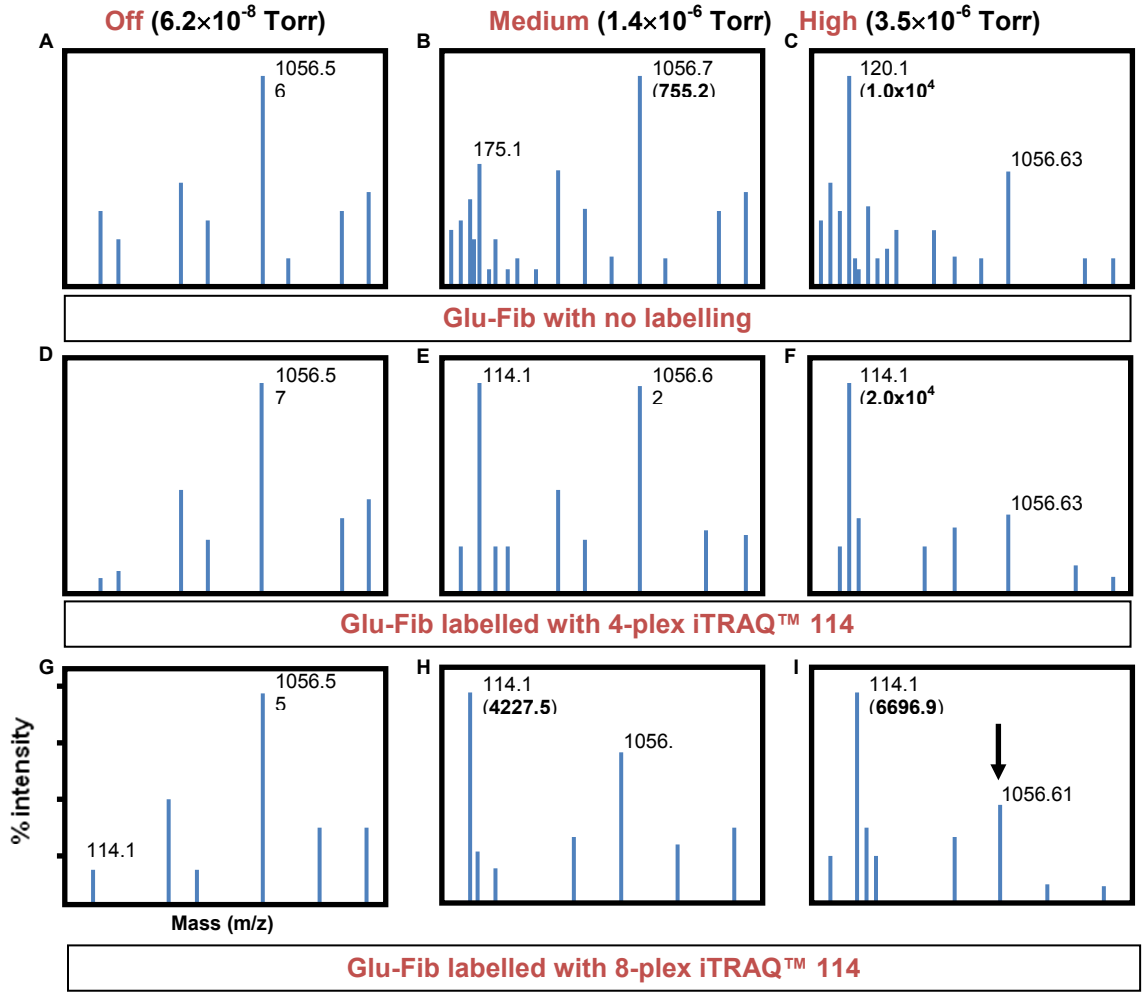

J

Theoretical ratio	2	5	10
Medium gas	2.4 ± 0.66	4.70 ± 0.84	8.01 ± 2.36
High gas	2.14 ± 0.41	5.14 ± 0.84	9.44 ± 1.76

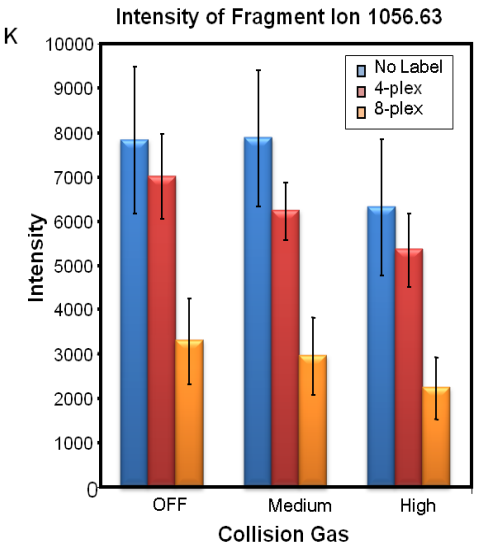

Figure 42. Optimising of collision energy for 8-plex iTRAQ™.
(A – I, K) Glu-fibrinopeptide B, labelled with channel 114 was used to optimise collision energy for a compromise between accurate and sensitive quantification of the peptide versus the iTRAQ™ reporter ion. (J & K) Quantification accuracy can be achieved with high collision gas energies but at a trade-off in the protein identification sensitivity.

The list of detected mitochondrial proteins was substantially physicochemically and functionally diverse; although the two combined proteomic methodology was not optimal for detecting certain classes of proteins such as the highly hydrophobic and small ones. This could partially stem from the intrinsic properties of MALDI that included the poorer ionization of hydrophobic peptides and the tendency to detect larger peptides (Lubec & Afjehi-Sadat, 2007) or insufficient solubilization of hydrophobic proteins.

In our analysis, we found the occurrence of a two-stage mitoproteome response after a short- or long-term administration of troglitazone. This was observed by proteomic shifts across the time-course in terms of (i) the ratio of up-regulated versus down-regulated proteins, (ii) the absolute number of differentially-expressed proteins, (iii) the functional classes of the differentially-expressed proteins and (iv) the minimal overlap in the proteins in the two groups. From 2D-DIGE, the modest number of differentially-modulated proteins (24) and that 83% of them increased in abundance suggested that troglitazone-induced early changes in the mitochondrial proteome were adaptive. Such greater proportion of up-regulated proteins was similarly reflected in the 8-plex iTRAQ™ study. An adaptive response to potential protoxicants typically involves transcriptional up-regulation of genes, changes to post-translational modifications and translocation of proteins into the mitochondria whose actions include eliminating the drug more efficiently and/or detoxifying reactive metabolites or ROS (antioxidant response), thus protecting the cell from initial damage (Ulrich & Friend, 2002). This was followed by a second phase where distinct proteome expression changes occurred that

were indicative of oxidative damage to a number of proteins as evidenced by decreased abundance of certain target proteins at 4 weeks. The small number of proteins common to both time-points (3 out of 70 proteins) reflected distinct and possibly stark changes that occurred at the molecular level.

This study confirms and extends previous data obtained with this model (Ong, et al., 2007) where we had found that 2-week treatment with troglitazone did not cause any apparent liver injury, while 4-week treatment caused decreased mitochondrial function (complex I activity) and oxidative injury to hepatic mitochondria. Furthermore, this study confirms that troglitazone, administered to HET mice at doses that resulted in systemic exposure levels similar to the clinical situation, caused, in some animals, overt hepatic necrosis.

4.2.2.1. Functional clustering of mitochondrial proteome

A logical and common step in analyzing genomic or proteomic data will be to examine the extremes of the data set (Lescuyer et al., 2007, Ransohoff, 2005). This simple yet efficient method is useful in the discovery of biomarkers, in selecting those that are most or least altered in terms of abundance given a biological state. However such analyses do not address the full potential of proteome-wide experiments; they also place assumptions that the most modulated proteins represent the functionally most important proteins or that they correlate specifically to the biological state of interest. In addition, automated generation of annotated pathways can present a few issues in

interpreting proteomic data. For example, IPA canonical pathways software considers individual protein fold-change but not overall directionality. Secondly, with respect to protein fold-change thresholds, it establishes limits that constraints the inclusion of low-to-moderately modulated proteins. Low-to-moderately modulated proteins are not necessarily functionally unimportant. By contrast, by capitalizing on the wider proteome coverage of MS-based proteomics, we took into account the entire range of differentially-expressed proteins, from mild to drastic fold changes and derived the mean centroid value or MCV of functional clusters. On doing so, one could faithfully index the overall modulation of a pathway, recapitulate the complexity of robust biological pathways and also maximise the real potential of global-scale technologies. Results from this approach demonstrated that there were several functional clusters which were more susceptible to troglitazone-toxic effects than others. For example, with prolonged troglitazone administration, the mitochondrial GSH transport system, ion transporters and β-oxidation were more likely to influence the phenotypic changes on the HET liver than components of ETC, urea cycle and TCA cycle.

4.2.2.2. Mitochondrial glutathione transport

Significantly, one fragile functional cluster is the mGSH cycling/transport system. The mGSH cycling/transport system was the most negatively-affected mitochondrial functional cluster with prolonged troglitazone administration. The mGSH is intrinsically perturbed by a compromised mitochondrial ROS defence in the HET mouse (Figure 23) and this fragile cluster could confer a point of sensitization for troglitazone to expose its

toxic effects. This suggests that the mGSH cluster is intolerant of unregulated elevated levels of ROS, even in the subtle redox imbalance of the HET mouse. This may stem from the lack of *de novo* GSH synthesis in the mitochondria (Griffith & Meister, 1985, Martensson et al., 1990) and the mitochondrion must replenish its pool of GSH by importing cytosolic GSH. Numerous studies have highlighted the importance of mGSH depletion and the association of hepatotoxicities (Das & Vasudevan, 2007, Fernandez-Checa & Kaplowitz, 2005, Zhao, et al., 2002).

The transport of GSH into the mitochondria is ATP-dependent and can be inhibited by a collapse of $\Delta\Psi_m$ (Martensson, et al., 1990). In addition, mGSH is an organic anion. Together, this suggest that GSH import cannot diffuse passively through the inner mitochondria membrane but require its active transport or exchange with another anion to reach the mitochondrial matrix (Lash, 2006). DIC, an anion carrier located on the inner mitochondrial membrane has been shown to function as a GSH transporter (Chen & Lash, 1998, Lluis et al., 2005, Zhong et al., 2008). The overexpression of rat kidney DIC, showing a two- to ten-fold increase in mGSH, confirmed the role of this carrier in the mitochondrial import of GSH in exchange for inorganic phosphate (Lash et al., 2002). In particular, DIC has three features that makes it a plausible target of troglitazone: (i) its temporal-based differential expression – up-regulation followed by down-regulation, fits well with the two-stage changes observed at tissue level, (ii) knockdown of DIC in *C. elegans* increases ROS production that could result in further oxidative damage (Lee et al., 2009) and (iii) the apparent compensatory response of OGC, the other mGSH transporter in isolated rat liver mitochondria (Zhong,

et al., 2008) to counteract the deleterious effect of DIC damage. Therefore, the data suggests that troglitazone exploited a diminished antioxidant environment due to *Sod2* haplodeficiency, and then apparently acting through a disrupted mGSH cluster to elicit damage via downstream mechanisms on the liver. Independent clinical studies support and extend this hypothesis further (Huang, et al., 2007, Lucena et al., 2008, Tafazoli et al., 2005a, Watanabe et al., 2003).

Association-studies on troglitazone-prescribed Japanese type II diabetes mellitus patients with elevated ALT (< 9 times upper limits of normal or ULN) and AST levels (< 5 times ULN) revealed gene-polymorphisms with combined null glutathione-S-transferase theta 1 (*Gstt1*) and glutathione-S-transferase mu1 (*Gstm1*) genotypes (Watanabe, et al., 2003). A correlation of $Gstt1^{-/-}$ and $Gstm1^{-/-}$ genotype in humans with troglitazone-associated liver transaminase elevation suggested that these acquired genetic factors at least partially predispose certain groups of patients to troglitazone-induced toxicity. Similar to this, but in a separate clinical retrospective study, $Gstm1^{-/-}$ genotype and *Sod2* polymorphisms increased the risk of anti-tuberculosis-DILI[5] (Huang, et al., 2007). Lastly and most importantly, Lucena and colleagues of the Spanish Group for the Study of Drug-Induced Liver Disease found that null mutations of *Gstt1*and *Gstm1* in Spanish patients exposed to a wide variety of drugs such as amoxicillin-clavulanate, nimsulide, flutamide and naproxen increased their susceptibility to DILI (Lucena, et al., 2008). Taken together, the large pool of clinical evidence highlighted the convergence of DILI susceptibility to perturbation in antioxidant defence, in particular GSH depletion. And because such sources of pathological changes are latent, there seems to be a

[5] Names of anti-tuberculosis drugs were not provided in the publication

potentially strong correlation of silent genetic abnormalities in ROS detoxification and GSH-cycling to the underlying factors or contributors to DILI outcomes such as troglitazone-induced liver toxicity. The HET mouse model and the clinical analysis suggest that the preclinical, inherited impairment of oxidative stress defence may proceed for many years in the absence of observable symptoms until drug exposure sensitizes these individuals to the adverse effects of drugs. This is consistent with the rarity and unpredictable nature of idiosyncratic DILI. Further verification studies extending to the review of patient records in larger study cohorts will be critical in determining the role of irregularities in GSH cluster in troglitazone-induced liver injuries in a feasible fashion. Further confirmation of the role of GSH imbalance is demonstrated in studies performed in rats which showed that troglitazone has the highest propensity to oxidize GSH, and the highest pro-oxidant activity that caused hepatocytotoxicity (Tafazoli et al., 2005b). If increased oxidant stress due to a compromised mitochondrial antioxidant defence is indeed a susceptibility factor in DILI, the HET mouse and the concomitted in-depth study on mGSH cycling could be a very promising tool for predicting not only troglitazone-toxicity but also other drugs such as the anti-tuberculosis drug mentioned above. Application of innovative molecular tools such as proteomics could signify a new paradigm in advancing mechanistic toxicity knowledge.

In this study and a recent publication, toxicological and biochemical evidence supported the hypothesis further of acquired mitochondrial dysfunction as a susceptibility factor in idiosyncratic DILI by showing how cellular and mitochondrial injuries translate to liver failure upon extended troglitazone administration (Ong, et al., 2007).

Furthermore, this study confirmed that troglitazone, when chronically administered to HET mice at doses that resulted in systemic exposure levels similar to the clinical situation, caused overt hepatic necrosis. Combining the results from proteomics with conventional toxicological endpoints and histopathological studies, we were able to correlate molecular level with cellular and tissue-level alterations. Such an approach is known as phenotypic anchoring and can be defined as "the process of determining the relationship between a particular expression profile and the pharmacological or toxicological phenotype of the organism for a particular exposure or dose and at a particular time" (Tennant, 2002, Waters & Fostel, 2004). Together with the use of conventional endpoints, the proteomic pattern is reinforced to visible phenotypic changes and therefore aids in the definition of the sequence of molecular events that corresponds to the dose, time and mode-of-action of the toxicant. This is crucial, because each individual toxicant exerts different effects at different doses and duration – acute or chronic, upon re-challenge and so forth, and phenotypic anchoring helps to establish the molecular changes at the proteome level, to the toxicant's specific mechanisms given a particular situation or condition.

4.2.2.3. PPAR-agonist mitochondrial targets

Among the changes in the mitoproteome, it is important but not always possible to distinguish between the drug-specific effects (including pharmacological effects) and non-specific, common toxic response pathways that merge or branch out more distally and that are shared with other hepatotoxicants (Kaplowitz, 2005). Specifically for troglitazone, effects on altered glucose and lipid homeostasis (PPARγ-dependent and –

independent processes) should therefore be differentiated from effects arising as a consequence of, for example, intramitochondrial oxidative stress that triggers the ASK1/JNK pathway that led to lethal hepatocyte injury. For example, compound-selective effects observed after 2 weeks included regulatory changes in fatty acid α- and β-oxidation, in particular upregulation of ACADM (the first step in β-oxidation) and HADH (the third step in β-oxidation), as well as 2-hydroxyacyl-CoA lyase (α-oxidation). Interestingly, the final step of β-oxidation (3-ketoacyl-CoA thiolase) was down-regulated at the protein level. Overall, this may reflect an adaptive response to the well-known inhibitory effects of thiazolidinediones on fatty acid oxidation, which is a consequence of an inhibition of acyl-CoA synthase (Fulgencio et al., 1996). Similarly, the observed up-regulation of HMG-CoA synthase after 2 weeks could be a result of TDZ binding to PPARα/γ, which would transactivate HMG-CoA synthase by binding to its promoter region (Hegardt, 1999). With continued troglitazone administration, some of the changes that reflect disturbances in fatty acyl metabolism were still obvious. For example, ketoacyl-CoA thiolase and palmitoyl-CoA oxidase levels were decreased.

The functional clustering analysis demonstrated that several of these clusters were less likely to play important roles in initiating or precipitating troglitazone-induced liver toxicity in the HET mouse. In some cases, it may be for the reason to curtail excessive cellular damage that the functional cluster remained at a basal state. For instance, the β-oxidation cluster remained at basal levels even with extended troglitazone-administration. This is crucial because free fatty acids can enhance mitochondrial-generated ROS by inhibiting the OXPHOS and by interfering with electron flow (Schonfeld & Wojtczak,

2008). Alternatively, this could also imply troglitazone's toxicity on this functional cluster given that this was opposite to troglitazone's role in restoring defective β-oxidation in human skeletal muscle and liver of the Zucker diabetic fatty rats (Cha, et al., 2005, Ide et al., 2000). In addition, disruption of β-oxidation will result in hepatic steatosis (Bartlett & Eaton, 2004, Eaton et al., 1994). As such, adverse consequences to the mitochondria can be minimized if β-oxidation is regulated. It is important to note that it is PPARα, which is highly expressed in the liver rather than PPARγ that is likely driving the expressions of these β-oxidation enzymes. This remains a paradox as to how troglitazone exerts its effects when the expression of its receptor is low in the liver (Citters & Forman, 2004). To this, it has been suggested that troglitazone is a dual agonist to PPARα and more strongly, PPARγ (Camp et al., 2000, Etgen et al., 2004, Lehmann et al., 1995).

The overall decrease in PPAR-responsive genes/proteins suggested an association of PPAR-dependent toxicity under increased mitochondrial oxidative stress. While this mechanism has been proposed before (Peraza et al., 2006), it did not account for the low incidence and delayed onset of troglitazone DILI. Rather, accumulating evidence pointed to mitochondria and ROS in predisposing individuals to troglitazone DILI (Julie et al., 2008). Such susceptibility factors could act in synergy with PPAR-ligand-induced toxicity and cause earlier and/or more severe manifestations of liver injuries potentially.

Although hepatic PPARγ levels did not increase appreciably upon troglitazone treatment, a notable point is the binding potencies of thiazolidinediones to PPARγ.

Previous studies have shown that the affinity of different thiazolidinediones species to PPARγ can be ranked in the following order: rosiglitazone > pioglitazone > troglitazone = ciglitazone (Camp, et al., 2000, Willson et al., 1996, Young et al., 1998) and this preferential affinity may have direct influence on the degree of expression of PPARγ-responsive genes/proteins.

4.2.2.4.OXHPOS

Sometimes, unbiased highthroughput approaches generate results that are counter-intuitive. Impairment of OXPHOS has been a logical area of focus for mechanistic information of troglitazone-induced cytotoxicity (Nadanaciva, et al., 2007, Tirmenstein, et al., 2002). However, our *in vivo* results suggested that troglitazone-mediated ETC-targeted toxicity may be early, if not transient, as denoted by healthy livers after 2 weeks of troglitazone treatment. In the *Sod2*$^{-/-}$ mouse brain, SDHB, a complex II subunit sensitive to *Sod2* loss was observed to decrease in abundance (Hinerfeld, et al., 2004). In contrast, in the HET mouse, SDHB remained at basal levels, and decreased marginally after 2 weeks of troglitazone administration. Interestingly, continual troglitazone treatment led to SDHB up-regulation, presumably as a compensatory response for any ROS-induced defects mediated by troglitazone. One ETC subunit was particularly interesting. In both short- and long-term troglitazone treatments, NDUFS4 was down-regulated. For this reason, NDUFS4, a nuclear-encoded ETC subunit, may be a sensitive protein biomarker to both early and sustained ROS toxicity. The potential value of using NDUFS4 as biomarker was demonstrated by the *Ndufs4*$^{-/-}$ mutant mouse. *Ndufs4*$^{-/-}$ mice

die by 7 weeks (the usual lifespan of WT mice ranges from 60 to 104 weeks), thus suggesting the detrimental cumulative effect of NDUFS4 deficiency (Kruse et al., 2008), which is a useful characteristic in predicting long-term mitochondrial toxicity.

4.2.2.5. Valine metabolism

Other changes (e.g., increases in 3-hydroxyisobutyryl-CoA hydrolase and isobutyryl-CoA dehydrogenase) include alterations of enzymes involved in valine catabolism. Valine catabolism occurs in the mitochondria, and among the metabolic intermediates, methacrylyl-CoA (MC-CoA) is potentially mitotoxic by reacting with thiol groups on proteins or GSH (Taniguchi et al., 1996). In addition, MC-CoA can inhibit sulfhydryl-containing mitochondrial enzymes which must be maintained in the reduced form for proper function. MC-CoA is detoxified by two steps by MC-CoA hydratase and 3-hydroxyisobutyryl-CoA (HIB-CoA) hydrolase. Interestingly, the subsequent catalysis of HIB-CoA by HIB-CoA hydrolase has been suggested to be cytoprotective against the toxic effects of MC-CoA (Taniguchi, et al., 1996). Thus, the increase in HIB-CoA hydrolase may be important in detoxifying MC-CoA as a result of increased valine catabolism. Preceding the formation of toxic MC-CoA is the catabolism of valine and isobutyryl-CoA. Unexpectedly, isobutyryl-CoA dehydrogenase (ACAD8) was shown to increase, which would result in more MC-CoA generated. Why this occurs is unclear. However, troglitazone reduces gluconeogenesis in the liver, and since valine is a glucogenic amino acid, upregulation of ACAD8 could generate more succinyl-CoA to enter the Krebs cycle for energy production.

4.2.2.6. Redox and Stress Response Proteins

In contrast, the most prominent effects pointing to a drug-induced non-specific cell stress was a clear stress response signal and upregulation of the mitochondrial protein import machinery. After 2-weeks of drug treatment, members of the heat shock protein superfamily, mortalin (HSPA9) and HSP7C were modified and predominantly down-regulated. These proteins are involved in refolding damaged proteins (chaperone function) and importing proteins into mitochondria; the changes may reflect adaptive responses that indicate underlying oxidant stress that can damage proteins including some stress response proteins themselves. Along the same line, Lon protease (LONP1), a matrix-selective protease that is involved in the removal of oxidatively damaged proteins was up-regulated (Bota & Davies, 2002). These data at the proteome level confirmed earlier findings obtained by Western blotting and showed that thiazolidinediones can induce members of HSP70 in non-hepatic and transformed liver cells *in vitro* (Maggi et al., 2000b, Maniratanachote, et al., 2005). Free and protein-bound methionine residues are oxidation-sensitive and readily oxidized to methionine sulfoxide derivatives which are in turn economically repaired by methionine sulfoxide reductase A (MSRA) (Moskovitz et al., 2001, Vogt, 1995). Methionine has been proposed to act as an intrinsic oxidation sink to protect other more oxidation-labile amino acids and structures (Levine et al., 1996, Stadtman et al., 2002), especially at sites with high ROS-production such as the mitochondria. Accordingly, the mitochondrial proteome contains more methionine than nuclear proteomes (Bender et al., 2008) and MSRA was found to be up-regulated in both 2- and 4-weeks study groups, possibly as a measure to repairing oxidized

methionine residues. In fact, the prolonged administration of troglitazone may have caused an overall up-regulation of stress response proteins and import proteins to cope with the challenge, but clearly, this compensatory response was insufficient and hepatic necrotic lesions ensued. With regards to drug-induced oxidant stress, additional markers indicative of mitochondrial oxidant stress thus became more apparent; for example, SOD2 was upregulated, while catalase was less abundant. In addition, Clp protease (an ATP-dependent protease) was up-regulated. These changes likely reflect adaptations to oxidative damage to proteins. In spite of this, mitochondrial protein carbonylation and nitration was significantly higher, indicating that there was an overwhelming oxidant stress on the mitoproteome which could neither be completely compensated by stress response proteins nor by the increased import of mitochondrial proteins.

4.2.3. Summary

Taken together, the proteomic results demonstrate that low repeated doses of troglitazone given to HET mice (whose mitochondrial antioxidant defence is slightly compromised) resulted in a two-stage oxidant injury to liver mitochondria by afflicting several sensitive functional clusters (Figure 43). The first phase was an adaptation to a prooxidant challenge, as reflected in the modification and up-regulation of stress genes/proteins and the lack of increases in levels of markers of protein oxidation. Such a cellular stress response can be viewed as an early marker of impending toxicity (Heinloth et al., 2004). The subsequent phase was characterized by oxidative damage to and decreased abundance of a number of key proteins, among which ACO2 was identified as a potential biomarker of oxidant stress in liver mitochondria. In accordance with this,

protein oxidative damage and overt liver necrosis were increased after 4-week treatment. It is not known what determines the shift from adaptive responses (without overt signs of toxicity) to a toxic response. Because troglitazone itself is not being accumulated in liver over time despite higher hepatic levels as compared to plasma (Chojkier, 2005), it is likely that a cumulative adverse effect was building up, again compatible with mitochondrial injury. It is important to understand that it is the accumulation of a drug's off-target effects that lead to liver injury, rather than the accumulation of troglitazone in the liver. The 2D-DIGE results have been published (Lee et al., 2008b) and our more recent findings based on 8-plex iTRAQ™ will be published shortly.

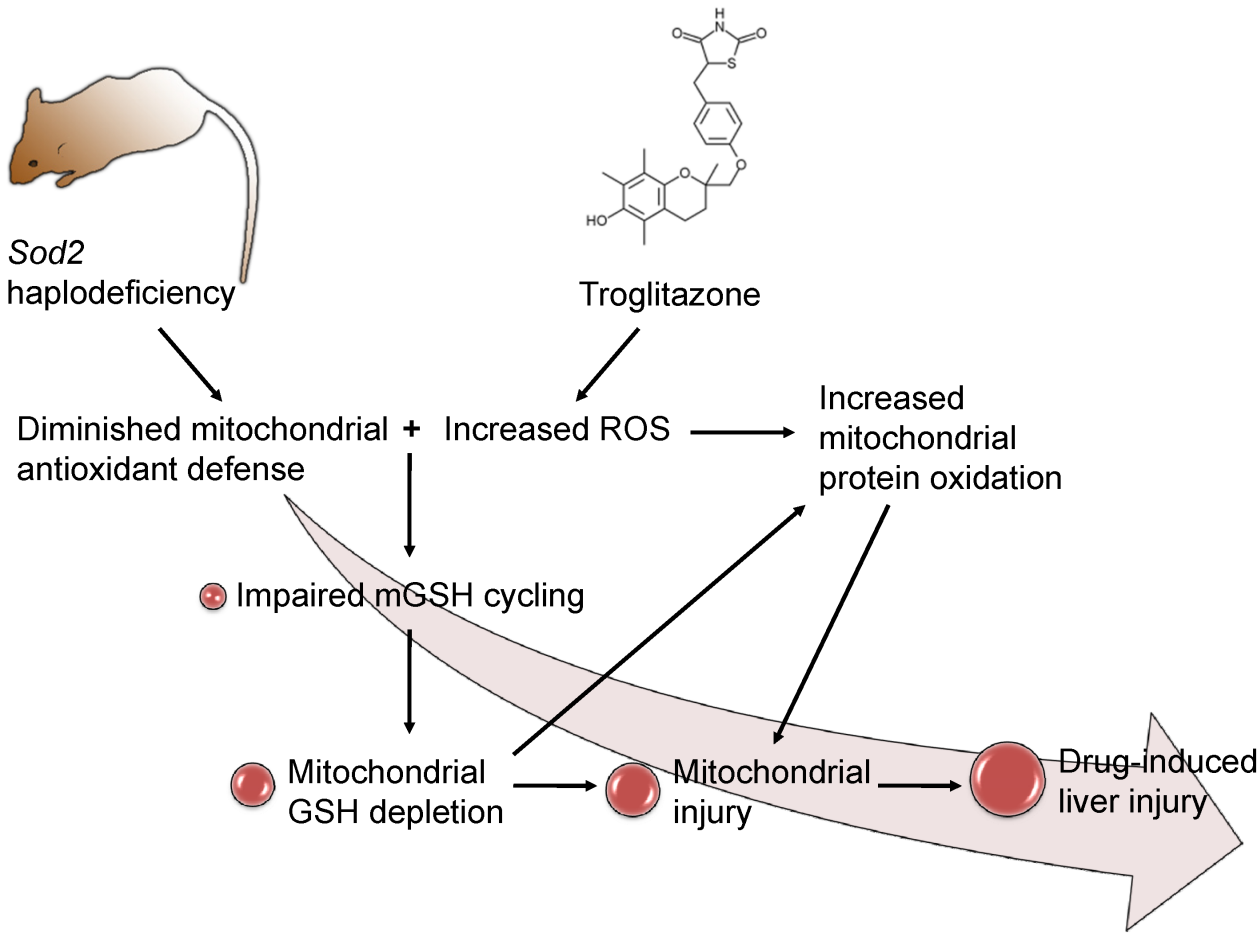

Figure 43. Proposed model of troglitazone-induced liver injury in the *Sod2*$^{+/-}$ mouse
The intrinsic diminished mitochondrial antioxidant defense, especially the mGSH cycling, acts as a fragile point of sensitazation for troglitazone-induced oxidative stress to extend its adverse effects on the liver. Alterations to mitoproteome and protein oxidation are some of the consequential effects that form a vicious cycle, ultimately leading to livery injury. The red balls represent the cumulative effect of troglitazone and its adverse effects that build up and lead to injury and eventually mitochondrial and liver injury

4.3. Aconitase-2 as a Potential Biomarker to Early Prediction of Toxicity

The terminology of biomarkers was defined by the Biomarkers Definitions Working Group under National Institutes of Health Director's Initiative on Biomarkers and Surrogate Endpoints as "a characteristic that is objectively measured and evaluated as an indicator of normal biological processes, pathogenic processes, or pharmacological responses to a therapeutic intervention" (Atkinson et al., 2001). Biomarkers contribute information of the pathophysiological state and are valuable in assessing the efficacy of certain treatments, and serving as proof-of-concept.

Because of the difficulty in picking up possible drug toxicities in normal and healthy murine models, there has been growing controversy on the value of using such mice as surrogates for studying human diseases (Dixit & Boelsterli, 2007, Nierkens & Pieters, 2005). In addition, there has been a recent change in strategies during toxicological evaluation by suggesting new mutant mouse models as surrogates to screen for drug toxicities (Dixit & Boelsterli, 2007, Griffin, 2006, Wallace, 1999). One strategy is to use the HET mouse in evaluating drug safety profiles. Hence in this study, proteomics and conventional toxicological endpoints were integrated to mine for potential protein signatures to predict idiosyncratic DILI. Importantly, the markers that most clearly pointed to a direct oxidative injury in mitochondria were associated with a decreased abundance of these proteins. Comparison between the 2 and 4 week study groups revealed only a few proteins which were concurrently affected by the toxicant in both groups. One such protein is ACO2. ACO2 is well recognized for its enhanced

sensitivity to oxidative stress due to its 4[Fe-s] clusters that are sensitive to prooxidants (Gardner et al., 1995; Nulton-Persson & Szweda, 2001) and has been proposed as a candidate biomarker in other proteomic studies (Bi et al., 2006, Hunzinger et al., 2006). Importantly, biochemical analysis has demonstrated that under increased oxidative stress, functional defects of ACO2 in the HET mouse do not necessarily correspond to significant changes in its activity (Williams, et al., 1998). This can be attributed to a known PTM of ACO2, known as carbonylation (Yan et al., 1997). Therefore ACO2 abundance alone is not sufficient to determine its utility as a sensitive and specific biomarker of oxidative stress. Note that iTRAQ™ did not detect changes in ACO's expression. ACO2 undergoes three different fates under varying stages of oxidative stress. Under mild oxidant stress, ACO2 is carbonylated. Following more oxidative stress, carbonylated ACO2 is marked for proteolysis by Lon protease (Delaval, et al., 2004). Lastly when exposed to more severe oxidant stress, ACO2 may form high-molecular weight aggregates which is no longer a substrate for Lon protease (Bota & Davies, 2002), which we also consistently found after troglitazone treatment.

Using 2D-DIGE, the changes occurring in ACO2 expression/PTM were partially demonstrated. In the 2 weeks study, the HET mouse is mildly sensitized by ROS-inducing troglitazone, the decrease in ACO2 abundance levels correlated well with increased Lon protease expression thus representing the increased Lon-mediated degradation of ACO2. This is consistent with biochemical studies that showed an increase in Lon protease, corresponding to increased degradation of oxidized ACO2 under mild prooxidant conditions (Bota & Davies, 2002). With prolonged troglitazone

treatment the HET mitochondria is subjected to chronic oxidative stress and ACO2 aggregated by becoming a poor substrate for Lon. However, aggregated ACO2 and Lon protease were not significantly modulated, as seen on the 2D-DIGE gels.

ACO2 has a peculiar sensitivity to oxidative damage and ability in distinguishing mild or chronic oxidative stress through a sustained change in expression and PTM over time. In addition, ACO2 function was also attenuated in *ex vivo* mitochondria from troglitazone-treated HET mice (Ong, et al., 2007). These factors make ACO2 a promising candidate for a biomarker of mitochondrial oxidant stress and ensuing toxicity. Although further in-depth studies are still required, ACO2 can be a promising oxidative stress marker for early detection as well as for diagnosing a biological system's redox status in response to oxidative insults, although not necessarily limited to troglitazone-induced ROS elevations but the early detection of ROS-inducing effects of drugs in general.

4.4. Mechanistic toxicology of troglitazone-induced DILI

Activation of JNK and p38 have been implicated as a mechanism in which troglitazone exerts its hepatocytotoxicity *in vitro* (Bae & Song, 2003, Lim et al., 2008). Here we show the *in vivo* ASK1-JNK1/2 activation in troglitazone-induced hepatotoxicity in the HET mouse, analogous to the major role JNK activation in acetaminophen-induced mouse liver injury (Gunawan et al., 2006, Tothova et al., 2007). There could be signalling crosstalk between ROS-mediated ASK1-JNK and FOXO3a through JNK-dependent phosphorylation of 14-3-3 (Sunayama et al., 2005, Sunters et al.,

2006, Tsuruta et al., 2004) which led to the activation of FOXO3a governing the mitoproteome. Interestingly, FOXO3a activation and translocation into the nucleus took place even when AKT remained phosphorylated. AKT phosphorylation regulates FOXO3a phosphorylation which in turn retains FOXO3a in the cytosol. This suggests that JNK antagonises AKT-mediated survival signals when the redox status is tipped towards that of a stressed one (Sunayama, et al., 2005). This was in parallel with a marked increase in *Sod2* expression following continual troglitazone treatment under inadequate mitochondrial oxidative stress management. Consistent with FOXO3a and its activation with a rise in ROS levels (Honda & Honda, 1999, Kops et al., 2002), prolonged troglitazone exposure in the HET liver led to dephosphorylation and nuclear translocation of FOXO3a to facilitate its role as a transcription factor. Such phenomenon can be intepreted as that of FOXO3a playing a significant role in modulating the mitochondrial antioxidant defence and possibly the mitoproteome during chronic toxicant-related liver injury. The ASK1-JNK-FOXO3a is therefore an attractive pathway for the development of toxicity tests ascribed to the detection of drugs with mitochondrial liability.

Although this model cannot explain idiosyncratic liver failure in patients (Jaeschke, 2007), it demonstrated that a small, discreet defect in a mitochondrial antioxidant system (heterozygous *Sod2* deficiency) can have dramatic consequences in vivo after challenge with therapeutic doses of troglitazone for a prolonged period of time. Furthermore, this model could help explain at the molecular level why patients who are exposed to drugs causing idiosyncratic DILI and who develop mild asymptomatic

transient increases in ALT most likely adapt to the potential prooxidant adverse effects of the drug (Abboud & Kaplowitz, 2007).

5. CONCLUSIONS

5.1. Implications of Studying the HET Hepatic Mitoproteome in Drug Safety Evaluation

Idiosyncratic drug-induced hepatotoxicity represents a major problem in drug development due to a paucity of suitable animal models to predict such unwanted side effects (Dixit & Boelsterli, 2007). Therefore the HET mouse has been suggested as a preclinical mouse model for toxicological evaluation of drugs. So how does this current study contribute to the toxicology field? Firstly, we were able to link impairment of mitochondrial function to phenotype relevant to humans by taking into account the presence of a clinically latent ailment. Such animals are sensitized to the toxic effects of normally-mild drugs not seen in healthy, normal laboratory mice (Boelsterli, 2003a). This also offers a mechanistic reasoning as to why small groups of patients may be more susceptible from the larger population exposed to the drug. Secondly, through the use of proteomics, we were able to globally analyze the mitochondrial proteome after troglitazone treatment. The functional consequences of short-term and long-term troglitazone administration on the hepatic mitochondria are important in defining the mechanisms that underlie the delayed toxicity in humans. Presently, this represents one of the few mouse models that can mimic the human situation. Therefore, this study, through the integration of proteomics with conventional toxicological endpoints achieved the

three objectives set out initially. This includes addressing the suitability of the HET mouse to unmask potential idiosyncratic drug-induced adverse events, the role of genetically-acquired mitochondrial dysfunction in predisposing individuals to toxic effects and finally, giving new insights to the mechanisms of rare, idiosyncratic DILI When such a strategy is employed, more efforts can be made to better understand the key mechanisms in off-target toxicities and improving drug safety.

5.2. Summary

In this study we sought to determine the potentiality of the HET mouse in unmasking normally undetected toxic effects of drugs meant for improving the well-being of patients. Because of the intrinsic redox disequilibrium in the HET mouse, it is a powerful animal model to study drug-induced pathogenesis under a lack of mitochondrial antioxidant protection. The absence of single *Sod2* allele led to the increased ROS levels and also altered the expression and modification of a collection of mitochondrial proteins involved in redox homeostasis such as GPX1, GSTK1 and MGST1 and mitochondrial metabolic functions. This sustained increase in ROS was neither sufficient to deplete mGSH, nor was it severe enough to adversely affect normal mitochondrial functioning of the urea cycle, TCA cycle, OXPHOS and β-oxidation. This discreet and small deficit in mitochondrial antioxidant defence represents a "1st hit" which is particularly useful for modelling toxicant-related diseases ("2nd hits") that converges on compromised mitochondrial function that progressively develops over a prolonged period of time.

We combined proteomics with classical toxicological endpoints in this study, generating a deeper understanding of the time-course and mechanisms of troglitazone-induced toxicity on the HET hepatic mitochondria. Our results clearly revealed a two-stage response which interestingly resembled the clinical outcome, showing a delayed toxic effect only after extended troglitazone exposure. Toxicoproteomic data revealed that the early mitochondrial response was compensatory, characterised by a larger proportion of up-regulated proteins (approximately 21% up-regulated versus 6% down-regulated), an induction of the mitochondrial stress response and a lack of oxidized mitochondrial proteins. Subsequently, the mitochondria and liver succumbed by 4-weeks. In an almost reversal of the 2-weeks situation, we found that approximately 8% of the mitoproteome were up-regulated whereas 20% were down-regulated. Mitochondrial protein carbonyls and 3-NT adducts were significantly increased, in spite of increased SOD2 levels, suggesting that the threshold for oxidative injury has been reached. In addition, the mitochondrial GSH transport system was perturbed, indicating this functional cluster as a critical cluster in precipitating troglitazone DILI. This is strongly supported by independent clinical studies demonstrating that GSH, in the form of GST mutations, are linked to troglitazone-induced liver injury (Watanabe, et al., 2003). Together, these results link mitoproteome changes to the phenotypic changes on the liver, which triggered the abrupt progression of necrotic hepatic lesions. Through our study, we found ACO2 to be a potential biomarker candidate for mitochondrial oxidative stress. Its exquisite sensitivity to oxidative stress, mitochondrial localization and its various protein modifications make ACO2 a highly appropriate protein biomarker for distinguishing the different degrees of mitochondrial oxidative stress.

At a time when drug-induced toxicities remain an important concern, the US. Food and Administration has initiated the Critical Path Activities to modernize the drug development process and drug safety evaluation, among which mechanisms underlying DILI and its prediction came under the priority topic of "Better Evaluation Tools" (Faca et al., 2008, Hennessy & Strom, 2007). The use of proteomics on a mutant mouse model of acquired mitochondrial abnormality may therefore tremendously enhance and augment our understanding on the association of risk factors in the pathogenesis of idiosyncratic DILI.

6. FUTURE WORK

In this study, we demonstrated that the HET mouse has the potential to reveal troglitazone's toxicity early. Toxicoproteomics was conducted in a comparative time-course manner to guide better understanding of the underlying mechanisms of troglitazone-induced DILI. We have several suggestions to improve this approach.

(1) To further accredit that this mutant mouse model is suitable for preclinical detection of drug-induced mitochondrial toxicity across a broader spectrum of drugs, it is necessary to rigorously assess the validity of this model across different drug classes. This validation of the HET mouse model as a proof-of-concept model was limited to troglitazone due to time constraints. Some drugs of different classes which may help to extend the HET mouse model's validity and show its sensitivity include tolcapone, an anti-Parkinson's disease drug and flutamide, an antiandrogen for the treatment of prostate cancer. Such drugs caused idiosyncratic liver injuries in certain patients and they have been linked to drug-induced mitochondrial toxicity (Coe et al., 2007, Haasio et al., 2002).

(2) On the basis that many drugs charged with causing idiosyncratic DILI affect the mitochondria, its functions or induction of cell death via the mitochondrial pathway, the HET mouse is potentially also an ideal surrogate mouse model to model the human clinical situation. While there is no conclusive experimental or clinical evidence to linking SOD2 deficiency/mutation in susceptible patients to idiosyncratic DILI,

association studies, GSH has emerged as a critical molecular in idiosyncratic DILI (Huang, et al., 2007, Lucena, et al., 2008, Tafazoli, et al., 2005a, Watanabe, et al., 2003). We could apply integrative proteomics to discover the perturbation of mGSH transport system with long-term troglitazone administration. We could also suggest the role of DIC in exposing hepatocytes to the toxic effects of troglitazone under a compromised mitochondrial antioxidative state. Manipulation of DIC by RNA interference can be used to investigate the toxicological consequences of altering mGSH upon troglitazone treatment and verify that DIC is an important determinant in precipitating troglitazone-induced hepatotoxicity. Any dramatic changes in sensitivity of cells proceeding after DIC knock-down will suggest a constant influx of mGSH levels to maintain resistance to troglitazone. Unfortunately, given the time constraints on this study, we were unable to conduct RNA interference experiments. This set of experiments remain the next critically-importantly experiment to verify the functional role of DIC and its (if any) association in precipitating troglitazone DILI.

(3) Historically, discovery proteomics generate a list of proteins which is validated based on immunological assays, thus providing the confidence to support the mass spectrometry data. In practice, a combination of factors, including the generation of redundant tryptic peptides, and thereafter varying ionization efficiencies for different amino acids, poor fragmentation and peptide identification resulted in only a fraction of the proteins being successfully detected in complex biological samples (Kuster et al., 2005, Malmstrom et al., 2007). The undetected proteins may represent key components of pathways and yet, commercially available antibodies exist for only a small fraction of

the proteome. Therefore, this implies that there is a technological gap in the detection and quantification of a majority of proteins by existing methodologies. More recently, mass spectrometric multiple reaction monitoring or MRM has emerged as a specific, quantitative tool for targeted proteomics (Fusaro et al., 2009, Kuhn et al., 2004). Therefore as part of any future work, MRM, in combination with large-scale, unbiased toxicoproteomics could be employed to measure the presence and abundance of any protein-of-interest to obtain a truly global view of a proteome upon drug treatment.

(4) It is worth mentioning that systems toxicology, a variant of systems biology has immense potential in advancing the understanding of toxicology in complex biological systems (Waters & Fostel, 2004). To leverage on our proteomic dataset and functional clustering, computational modelling can also be developed to create dense protein-interaction networks to help us understand the adverse effects of oxidative stress and troglitazone-induced pathological processes at the functional level. Although systemic integration of proteomic information with interactions is useful, they require high-quality protein-interaction datasets based on experimentally- and/or computationally-derived results. Reports of large-scale mouse protein-protein interactions remain modest (Li et al., 2009) and it limits our ability to generate a map of mouse protein-interactions using our HET mouse dataset. Mitochondrial protein-interaction maps are virtually absent to the best of our knowledge. We eagerly await further developments of such databases.

In summary, we have shown that toxicoproteomics of the HET mouse is a robust method in evaluating the time-course and mechanisms of troglitazone DILI. This fills a critical gap in understanding the progression of idiosyncratic DILI, albeit in troglitazone-induced toxicity only. We hope that with improvements in technologies and methodologies such as MRM and protein-interaction networks, greater use of such an approach can be better applied to advance our understanding of toxicology in basic research and healthcare. Ultimately such knowledge should tremendously reduce drug attrition and yield safer drugs in the future.

7. APPENDIX

7.1. MS/MS spectrum

- 3-hydroxyisobutyrate dehydrogenase

IPI00116222 (IPI_mouse_v.3.23)
Best-scored peptide: MS/MS Fragmentation of **HGYPLILYDVFPDVCK**
MONOISOTOPIC mass of neutral peptide *Mr*: 1934.96
Variable modifications:
C15 : Carbamidomethyl (C)
Ions Score: 32 **Expect:** 0.13
Matches (Bold Red): 13/201 fragment ions using 11 most intense peaks

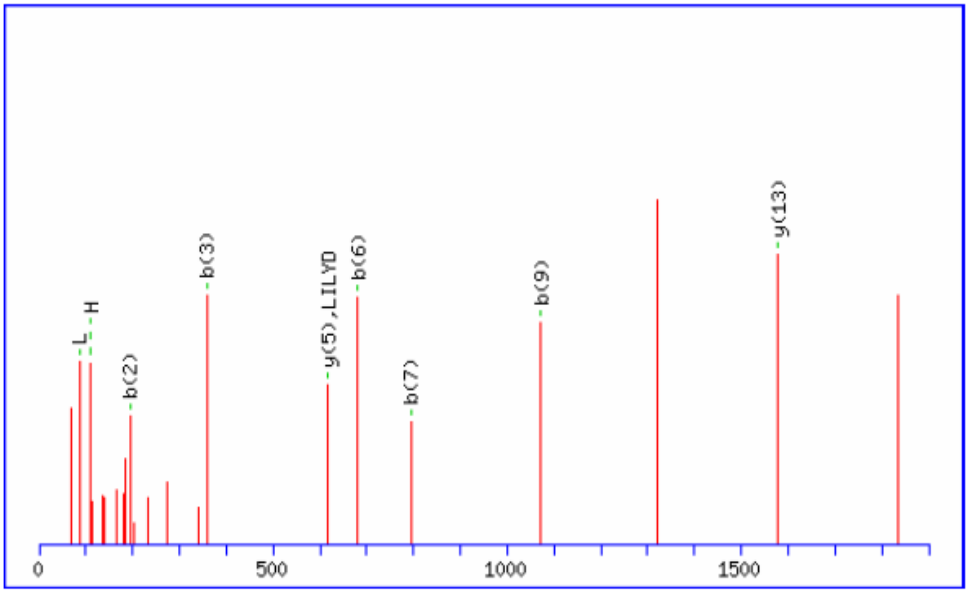

esidue	*b*
	138.07
	195.09
	358.15
	455.20
	568.29
	681.37
	794.46
	957.52
	1072.55
	1171.61
	1318.68
	1415.74
	1530.76
	1629.83
C	1789.86
K	

Figure 44. Supplemental data of best scoring MS/MS of 3-hydroxyisobutyrate dehydrogenase

- Enoyl-CoA hydratase

IPI00454049 (IPI_mouse_v.3.23)
Best-scored peptide: MS/MS Fragmentation of **AQFGQPEILLGTIPGAGGTQR**
MONOISOTOPIC mass of neutral peptide *Mr*: 2110.12
Ions Score: 33 **Expect:** 0.088
Matches (Bold Red): 22/402 fragment ions using 13 most intense peaks

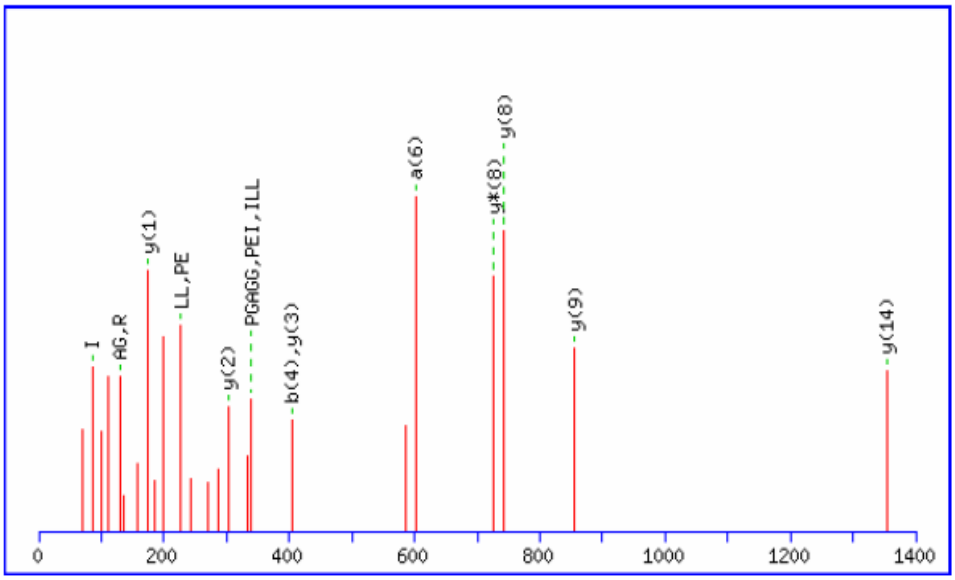

Residue	y
A	
Q	2040.09
F	1912.03
G	1764.96
Q	1707.94
P	1579.88
E	1482.83
I	**1353.78**
L	1240.7
L	1127.62
G	1014.53
T	957.51
I	**856.46**
P	**743.38**
G	646.33
A	589.31
G	518.27
G	461.25
T	**404.23**
Q	**303.18**
R	**175.12**

Figure 45. Supplemental data of best scoring MS/MS of enoyl-CoA hydratase

- Hydroxymethylglutaryl-CoA synthase
  IPI00420718 (IPI_mouse_v.3.23)

Best-scored peptide: MS/MS Fragmentation of **APLVLEQGLR**
MONOISOTOPIC mass of neutral peptide *Mr*: 1094.64
Ions Score: 33 **Expect:** 0.069
Matches (Bold Red): 22/131 fragment ions using 22 most intense peaks

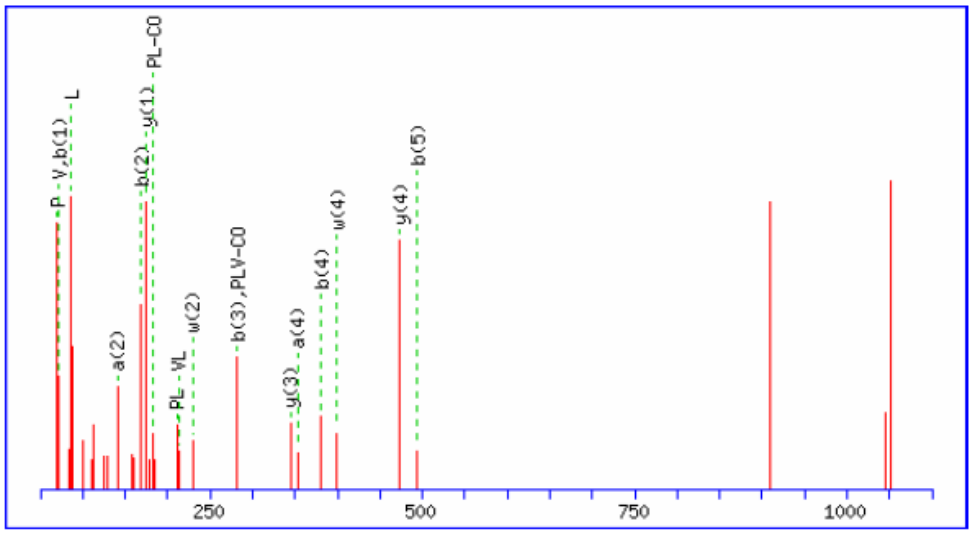

Residue	*b*	*y*
A	**72.04**	
P	**169.1**	1024.61
L	**282.18**	927.56
V	**381.25**	814.48
L	**494.33**	715.41
E	623.38	602.33
Q	751.43	**473.28**
G	808.46	**345.22**
L	921.54	288.2
R		**175.12**

Figure 46. Supplemental data of best scoring MS/MS of hydroxymethylglutaryl-CoA synthase

7.2. Protein Tables

Mean Centroid Values obtained from proteomic data

Table 11. List of detected proteins used to calculate MCV

B oxidation			
Accession #	**Name**	**2 weeks**	**4 weeks**
IPI:IPI00875372.1	Gene_Symbol=Echdc2 Isoform 2 of Enoyl-CoA hydratase domain-containing protein 2, mitochondrial	0.9463	1.2904
IPI:IPI00387379.1	Gene_Symbol=Decr1 2,4-dienoyl-CoA reductase, mitochondrial	1.0006	0.9821
IPI:IPI00121322.2	Gene_Symbol=Etfdh Electron transfer flavoprotein-ubiquinone oxidoreductase, mitochondrial	1.0268	1.0189
IPI:IPI00116753.4	Gene_Symbol=Etfa Electron transfer flavoprotein subunit alpha, mitochondrial	0.9453	1.0663
IPI:IPI00848492.1	Gene_Symbol=LOC100045699 similar to Electron transferring flavoprotein, beta polypeptide isoform 2	0.9180	1.0153
IPI:IPI00134961.1	Gene_Symbol=Acadm Medium-chain specific acyl-CoA dehydrogenase, mitochondrial	0.9654	0.9922
IPI:IPI00119203.4	Gene_Symbol=Acadvl Very long-chain specific acyl-CoA dehydrogenase, mitochondrial	1.0590	1.0966
IPI:IPI00894588.1	Gene_Symbol=Acadl Long-chain specific acyl-CoA dehydrogenase, mitochondrial	1.0603	1.0329
IPI:IPI00331251.1	Gene_Symbol=Acads Acyl-Coenzyme A dehydrogenase, short chain, isoform CRA_a	0.9653	1.0460
IPI:IPI00330094.4	Gene_Symbol=Cpt1a Carnitine O-palmitoyltransferase I, liver isoform	1.2898	0.9966
IPI:IPI00881401.1	Gene_Symbol=Cpt2 carnitine palmitoyltransferase 2	1.1047	1.0996
IPI:IPI00130804.1	Gene_Symbol=Ech1 Delta(3,5)-Delta(2,4)-dienoyl-CoA isomerase, mitochondrial	0.9423	0.8760
IPI:IPI00454049.4	Gene_Symbol=Echs1 Enoyl-CoA hydratase, mitochondrial	0.9221	1.1311
IPI:IPI00121105.2	Gene_Symbol=Hadh Hydroxyacyl-coenzyme A dehydrogenase, mitochondrial	0.9911	0.9936
IPI:IPI00223092.5	Gene_Symbol=Hadha Trifunctional enzyme subunit alpha, mitochondrial	1.0484	0.9273
IPI:IPI00115607.3	Gene_Symbol=Hadhb Trifunctional enzyme subunit beta, mitochondrial	1.0446	0.9955
IPI:IPI00131584.1	Gene_Symbol=Slc25a20 Mitochondrial carnitine/acylcarnitine carrier protein	1.1764	1.0216
IPI:IPI00653158.1	Gene_Symbol=Acaa2 Acetyl-Coenzyme A acyltransferase 2 (Mitochondrial 3-oxoacyl-Coenzyme A thiolase), isoform CRA_k	0.9729	1.0094
IPI:IPI00122139.3	Gene_Symbol=Acaa1b;Acaa1a 3-ketoacyl-CoA thiolase B, peroxisomal	1.8786	0.4855
IPI:IPI00154054.1	Gene_Symbol=Acat1 Acetyl-CoA acetyltransferase, mitochondrial	0.9671	0.9511
IPI:IPI00331692.1	Gene_Symbol=Dci Putative uncharacterized protein	1.0440	1.0077

	MCV	1.0604	1.0017

GSH recycling			
Accession #	**Name**	**2 weeks**	**4 weeks**
IPI:IPI00135231.2	Gene_Symbol=Idh1 0 day neonate lung cDNA, RIKEN full-length enriched library, clone:E030024J03 product:isocitrate dehydrogenase 1 (NADP+), soluble, full insert sequence	1.0745	0.5321
IPI:IPI00273164.1	Gene_Symbol=Aldh5a1 Succinate-semialdehyde dehydrogenase, mitochondrial	0.8826	1.0085
IPI:IPI00121051.3	Gene_Symbol=Gstk1 Glutathione S-transferase kappa 1	1.0470	0.8088
IPI:IPI00230754.5	Gene_Symbol=Slc25a11 Mitochondrial 2-oxoglutarate/malate carrier protein	1.0523	1.0804
IPI:IPI00317074.3	Gene_Symbol=Slc25a10 Mitochondrial dicarboxylate carrier	1.2446	0.8863
IPI:IPI00319652.2	Gene_Symbol=Gpx1 Glutathione peroxidase 1	0.8510	1.0472
IPI:IPI00109109.1	Gene_Symbol=Sod2 Superoxide dismutase [Mn], mitochondrial	0.9572	1.2302
IPI:IPI00135857.3	Gene_Symbol=Sod1 (BLAST score 313, P = 3e-84) EG667310;LOC545845 hypothetical protein isoform 4	0.9004	0.7967
	MCV	1.0012	0.9238

Redox detoxification			
Accession #	**Name**	**2 weeks**	**4 weeks**
IPI:IPI00109109.1	Gene_Symbol=Sod2 Superoxide dismutase [Mn], mitochondrial	0.9572	1.2302
IPI:IPI00121051.3	Gene_Symbol=Gstk1 Glutathione S-transferase kappa 1	1.0470	0.8088
IPI:IPI00135857.3	Gene_Symbol=Sod1 (BLAST score 313, P = 3e-84) EG667310;LOC545845 hypothetical protein isoform 4	0.9004	0.7967
IPI:IPI00319652.2	Gene_Symbol=Gpx1 Glutathione peroxidase 1	0.8510	1.0472
IPI:IPI00378120.2	Gene_Symbol=Glrx5 Glutaredoxin-related protein 5	0.9794	1.1829
IPI:IPI00896110.1	Gene_Symbol=Prdx5 Prdx5 protein	0.8965	1.0364
IPI:IPI00116192.1	Gene_Symbol=Prdx3 Thioredoxin-dependent peroxide reductase, mitochondrial	1.0291	1.2911
IPI:IPI00223367.5	Gene_Symbol=Uox Uricase	1.6255	0.5534
IPI:IPI00111218.1	Gene_Symbol=Aldh2 Aldehyde dehydrogenase, mitochondrial	1.0188	1.0302
	MCV	1.0339	0.9974

Import Machinery			
Accession #	**Name**	**2 weeks**	**4 weeks**
IPI:IPI00751137.1	Gene_Symbol=Tomm70a Adult male thymus cDNA, RIKEN full-length enriched library, clone:5830412L10 product:Mitochondrial proteins import receptor (Translocase of outer membrane TOM70), full insert sequence	1.114	0.846
IPI:IPI00125776.1	Gene_Symbol=ENSMUSG00000045455;Timm8a1 Mitochondrial import inner membrane translocase	0.655	1.070

	subunit Tim8 A		
IPI:IPI00134484.1	Gene_Symbol=Timm10;Timm13 Mitochondrial import inner membrane translocase subunit Tim13	0.709	1.222
IPI:IPI00221608.3	Gene_Symbol=Samm50 Sorting and assembly machinery component 50 homolog	1.372	1.007
IPI:IPI00170126.4	Gene_Symbol=Pitrm1 Isoform 1 of Presequence protease, mitochondrial	0.942	1.109
IPI:IPI00117083.1	Gene_Symbol=Grpel1 GrpE protein homolog 1, mitochondrial	0.981	1.302
IPI:IPI00274656.6	Gene_Symbol=Pmpcb Mitochondrial-processing peptidase subunit beta	0.889	1.286
	MCV	0.952	1.120

Tricarboxylic acid cycle

Accession #	Name	2 weeks	4 weeks
IPI:IPI00405699.2	Gene_Symbol=Aldh4a1 Delta-1-pyrroline-5-carboxylate dehydrogenase, mitochondrial	0.9840	1.0870
IPI:IPI00109169.1	Gene_Symbol=Idh3g Isocitrate dehydrogenase [NAD] subunit gamma, mitochondrial	0.8768	1.0186
IPI:IPI00126635.1	Gene_Symbol=Idh3b Tumor-related protein	0.9022	0.9376
IPI:IPI00874456.1	Gene_Symbol=Dld Dihydrolipoyl dehydrogenase, mitochondrial	0.9035	1.0850
IPI:IPI00134809.2	Gene_Symbol=Dlst Isoform 1 of Dihydrolipoyllysine-residue succinyltransferase component of 2-oxoglutarate dehydrogenase complex, mitochondrial	0.9075	1.0970
IPI:IPI00459725.2	Gene_Symbol=Idh3a Isoform 1 of Isocitrate dehydrogenase [NAD] subunit alpha, mitochondrial	0.9180	1.0072
IPI:IPI00114710.2	Gene_Symbol=Pcx Activated spleen cDNA, RIKEN full-length enriched library, clone:F830201B12 product:pyruvate carboxylase, full insert sequence	1.0633	1.4495
IPI:IPI00261627.1	Gene_Symbol=Sucla2 Succinyl-CoA ligase [ADP-forming] subunit beta, mitochondrial	0.9228	1.0914
IPI:IPI00338536.1	Gene_Symbol=Sdhb Succinate dehydrogenase [ubiquinone] iron-sulfur subunit, mitochondrial	0.9480	1.1639
IPI:IPI00113141.1	Gene_Symbol=Cs Citrate synthase, mitochondrial	0.9570	1.0160
IPI:IPI00337893.2	Gene_Symbol=Pdha1 Pyruvate dehydrogenase E1 component subunit alpha, somatic form, mitochondrial	0.9690	0.9875
IPI:IPI00129928.2	Gene_Symbol=Fh1 Isoform Mitochondrial of Fumarate hydratase, mitochondrial	0.9707	1.1420
IPI:IPI00323592.2	Gene_Symbol=Mdh2 Malate dehydrogenase, mitochondrial	0.9712	1.1020
IPI:IPI00153660.4	Gene_Symbol=Dlat Dihydrolipoyllysine-residue acetyltransferase component of pyruvate dehydrogenase complex, mitochondrial	0.9753	0.9653
IPI:IPI00116074.1	Gene_Symbol=Aco2 Aconitate hydratase, mitochondrial	0.9813	1.0820
IPI:IPI00845652.1	Gene_Symbol=Ogdh Isoform 3 of 2-oxoglutarate dehydrogenase E1 component, mitochondrial	1.0010	1.0916
IPI:IPI00132042.1	Gene_Symbol=Pdhb Pyruvate dehydrogenase E1 component subunit beta, mitochondrial	1.0197	1.0619
IPI:IPI00461197.1	Gene_Symbol=Ldhd 10 days neonate skin cDNA,	1.0394	1.5385

	RIKEN full-length enriched library, clone:4733401P21 product:weakly similar to PUTATIVE D-LACTATE DEHYDROGENASE (CYTOCHROME) OXIDOREDUCTASE PROTEIN		
IPI:IPI00406442.2	Gene_Symbol=Suclg1 Succinyl-CoA ligase [GDP-forming] subunit alpha, mitochondrial	1.0159	1.0708
IPI:IPI00459487.3	Gene_Symbol=Suclg2 Isoform 1 of Succinyl-CoA ligase [GDP-forming] subunit beta, mitochondrial	1.0329	1.0502
IPI:IPI00875110.1	Gene_Symbol=Idh2 52 kDa protein	1.2126	0.9286
IPI:IPI00117312.1	Gene_Symbol=Got2 Aspartate aminotransferase, mitochondrial	0.9640	1.1201
IPI:IPI00230351.1	Gene_Symbol=Sdha Succinate dehydrogenase [ubiquinone] flavoprotein subunit, mitochondrial	0.9884	1.1603
IPI:IPI00556699.1	Gene_Symbol=Gcsh Putative uncharacterized protein	0.9494	1.2510
IPI:IPI00121218.5	Gene_Symbol=Fahd2a Fumarylacetoacetate hydrolase domain-containing protein 2A	1.0118	1.1611
IPI:IPI00135231.2	Gene_Symbol=Idh1 0 day neonate lung cDNA, RIKEN full-length enriched library, clone:E030024J03 product:isocitrate dehydrogenase 1 (NADP+), soluble, full insert sequence	1.0745	0.5321
	MCV	0.9831	1.0845

Urea cycle

Accession #	Name	2 weeks	4 weeks
IPI:IPI00405699.2	Gene_Symbol=Aldh4a1 Delta-1-pyrroline-5-carboxylate dehydrogenase, mitochondrial	0.9840	1.0870
IPI:IPI00114209.1	Gene_Symbol=Glud1 Glutamate dehydrogenase 1, mitochondrial	0.9862	1.2509
IPI:IPI00776257.1	Gene_Symbol=Otc Otc protein	0.9645	1.0244
IPI:IPI00111908.8	Gene_Symbol=Cps1 Carbamoyl-phosphate synthase [ammonia], mitochondrial	0.9196	1.2264
IPI:IPI00223367.5	Gene_Symbol=Uox Uricase	1.6255	0.5534
IPI:IPI00119945.1	Gene_Symbol=Nit2 Nitrilase homolog 2	0.9843	0.9547
IPI:IPI00117312.1	Gene_Symbol=Got2 Aspartate aminotransferase, mitochondrial	0.9640	1.1201
IPI:IPI00110843.3	Gene_Symbol=Agmat Agmatinase, mitochondrial	0.7623	1.0844
IPI:IPI00113073.3	Gene_Symbol=Aldh1b1 Aldehyde dehydrogenase X, mitochondrial	0.8547	1.4719
IPI:IPI00124372.3	Gene_Symbol=Aldh9a1 aldehyde dehydrogenase 9, subfamily A1	0.9230	0.9621
IPI:IPI00230084.5	Gene_Symbol=Aldh7a1 aldehyde dehydrogenase family 7, member A1 isoform a	1.0447	1.1818
	MCV	1.0012	1.0834

Transporters

Accession #	Name	2 weeks	4 weeks
IPI:IPI00125853.1	Gene_Symbol=Slc25a15 Mitochondrial ornithine transporter 1	1.031	1.267
IPI:IPI00109275.1	Gene_Symbol=Slc25a22 Mitochondrial glutamate carrier 1	1.052	0.972

IPI:IPI00230754.5	Gene_Symbol=Slc25a11 Mitochondrial 2-oxoglutarate/malate carrier protein	1.052	1.080
IPI:IPI00850430.1	Gene_Symbol=Slc25a3 LOC100046151 similar to Solute carrier family 25 (mitochondrial carrier, phosphate carrier), member 3	1.084	1.059
IPI:IPI00131584.1	Gene_Symbol=Slc25a20 Mitochondrial carnitine/acylcarnitine carrier protein	1.176	1.022
IPI:IPI00276926.3	Gene_Symbol=Slc25a1 NOD-derived CD11c +ve dendritic cells cDNA, RIKEN full-length enriched library, clone:F630026H16 product:solute carrier family 25 (mitochondrial carrier	1.177	1.158
IPI:IPI00135651.1	Gene_Symbol=Slc25a13 Calcium-binding mitochondrial carrier protein Aralar2	1.226	1.076
IPI:IPI00317074.3	Gene_Symbol=Slc25a10 Mitochondrial dicarboxylate carrier	1.245	0.886
IPI:IPI00127841.3	Gene_Symbol=Slc25a5 ADP/ATP translocase 2	1.385	1.116
IPI:IPI00117312.1	Gene_Symbol=Got2 Aspartate aminotransferase, mitochondrial	0.964	1.120
IPI:IPI00230540.1	Gene_Symbol=Vdac1 Isoform Mt-VDAC1 of Voltage-dependent anion-selective channel protein 1	1.068	1.082
IPI:IPI00122547.1	Gene_Symbol=Vdac2 Voltage-dependent anion-selective channel protein 2	1.147	1.101
IPI:IPI00876341.1	Gene_Symbol=Vdac3 Voltage-dependent anion-selective channel protein 3	1.495	1.096
IPI:IPI00648829.1	Gene_Symbol=Nipsnap3a Nipsnap homolog 3A	0.861	1.116
	MCV	1.140	1.082

Stress response			
Accession #	**Name**	**2 weeks**	**4 weeks**
IPI:IPI00133270.1	Gene_Symbol=Clpp Putative ATP-dependent Clp protease proteolytic subunit, mitochondrial	0.918	1.272
IPI:IPI00880839.1	Gene_Symbol=Hspa9 heat shock protein 9	0.963	1.127
IPI:IPI00788396.1	Gene_Symbol=Clpx caseinolytic protease X isoform 2	1.068	1.025
IPI:IPI00475322.1	Gene_Symbol=Msra Msra protein	1.109	1.116
IPI:IPI00761408.2	Gene_Symbol=Lonp1 Lon protease homolog, mitochondrial	1.133	1.096
IPI:IPI00132762.1	Gene_Symbol=Trap1 Heat shock protein 75 kDa, mitochondrial	1.065	1.004
IPI:IPI00308885.6	Gene_Symbol=Hspd1 Isoform 1 of 60 kDa heat shock protein, mitochondrial	0.867	1.138
IPI:IPI00263863.8	Gene_Symbol=Hspe1 10 kDa heat shock protein, mitochondrial	0.865	1.112
IPI:IPI00319992.1	Gene_Symbol=Hspa5 78 kDa glucose-regulated protein	1.045	0.662
IPI:IPI00223216.5	Gene_Symbol=Tst Thiosulfate sulfurtransferase	1.014	1.096
	MCV	1.005	1.065

Fatty acid metabolism			
Accession #	**Name**	**2 weeks**	**4 weeks**
IPI:IPI00126625.1	Gene_Symbol=Acsm1 Isoform 1 of Acyl-coenzyme A	1.062	1.119

	synthetase ACSM1, mitochondrial		
IPI:IPI00886014.1	Gene_Symbol=Acss3 Isoform 1 of Acyl-CoA synthetase short-chain family member 3, mitochondrial	0.965	1.018
IPI:IPI00122633.3	Gene_Symbol=Acsf2 Acyl-CoA synthetase family member 2, mitochondrial	1.025	1.018
IPI:IPI00230113.5	Gene_Symbol=Cyb5 Cytochrome b5	1.050	0.594
IPI:IPI00874376.1	Gene_Symbol=Apool 10, 11 days embryo whole body cDNA, RIKEN full-length enriched library, clone:2810024N24 product:hypothetical protein, full insert sequence	1.336	1.203
IPI:IPI00831119.1	Gene_Symbol=Lypla1 21 kDa protein	0.931	0.918
IPI:IPI00130804.1	Gene_Symbol=Ech1 Delta(3,5)-Delta(2,4)-dienoyl-CoA isomerase, mitochondrial	0.942	0.876
IPI:IPI00222430.5	Gene_Symbol=Dbi diazepam binding inhibitor isoform 1	0.702	1.193
IPI:IPI00113073.3	Gene_Symbol=Aldh1b1 Aldehyde dehydrogenase X, mitochondrial	0.855	1.472
IPI:IPI00273164.1	Gene_Symbol=Aldh5a1 Succinate-semialdehyde dehydrogenase, mitochondrial	0.883	1.009
IPI:IPI00124372.3	Gene_Symbol=Aldh9a1 aldehyde dehydrogenase 9, subfamily A1	0.923	0.962
IPI:IPI00379694.4	Gene_Symbol=Hmgcl 3-hydroxy-3-methylglutaryl-Coenzyme A lyase	0.937	1.012
IPI:IPI00875372.1	Gene_Symbol=Echdc2 Isoform 2 of Enoyl-CoA hydratase domain-containing protein 2, mitochondrial	0.946	1.290
IPI:IPI00230084.5	Gene_Symbol=Aldh7a1 aldehyde dehydrogenase family 7, member A1 isoform a	1.045	1.182
	MCV	0.972	1.062

Nucleobase, nucleoside, nucleotide and nucleic acid metabolic process			
Accession #	**Name**	**2 weeks**	**4 weeks**
IPI:IPI00855212.1	Gene_Symbol=1110020G09Rik Isoform 2 of UPF0465 protein C5orf33 homolog	0.8837	1.0150
IPI:IPI00648318.1	Gene_Symbol=Ak2 Adult male liver tumor cDNA, RIKEN full-length enriched library, clone:C730019E03 product:ADENYLATE KINASE 2 homolog	0.8764	1.0009
IPI:IPI00742309.1	Gene_Symbol=Kmo Isoform 2 of Kynurenine 3-monooxygenase	1.2105	1.1066
IPI:IPI00133034.3	Gene_Symbol=Hint2 Histidine triad nucleotide-binding protein 2	0.9080	1.0788
IPI:IPI00221769.5	Gene_Symbol=Ak3 GTP:AMP phosphotransferase mitochondrial	0.9106	1.0956
	MCV		

PPAR signalling			
Accession #	**Name**	**2 weeks**	**4 weeks**
IPI:IPI00420718.4	Gene_Symbol=Hmgcs2 Hydroxymethylglutaryl-CoA synthase, mitochondrial	1.069	0.992

IPI:IPI00222430.5	Gene_Symbol=Dbi diazepam binding inhibitor isoform 1	0.702	1.193
IPI:IPI00134961.1	Gene_Symbol=Acadm Medium-chain specific acyl-CoA dehydrogenase, mitochondrial	0.965	0.992
IPI:IPI00119203.4	Gene_Symbol=Acadvl Very long-chain specific acyl-CoA dehydrogenase, mitochondrial	1.059	1.097
IPI:IPI00330094.4	Gene_Symbol=Cpt1a Carnitine O-palmitoyltransferase I, liver isoform	1.290	0.997
IPI:IPI00881401.1	Gene_Symbol=Cpt2 carnitine palmitoyltransferase 2	1.105	1.100
	MCV	1.032	1.062

Electron Transport Chain

Accession #	Name	2 weeks	4 weeks
IPI:IPI00133006.1	Gene_Symbol=Ndufab1 Acyl carrier protein, mitochondrial	1.147	1.049
IPI:IPI00130460.1	Gene_Symbol=Ndufv1 NADH dehydrogenase [ubiquinone] flavoprotein 1, mitochondrial	1.045	1.073
IPI:IPI00120212.1	Gene_Symbol=Ndufa9 NADH dehydrogenase [ubiquinone] 1 alpha subcomplex subunit 9, mitochondrial	1.138	0.955
IPI:IPI00125929.2	Gene_Symbol=Ndufa4 NADH dehydrogenase [ubiquinone] 1 alpha subcomplex subunit 4	0.871	1.134
IPI:IPI00130322.5	Gene_Symbol=Ndufa7 NADH dehydrogenase [ubiquinone] 1 alpha subcomplex subunit 7	0.969	1.132
IPI:IPI00116748.1	Gene_Symbol=Ndufa10 NADH dehydrogenase [ubiquinone] 1 alpha subcomplex subunit 10, mitochondrial	1.169	1.144
IPI:IPI00169925.2	Gene_Symbol=Ndufv2 Isoform 1 of NADH dehydrogenase [ubiquinone] flavoprotein 2, mitochondrial	1.069	0.986
IPI:IPI00387430.1	Gene_Symbol=Ndufb8 NADH dehydrogenase [ubiquinone] 1 beta subcomplex subunit 8, mitochondrial	0.998	1.145
IPI:IPI00120232.1	Gene_Symbol=Ndufs7 NADH dehydrogenase [ubiquinone] iron-sulfur protein 7, mitochondrial	1.134	1.172
IPI:IPI00308882.4	Gene_Symbol=Ndufs1 NADH-ubiquinone oxidoreductase 75 kDa subunit, mitochondrial	1.064	1.054
IPI:IPI00230715.5	Gene_Symbol=Ndufa13 NADH dehydrogenase [ubiquinone] 1 alpha subcomplex subunit 13	1.200	0.983
IPI:IPI00170093.3	Gene_Symbol=Ndufs8 NADH dehydrogenase [ubiquinone] iron-sulfur protein 8, mitochondrial	0.943	1.009
IPI:IPI00881750.1	Gene_Symbol=Ndufb5 14 kDa protein	1.117	1.032
IPI00880613.1	Gene_Symbol=Ndufb10 18 kDa protein	1.023	1.109
IPI:IPI00132623.3	Gene_Symbol=Ndufb9 NADH dehydrogenase [ubiquinone] 1 beta subcomplex subunit 9	0.827	1.130
IPI:IPI00133403.1	Gene_Symbol=Ndufb3 NADH dehydrogenase [ubiquinone] 1 beta subcomplex subunit 3	1.063	0.991
IPI:IPI00133399.1	Gene_Symbol=Ndufa6 NADH dehydrogenase [ubiquinone] 1 alpha subcomplex subunit 6	0.995	1.126
IPI:IPI00662861.1	Gene_Symbol=LOC635087 similar to NADH dehydrogenase (ubiquinone) 1, subcomplex unknown,	1.219	0.976

	2		
IPI:IPI00229008.2	Gene_Symbol=Ndufs4 NADH dehydrogenase [ubiquinone] iron-sulfur protein 4, mitochondrial	0.774	0.875
IPI:IPI00128023.3	Gene_Symbol=Ndufs2 NADH dehydrogenase [ubiquinone] iron-sulfur protein 2, mitochondrial	0.828	1.259
IPI:IPI00114246.2	Gene_Symbol=Ndufb11 NADH dehydrogenase [ubiquinone] 1 beta subcomplex subunit 11, mitochondrial	0.922	1.090
IPI:IPI00121309.2	Gene_Symbol=Ndufs3 NADH dehydrogenase [ubiquinone] iron-sulfur protein 3, mitochondrial	0.774	0.957
IPI:IPI00648743.1	Gene_Symbol=Ndufb6 NADH dehydrogenase (Ubiquinone) 1 beta subcomplex, 6	0.924	1.333
IPI:IPI00315302.5	Gene_Symbol=Ndufa2 NADH dehydrogenase [ubiquinone] 1 alpha subcomplex subunit 2	0.507	0.998
IPI:IPI00230351.1	Gene_Symbol=Sdha Succinate dehydrogenase [ubiquinone] flavoprotein subunit, mitochondrial	1.017	1.171
IPI:IPI00338536.1	Gene_Symbol=Sdhb Succinate dehydrogenase [ubiquinone] iron-sulfur subunit, mitochondrial	0.948	1.164
IPI:IPI00119138.1	Gene_Symbol=Uqcrc2 Cytochrome b-c1 complex subunit 2, mitochondrial	0.986	1.040
IPI:IPI00555000.2	Gene_Symbol=Uqcrb Cytochrome b-c1 complex subunit 7	0.964	1.118
IPI:IPI00653598.2	Gene_Symbol=Uqcrc1 ubiquinol-cytochrome c reductase core protein 1	1.035	1.171
IPI:IPI00224210.5	Gene_Symbol=Uqcrq Cytochrome b-c1 complex subunit 8	0.908	0.986
IPI:IPI00133240.1	Gene_Symbol=Uqcrfs1 Cytochrome b-c1 complex subunit Rieske, mitochondrial	0.971	0.988
IPI:IPI00230113.5	Gene_Symbol=Cyb5 Cytochrome b5	1.050	0.594
IPI:IPI00222419.5	Gene_Symbol=ENSMUSG00000058927;Cycs Cytochrome c, somatic	0.899	1.128
IPI:IPI00117978.1	Gene_Symbol=Cox4i1 Cytochrome c oxidase subunit 4 isoform 1, mitochondrial	0.962	1.130
IPI:IPI00785410.1	Gene_Symbol=Cox5b Cytochrome c oxidase subunit 5B, mitochondrial	0.848	1.028
IPI:IPI00131771.3	Gene_Symbol=Cox6c Cytochrome c oxidase polypeptide VIc	0.978	1.049
IPI:IPI00225390.5	Gene_Symbol=Cox6b1 Cytochrome c oxidase subunit VIb isoform 1	0.809	1.132
IPI:IPI00120719.4	Gene_Symbol=Cox5a Cytochrome c oxidase subunit 5A, mitochondrial	0.931	1.129
IPI:IPI00131176.1	Gene_Symbol=mt-Co2 Cytochrome c oxidase subunit 2	1.255	1.030
IPI:IPI00355248.5	Gene_Symbol=mt-Co1 cytochrome c oxidase subunit I	1.304	0.815
IPI:IPI00132728.2	Gene_Symbol=Cyc1 Isoform 1 of Cytochrome c1, heme protein, mitochondrial	1.187	1.003
IPI:IPI00468481.2	Gene_Symbol=Atp5b ATP synthase subunit beta, mitochondrial	0.946	1.065
IPI:IPI00130280.1	Gene_Symbol=Atp5a1 ATP synthase subunit alpha, mitochondrial	0.968	1.052
IPI:IPI00623553.1	Gene_Symbol=Atp5h (BLAST score: 326, P = 4e-88)	1.068	0.969

	LOC100044492;ENSMUSG00000068706 hypothetical protein		
IPI:IPI00341282.2	Gene_Symbol=Atp5f1 ATP synthase subunit b, mitochondrial	1.120	0.909
IPI:IPI00118986.1	Gene_Symbol=Atp5o;LOC100047429 ATP synthase subunit O, mitochondrial	1.008	1.030
IPI:IPI00776084.1	Gene_Symbol=Atp5c1 ATP synthase gamma chain	1.100	1.137
IPI:IPI00125460.1	Gene_Symbol=Atp5j;LOC674583 ATP synthase-coupling factor 6, mitochondrial	0.726	1.028
IPI:IPI00271986.6	Gene_Symbol=Atp5j2 ATP synthase subunit f, mitochondrial	0.956	1.084
IPI:IPI00453777.2	Gene_Symbol=Atp5d ATP synthase subunit delta, mitochondrial	0.852	1.055
IPI:IPI00116896.1	Gene_Symbol=mt-Atp8 ATP synthase protein 8	1.005	1.116
IPI:IPI00111770.7	Gene_Symbol=Atp5k ATP synthase subunit e, mitochondrial	0.804	0.987
IPI:IPI00169862.1	Gene_Symbol=Coq9 Ubiquinone biosynthesis protein COQ9, mitochondrial	0.824	1.101
IPI:IPI00273164.1	Gene_Symbol=Aldh5a1 Succinate-semialdehyde dehydrogenase, mitochondrial	0.883	1.009
IPI:IPI00848492.1	Gene_Symbol=LOC100045699 similar to Electron transferring flavoprotein, beta polypeptide isoform 2	0.918	1.015
IPI:IPI00116753.4	Gene_Symbol=Etfa Electron transfer flavoprotein subunit alpha, mitochondrial	0.945	1.066
IPI:IPI00121322.2	Gene_Symbol=Etfdh Electron transfer flavoprotein-ubiquinone oxidoreductase, mitochondrial	1.027	1.019
	MCV	0.981	1.053

Ca^{2+}			
Accession #	Name	2 weeks	4 weeks
IPI:IPI00131177.1	Gene_Symbol=Letm1 LETM1 and EF-hand domain-containing protein 1, mitochondrial	0.906	0.927
IPI:IPI00135651.1	Gene_Symbol=Slc25a13 Calcium-binding mitochondrial carrier protein Aralar2	1.226	1.076
IPI:IPI00115824.1	Gene_Symbol=Nipsnap1 Protein NipSnap homolog 1	1.063	1.139
	MCV	1.065	1.047

Detoxification			
Accession #	**Name**	**2 weeks**	**4 weeks**
IPI:IPI00226140.5	Gene_Symbol=Maob Amine oxidase [flavin-containing] B	1.139	1.051
IPI:IPI00223216.5	Gene_Symbol=Tst Thiosulfate sulfurtransferase	1.014	1.096
IPI:IPI00230113.5	Gene_Symbol=Cyb5 Cytochrome b5	1.050	0.594
IPI:IPI00895177.1	Gene_Symbol=Cyb5r3 13 days embryo liver cDNA, RIKEN full-length enriched library, clone:2500002N19 product:NADH-CYTOCHROME B5 REDUCTASE homolog	1.050	0.932
IPI:IPI00123276.1	Gene_Symbol=Mosc2 MOSC domain-containing protein 2, mitochondrial	1.598	0.898
IPI:IPI00762185.2	Gene_Symbol=Mpst 3-mercaptopyruvate sulfurtransferase	0.967	0.967
IPI:IPI00318750.4	Gene_Symbol=Dhrs4 NADPH-dependent retinol dehydrogenase/reductase isoform 1	1.156	0.631

IPI:IPI00111218.1	Gene_Symbol=Aldh2 Aldehyde dehydrogenase, mitochondrial	1.019	1.030
IPI:IPI00113073.3	Gene_Symbol=Aldh1b1 Aldehyde dehydrogenase X, mitochondrial	0.855	1.472
IPI:IPI00153144.3	Gene_Symbol=Suox Sulfite oxidase, mitochondrial	0.862	1.038
	MCV	1.071	0.971

Morpholgy and structure

Accession #	Name	2 weeks	4 weeks
IPI:IPI00875638.1	Gene_Symbol=Immt Isoform 3 of Mitochondrial inner membrane protein	0.840	1.037
IPI:IPI00653064.1	RANDOMIZED Gene_Symbol=Mfn1 Mitofusin-1	1.275	1.311
IPI:IPI00855011.1	Gene_Symbol=LOC100046998 similar to optic atrophy 1	0.872	0.900
IPI:IPI00131177.1	Gene_Symbol=Letm1 LETM1 and EF-hand domain-containing protein 1, mitochondrial	0.906	0.927
IPI:IPI00420706.4	Gene_Symbol=Lrpprc Leucine-rich PPR motif-containing protein, mitochondrial	1.026	0.988
IPI:IPI00317074.3	Gene_Symbol=Slc25a10 Mitochondrial dicarboxylate carrier	1.245	0.886
	MCV	1.027	1.008

Apoptosis

Accession #	Name	2 weeks	4 weeks
IPI:IPI00776047.1	Gene_Symbol=Aifm1 Apoptosis-inducing factor, mitochondrion-associated 1	1.051	1.103
IPI:IPI00222419.5	Gene_Symbol=ENSMUSG00000058927;Cycs Cytochrome c, somatic	0.905	1.155
IPI:IPI00127841.3	Gene_Symbol=Slc25a5 ADP/ATP translocase 2	1.385	1.116
IPI:IPI00230540.1	Gene_Symbol=Vdac1 Isoform Mt-VDAC1 of Voltage-dependent anion-selective channel protein 1	1.068	1.082
IPI:IPI00122547.1	Gene_Symbol=Vdac2 Voltage-dependent anion-selective channel protein 2	1.147	1.101
IPI:IPI00876341.1	Gene_Symbol=Vdac3 Voltage-dependent anion-selective channel protein 3	1.495	1.096
IPI:IPI00648318.1	Gene_Symbol=Ak2 Adult male liver tumor cDNA, RIKEN full-length enriched library, clone:C730019E03 product:ADENYLATE KINASE 2 homolog	0.876	1.001
	MCV	1.132	1.093

Amino acid metabolism

Accession #	Name	2 weeks	4 weeks
IPI:IPI00273146.1	Gene_Symbol=Chdh Choline dehydrogenase, mitochondrial	1.095	1.137
IPI:IPI00136213.5	Gene_Symbol=Sardh Sarcosine dehydrogenase, mitochondrial	0.953	1.065
IPI:IPI00226140.5	Gene_Symbol=Maob Amine oxidase [flavin-containing] B	1.139	1.051
IPI:IPI00130535.1	Gene_Symbol=Dbt Lipoamide acyltransferase component of branched-chain alpha-keto acid dehydrogenase complex, mitochondrial	0.933	1.054
IPI:IPI00762346.1	Gene_Symbol=Aadat Kynurenine/alpha-aminoadipate aminotransferase mitochondrial	1.114	0.998
IPI:IPI00114209.1	Gene_Symbol=Glud1 Glutamate dehydrogenase 1, mitochondrial	0.986	1.251
IPI:IPI00129178.1	Gene_Symbol=Oat Ornithine aminotransferase, mitochondrial	1.148	1.041

IPI:IPI00405699.2	Gene_Symbol=Aldh4a1 Delta-1-pyrroline-5-carboxylate dehydrogenase, mitochondrial	0.984	1.087
IPI:IPI00320850.3	Gene_Symbol=Mccc1 Methylcrotonoyl-CoA carboxylase subunit alpha, mitochondrial	0.900	0.976
IPI:IPI00454008.1	Gene_Symbol=Shmt2 Serine hydroxymethyltransferase	0.979	1.166
IPI:IPI00468653.3	Gene_Symbol=Pccb Propionyl Coenzyme A carboxylase, beta polypeptide	0.951	1.168
IPI:IPI00117312.1	Gene_Symbol=Got2 Aspartate aminotransferase, mitochondrial	0.964	1.120
IPI:IPI00274222.2	Gene_Symbol=Acad8 Isobutyryl-CoA dehydrogenase, mitochondrial	1.206	1.124
IPI:IPI00116222.1	Gene_Symbol=Hibadh 3-hydroxyisobutyrate dehydrogenase, mitochondrial	0.879	0.910
IPI:IPI00471246.2	Gene_Symbol=Ivd Isovaleryl-CoA dehydrogenase, mitochondrial	0.960	1.046
IPI:IPI00127267.4	Gene_Symbol=Gldc Glycine dehydrogenase [decarboxylating], mitochondrial	0.939	1.277
IPI:IPI00624210.3	Gene_Symbol=Glyal (BLAST score 619, P = 1e-176) EG240549 Glycine N-acyltransferase-like protein	1.052	1.076
IPI:IPI00121218.5	Gene_Symbol=Fahd2a Fumarylacetoacetate hydrolase domain-containing protein 2A	1.012	1.161
IPI:IPI00130804.1	Gene_Symbol=Ech1 Delta(3,5)-Delta(2,4)-dienoyl-CoA isomerase, mitochondrial	0.942	0.876
IPI:IPI00553717.6	Gene_Symbol=Mccc2 Methylcrotonoyl-CoA carboxylase beta chain, mitochondrial	0.810	1.130
IPI:IPI00265352.1	Gene_Symbol=Gpt2 Alanine aminotransferase 2	0.827	1.230
IPI:IPI00120123.1	Gene_Symbol=Dmgdh Dimethylglycine dehydrogenase, mitochondrial	0.853	1.072
IPI:IPI00113073.3	Gene_Symbol=Aldh1b1 Aldehyde dehydrogenase X, mitochondrial	0.855	1.472
IPI:IPI00556699.1	Gene_Symbol=Gcsh Putative uncharacterized protein	0.949	1.251
IPI:IPI00273164.1	Gene_Symbol=Aldh5a1 Succinate-semialdehyde dehydrogenase, mitochondrial	0.883	1.009
IPI:IPI00136655.1	Gene_Symbol=Gcat 2-amino-3-ketobutyrate coenzyme A ligase, mitochondrial	0.906	1.080
IPI:IPI00461964.3	Gene_Symbol=Aldh6a1 Methylmalonate-semialdehyde dehydrogenase [acylating], mitochondrial	0.915	1.071
IPI:IPI00848492.1	Gene_Symbol=LOC100045699 similar to Electron transferring flavoprotein, beta polypeptide isoform 2	0.918	1.015
IPI:IPI00124372.3	Gene_Symbol=Aldh9a1 aldehyde dehydrogenase 9, subfamily A1	0.923	0.962
IPI:IPI00379694.4	Gene_Symbol=Hmgcl 3-hydroxy-3-methylglutaryl-Coenzyme A lyase	0.937	1.012
IPI:IPI00330523.1	Gene_Symbol=Pcca Propionyl-CoA carboxylase alpha chain, mitochondrial	0.941	1.038
IPI:IPI00420718.4	Gene_Symbol=Hmgcs2 Hydroxymethylglutaryl-CoA synthase, mitochondrial	1.069	0.992
IPI:IPI00230084.5	Gene_Symbol=Aldh7a1 aldehyde dehydrogenase family 7, member A1 isoform a	1.045	1.182
	MCV	0.969	1.094

Gluconeogenesis			
Accession #	**Name**	**2 weeks**	**4 weeks**
IPI:IPI00760085.1	Gene_Symbol=Agxt Isoform Peroxisomal of Serine--pyruvate aminotransferase, mitochondrial	0.9617	0.7917
IPI:IPI00114710.2	Gene_Symbol=Pcx Activated spleen cDNA, RIKEN full-length enriched library, clone:F830201B12 product:pyruvate carboxylase, full insert sequence	1.0633	1.4495
IPI:IPI00113073.3	Gene_Symbol=Aldh1b1 Aldehyde dehydrogenase X, mitochondrial	0.8547	1.4719
IPI:IPI00230084.5	Gene_Symbol=Aldh7a1 aldehyde dehydrogenase family 7, member A1 isoform a	1.0447	1.1818
	MCV	0.9811	1.2237

Mito translation/transcription			
Accession #	**Name**	**2 weeks**	**4 weeks**
IPI:IPI00830581.1	Gene_Symbol=Hsd17b10 hydroxyacyl-Coenzyme A dehydrogenase type II	1.108	1.211
IPI:IPI00118963.1	Gene_Symbol=Mrpl12 39S ribosomal protein L12, mitochondrial	0.897	1.064
IPI:IPI00126634.1	Gene_Symbol=Poldip2 Polymerase delta-interacting protein 2	0.910	1.091
IPI:IPI00130640.5	Gene_Symbol=Hrsp12 Ribonuclease UK114	0.948	0.801
	MCV	0.965	1.042

7.3. List of PPAR-responsive genes

Table 12. List of PPAR-responsive genes/products using bioinformatics

No.	Gene	Present	2-week	4-week		No.	Gene	Present	2-week	4-week
1	Btbd17	NO				41	Iqcf3	NO		
2	Lck	NO				42	Abca3	NO		
3	Pparg	NO				43	Gbl	NO		
4	Sept1	NO				44	Asrgl1	NO		
5	Acvrl1	NO				45	AC121967.3-2	NO		
6	Fkbp10	NO				46	Lgals12	NO		
7	Tmem143	NO				47	Ablim1	NO		
8	S3-12	NO				48	Maged1	NO		
9	Etv1	NO				49	Cbx8	NO		
10	Etfb	YES	0.918	1.015		50	Slc25a10	YES	1.2446	0.886
11	Ubqln1	NO				51	Acat1	YES	1.0454	0.951
12	Pan2	NO				52	Mobkl3	NO		
13	Cd247	NO				53	Il8rb	NO		
14	Pknox1	NO				54	Abcb6	NO		
15	1110036O03Rik	NO				55	Nr5a2	NO		
16	Ly6g6c	NO				56	BC005624	NO		
17	Abhd8	NO				57	Usp20	NO		
18	Mgst1	NO				58	Api5	NO		
19	Clec4f	NO				59	Csrp2bp	NO		
20	Ppt2	NO				60	Defb22	NO		
21	Prrt1	NO				61	Etfdh	YES	1.0268	1.019
22	Lpl	NO				62	Nphp3	YES	1.3297	0.469
23	Qdpr	NO				63	Cyr61	NO		
24	Eapa2	NO				64	Gcat	YES	1.3855	1.08
25	Dnahc1	NO				65	5430416O09Rik	NO		
26	Aifm2	NO				66	Sema3c	NO		
27	Lyrm7	NO				67	Slc4a2	NO		
28	Rrm2	NO				68	Cdk5	NO		
29	Cdc27	NO				69	Mthfr	NO		
30	Nt5c	NO				70	Clcn6	NO		
31	Txndc17	NO				71	Chic2	NO		
32	Zfyve21	NO				72	Zfp326	NO		
33	Xrcc3	NO				73	Mmab	NO		
34	Cast	NO				74	1700012A03Rik	NO		
35	C9	NO				75	Chl1	NO		
36	Cd96	NO				76	Aldh1l1	NO		
37	Ccdc80	NO				77	4632434I11Rik	NO		
38	Fyttd1	NO				78	Pdha1	YES	0.969	0.988
39	Adipoq	NO				79	Angpt2	NO		
40	Tuba1b	NO				80	Cd209d	NO		

No.	Gene	Present	2-week	4-week		No.	Gene	Present	2-week	4-week
81	Carkd	NO				121	BC027072	NO		
82	Wrn	NO				122	Lrtm1	NO		
83	Hp	NO				123	Ppp1r15b	NO		
84	2400003C14Rik	NO				124	Myct1	NO		
85	2310065K24Rik	NO				125	C230078M08Rik	NO		
86	Crispld2	NO				126	Lonp2	NO		
87	Pla2g15	NO				127	D930001I22Rik	NO		
88	Abcg4	NO				128	1110034B05Rik	NO		
89	Nudt16	NO				129	Purg	NO		
90	Ilvbl	NO				130	Clrn2	NO		
91	Tpsg1	NO				131	Rspry1	NO		
92	Reep4	NO				132	Tmc8	NO		
93	Clec18a	NO				133	Olfr690	NO		
94	Vav3	NO				134	BC030396	NO		
95	Tpsb2	NO				135	1100001G20Rik	NO		
96	Gpr142	NO				136	Olfr284	NO		
97	Plvap	NO				137	Ubxn8	NO		
98	Mrpl34	NO				138	2310001K24Rik	NO		
99	Ubd	NO				139	F730015K02Rik	NO		
100	Wdr38	NO				140	Olfr354	NO		
101	Fbxl21	NO				141	Gapdh	NO		
102	Pkd2l1	NO				142	Sh2d3c	NO		
103	EG70793	NO				143	Slc35e3	NO		
104	Scarf1	NO				144	V1re3	NO		
105	Rras	NO				145	Myl4	NO		
106	Scaf1	NO				146	Prcp	NO		
107	Gdf15	NO				147	Olfr525	NO		
108	Ubn2	NO				148	Cfd	NO		
109	Gcnt1	NO				149	Fabp4	NO		
110	Orm1	NO				150	Olfr1351	NO		
111	Sec24c	NO				151	U6	NO		
112	Syngr4	NO				152	U6	NO		
113	Cmtm5	NO				153	mmu-mir-218-2	NO		
114	Mslnl	NO				154	Cd209b	NO		
115	Gpr110	NO				155	Olfr1143	NO		
116	Ccnb1	NO				156	Lyz2	NO		
117	Mvk	NO				157	Ddx43	NO		
118	Kcna4	NO				158	Utp3	NO		
119	Pars2	NO				159	AU023871	NO		
120	BC037703	NO				160	ACADM	YES	0.9654	0.992

No.	Gene	Present	2-week	4-week
161	ACADVL	NO	1.059	1.097
162	GK	NO		
163	HADHA	YES	1.0484	0.927
164	HADHB	YES	1.0446	0.995
165	LIPC	NO		
166	SLC25A20	YES	1.1764	1.022
167	BLVRB	NO		
168	ADFP	NO		
169	ECH1	YES	0.9423	0.876
170	FABP1	YES	1.2179	0.541
171	ACAA1	YES	0.9482	0.485
172	CAT	YES	1.0682	0.435
173	CPT1A	YES	1.1457	0.997
174	ACSL1	YES	1.0252	0.731
175	HMOX1	NO		
176	PCK1	NO		
177	PDZK1	NO		
178	SULT2A1	NO		
179	VNN1	NO		
180	AQP3	NO		
181	HMGCS2	YES	1.0693	0.992
182	ACAA2	YES	0.9671	1.009
183	ANGPTL4	NO		
184	ABHD3	NO		

Combined list of PPAR-responsive genes from proteomic datasets. In order to screen for PPAR-responsive genes, accession numbers were first extracted from IPI and converted to Ensembl accession numbers and compared against the reference. Genes highlighted in grey were detected in the proteomics screen. Their associating fold change in 2 weeks and 4 weeks are shown.

7.4. iTRAQ™ supplementary data

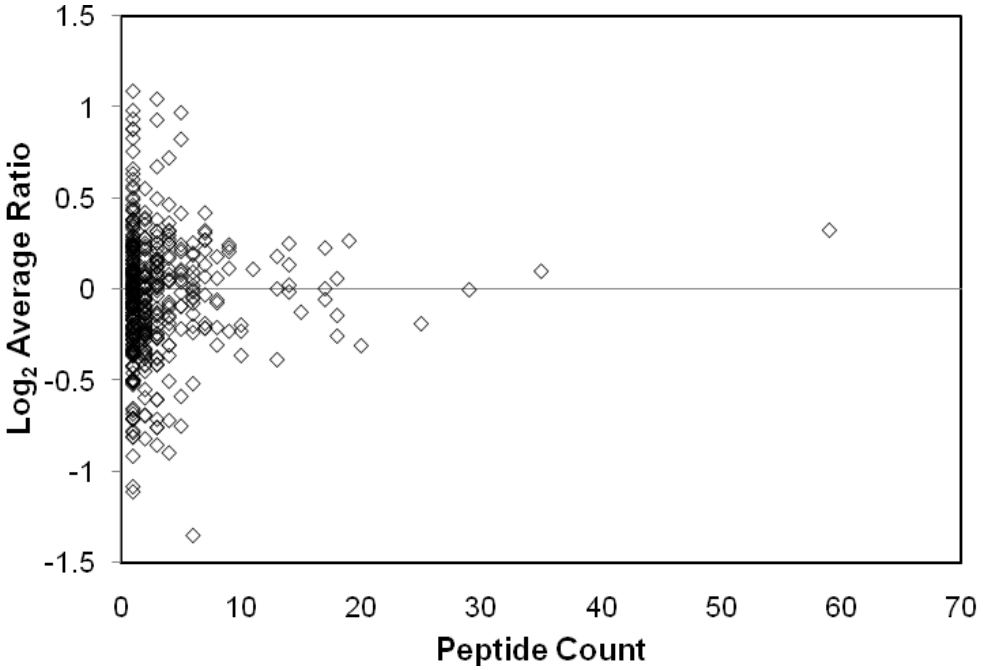

Figure 47. Scatterplot of fold change ratios against peptides
Plot showing the distribution of averaged fold change ratios (115/114 and 117/16) identified proteins against the number of peptide identified using MS/MS. A normal distribution can be observed. Each spot represents one protein.

7.5. List of publications

1. Boelsterli UA, Lee YH. 2008. Development of animal models of drug-induced mitochondrial toxicity. In: Will Y, Dykens JA, Editors. Mitochondrial Dysfunction in Drug-induced Toxicity. Hoboken, N.J.: Wiley
2. Lee YH, Boelsterli UA, Lin Q, Chung MC. 2008. Proteomics profiling of hepatic mitochondria in heterozygous HET mice, an animal model of discreet mitochondrial oxidative stress. *Proteomics* 8:555-568
3. Lee YH, Chung MC, Lin Q, Boelsterli UA. 2008. Troglitazone-induced hepatic mitochondrial proteome expression dynamics in heterozygous *Sod2*$^{+/-}$ mice: Two-stage oxidative injury. *Toxicology and Applied Pharmacology* 231:43-51.
4. Lee YH, Lin Q, Boelsterli UA, Chung MC. In press. The *Sod2* transgenic mouse as a model for oxidative stress: A functional proteomics perspective. Mass Spectrometry Reviews. Available online: DOI: 10.1002/mas.20226
5. Lee YH, et al. Differential effects on *Sod2*$^{+/-}$ mitochondrial proteome clusters accompanying troglitazone-induced hepatic injury. Manuscript in preparation

7.6. Posters and Presentations

1. Lee YH, Boelsterli, UA, Lin, Q. and Chung, MC. "Integrative Toxicoproteomics of mitochondrial oxidative stress-potentiated troglitazone-induced hepatic injury." 2nd Biochemistry Student Symposium.
2. Lee YH, Boelsterli, UA and Chung, MC. "Drug stress-induced alterations in the mitochondrial proteome".
   Joint Third Asia Oceania Human Proteome Organisation (AOHUPO) and Fourth Structural Biology and Functional Genomics Conference, Singapore
3. Lee YH, Boelsterli, UA and Chung, MC. "2D-DIGE identification of Troglitazone-induced mitochondrial proteome changes".
   Human Proteome Organisation (HUPO) 6th Annual World Congress, Seoul
   * Received AOHUPO/KSMS Young Scientist Award
4. Lee YH, Lin, Q and Chung, MC. "Impact on the heterozygous loss of SOD2 on the mitochondrial proteome."
   5th Structural Biology & Functional Genomics and Biological Physics International Conference, Singapore
5. Lee YH, Lin, Q and Chung, MC. "Troglitazone-induced two-staged hepatic mitochondrial proteome changes in *Sod2*$^{+/-}$ mice". Singapore Proteomics Forum

8. BIBLIOGRAPHY

Aardema MJ, MacGregor JT. 2002. Toxicology and genetic toxicology in the new era of "toxicogenomics": impact of "-omics" technologies. Mutat Res 499:13-25.

Abboud G, Kaplowitz N. 2007. Drug-induced liver injury. Drug Saf 30:277-294.

Abello N, Kerstjens HA, Postma DS, Bischoff R. 2009. Protein Tyrosine Nitration: Selectivity, Physicochemical and Biological Consequences, Denitration, and Proteomics Methods for the Identification of Tyrosine-Nitrated Proteins. J Proteome Res.

Adam-Vizi V, Chinopoulos C. 2006. Bioenergetics and the formation of mitochondrial reactive oxygen species. Trends Pharmacol Sci 27:639-645.

Alamdari DH, Kostidou E, Paletas K, Sarigianni M, Konstas AG, Karapiperidou A, Koliakos G. 2005. High sensitivity enzyme-linked immunosorbent assay (ELISA) method for measuring protein carbonyl in samples with low amounts of protein. Free Radic Biol Med 39:1362-1367.

Andersen JS, Mann M. 2006. Organellar proteomics: turning inventories into insights. EMBO Rep 7:874-879.

Aslan M, Ryan TM, Adler B, Townes TM, Parks DA, Thompson JA, Tousson A, Gladwin MT, Patel RP, Tarpey MM, Batinic-Haberle I, White CR, Freeman BA. 2001. Oxygen radical inhibition of nitric oxide-dependent vascular function in sickle cell disease. Proc Natl Acad Sci U S A 98:15215-15220.

Atkinson AJ, Colburn WA, DeGruttola VG, DeMets DL, Downing GJ, Hoth DF, Oates JAP, Carl C., Schooley RT, Spilker BA, Woodcock J, Zeger SL. 2001. Biomarkers and surrogate endpoints: preferred definitions and conceptual framework. Clin Pharmacol Ther 69:89-95.

Bae MA, Song BJ. 2003. Critical role of c-Jun N-terminal protein kinase activation in troglitazone-induced apoptosis of human HepG2 hepatoma cells. Mol Pharmacol 63:401-408.

Barreiro E, Coronell C, Lavina B, Ramirez-Sarmiento A, Orozco-Levi M, Gea J. 2006. Aging, sex differences, and oxidative stress in human respiratory and limb muscles. Free Radic Biol Med 41:797-809.

Bauer S, Grossmann S, Vingron M, Robinson PN. 2008. Ontologizer 2.0--a multifunctional tool for GO term enrichment analysis and data exploration. Bioinformatics 24:1650-1651.

Bender A, Hajieva P, Moosmann B. 2008. Adaptive antioxidant methionine accumulation in respiratory chain complexes explains the use of a deviant genetic code in mitochondria. Proc Natl Acad Sci U S A 105:16496-16501.

Bi X, Lin Q, Foo TW, Joshi S, You T, Shen HM, Ong CN, Cheah PY, Eu KW, Hew CL. 2006. Proteomic analysis of colorectal cancer reveals alterations in metabolic pathways: mechanism of tumorigenesis. Mol Cell Proteomics 5:1119-1130.

Biggs WH, 3rd, Meisenhelder J, Hunter T, Cavenee WK, Arden KC. 1999. Protein kinase B/Akt-mediated phosphorylation promotes nuclear exclusion of the winged helix transcription factor FKHR1. Proc Natl Acad Sci U S A 96:7421-7426.

Boelsterli UA. 2003a. Animal models of human disease in drug safety assessment. J Toxicol Sci 28:109-121.

Boelsterli UA. 2003b. Idiosyncratic drug hepatotoxicity revisited: new insights from mechanistic toxicology. Toxicol. Mech. Methods 13:3–20.

Boelsterli UA, Hsiao CJ. 2008. The heterozygous Sod2(+/-) mouse: modeling the mitochondrial role in drug toxicity. Drug Discov Today 13:982-988.

Boelsterli UA, Lee YH. 2008. Development of animal models of drug-induced mitochondrial toxicity. In: Will Y, Dykens JA, Editors. Mitochondrial Dysfunction in Drug-induced Toxicity. Hoboken, N.J.: Wiley.

Boelsterli UA, Lim PL. 2007. Mitochondrial abnormalities--a link to idiosyncratic drug hepatotoxicity? Toxicol Appl Pharmacol 220:92-107.

Bogacka I, Xie H, Bray GA, Smith SR. 2005. Pioglitazone induces mitochondrial biogenesis in human subcutaneous adipose tissue in vivo. Diabetes 54:1392-1399.

Borniquel S, Valle I, Cadenas S, Lamas S, Monsalve M. 2006. Nitric oxide regulates mitochondrial oxidative stress protection via the transcriptional coactivator PGC-1alpha. Faseb J 20:1889-1891.

Bota DA, Davies KJ. 2002. Lon protease preferentially degrades oxidized mitochondrial aconitase by an ATP-stimulated mechanism. Nat Cell Biol 4:674-680.

Bota DA, Van Remmen H, Davies KJ. 2002. Modulation of Lon protease activity and aconitase turnover during aging and oxidative stress. FEBS Lett 532:103-106.

Brinton RD. 2008. The healthy cell bias of estrogen action: mitochondrial bioenergetics and neurological implications. Trends Neurosci 31:529-537.

Brown GC, Borutaite V. 2002. Nitric oxide inhibition of mitochondrial respiration and its role in cell death. Free Radic Biol Med 33:1440-1450.

Buss H, Chan TP, Sluis KB, Domigan NM, Winterbourn CC. 1997. Protein carbonyl measurement by a sensitive ELISA method. Free Radic Biol Med 23:361-366.

Camp HS, Li O, Wise SC, Hong YH, Frankowski CL, Shen X, Vanbogelen R, Leff T. 2000. Differential activation of peroxisome proliferator-activated receptor-gamma by troglitazone and rosiglitazone. Diabetes 49:539-547.

Chandra V, Huang P, Hamuro Y, Raghuram S, Wang Y, Burris TP, Rastinejad F. 2008. Structure of the intact PPAR-gamma-RXR- nuclear receptor complex on DNA. Nature 456:350-356.

Chen Z, Lash LH. 1998. Evidence for mitochondrial uptake of glutathione by dicarboxylate and 2-oxoglutarate carriers. J Pharmacol Exp Ther 285:608-618.

Chinnery PF, Turnbull DM. 2001. Epidemiology and treatment of mitochondrial disorders. Am J Med Genet 106:94-101.

Chojkier M. 2005. Troglitazone and liver injury: in search of answers. Hepatolog 41:237-246.

Citters GWV, Forman BM. 2004. Molecular Links Between Peroxisome Proliferator-γ Activated Receptor-γ and Metabolic Disease. In: LeRoith D, Taylor SI, Olefsky JM, Editors. Diabetes mellitus : a fundamental and clinical text. Philadelphia: Lippincott Williams & Wilkins. p 442-454.

Coe KJ, Jia Y, Ho HK, Rademacher P, Bammler TK, Beyer RP, Farin FM, Woodke L, Plymate SR, Fausto N, Nelson SD. 2007. Comparison of the cytotoxicity of the nitroaromatic drug flutamide to its cyano analogue in the hepatocyte cell line TAMH: evidence for complex I inhibition and mitochondrial dysfunction using toxicogenomic screening. Chem Res Toxicol 20:1277-1290.

Colca JR, McDonald WG, Waldon DJ, Leone JW, Lull JM, Bannow CA, Lund ET, Mathews WR. 2004. Identification of a novel mitochondrial protein ("mitoNEET")

cross-linked specifically by a thiazolidinedione photoprobe. Am J Physiol Endocrinol Metab 286:E252-260.

Cooper MP, Qu L, Rohas LM, Lin J, Yang W, Erdjument-Bromage H, Tempst P, Spiegelman BM. 2006. Defects in energy homeostasis in Leigh syndrome French Canadian variant through PGC-1alpha/LRP130 complex. Genes Dev 20:2996-3009.

Corral-Debrinski M, Horton T, Lott MT, Shoffner JM, Beal MF, Wallace DC. 1992a. Mitochondrial DNA deletions in human brain: regional variability and increase with advanced age. Nat Genet 2:324-329.

Corral-Debrinski M, Shoffner JM, Lott MT, Wallace DC. 1992b. Association of mitochondrial DNA damage with aging and coronary atherosclerotic heart disease. Mutat Res 275:169-180.

Cox J, Mann M. 2007. Is proteomics the new genomics? Cell 130:395-398.

Das SK, Vasudevan DM. 2007. Alcohol-induced oxidative stress. Life Sci 81:177-187.

Dasgupta T, Hebbel RP, Kaul DK. 2006. Protective effect of arginine on oxidative stress in transgenic sickle mouse models. Free Radic Biol Med 41:1771-1780.

Davies GF, Khandelwal RL, Roesler WJ. 1999. Troglitazone induces expression of PPARgamma in liver. Mol Cell Biol Res Commun 2:202-208.

Dawson TL, Gores GJ, Nieminen AL, Herman B, Lemasters JJ. 1993. Mitochondria as a source of reactive oxygen species during reductive stress in rat hepatocytes. Am J Physiol 264:C961-967.

Day C. 1999. Thiazolidinediones: a new class of antidiabetic drugs. Diabet Med 16:179-192.

Delaval E, Perichon M, Friguet B. 2004. Age-related impairment of mitochondrial matrix aconitase and ATP-stimulated protease in rat liver and heart. Eur J Biochem 271:4559-4564.

Dennis G, Jr., Sherman BT, Hosack DA, Yang J, Gao W, Lane HC, Lempicki RA. 2003. DAVID: Database for Annotation, Visualization, and Integrated Discovery. Genome Biol 4:P3.

Desmet C, Warzee B, Gosset P, Melotte D, Rongvaux A, Gillet L, Fievez L, Seumois G, Vanderplasschen A, Staels B, Lekeux P, Bureau F. 2005. Pro-inflammatory properties for thiazolidinediones. Biochem Pharmacol 69:255-265.

DiMauro S, Schon EA. 2003. Mitochondrial respiratory-chain diseases. N Engl J Med 348:2656-2668.

Dixit R, Boelsterli UA. 2007. Healthy animals and animal models of human disease(s) in safety assessment of human pharmaceuticals, including therapeutic antibodies. Drug Discov Today 12:336-342.

Droge W. 2002. Free radicals in the physiological control of cell function. Physiol Rev 82:47-95.

Duckles SP, Krause DN, Stirone C, Procaccio V. 2006. Estrogen and mitochondria: a new paradigm for vascular protection? Mol Interv 6:26-35.

Dunkley TP, Hester S, Shadforth IP, Runions J, Weimar T, Hanton SL, Griffin JL, Bessant C, Brandizzi F, Hawes C, Watson RB, Dupree P, Lilley KS. 2006. Mapping the Arabidopsis organelle proteome. Proc Natl Acad Sci U S A 103:6518-6523.

Dykens JA, Will Y. 2007. The significance of mitochondrial toxicity testing in drug development. Drug Discov Today 12:777-785.

Eravci M, Fuxius S, Broedel O, Weist S, Krause E, Stephanowitz H, Schluter H, Eravci S, Baumgartner A. 2008. The whereabouts of transmembrane proteins from rat brain synaptosomes during two-dimensional gel electrophoresis. Proteomics 8:1762-1770.

Essers MA, Weijzen S, de Vries-Smits AM, Saarloos I, de Ruiter ND, Bos JL, Burgering BM. 2004. FOXO transcription factor activation by oxidative stress mediated by the small GTPase Ral and JNK. Embo J 23:4802-4812.

Etgen GJ, Prince MJ, Caro JF. 2004. Peroxisome Proliferator-Activated Receptor Modulators. In: LeRoith D, Taylor SI, Olefsky JM, Editors. Diabetes mellitus : a fundamental and clinical text. Philadelphia: Lippincott Williams & Wilkins. p 1140-1150.

Faca VM, Song KS, Wang H, Zhang Q, Krasnoselsky AL, Newcomb LF, Plentz RR, Gurumurthy S, Redston MS, Pitteri SJ, Pereira-Faca SR, Ireton RC, Katayama H, Glukhova V, Phanstiel D, Brenner DE, Anderson MA, Misek D, Scholler N, Urban ND, Barnett MJ, Edelstein C, Goodman GE, Thornquist MD, McIntosh MW, DePinho RA, Bardeesy N, Hanash SM. 2008. A mouse to human search for plasma proteome changes associated with pancreatic tumor development. PLoS Med 5:e123.

FDA. 2008. Key FDA Critical Path Activities Under Way in 2007. In: U.S. Department of Health and Human Services FaDA, Editor.

Feng J, Naiman DQ, Cooper B. 2007. Probability-based pattern recognition and statistical framework for randomization: modeling tandem mass spectrum/peptide sequence false match frequencies. Bioinformatics 23:2210-2217.

Fernandez-Checa JC, Kaplowitz N. 2005. Hepatic mitochondrial glutathione: transport and role in disease and toxicity. Toxicol Appl Pharmacol 204:263-273.

Fountoulakis M, Berndt P, Boelsterli UA, Crameri F, Winter M, Albertini S, Suter L. 2000. Two-dimensional database of mouse liver proteins: changes in hepatic protein levels following treatment with acetaminophen or its nontoxic regioisomer 3-acetamidophenol. Electrophoresis 21:2148-2161.

Fountoulakis M, de Vera MC, Crameri F, Boess F, Gasser R, Albertini S, Suter L. 2002. Modulation of gene and protein expression by carbon tetrachloride in the rat liver. Toxicol Appl Pharmacol 183:71-80.

Fulgencio JP, Kohl C, Girard J, Pegorier JP. 1996. Troglitazone inhibits fatty acid oxidation and esterification, and gluconeogenesis in isolated hepatocytes from starved rats. Diabetes 45:1556-1562.

Fusaro VA, Mani DR, Mesirov JP, Carr SA. 2009. Prediction of high-responding peptides for targeted protein assays by mass spectrometry. Nat Biotechnol 27:190-198.

Germain P, Iyer J, Zechel C, Gronemeyer H. 2002. Co-regulator recruitment and the mechanism of retinoic acid receptor synergy. Nature 415:187-192.

Gilar M, Olivova P, Daly AE, Gebler JC. 2005. Two-dimensional separation of peptides using RP-RP-HPLC system with different pH in first and second separation dimensions. J Sep Sci 28:1694-1703.

Girnun GD, Domann FE, Moore SA, Robbins ME. 2002. Identification of a functional peroxisome proliferator-activated receptor response element in the rat catalase promoter. Mol Endocrinol 16:2793-2801.

Gorg A, Weiss W, Dunn MJ. 2004. Current two-dimensional electrophoresis technology for proteomics. Proteomics 4:3665-3685.

Graham DJ, Green L, Senior JR, Nourjah P. 2002. Troglitazone-induced liver failure: A case study. Am. J. Med. 114:299-306.

Griffith OW, Meister A. 1985. Origin and turnover of mitochondrial glutathione. Proc Natl Acad Sci U S A 82:4668-4672.

Grune T, Merker K, Sandig G, Davies KJ. 2003. Selective degradation of oxidatively modified protein substrates by the proteasome. Biochem Biophys Res Commun 305:709-718.

Guengerich FP, MacDonald JS. 2007. Applying mechanisms of chemical toxicity to predict drug safety. Chem Res Toxicol 20:344-369.

Gulick T, Cresci S, Caira T, Moore DD, Kelly DP. 1994. The peroxisome proliferator-activated receptor regulates mitochondrial fatty acid oxidative enzyme gene expression. Proc Natl Acad Sci U S A 91:11012-11016.

Gunawan B, Kaplowitz N. 2004. Clinical perspectives on xenobiotic-induced hepatotoxicity. Drug Metab Rev 36:301-312.

Gunawan BK, Liu ZX, Han D, Hanawa N, Gaarde WA, Kaplowitz N. 2006. c-Jun N-terminal kinase plays a major role in murine acetaminophen hepatotoxicity. Gastroenterology 131:165-178.

Guo LJ, Oshida Y, Fuku N, Takeyasu T, Fujita Y, Kurata M, Sato Y, Ito M, Tanaka M. 2005. Mitochondrial genome polymorphisms associated with type-2 diabetes or obesity. Mitochondrion 5:15-33.

Gutteridge JM, Halliwell B. 2000. Free radicals and antioxidants in the year 2000. A historical look to the future. Ann N Y Acad Sci 899:136-147.

Haasio K, Koponen A, Penttila KE, Nissinen E. 2002. Effects of entacapone and tolcapone on mitochondrial membrane potential. Eur J Pharmacol 453:21-26.

Hamdan M, Righetti PG. 2002. Modern strategies for protein quantification in proteome analysis: advantages and limitations. Mass Spectrom Rev 21:287-302.

Han D, Matsumaru K, Rettori D, Kaplowitz N. 2004. Usnic acid-induced necrosis of cultured mouse hepatocytes: inhibition of mitochondrial function and oxidative stress. Biochem Pharmacol 67:439-451.

Hanson BJ, Schulenberg B, Patton WF, Capaldi RA. 2001. A novel subfractionation approach for mitochondrial proteins: a three-dimensional mitochondrial proteome map. Electrophoresis 22:950-959.

Hegardt FG. 1999. Mitochondrial 3-hydroxy-3-methylglutaryl-CoA synthase: a control enzyme in ketogenesis. Biochem J 338 (Pt 3):569-582.

Heijne WH, Kienhuis AS, van Ommen B, Stierum RH, Groten JP. 2005. Systems toxicology: applications of toxicogenomics, transcriptomics, proteomics and metabolomics in toxicology. Expert Rev Proteomics 2:767-780.

Heinaniemi M, Carlberg C. 2008. Screening for PPAR Responsive Regulatory Modules in Cancer. PPAR Res 2008:749073.

Heinloth AN, Irwin RD, Boorman GA, Nettesheim P, Fannin RD, Sieber SO, Snell ML, Tucker CJ, Li L, Travlos GS, Vansant G, Blackshear PE, Tennant RW, Cunningham ML, Paules RS. 2004. Gene expression profiling of rat livers reveals indicators of potential adverse effects. Toxicol. Sci. 80:193-202.

Helledie T, Grontved L, Jensen SS, Kiilerich P, Rietveld L, Albrektsen T, Boysen MS, Nohr J, Larsen LK, Fleckner J, Stunnenberg HG, Kristiansen K, Mandrup S. 2002. The gene encoding the Acyl-CoA-binding protein is activated by peroxisome

proliferator-activated receptor gamma through an intronic response element functionally conserved between humans and rodents. J Biol Chem 277:26821-26830.

Hennessy S, Strom BL. 2007. PDUFA reauthorization--drug safety's golden moment of opportunity? N Engl J Med 356:1703-1704.

Hinerfeld D, Traini MD, Weinberger RP, Cochran B, Doctrow SR, Harry J, Melov S. 2004. Endogenous mitochondrial oxidative stress: neurodegeneration, proteomic analysis, specific respiratory chain defects, and efficacious antioxidant therapy in superoxide dismutase 2 null mice. J Neurochem 88:657-667.

Honda Y, Honda S. 1999. The daf-2 gene network for longevity regulates oxidative stress resistance and Mn-superoxide dismutase gene expression in Caenorhabditis elegans. Faseb J 13:1385-1393.

Huang TT, Carlson EJ, Kozy HM, Mantha S, Goodman SI, Ursell PC, Epstein CJ. 2001. Genetic modification of prenatal lethality and dilated cardiomyopathy in Mn superoxide dismutase mutant mice. Free Radic Biol Med 31:1101-1110.

Huang YS, Su WJ, Huang YH, Chen CY, Chang FY, Lin HC, Lee SD. 2007. Genetic polymorphisms of manganese superoxide dismutase, NAD(P)H:quinone oxidoreductase, glutathione S-transferase M1 and T1, and the susceptibility to drug-induced liver injury. J Hepatol 47:128-134.

Humphries KM, Szweda LI. 1998. Selective inactivation of alpha-ketoglutarate dehydrogenase and pyruvate dehydrogenase: reaction of lipoic acid with 4-hydroxy-2-nonenal. . Biochemistry 37:15 835-815 841.

Hunzinger C, Wozny W, Schwall GP, Poznanovic S, Stegmann W, Zengerling H, Schoepf R, Groebe K, Cahill MA, Osiewacz HD, Jagemann N, Bloch M, Dencher NA, Krause F, Schrattenholz A. 2006. Comparative profiling of the mammalian mitochondrial proteome: multiple aconitase-2 isoforms including N-formylkynurenine modifications as part of a protein biomarker signature for reactive oxidative species. J Proteome Res 5:625-633.

Iannaccone PM. 2001. Toxicogenomics: "the call of the wild chip". Environ Health Perspect 109:A8-11.

Ide T, Nakazawa T, Mochizuki T, Murakami K. 2000. Tissue-specific actions of antidiabetic thiazolidinediones on the reduced fatty acid oxidation in skeletal muscle and liver of Zucker diabetic fatty rats. Metabolism 49:521-525.

Iwase M, Yamaguchi M, Yoshinari M, Okamura C, Hirahashi T, Tsuji H, Fujishima M. 1999. A Japanese case of liver dysfunction after 19 months of troglitazone treatment. Diabetes Care 22:1382-1384.

Jaeschke H. 2002. Inflammation in response to hepatocellular apoptosis. Hepatology 35:964-966.

Jaeschke H. 2007. Troglitazone hepatotoxicity: are we getting closer to understanding idiosyncratic liver injury? Toxicol Sci 97:1-3.

Jiang X-S, Dai J, Sheng Q-H, Zhang L, Xia Q-C, Wu J-R, Zeng R. 2005. A Comparative Proteomic Strategy for Subcellular Proteome Research. Molecular & Cellular Proteomics 4:12–34.

Jove M, Salla J, Planavila A, Cabrero A, Michalik L, Wahli W, Laguna JC, Vazquez-Carrera M. 2004. Impaired expression of NADH dehydrogenase subunit 1 and PPARgamma coactivator-1 in skeletal muscle of ZDF rats: restoration by troglitazone. J Lipid Res 45:113-123.

Julie NL, Julie IM, Kende AI, Wilson GL. 2008. Mitochondrial dysfunction and delayed hepatotoxicity: another lesson from troglitazone. Diabetologia 51:2108-2116.

Kalueff AV, Ren-Patterson RF, Murphy DL. 2007. The developing use of heterozygous mutant mouse models in brain monoamine transporter research. Trends Pharmacol Sci 28:122-127.

Kaplowitz N. 2005. Idiosyncratic drug hepatotoxicity. Nature Reviews: Drug Discovery 4 489 - 499.

Kersey PJ, Duarte J, Williams A, Karavidopoulou Y, Birney E, Apweiler R. 2004. The International Protein Index: An integrated database for proteomics experiments. Proteomics 4:1985-1988.

Kirman CR, Sweeney LM, Meek ME, Gargas ML. 2005. Assessing the dose-dependency of allometric scaling performance using physiologically based pharmacokinetic modeling. Reg. Toxicol. Pharmacol. 38:345-367.

Kislinger T, Cox B, Kannan A, Chung C, Hu P, Ignatchenko A, Scott MS, Gramolini AO, Morris Q, Hallett MT, Rossant J, Hughes TR, Frey B, Emili A. 2006. Global survey of organ and organelle protein expression in mouse: combined proteomic and transcriptomic profiling. Cell 125:173-186.

Kliewer SA, Umesono K, Noonan DJ, Heyman RA, Evans RM. 1992. Convergence of 9-cis retinoic acid and peroxisome proliferator signalling pathways through heterodimer formation of their receptors. Nature 358:771-774.

Kops GJ, Dansen TB, Polderman PE, Saarloos I, Wirtz KW, Coffer PJ, Huang TT, Bos JL, Medema RH, Burgering BM. 2002. Forkhead transcription factor FOXO3a protects quiescent cells from oxidative stress. Nature 419:316-321.

Kramer JA, Sagartz JE, Morris DL. 2007. The application of discovery toxicology and pathology towards the design of safer pharmaceutical lead candidates. Nat Rev Drug Discov 6:636-649.

Kuhn E, Wu J, Karl J, Liao H, Zolg W, Guild B. 2004. Quantification of C-reactive protein in the serum of patients with rheumatoid arthritis using multiple reaction monitoring mass spectrometry and 13C-labeled peptide standards. Proteomics 4:1175-1186.

Lanne B, Dahllof B, Lindahl C, Ebefors K, Kanmert I, von Bahr H, Miliotis T, Nystrom AC, Arnerup G, Paulsons I, Kerb S, Oakes N. 2006. PPARalpha and PPARgamma regulation of liver and adipose proteins in obese and dyslipidemic rodents. J Proteome Res 5:1850-1859.

Lash LH. 2006. Mitochondrial glutathione transport: physiological, pathological and toxicological implications. Chem Biol Interact 163:54-67.

Lash LH, Putt DA, Matherly LH. 2002. Protection of NRK-52E cells, a rat renal proximal tubular cell line, from chemical-induced apoptosis by overexpression of a mitochondrial glutathione transporter. J Pharmacol Exp Ther 303:476-486.

Lebovitz RM, Zhang H, Vogel H, Cartwright J, Dionne L, Lu N, Huang S, Matzuk MM. 1996. Neurodegeneration, myocardial injury, and perinatal death in mitochondrial superoxide dismutase-deficient mice. Proc. Natl. Acad. Sci. U. S. A. 93:9782–9787.

Lee TH, Mun JY, Han SM, Yoon G, Han SS, Koo HS. 2009. DIC-1 over-expression enhances respiratory activity in Caenorhabditis elegans by promoting mitochondrial cristae formation. Genes Cells 14:319-327.

Lee YH, Boelsterli UA, Lin Q, Chung MC. 2008a. Proteomics profiling of hepatic mitochondria in heterozygous Sod2(+/-) mice, an animal model of discreet mitochondrial oxidative stress. Proteomics 8:555-568.

Lee YH, Chung MC, Lin Q, Boelsterli UA. 2008b. Troglitazone-induced hepatic mitochondrial proteome expression dynamics in heterozygous Sod2(+/-) mice: two-stage oxidative injury. Toxicol Appl Pharmacol 231:43-51.

Lehmann JM, Moore LB, Smith-Oliver TA, Wilkison WO, Willson TM, Kliewer SA. 1995. An antidiabetic thiazolidinedione is a high affinity ligand for peroxisome proliferator-activated receptor gamma (PPAR gamma). J Biol Chem 270:12953-12956.

Lemay DG, Hwang DH. 2006. Genome-wide identification of peroxisome proliferator response elements using integrated computational genomics. J Lipid Res 47:1583-1587.

Lescuyer P, Hochstrasser D, Rabilloud T. 2007. How shall we use the proteomics toolbox for biomarker discovery? J Proteome Res 6:3371-3376.

Levine RL, Mosoni L, Berlett BS, Stadtman ER. 1996. Methionine residues as endogenous antioxidants in proteins. Proc Natl Acad Sci U S A 93:15036-15040.

Li X, Cai H, Xu J, Ying S, Zhang Y. 2009. A mouse protein interactome through combined literature mining with multiple sources of interaction evidence. Amino Acids.

Lim PL, Liu J, Go ML, Boelsterli UA. 2008. The Mitochondrial Superoxide/Thioredoxin-2/Ask1 Signaling Pathway is Critically Involved in Troglitazone-Induced Cell Injury to Human Hepatocytes. Toxicol Sci 101:341-349.

Lin MT, Beal MF. 2006. Mitochondrial dysfunction and oxidative stress in neurodegenerative diseases. Nature 443:787-795.

Lluis JM, Morales A, Blasco C, Colell A, Mari M, Garcia-Ruiz C, Fernandez-Checa JC. 2005. Critical role of mitochondrial glutathione in the survival of hepatocytes during hypoxia. J Biol Chem 280:3224-3232.

Loi CM, Young M, Randinitis E, Vassos A, Koup JR. 1999. Clinical pharmacokinetics of troglitazone. Clin Pharmacokinet 37:91-104.

Lubec G, Afjehi-Sadat L. 2007. Limitations and pitfalls in protein identification by mass spectrometry. Chem Rev 107:3568-3584.

Lucena MI, Andrade RJ, Martinez C, Ulzurrun E, Garcia-Martin E, Borraz Y, Fernandez MC, Romero-Gomez M, Castiella A, Planas R, Costa J, Anzola S, Agundez JA. 2008. Glutathione S-transferase m1 and t1 null genotypes increase susceptibility to idiosyncratic drug-induced liver injury. Hepatology 48:588-596.

Lynn S, Huang EJ, Elchuri S, Naeemuddin M, Nishinaka Y, Yodoi J, Ferriero DM, Epstein CJ, Huang TT. 2005. Selective neuronal vulnerability and inadequate stress response in superoxide dismutase mutant mice. Free Radic Biol Med 38:817-828.

Maggi LB, Jr., Sadeghi H, Weigand C, Scarim AL, Heitmeier MR, Corbett JA. 2000a. Anti-inflammatory actions of 15-deoxy-delta 12,14-prostaglandin J2 and troglitazone: evidence for heat shock-dependent and -independent inhibition of cytokine-induced inducible nitric oxide synthase expression. Diabetes 49:346-355.

Maggi LB, Sadeghi H, Weigand C, Scarim AL, Heitmeier MR, Corbett JA. 2000b. Anti-inflammatory actions of 15-deoxy-delta 12,14-prostaglandin J2 and troglitazone: Evidence for heat shock-dependent and -independent inhibition of cytokine-induced inducible nitric oxide synthase expression. Diabetes 49:346-355.

Majamaa K, Moilanen JS, Uimonen S, Remes AM, Salmela PI, Karppa M, Majamaa-Voltti KA, Rusanen H, Sorri M, Peuhkurinen KJ, Hassinen IE. 1998. Epidemiology of A3243G, the mutation for mitochondrial encephalomyopathy, lactic acidosis, and strokelike episodes: prevalence of the mutation in an adult population. Am J Hum Genet 63:447-454.

Maniratanachote R, Keiichi M, Katoh M, Nakajima M, Yokoi T. 2005. Chaperone Proteins Involved in Troglitazone-Induced Toxicity in Human Hepatoma Cell Lines. Toxicol. Sci. 83:293-302.

Mantena SK, King AL, Andringa KK, Eccleston HB, Bailey SM. 2008. Mitochondrial dysfunction and oxidative stress in the pathogenesis of alcohol- and obesity-induced fatty liver diseases. Free Radic Biol Med 44:1259-1272.

Marla SS, Lee J, Groves JT. 1997. Peroxynitrite rapidly permeates phospholipid membranes. Proc Natl Acad Sci U S A 94:14243-14248.

Martensson J, Lai JC, Meister A. 1990. High-affinity transport of glutathione is part of a multicomponent system essential for mitochondrial function. Proc Natl Acad Sci U S A 87:7185-7189.

Meisinger C, Sommer T, Pfanner N. 2000. Purification of Saccharomcyes cerevisiae mitochondria devoid of microsomal and cytosolic contaminations. Anal Biochem 287:339-342.

Minin EA, Buchwalow IB, Wellner M, Palmes D, Spiegel HU, Neumann J, Boecker W, Herbst H. 2005. L-Arginine-NO-cGMP signaling following acute liver injury in the rat. Exp Toxicol Pathol 57:161-171.

Mootha VK, Lindgren CM, Eriksson KF, Subramanian A, Sihag S, Lehar J, Puigserver P, Carlsson E, Ridderstrale M, Laurila E, Houstis N, Daly MJ, Patterson N, Mesirov JP, Golub TR, Tamayo P, Spiegelman B, Lander ES, Hirschhorn JN, Altshuler D, Groop LC. 2003. PGC-1alpha-responsive genes involved in oxidative phosphorylation are coordinately downregulated in human diabetes. Nat Genet 34:267-273.

Mortz E, Krogh TN, Vorum H, Görg A. 2001. Improved silver staining protocols for high sensitivity protein identification using matrix-assisted laser desorption/ionization-time of flight analysis. Proteomics 1:1359–1363.

Moskovitz J, Bar-Noy S, Williams WM, Requena J, Berlett BS, Stadtman ER. 2001. Methionine sulfoxide reductase (MsrA) is a regulator of antioxidant defense and lifespan in mammals. Proc Natl Acad Sci U S A 98:12920-12925.

Murray AJ, Edwards LM, Clarke K. 2007. Mitochondria and heart failure. Curr Opin Clin Nutr Metab Care 10:704-711.

Nahon P, Sutton A, Pessayre D, Rufat P, Degoul F, Ganne-Carrie N, Ziol M, Charnaux N, N'Kontchou G, Trinchet JC, Gattegno L, Beaugrand M. 2005. Genetic dimorphism in superoxide dismutase and susceptibility to alcoholic cirrhosis, hepatocellular carcinoma, and death. Clin Gastroenterol Hepatol 3:292-298.

Nakachi Y, Yagi K, Nikaido I, Bono H, Tonouchi M, Schonbach C, Okazaki Y. 2008. Identification of novel PPARgamma target genes by integrated analysis of ChIP-on-chip and microarray expression data during adipocyte differentiation. Biochem Biophys Res Commun 372:362-366.

Navarro VJ, Senior JR. 2006. Drug-related hepatotoxicity. N Engl J Med 354:731-739.

New L-S, Saha S, Ong MMK, Boelsterli UA, Chan ECY. 2007 Pharmacokinetic study of intraperitoneally administered troglitazone in mice using ultra-performance liquid chromatography/tandem mass spectrometry. Rapid Commun. Mass Spectrom. 21:982–988.

Nilsen J, Diaz Brinton R. 2003. Mechanism of estrogen-mediated neuroprotection: regulation of mitochondrial calcium and Bcl-2 expression. Proc Natl Acad Sci U S A 100:2842-2847.

Nilsen J, Irwin RW, Gallaher TK, Brinton RD. 2007. Estradiol in vivo regulation of brain mitochondrial proteome. J Neurosci 27:14069-14077.

Nulton-Persson AC, Szweda LI. 2001. Modulation of mitochondrial function by hydrogen peroxide. J Biol Chem 276:23357-23361.

Nystrom T. 2005. Role of oxidative carbonylation in protein quality control and senescence. Embo J 24:1311-1317.

Okado-Matsumoto A, Fridovich I. 2001. Subcellular distribution of superoxide dismutases (SOD) in rat liver: Cu, Zn-SOD in mitochondria. J. Biol. Chem. 276:38388–38393.

Omura T. 2006. Mitochondrial P450s. Chem Biol Interact 163:86-93.

Ong MMK, Latchoumycandane C, Boelsterli UA. 2007. Troglitazone-induced hepatic necrosis in an animal model of silent mitochondrial abnormalities. Toxicol. Sci. 97:205-213.

Orrenius S, Gogvadze V, Zhivotovsky B. 2007. Mitochondrial oxidative stress: implications for cell death. Annu Rev Pharmacol Toxicol 47:143-183.

Ott M, Gogvadze V, Orrenius S, Zhivotovsky B. 2007. Mitochondria, oxidative stress and cell death. Apoptosis 12:913-922.

Paddock ML, Wiley SE, Axelrod HL, Cohen AE, Roy M, Abresch EC, Capraro D, Murphy AN, Nechushtai R, Dixon JE, Jennings PA. 2007. MitoNEET is a uniquely folded 2Fe 2S outer mitochondrial membrane protein stabilized by pioglitazone. Proc Natl Acad Sci U S A 104:14342-14347.

Pagliarini DJ, Calvo SE, Chang B, Sheth SA, Vafai SB, Ong SE, Walford GA, Sugiana C, Boneh A, Chen WK, Hill DE, Vidal M, Evans JG, Thorburn DR, Carr SA, Mootha VK. 2008. A mitochondrial protein compendium elucidates complex I disease biology. Cell 134:112-123.

Patti ME, Butte AJ, Crunkhorn S, Cusi K, Berria R, Kashyap S, Miyazaki Y, Kohane I, Costello M, Saccone R, Landaker EJ, Goldfine AB, Mun E, DeFronzo R, Finlayson J, Kahn CR, Mandarino LJ. 2003. Coordinated reduction of genes of oxidative metabolism in humans with insulin resistance and diabetes: Potential role of PGC1 and NRF1. Proc Natl Acad Sci U S A 100:8466-8471.

Peng J, Elias JE, Thoreen CC, Licklider LJ, Gygi SP. 2003. Evaluation of multidimensional chromatography coupled with tandem mass spectrometry (LC/LC-MS/MS) for large-scale protein analysis: the yeast proteome. J Proteome Res 2:43-50.

Peraza MA, Burdick AD, Marin HE, Gonzalez FJ, Peters JM. 2006. The toxicology of ligands for peroxisome proliferator-activated receptors (PPAR). Toxicol Sci 90:269-295.

Pessayre D, Mansouri A, Haouzi D, Fromenty B. 1999. Hepatotoxicity due to mitochondrial dysfunction. Cell Biol Toxicol 15:367-373.

Petersen KF, Dufour S, Befroy D, Garcia R, Shulman GI. 2004. Impaired mitochondrial activity in the insulin-resistant offspring of patients with type 2 diabetes. N Engl J Med 350:664-671.

Pierce A, Unwin RD, Evans CA, Griffiths S, Carney L, Zhang L, Jaworska E, Lee CF, Blinco D, Okoniewski MJ, Miller CJ, Bitton DA, Spooncer E, Whetton AD. 2008. Eight-channel iTRAQ enables comparison of the activity of six leukemogenic tyrosine kinases. Mol Cell Proteomics 7:853-863.

Poyton RO. 1996. Crosstalk between nuclear and mitochondrial genomes. Annu. Rev. Biochem. 65:563-607.

Radi R. 2004. Nitric oxide, oxidants, and protein tyrosine nitration. Proc Natl Acad Sci U S A 101:4003-4008.

Radi R, Turrensll JF, Chang LY, Bush KM, Crapo JD, Freeman BA. 1991. Detection of Catalase in Rat Heart Mitochondria. The Journal of Biological Chemistry 266:22028-22034.

Ransohoff DF. 2005. Bias as a threat to the validity of cancer molecular-marker research. Nat Rev Cancer 5:142-149.

Reznick AZ, Packer L. 1994. Oxidative damage to proteins: spectrophotometric method for carbonyl assay. Methods Enzymol 233:357-363.

Rodriguez JC, Gil-Gomez G, Hegardt FG, Haro D. 1994. Peroxisome proliferator-activated receptor mediates induction of the mitochondrial 3-hydroxy-3-methylglutaryl-CoA synthase gene by fatty acids. J Biol Chem 269:18767-18772.

Ruepp SU, Tonge RP, Shaw J, Wallis N, Pognan Fo. 2002. Genomics and Proteomics Analysis of Acetaminophen Toxicity in Mouse Liver. Toxicology Sciences 65:135–150.

Schon EA. 2000. Mitochondrial genetics and disease. Trends Biochem Sci 25:555-560.

Schonfeld P, Wojtczak L. 2008. Fatty acids as modulators of the cellular production of reactive oxygen species. Free Radic Biol Med 45:231-241.

Shilov IV, Seymour SL, Patel AA, Loboda A, Tang WH, Keating SP, Hunter CL, Nuwaysir LM, Schaeffer DA. 2007. The Paragon Algorithm, a next generation search engine that uses sequence temperature values and feature probabilities to identify peptides from tandem mass spectra. Mol Cell Proteomics 6:1638-1655.

Shimoda-Matsubayashi S, Matsumine H, Kobayashi T, Nakagawa-Hattori Y, Shimizu Y, Mizuno Y. 1996. Structural dimorphism in the mitochondrial targeting sequence in the human manganese superoxide dismutase gene. A predictive evidence for conformational change to influence mitochondrial transport and a study of allelic association in Parkinson's disease. Biochem Biophys Res Commun 226:561-565.

Sigrist S, Bedoucha M, Boelsterli UA. 2000. Down-regulation by troglitazone of hepatic tumor necrosis factor-alpha and interleukin-6 mRNA expression in a murine model of non-insulin-dependent diabetes. Biochem Pharmacol 60:67-75.

Slonecker PJ, Li X, Ridgway TH, Dorsey JG. 1996. Informational orthogonality of two-dimensional chromatographic separations. Anal Chem 68:682-689.

Smith MT. 2003. Mechanisms of troglitazone hepatotoxicity. Chem Res Toxicol 16:679-687.

Souza JM, Peluffo G, Radi R. 2008. Protein tyrosine nitration--functional alteration or just a biomarker? Free Radic Biol Med 45:357-366.

St-Pierre J, Drori S, Uldry M, Silvaggi JM, Rhee J, Jager S, Handschin C, Zheng K, Lin J, Yang W, Simon DK, Bachoo R, Spiegelman BM. 2006. Suppression of reactive oxygen species and neurodegeneration by the PGC-1 transcriptional coactivators. Cell 127:397-408.

Stadtman ER, Moskovitz J, Berlett BS, Levine RL. 2002. Cyclic oxidation and reduction of protein methionine residues is an important antioxidant mechanism. Mol Cell Biochem 234-235:3-9.

Stirone C, Duckles SP, Krause DN, Procaccio V. 2005. Estrogen increases mitochondrial efficiency and reduces oxidative stress in cerebral blood vessels. Mol Pharmacol 68:959-965.

Strehlow K, Rotter S, Wassmann S, Adam O, Grohe C, Laufs K, Bohm M, Nickenig G. 2003. Modulation of antioxidant enzyme expression and function by estrogen. Circ Res 93:170-177.

Sunayama J, Tsuruta F, Masuyama N, Gotoh Y. 2005. JNK antagonizes Akt-mediated survival signals by phosphorylating 14-3-3. J Cell Biol 170:295-304.

Sutton A, Khoury H, Prip-Buus C, Cepanec C, Pessayre D, Degoul F. 2003. The Ala16Val genetic dimorphism modulates the import of human manganese superoxide dismutase into rat liver mitochondria. Pharmacogenetics 13:145-157.

Sutton A, Nahon P, Pessayre D, Rufat P, Poire A, Ziol M, Vidaud D, Barget N, Ganne-Carrie N, Charnaux N, Trinchet JC, Gattegno L, Beaugrand M. 2006. Genetic polymorphisms in antioxidant enzymes modulate hepatic iron accumulation and hepatocellular carcinoma development in patients with alcohol-induced cirrhosis. Cancer Res 66:2844-2852.

Taanman JW. 1997. Human cytochrome c oxidase: structure, function, and deficiency. J Bioenerg Biomembr 29:151-163.

Tafazoli S, Spehar DD, O'Brien PJ. 2005a. Oxidative stress mediated idiosyncratic drug toxicity. Drug Metab Rev 37:311-325.

Tafazoli S, Wright JS, O'Brien PJ. 2005b. Prooxidant and antioxidant activity of vitamin E analogues and troglitazone. Chem Res Toxicol 18:1567-1574.

Takeda K, Noguchi T, Naguro I, Ichijo H. 2008. Apoptosis signal-regulating kinase 1 in stress and immune response. Annu Rev Pharmacol Toxicol 48:199-225.

Tamai S, Iida H, Yokota S, Sayano T, Kiguchiya S, Ishihara N, Hayashi J, Mihara K, Oka T. 2008. Characterization of the mitochondrial protein LETM1, which maintains the mitochondrial tubular shapes and interacts with the AAA-ATPase BCS1L. J Cell Sci 121:2588-2600.

Tang WH, Shilov IV, Seymour SL. 2008. Nonlinear fitting method for determining local false discovery rates from decoy database searches. J Proteome Res 7:3661-3667.

Taniguchi K, Nonami T, Nakao A, Harada A, Kurokawa T, Sugiyama S, Fujitsuka N, Shimomura Y, Hutson SM, Harris RA, Takagi H. 1996. The valine catabolic pathway in human liver: effect of cirrhosis on enzyme activities. Hepatology 24:1395-1398.

Taylor SW, Fahy E, Ghosh SS. 2003. Global organellar proteomics. Trends Biotechnol 21:82-88.

Tothova Z, Kollipara R, Huntly BJ, Lee BH, Castrillon DH, Cullen DE, McDowell EP, Lazo-Kallanian S, Williams IR, Sears C, Armstrong SA, Passegue E, DePinho

RA, Gilliland DG. 2007. FoxOs are critical mediators of hematopoietic stem cell resistance to physiologic oxidative stress. Cell 128:325-339.

Tretter L, Adam-Vizi V. 2005. Alpha-ketoglutarate dehydrogenase: a target and generator of oxidative stress. Phil. Trans. R. Soc. B. 360:2335–2345.

Tretter LA-V, V. . 2000. Inhibition of Krebs cycle enzymes by hydrogen peroxide: A key role of [alpha]-ketoglutarate dehydrogenase in limiting NADH production under oxidative stress. J. Neurosci. 20:8972–8979.

U.S. Department of Health and Human Services FaDA. March 21, 2000 Rezulin to be withdrawn from the market.

Uetrecht J. 2007. Idiosyncratic drug reactions: current understanding. Annu Rev Pharmacol Toxicol 47:513-539.

Uetrecht J. 2008. Idiosyncratic drug reactions: past, present, and future. Chem Res Toxicol 21:84-92.

Uetrecht J. 2009. Immune-mediated adverse drug reactions. Chem Res Toxicol 22:24-34.

Ulrich R, Friend SH. 2002. Toxicogenomics and drug discovery: will new technologies help us produce better drugs? Nat Rev Drug Discov 1:84-88.

Ulrich RG. 2007. Idiosyncratic toxicity: a convergence of risk factors. Annu Rev Med 58:17-34.

Unlu M, Morgan ME, Minden JS. 1997. Difference gel electrophoresis: a single gel method for detecting changes in protein extracts. Electrophoresis 18:2071-2077.

Valle I, Alvarez-Barrientos A, Arza E, Lamas S, Monsalve M. 2005. PGC-1alpha regulates the mitochondrial antioxidant defense system in vascular endothelial cells. Cardiovasc Res 66:562-573.

Vance JE. 1990. Phospholipid synthesis in a membrane fraction associated with mitochondria. J Biol Chem 265:7248-7256.

Varanasi U, Chu R, Huang Q, Castellon R, Yeldandi AV, Reddy JK. 1996. Identification of a peroxisome proliferator-responsive element upstream of the human peroxisomal fatty acyl coenzyme A oxidase gene. J Biol Chem 271:2147-2155.

Vogt W. 1995. Oxidation of methionyl residues in proteins: tools, targets, and reversal. Free Radic Biol Med 18:93-105.

Walgren JL, Thompson DC. 2004. Application of proteomic technologies in the drug development process. Toxicol Lett 149:377-385.

Wallace DC. 1999. Mitochondrial diseases in man and mouse. Science 283:1482-1488.

Wallace KB. 2008. Mitochondrial off targets of drug therapy. Trends Pharmacol Sci 29:361-366.

Wallace KB, Starkov AA. 2000. Mitochondrial targets of drug toxicity. Annual review of pharmacology & toxicology 40:353–388.

Washburn MP, Wolters D, Yates JR, 3rd. 2001. Large-scale analysis of the yeast proteome by multidimensional protein identification technology. Nat Biotechnol 19:242-247.

Watanabe I, Tomita A, Shimizu M, Sugawara M, Yasumo H, Koishi R, Takahashi T, Miyoshi K, Nakamura K, Izumi T, Matsushita Y, Furukawa H, Haruyama H, Koga T. 2003. A study to survey susceptible genetic factors responsible for troglitazone-

associated hepatotoxicity in Japanese patients with type 2 diabetes mellitus. Clin Pharmacol Ther 73:435-455.

Waters MD, Fostel JM. 2004. Toxicogenomics and systems toxicology: aims and prospects. Nat Rev Genet 5:936-948.

Wei J, Kang HW, Cohen DE. 2009. Thioesterase superfamily member 2 (Them2)/acyl-CoA thioesterase 13 (Acot13): A homotetrameric hotdog fold thioesterase with selectivity for long chain fatty acyl-CoAs. Biochem J.

Wiese S, Reidegeld KA, Meyer HE, Warscheid B. 2007. Protein labeling by iTRAQ: a new tool for quantitative mass spectrometry in proteome research. Proteomics 7:340-350.

Williams MD, Van Remmen H, Conrad CC, Huang TT, Epstein CJ, Richardson A. 1998. Increased oxidative damage is correlated to altered mitochondrial function in heterozygous manganese superoxide dismutase knockout mice. J Biol Chem 273:28510-28515.

Willson TM, Cobb JE, Cowan DJ, Wiethe RW, Correa ID, Prakash SR, Beck KD, Moore LB, Kliewer SA, Lehmann JM. 1996. The structure-activity relationship between peroxisome proliferator-activated receptor gamma agonism and the antihyperglycemic activity of thiazolidinediones. J Med Chem 39:665-668.

Winterbourn CC. 2008. Reconciling the chemistry and biology of reactive oxygen species. Nat Chem Biol 4:278-286.

Yan L-J, Levine RL, Sohal RS. 1997. Oxidative damage during aging targets mitochondrial aconitase. Proc. Natl. Acad. Sci. USA 94:11168-11172.

Yates JR, 3rd, Gilchrist A, Howell KE, Bergeron JJ. 2005. Proteomics of organelles and large cellular structures. Nat Rev Mol Cell Biol 6:702-714.

Young PW, Buckle DR, Cantello BC, Chapman H, Clapham JC, Coyle PJ, Haigh D, Hindley RM, Holder JC, Kallender H, Latter AJ, Lawrie KW, Mossakowska D, Murphy GJ, Roxbee Cox L, Smith SA. 1998. Identification of high-affinity binding sites for the insulin sensitizer rosiglitazone (BRL-49653) in rodent and human adipocytes using a radioiodinated ligand for peroxisomal proliferator-activated receptor gamma. J Pharmacol Exp Ther 284:751-759.

Yu L, Strandberg L, Lenardo MJ. 2008. The selectivity of autophagy and its role in cell death and survival. Autophagy 4:567-573.

Zhang L, Yu L, Yu CA. 1998. Generation of superoxide anion by succinate-cytochrome c reductase from bovine heart mitochondria. J Biol Chem 273:33972-33976.

Zhao P, Kalhorn TF, Slattery JT. 2002. Selective mitochondrial glutathione depletion by ethanol enhances acetaminophen toxicity in rat liver. Hepatology 36:326-335.

Zhong Q, Putt DA, Xu F, Lash LH. 2008. Hepatic mitochondrial transport of glutathione: studies in isolated rat liver mitochondria and H4IIE rat hepatoma cells. Arch Biochem Biophys 474:119-127.

Zimmerman HJ. 1976. Various forms of chemically induced liver injury and their detection by diagnostic procedures. Environ Health Perspect 15:3-12.